UCLouvain

École polytechnique de Louvain

Study and Optimisation of Flax Fibers Reinforced Bio-Sourced Epoxy Resin Composites Interfacial Adhesion and Compatibility

Author: **João Ítalo Lopes Amaro**
Supervisor: **Christian Bailly**
Readers: **Wael Ballout, Christine Dupont, Carlos Fuentes**
Academic year 2018–2019
Master [120] in Chemical and Materials Engineering

Abstract

Recent advances in the field of natural fibre reinforced composites, allowing to better understand and control their properties, the raise of environmental awareness amongst costumers and the need for low-weight, cost-effective materials in industries such as the automotive contribute to promising projections for the increase in demand of natural fibre reinforced composites. Flax fibres present the best combination of mechanical proprieties, whose specific values are comparable to those of glass fibres. However, the specific strength of composites made with untreated flax is still much lower than that of glass fibres composites, most probably due to poor load transfer. This indicates a need for interface improvement. Essentially controlled by the chemistry and morphology of the interface, interfacial compatibility and adhesion in fibre reinforced composites can be described in terms of physicochemical interactions, chemical bonding and mechanical interlocking. This work was mostly devoted to characterising the effects of chemical and mechanical surface properties of flax fibres as a means to optimise their adhesion and compatibility with the matrix. Fibres were either untreated, aminosilane-treated or washed via one of two different mild treatments with ethanol or water selected from the literature. Changes in physicochemical interactions were investigated using the Wilhelmy technique to assess fibres wettability. In parallel, X-ray photoelectric spectroscopy (XPS) analysis was performed to study surface chemical composition of untreated and aminosilane-treated fibres. The combined effect of those parameters and mechanical interlocking on interface mechanical properties due to fibres treatments were characterised via microbond tests. Single-fibre tensile tests were also performed, proving no significant degree of degradation due to storage conditions or handling of the fibres. Treatment with Bis(trimethoxysilylpropyl)amine was the only modification effective in improving the practical adhesion and was demonstrated to be strongly determined by chemical bonding, while, contrary to what was expected, washing methods seemed to worsen interface strength. Although the root causes of this phenomena may lay in the frictional stresses, it could not be assessed by the approach used.

Contents

1 Introduction **1**
- 1.1 Flax Facts . . . 1
  - 1.1.1 Flax History . . . 1
  - 1.1.2 Flax Processing . . . 2
  - 1.1.3 World Production . . . 4
- 1.2 New Applications: A Demand for Greener Composites . . . 5
- 1.3 Towards High-Performance Environmentally Friendly Composites . . . 8
- 1.4 Recent Applications . . . 9
- 1.5 The Present Work . . . 10

2 Literature Review **12**
- 2.1 Theoretical Background . . . 12
  - 2.1.1 Flax Fibres Structure . . . 12
  - 2.1.2 Flax Fibres Composition . . . 14
  - 2.1.3 Interfacial Compatibility and Adhesion in Natural Fibre Composites . . . 16
  - 2.1.4 Wettability Models and Assessment . . . 18
  - 2.1.5 Interface Mechanical Characterisation . . . 32
  - 2.1.6 Experiment Description and Modelling . . . 33
  - 2.1.7 Tensile Properties of Flax Fibres . . . 40
- 2.2 State of the Art . . . 43
  - 2.2.1 Physicochemical Interactions . . . 43
  - 2.2.2 Interface Mechanical Characterisation . . . 52
  - 2.2.3 Tensile Properties . . . 64
  - 2.2.4 Silanisation . . . 70

3 Experimental Section **73**
- 3.1 Materials . . . 73
  - 3.1.1 Flax Fibres . . . 73
  - 3.1.2 Bio-Epoxy Resin . . . 73
- 3.2 Methods . . . 74
  - 3.2.1 Elementary Fibres Isolation . . . 74
  - 3.2.2 Tensile Test and Microbond Specimens Preparation . . . 75
  - 3.2.3 Elementary Fibres Cleaning . . . 78
  - 3.2.4 Surface Chemical Analysis . . . 79
  - 3.2.5 Wilhelmy Technique . . . 80
  - 3.2.6 Microbond Test . . . 85
  - 3.2.7 Tensile Test . . . 87

4 Results and Discussion **90**
- 4.1 Chemical Analysis . . . 90
- 4.2 Physicochemical Interactions . . . 91
  - 4.2.1 Surface Energy Results Presentation . . . 92
  - 4.2.2 Critical Comparison with the Literature . . . 94
  - 4.2.3 Partial Conclusion . . . 96

4.3 Interface Mechanical Properties . . . 96
4.3.1 Interface Mechanical Properties Results Presentation . . . 97
4.3.2 Critical Comparison with the Literature . . . 99
4.3.3 Partial Conclusion . . . 99
4.4 Tensile Properties . . . 101

5 Conclusion and Perspectives **102**
5.1 Silanisation Effect . . . 102
5.2 Ethylene and Water Washing Effect . . . 103
5.2.1 Tensile Properties . . . 103
5.3 Overall Perspectives . . . 104

6 Appendix A: MKT Impracticability **117**

7 Appendix B: Energy-Based Equation Coefficients **119**

8 Appendix C: An Approach to Drop-on-Fibre Measurements **120**

9 Appendix D: System Compliance **123**

List of Figures

1.1 Different Structures of Linum usitatissimum (flax). Köhler's Medizinal-Pflanzen [1]. 1
1.2 Bandage made of linen (flax textile) from Tutankhamun's Embalming Cache (ca. 1336-1327 B.C.) [2]. . . . 2
1.3 The traditional value-added chain from flax plant to textile products [3]. 3
1.4 (a) A flax field in bloom in Normandy, France [4]; (b) Flax fibres let to dew-ret in the field [4] 3
1.5 Overview of flax processing [5] 4
1.6 Main Flax Producers in the North hemisphere (not accounting for Canada). As per 2014 production [6] . . 4
1.7 (a) Comparison of potential specific modulus, natural fibres and glass fibres; (b) Cost per weight comparison between glass and natural fibres [7] 6
1.8 Environmental impacts during the production of hackled flax fibres compared to those for glass fibres [8] . . 6
1.9 The absolute (a) and specific (b in tension, c in plate bending) longitudinal stiffness of flax, glass, carbon fibre UD composites, steel and aluminium as a function of the fibre volume fraction (calculated properties, based on average data) [3]. 7
1.10 Tesla-based EPCS Series. Body works in high-performance, lightweight natural flax fibre composite (powerRibs^{TM} and ampliTex^{TM}). Thanks to the fibre translucency, the roof can have an internal, fully integrated LED screen that shows live-information during races. [9] 8
1.11 Mercedes S class natural fibre reinforced composite parts [10] 9
1.12 Various applications of flax composites in sporting goods: a) Artengo tennis racket, b) Notox surfboard, c) Caperlan fishing rod, d) ArcWin Archery bow, e) Kang flax ski poles and f) Le Ventoux bamboo-flax bike. [11] 10
1.13 a) Aria column speaker 900 and flax cone from FOCAL, b) El Capitan Blackbird Guitar, c) Blackbird flax Ukulele and d) Flax electric Guitar from Depestele. From [11] 10

2.1 Flax structure, from stem to cellulosic fibrils [12] 12
2.2 Defects on fibres observed by polarised optical microscope. Fibre diameters in all images are ca. 20µm [13] 13
2.3 Field-emission SEM image of an elementary flax fibre showing transverse defects and longitudinal defects [14] 14
2.4 Cellulose structure. Inter and Intramolecular hydrogen bonds are presented as dashed lines [15] 15
2.5 A) Schematic structure of pectin, with approximate relative abundance between groups [16]; B) Schematics of an "eggbox" structure consisting of two antiparallel poly-galacturonic acid chains complexed by Ca^{2+} [17] 15
2.6 Example of a common hemicellulose repeating motif: L-arabino-D-xylane [18] 16
2.7 Scheme illustrating the Young equation, which relates the characteristic ideal contact angle of a liquid droplet (θ) on a solid surface and the surface free energy (γ) of the different phases in equilibrium at the triple line where solid (s), liquid (l), and gaseous (g) phases meet [19]. 18
2.8 Owens-Wendt plot used to estimate the surface energy of coir fibres employing the contact angles obtained from different approaches (Molecular-Kinetic Theory [MKT], mean advancing and receding contact angles in Wilhelmy Balance (W1) and linear trend (W2)). [20] 20
2.9 Schematic of the force balance diagram model assumed in the Wilhelmy technique method to calculate the advancing dynamic contact angle as the liquid contact line (i.e. solid-liquid-air interface line) moves due to immersion of the fibre into the probe liquid vessel [21]. (Ideal perfectly fat surface). 22
2.10 Schematic representation of the velocity dependence of the experimentally determined contact angle θ, showing static advancing and receding limits, and the equilibrium angle θ_{eq} (Young's contact angle) [22]. . 23
2.11 Thin liquid film formed during liquid retreat can be thicker from precursor film formed during spreading. Contact angle hysteresis is caused by different disjoining pressure [23] 24

2.12 (a) Typical dynamic contact angle measurements of coir and PET fibres [24]; (b) Contact angle as a function of the wetting force according to Eq. 2.15 for Water (WT), Ethylene Glycol (EG) and Diiodomethane (DIM). Weight and buoyancy were assumed negligible and the fibre diameter set to an average value of 20 µm . . . 25
2.13 Effect of surface heterogeneity on the three-phase contact line and contact angle. The graph presents correlations between advancing and receding contact angles and the fractional area of the solid covered by inclusions (heterogeneity with apolar character). Rec, St, Adv, receding, static and advancing contact lines, respectively; θ_R, θ, θ_A, receding, static and advancing contact angles, respectively . . . 26
2.14 Cassie–Baxter wetting of flat chemically heterogeneous surfaces (various grey scale colours correspond to different chemical species) [19] . . . 27
2.15 Wenzel wetting of a chemically homogeneous rough surface: liquid completely wets the grooves coming representing the surface roughness [19]. . . . 28
2.16 Wetting of a substrate built of conical posts. The external and internal triple lines are shown [25]. . . . 28
2.17 SEM micrographs of flax fibres with defect regions. Arrows show the kink bands on flax fibre surfaces [13] . 29
2.18 The radius of curvature of the fibre surface is constantly changing during the movement of the meniscus over the fibre body, and so the direction of the wetting force, r–curvature radius, F_{lv}–liquid–vapour interfacial force (or wetting force). Position (1): smooth fibre and position (2): fibre with surface irregularities [26] . . 29
2.19 (A) Optical microscopy of non-autoclave treated bamboo fibre and SEM image of disjointed elementary fibres, the scale bar in (a) is 10 m. (B) Optical microscopy image of altered PET fibre [26] . . . 30
2.20 Usual morphologies assumed by a droplet wetting a fibre surface [27]. . . . 31
2.21 (A) PLA microdroplet on single flax fibre [28]; (B) Debonded sample without peeling [29] . . . 33
2.22 Fibre surfaces after microdroplet sliding, glass/PLLA (A), flax/PLLA (type A) (B), flax/PLLA (type B) (C1-C3), (D) schematic diagram of the structure of a flax (Reminder) [28] . . . 33
2.23 Variations of the total interfacial shear stress and its components along the axial coordinate in a microbond or pullout specimen. The horizontal line shows the apparent shear strength value for this specimen [30] . . 34
2.24 An idealised force–displacement curve in the pullout test [31]. A similar behaviour is observed for microbond test, except for a constant friction force resulting in a plateau after point D . . . 35
2.25 Typical Force versus Position curve obtained from microbond tests using Bio-epoxy resin and Flax Fibres. Debonding (F_d) and Maximum (F_{max}) forces are indicated, they correspond respectively to the initial force at which crack propagation starts and the force at the moment in which the sum of the frictional and interfacial adhesion forces are surpassed by the tensile force, resulting in catastrophic failure of remaining bonded surface . . . 36
2.26 The left side shows the microbond (top) and pullout (bottom) specimen geometries. The right side shows the equivalent concentric cylinder model where the embedded length of fiber is in a cylinder of matrix. The fibre in both specimens is loaded with stress σ_d. The "dotted" arrows are the remaining microbond specimen boundary conditions; the solid arrows on the bottom of the specimen are the remaining pullout specimen boundary conditions [32] . . . 37
2.27 Example of a stress-strain curve of an elementary flax fibre. Modified from K. Charlet et al. [33] . . . 39
2.28 Schematics of the main flax fibres secondary wall structural components and defects: a) Under rest condition; b) Under tensile load [34]. . . . 40
2.29 Schematic representation of microfibrils alignment with respect to the tensile axis under tensile loading [34] 40
2.30 Fracture behaviour of a flax fibre showed a by optical microscope images of a fibre before and after fracture and b in a schematic view. The locations of small and large transverse defects are indicated [14] . . . 41
2.31 Scanning electron microscope image of a large fracture zone in a single flax fibre. Magnified views (1 and 2) are presented to highlight the longitudinal cracks along the fibre, and the formed microfibrillar units at the inner layers at both fractured ends [14] . . . 42
2.32 Schematic representation of the transverse tensile test and the transverse three point bending test (transverse 3PBT) on unidirectional (UD) composites [35] . . . 53
2.33 Tensile strength in transverse direction of UD flax/epoxy composites (v_f=40 vol%). The data are grouped per processing step of the flax reinforcement: S-Scutched; H-Hackled; C-Carded. Different fibre types are used as reinforcement: L-Long; S-Slivers; T-Tow;. Fibres with different degrees of retting were used: G-Green; GH-Green Half Retted; N-Normal Retted [35] . . . 54
2.34 The transverse three point bending strength for several flax/epoxy systems. For the specimens code, please refer to Fig. 2.35. Only optimal results are presented. For details about the procedure and the complete set of results, please refer to the source. Modified from [35] . . . 55

2.35 Comparison between the interfacial shear strength, obtained from a stress-based approach similar to that presented in section 2.1.6.2, added of an experimental frictional stress (constant stress observed after debonding) (X-axis), and the transverse flexural composite strength, measured by three point bending (Y-axis). A positive correlation between both data series can be noticed, with a correlation coefficient of 0.6409. Different numbers refer to modified silanisation treatment. UT symbolises the untreated fibre. Specimens 2 and 7 are identical and underwent the standard treatment, Specimens 31 and 32 are also identical and underwent the same treatment with slightly modified parameters (ethanol silane solution instead of water/acetone and 50 °C instead of 105 °C after silane-curing step). 33 correspond to a specimen that underwent the same treatment as 31 and 33, but was not degreased. For details about the procedure and the complete set of results, please refer to the source. Modified from [35]. 56
2.36 Transverse 3PBT failure surfaces showing the correlation between high flexural strength specimens and matrix failure, leaving resin remainders on the surface of the fibres a), poor flexural strength specimens and interface failure, resulting in a clean fibre surface and clean and smooth matrix surface in places from which the fibres were removed (canals); moreover, a gap can be seen between the matrix and a still embedded fibre, further indicating bad adhesion. b) In both cases, poor internal fibre adhesion caused either out cell wall decohesion, revealing aligned microfibrils structure c) or fibre splitting in longitudinal direction d). Modified from [35]. 56
2.37 Schematic representation of different micromechanical tests for interface characterisation. Modified from [36]. 58
2.38 Specimen with increasing number of fibre breaks due to increased strain levels in the matrix. Right: Stress in fibre as function of position for the respective matrix strain levels. Zero stress corresponds to a position with a fibre break [37] 59
2.39 Tensile strength-strain curves for untreated and treated flax fibres [38] 65
2.40 Definition of the three locations from which fibres were extracted from oriented tows [12]. 66
2.41 Tensile strength of flax bundles as a function of gauge length (the dotted line is an approximation). Compilation from different studies [39–41]. From [42]. 67
2.42 a) Specific Young's modulus for each flax sample as compared to glass fibres; b) Specific stress at break for each flax sample as compared to glass fibres. In both cases, the solid line represents average values for oleaginous flax and dash lines their standard deviation [43]. 68
2.43 Back-calculated technical flax fibres tensile obtained by different laboratories using IFBT for the same batch of fibres. Dotted horizontal lines (E1 and E2) represent the average values, as calculated by fitting the rule-of-mixtures equation through all the experimental data [11] 69
2.44 Reactions taking place in the sizing treatment: a) Catalysed hydrolysis of silane monomers forming Silanol groups (-Si-OH); b) Undesirable Self-Condensation of Silanols reducing the available sizing acitve sites and reducing the molecule diffusivity (acidic pH can be used to accelerate hydrolysis rate while slowing down self condensation [44]); c) Physical Adsorption of Silanol groups to Hydroxyl groups on the surface of natural fibres by hydrogen bonding (surface coating) and/or in the cell walls (cell wall bulking) 70
2.45 Reaction between an amino group from the sizing and epoxide group from the epoxy resin (most common Epoxy matrix - Aminosilane coupling agent reaction) 71
2.46 The degradation of interfacial adhesion due to moisture absorption: (a) development of micro-cracks due to expansion of swollen fibre, (b) water molecules diffused in the bulk matrix flow along the fibre–matrix interface, (c) water-soluble components leach from fibre, (d) ultimate matrix–fibre debonding takes place [45]. Copied modified from [46]. 71

3.1 a) As-received UD sample composed of untreated technical fibres, its entire length (not shown in the figure) is about 1m; b) Silane compound used as surface sizing agent 73
3.2 a) Schematics of microdroplet deposition setup, composed of microscope slides as supports and a fixed elementary fibre with microdroplet deposited using a Teflon stick. b) Schematics of the tensile and microbond tests specimen support. It was used to facilitate fibres handling and fixation in the equipment. Dimensions of support for elementary are presented 75
3.3 Microbond specimen characteristic dimensions measurement: A) Typical specimen presenting characteristic dimensions; B) Typical specimen presenting small-diameter "neighbours" (their diameter was taken into account when determining the distance between support knives, see section 3.2.6), Scale bar: 200 µm 76
3.4 Measurement of Gauge length and Diameter of Fibres Bundle Tensile Test Specimen 77
3.5 Cleaning methods and chemical treatments apparatus: a) Caged fibres. The inset shows the stainless steel mesh used to hold the fibres during the treatment; b) Caged fibres in a beaker with cleaning liquid in a hot plate 78
3.6 C 1s spectra, decomposed into four components C1–C4 for Unmodified Flax Fibres. 79

3.7 A) 1μg-resolution Kruss tensiometer K100 SF, B) Schematic drawing of the K100 SF tensiometer indicating each component [47] . . . 80
3.8 A) Detail of Wilhelmy Balance Fibre Specimen mounted on tensiometer holder; B) Detail of Fibre Specimen placed in the close vicinity of the test liquid surface before measurement is started . . . 81
3.9 Typical Force versus Position result obtained for Flax Fibres when the device sensitivity is set to its minimum (1 µg). The force measured before the contact point (pre-force) is attribute environmental interference and must be subtracted from the values after contact point (corresponding to a jump in the curve, which is related to the wetting force) [47]. Results from untreated fibres tested using ethylene glycol. . . . 82
3.10 Illustration of the raw force data treatment procedure. The curve presented in the inset had the pre-force subtracted and contact-point set to zero. Results from untreated fibres tested using ethylene glycol. . . . 82
3.11 Typical Wetting Force versus Immersion Depth curve for Flax Fibres using hexane as probe liquid. The force at zero immersion, obtained by linear regression, is used to calculate the wetted perimeter, which is then employed in the subsequent contact angle calculations. . . . 83
3.12 Typical contact angle curve presenting waviness signature (sudden drop to $\theta = 0°$). Results from untreated fibres tested using water. . . . 84
3.13 Typical raw data force curve presenting bending signature (negative-force regions followed, or not, by sudden peaks). Results from water-washed fibres tested using water. . . . 84
3.14 Gripped Microbond Specimen: A) Elementary fibre with deposited microdroplet placed in paper support; B) schematic representation of a microbond test setup with identified components [48] C) Microdroplet held by caliper. Caliper's knives gap was adjusted for each specimen according to the measured fibre diameter . 85
3.15 Optical Micrographs of Microbond specimen: A) Before experiment (Bright Field, Scale Bar 100 µm); B) After experiment (Bright Field, Scale Bar 100 µm); B) After experiment (Bright Field, Scale Bar 100µm); C) After experiment, broken droplet meniscus and debonded region in the fibre (Bright Field, Scale Bar 25 µm); D) After experiment, highlighting broken interface inside drop (Dark Field Field, Scale Bar 100 µm). 86
3.16 Typical Force versus Position curve obtained from microbond tests using Bio-epoxy resin and Flax Fibres. Debonding (F_d) and Maximum (F_{max}) are indicated, they correspond respectively to the initial force at which crack propagation starts and the force at the moment in which the sum of the friction and interfacial adhesion forces are surpassed by the tensile force, resulting in catastrophic failure of remaining bonded surface 86
3.17 A) Bruker's Universal Mechanical Tester (UMT) - machine used for Microbond and Tensile Tests. B) Gripped Tensile Test Specimen . . . 87
3.18 Typical curve strain-stress for non-(pre)strained elementary flax fibres. The Young's Modulus is obtained from the slope of the linear region according to the Standard for determination of tensile properties of elementary flax fibres NF T25-501-2 . . . 88
3.19 Load cell calibration curve for force values from 0.1 N to 1 N using standard specimens whose weight was assessed with $\sim$ 1 mN precision. Correlation was demonstrated to the 4th decimal digit of the coefficient of determination three times. . . . 89

4.1 Total Surface Free Energy divided in acid-base (AB) and Lifshitz van der Waals (LW) components, and respective work of Adhesion with Epoxy Resin with properties presented in table 4.2 for NT:Untreated; S: Silane-Treated; EtT: Ethanol-Washed and WTT: Water-Washed Fibres . . . 92
4.2 Example of non-usual results presenting non-zero receding angles. Obtained from untreated fibres using water as probe liquid. . . . 94
4.3 Apparent IFSS from Microbond test for NT: Untreated; S: Silane-Treated; EtT: Ethanol-Washed and WTT: Water-Washed Fibres (F). . . . 97
4.4 Apparent IFSS as a function of Work of Adhesion NT: Untreated; S: Silane Treated; EtT: Ethanol Washed and WTT: Water Washed Fibres (F). . . . 98
4.5 Summary of the Young's Modulus values obtained as determined by the Standard NF T25-501-2 from tensile tests performed on three untreated elementary flax fibres . . . 100

8.1 Morphology diagram of millimetre-sized drops on fibres as a function of contact angle θ and reduced volume $\tilde{V}$. Black and red symbols indicate the experimentally observed barrel-to-clamshell (θ_{c1}) and clamshell-to-barrel (θ_{c2}) transitions, respectively. Symbol shapes indicate different fibre diameters: (■) 0.2, (▲) 0.3, and (♦) 0.5 mm. The solid lines indicate the numerically determined stability limit of the clamshell (upper red) and the (coinciding) analytically and numerically determined stability limit of the barrel (lower black). The dashed line indicates the condition of equal absolute energy of both states [49]. . . . 120
8.2 Schematic diagram of a microdroplet on a fibre. . . . 121

List of Tables

1.1 Compilation Properties and Composition of Natural Fibres from various sources [7] 5

2.1 Description of identifiable tissues and cells on the transverse cross-section in the bottom part of a growing flax stained with toluidine blue [50] 13
2.2 Main tissues and cell types composing flax stems [50] 13
2.3 Surface energy components of suggested liquids according to C. Della Volpe and S. Siboni scale [51] 21
2.4 Summary of flax fibres surface energy values available in the literature divided by technique employed and model/method used to interpreter the results (Owens - Wendt - Rabel - Kaelble [OWRK]; Good - van Oss - Chaudhury [GvOC]; Johnson–Kendall–Roberts [JKR]). 44
2.5 Typical SEM images of the fracture surface of flax fibre composites in transverse 3PBT [52] 57
2.6 Work of adhesion, interfacial energy, transverse strength and efficiency factor of longitudinal strength of different fiber-matrix systems 57
2.7 Compilation of IFSS values available in the literature for various systems Flax-Epoxy Resin. Typical Glass Fibres-Epoxy Resin and Regenerated Cellulose(Lyocell)-Epoxy Resin IFSS values are presented for comparison. 61
2.8 Apparent IFSS calculated for flax fibres that underwent extraction increasingly removing the polysaccharides in their structure [53] 63
2.9 Factors affecting the mechanical properties of flax fibres. Modified from [54] 64
2.10 Tensile properties of elementary and technical flax fibres [13] 64
2.11 Tensile properties of untreated and chemically treated technical flax fibres. Treatment agents: Anhydride (MA), acetic anhydride (Ac), silane (Si), ethanedial (glyoxal), 3-aminopropyltriethoxysilane (APS) and dimethyloldihydroxyethylene urea (DMDHEU) [38, 55] 65
2.12 Tensile properties of flax fibres according to their location in the stem [12, 56] 66
2.13 Elementary flax fibre properties vs back-calculated technical fibre properties. E_{f1}: Stiffness calculated between 0% and 0.1% strain; E_{f2}: Stiffness calculated between 0.3% and 0.5% strain; $\sigma_{f,u}$: Tensile strength [11] 68

3.1 Mechanical properties and Glass Transition Temperature (T_g) of a typical cast SR InfuGreen 810 obtained using SD 4771 Ultra-Slow as hardener and curing cycle: AT + 16h at 60°C [57]. 74

4.1 XPS analysis of Untreated and Silane-Treated Flax Technical Fibres presenting Elemental Surface Atomic Fraction (s.at.%) and Binding Energy (B.E. - eV) by bond. Silane-Treated Fibres were analysed twice in different locations proving chemical heterogeneity. 90
4.2 Surface Energy components of Natural fibres submitted to different treatments (NT: Untreated; S: Silane-Treated; EtT: Ethanol-Washed and WTT: Water-Washed Fibres) according to the van Oss model (γ^{LW} : Lifshitz–van der Waals, γ^{+} : Acid or Electron Acceptor, γ^{-} : Basic or Electron Donor, γ^{AB} : Acid-Base or Lewis-like, γ^{Total} : Total surface free energy components) using the Wilhlemy Technique with three probe liquids (WT: Water; EG: Ethylene Glycol; DIM: Diiodomethane) to characterise the fibres contact angle θ. The Work of Adhesion (W_A) is calculated using the surface free energy components of a DGEBA-base system [58], similar to the one used in the present work. 92
4.3 Dispersive (W_A^d) and Acid-Base (W_A^{AB}) components to the total work of adhesion of Ethylene-washed (EtT) and Water-washed (WTT) fibres 93
4.4 Polar and dispersive components of some of main biomolecules contributing to flax surface energy according to various sources 95

4.5 Mean Apparent IFSS and Embedded length from various Microbond test specimens for NT: Untreated; S: Silane Treated; EtT: Ethanol Washed and WTT: Water Washed Fibres (F). 97
4.6 Summary of the tensile test results performed on untreated elementary flax fibres 100

1 Introduction

Over the last two decades, it has been proved that natural fibre composites can have high mechanical properties and be produced at low, competitive cost [35]. These qualities and their inherent environmental friendly character, have attracted increasing attention of both academics and several different industry segments, leading to promising projections to the future of these materials. When compared to other natural fibres, flax fibres present the best combination of mechanical proprieties, whose specific values are comparable to those of glass fibres. However, although remarkably stiff composites can be made with flax, their strength does not reflect the properties of the fibres, being considerably lower than that of glass fibre composites [35]. Among the causes of this discrepancy there are the intrinsic natural character of the fibres, causing properties variation, damage during processing and low interface quality affecting load transfer [35]. The last one being the main focus of the present work. This chapter begins with a contextualisation, presenting some of the reasons that have made flax a crucial fibre crop for the development of modern society, a brief introduction to their processing technology, production worldwide and the factors that have promoted their current development as a composite reinforcement material. Stemming from this these facts, the motivations supporting the current work are stated, the approach followed presented and its methodlogy summarised.

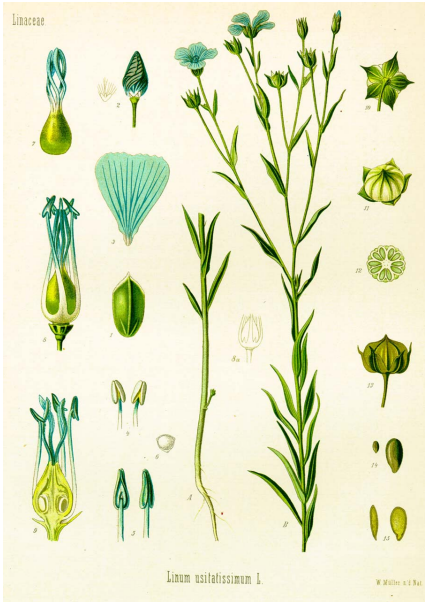


Figure 1.1: Different Structures of Linum usitatissimum (flax). Köhler's Medizinal-Pflanzen [1].

1.1 Flax Facts

1.1.1 Flax History

Linum usitatissimum (flax) is a flowering crop from the Linaceae family mostly cultivated for oil and fibre production [59], it is the first known fibre to be employed for textiles production. First

traces of linen, the textile made from the fibres of the flax plant, were found in a Georgian cave in the Caucasus dating from 36,000 B.C. [60]. Flax was domesticated in parallel with the birth of agriculture in Mesopotamia and through the Fertile Crescent, during the Neolithic period, 10,000 BC [61]. The first evidences of flax technology development come from samples found in Swiss lakes, dating back to 8,000 B.C, those samples were treated by water-retting, a process involving the degradation of pectins and other biomolecules that hold the fibres in bundles in the flax plant by anaerobic bacteria, facilitating their individualisation. Retting is one of the oldest known examples of biotechnology use by mankind [62]. Linen also played an important economic and cultural role in Ancient Egypt, being used to wrap bodies in the burial ritual of mummification [63]. Egyptian linen was first brought to Europe by the Phoenician, around 1,200 to 800 B.C. [64].



Figure 1.2: Bandage made of linen (flax textile) from Tutankhamun's Embalming Cache (ca. 1336-1327 B.C.) [2].

Flax can grow in a variety of climates, but it flourishes in cool, damp environments. It cannot withstand extreme heat, and thus its planting schedule varies from country to country depending upon regional climatic conditions [65] (see Fig. 1.3). Additionally, the quality of the linen fabric is strongly dependent on the retting process [1]. The linen retted in Northern France and Belgium is widely known for having the best quality the world [65]. The climate and soil in the region, interlaced with many small rivers, make it favourable for linen production [66]. The tradition of Belgian and French linen finds its roots thousands of years ago. Indeed, the name Belgium stems from Celtic language "Bel'ch", which means linen. This name (or a similar Latin version, "Belgae") was attributed to the region by Julius Caeser after the Gallic wars in 50 B.C., due to the high-quality of its linen textiles [60]. Since then, flax has been used as a textile fibre for multiple purposes, notably fashionable garments or high-quality fabric upholstery [50]. However this is not the end of the story (or we hope so).

1.1.2 Flax Processing

As previously mentioned, flax planting schedule depends on the climate of the region where the crop grows, Fig. 1.3 shows an example of plating schedule for the climate in Belgium and Northern France. The plant takes about four months to grow from April to June/July, according to the climate and soil conditions. After flowering (see Fig. 1.4a), it is pulled out from the ground and placed in the field for about 6 weeks for dew-retting (see Fig. 1.4b). As previously mentioned, retting is a process used to facilitate individualisation of the fibre bundles in the plant stem. Basically, during dew-retting the cellular tissue and pectins that join the fibres are either dissolved or rot away due to environmental

[1] Still the processes developed more than 10,000 years ago!

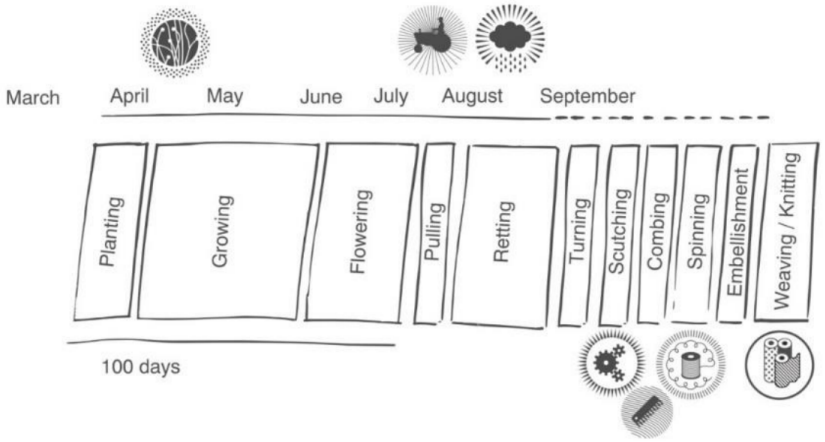


Figure 1.3: The traditional value-added chain from flax plant to textile products [3].



(a) **(b)**

Figure 1.4: (a) A flax field in bloom in Normandy, France [4]; (b) Flax fibres let to dew-ret in the field [4]

moisture, heating from the sun and fungi degradation [67]. Retting is strongly dependent on weather conditions, and thus the timing of the process. The degree of retting, measured by the extent of pectins dissolved, is an important variable, defining the quality of the final fibres [68–70].

Following harvesting and retting, as presented in Fig. 1.5, the stem and woody core, are broken in small parts, so-called shives, and the loosen fibres are extraction from the reaming plant cortical tissue by a process called scutching, this allows to separate the fibres (long and short fibres) and shives. Fibres from scutching are still rough and thick, requiring purification and refining, which is done by a process called hackling, resulting in a fine pure technical fibre (a bundle of elementary fibres that has been extracted, partially individualised and purified [2]. Shives and tows are produced as byproducts of hackling, these are composed of short fibres that can be converted into silvers by carding or used to produce flax mats or low-cost compounds for injection moulding [11]. Fibres from hackling are then spun into yarns or used as roving to produce unidirectional structures (see Fig. 1.5).

[2]More about nomenclature of the different type of fibres is provided in section 2.1.1

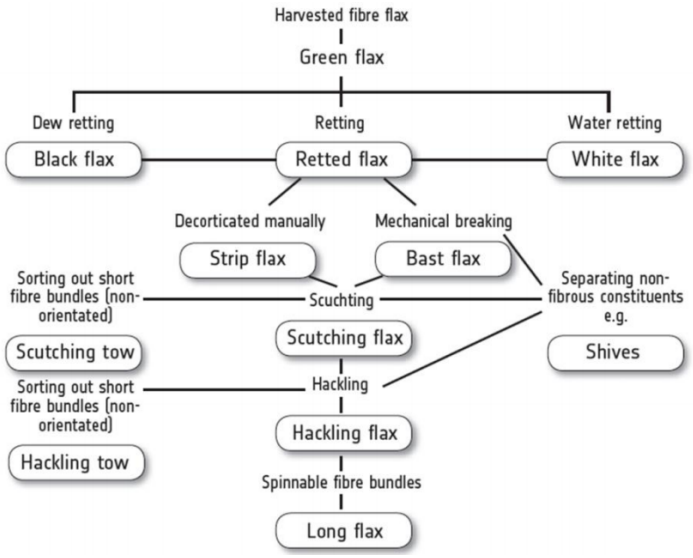


Figure 1.5: Overview of flax processing [5]

1.1.3 World Production

Fig. 1.6 shows the distribution of flax producers in the North Hemisphere except for Canada. In Europe, French production accounts for about 50% (as per values from 2014 [6]). Worldwide European production of flax represents about two thirds of the total, presenting high yields of around 1.5 t/ha. Russia, China and Belarus also produce flax in a smaller scale, as well as other countries from the Balticks and Egypt [6].

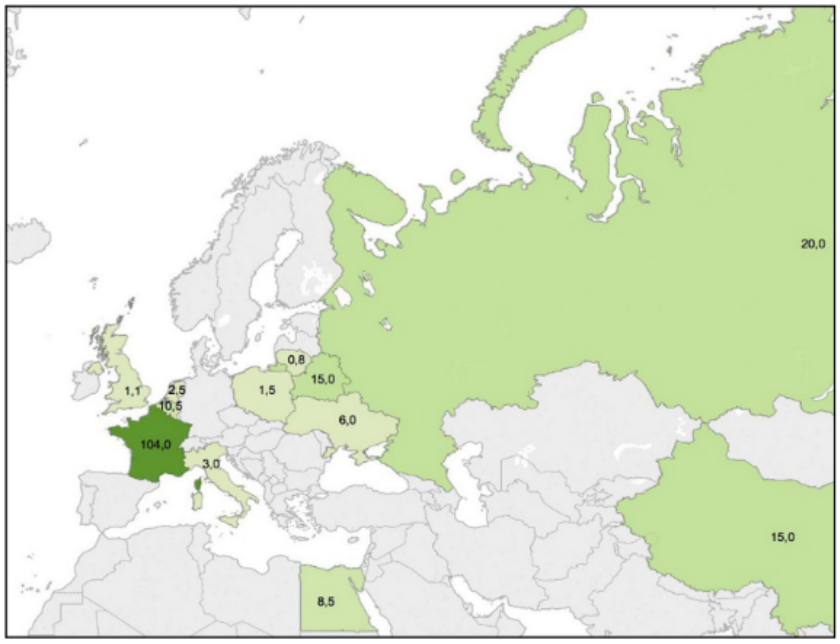


Figure 1.6: Main Flax Producers in the North hemisphere (not accounting for Canada). As per 2014 production [6]

1.2 New Applications: A Demand for Greener Composites

Fibre reinforced composites (FRCs[3]) are lightweight and present mechanical properties that can match or even overcome those of metals. Starting from the late 30's, composites industry gained traction in the second half of the 20th century, with glass fibre reinforced polymer composites, these materials have found increasingly more applications in industries that benefit from their high specific mechanical properties, including the automotive, aerospace, marine and civil construction [71]. Nonetheless, being based on petrochemical polymers, as well as materials that have energy-intensive production processes, such glass-fibres, which have an important contribution to CO_2 emissions [8], FRCs raise important environmental concerns.

Bio-polymers, polymers completely or partially based on bio-sourced carbon (e.g., from biomass) with composition and properties similar to those based on petrochemicals [72], are a suitable environmentally friendly option for FRCs matrices. It has been proved that, in terms of interfacial adhesion, the properties of some bio-polymers, such as bio-epoxy resins, can actually surpass that of their petrochemical counterparts [53]. In the present work, a DGEBA bio-epoxy resin with 38% of carbon from plant origin was used.

Table 1.1: Compilation Properties and Composition of Natural Fibres from various sources [7]

Fiber type	Density (g/cm3)	Length (mm)	Diameter (μm)	Tensile strength (MPa)	Tensile modulus (GPa)	Specific modulus (approx)	Elongation (%)	Cellulose (wt.%)	Hemi-cellulose (wt.%)	Lignin (wt.%)	Pectin (wt.%)	Waxes (wt.%)	Micro-fibrillar angle (deg)	Moisture content (wt.%)
E-glass	2.5–2.59	–	<17	2000–3500	70–76	29	1.8–4.8	–	–	–	–	–	–	–
Abaca	1.5	–	–	400–980	6.2–20	9	1.0–10	56–63	20–25	7–13	1	3	–	5–10
Alfa	9	–	–	35	22	25	5.8	45.4	38.5	14.9	–	2	–	–
Bagasse	1.25	10–300	10–34	222–290	17–27.1	18	1.1	32–55.2	16.8	19–25.3	–	–	–	–
Bamboo	–1.1	1.5–4	25–40	140–800	11–32	25	2.5–3.7	26–65	30	5–31	–	–	–	–
Banana	1.35	300–900	12–30	500	12	9	1.5–9	63–67.6	10–19	5	–	–	–	8.7–12
Coir	1.15–1.46	20–150	10–460	95–230	2.8–6	4	15–51.4	32–43.8	0.15–20	40–45	3–4	–	30–49	8.0
Cotton	1.5–1.6	10–60	10–45	287–800	5.5–12.6	6	3–10	82.7–90	5.7	<2	0–1		–	7.85–8.5
Curaua	1.4	35	7–10	87–1150	11.8–96	39	1.3–4.9	70.7–73.6	9.9	7.5–11.1	–	–	–	–
Flax	1.4–1.5	5–900	12–600	343–2000	27.6–103	45	1.2–3.3	62–72	18.6–2	2–5	2.3	1.5–1.7	5–10	8–12
Hemp	1.4–1.5	5–55	25–500	270–900	23.5–90	40	1–3.5	68–74.4	15–22.4	3.7–10	0.9		2–6.2	6.2–12
Henequen	1.2	–	–	430–570	10.1–16.3	11	3.7–5.9	60–77.6	4–28	8–13.1	–	0.5	–	–
Isora	1.2–1.3	–	–	500–600	–	–	5–6	74	–	23	–	1.09	–	–
Jute	1.3–1.49	1.5–120	20–200	320–800	8–78	30	1–1.8	59–71.5	13.6–20.4	11.8–13	0.2–0.4	0.5	8.0	12.5–13.7
Kenaf	1.4	–	–	223–930	14.5–53	24	1.5–2.7	31–72	20.3–21.5	8–19	3–5	–	–	–
Nettle	–	–	–	650	38	–	1.7	86	10	–	–	4	–	11–17
Oil palm	0.7–1.55	–	150–500	80–248	0.5–3.2	2	17–25	60–65	–	11–29	–	–	42–46	–
Piassava	1.4	–	–	134–143	1.07–4.59	2	7.8–21.9	28.6	25.8	45	–	–	–	–
PALF	–1.6	900–1500	20–80	180–1627	1.44–82.5	35	1.6–14.5	70–83	–	5–12.7	–	–	14.0	11.8
Ramie	1.0–1.55	900–1200	20–80	400–1000	24.5–128	60	1.2–4.0	68.6–85	13–16.7	0.5–0.7	1.9	0.3	7.5	7.5–17
Sisal	1.33–1.5	900	8–200	363–700	9.0–38	17	2.0–7.0	60–78	10.0–14.2	8.0–14	10.0	2.0	10–22	10–22

When it comes to the fibres, even though no natural or bio-sourced material has been found to compete with the impressive properties of carbon fibres, the mechanical properties of glass fibres can be matched or overcome. Flax fibres also standout for their mechanical properties. When compared to other natural fibres, see table 1.1 and Fig. 1.7, flax presents the best combination of tensile strength, which can reach 2000 MPa, tensile modulus, up to 103 GPa, and low density, 1.4 - 1.5 g/cm^3 [7]. Its mean specific tensile modulus is approximately 45 GPa.cm^3/g, which is 84% higher than that of E-glass fibres [7] (see Fig. 1.7a). Furthermore, flax fibres present a remarkable aspect ratio ($\sim$ 1250 [73][4]), which

[3]Here used as synonym for fibre reinforced polymer composites.

[4]Considering elementary fibres

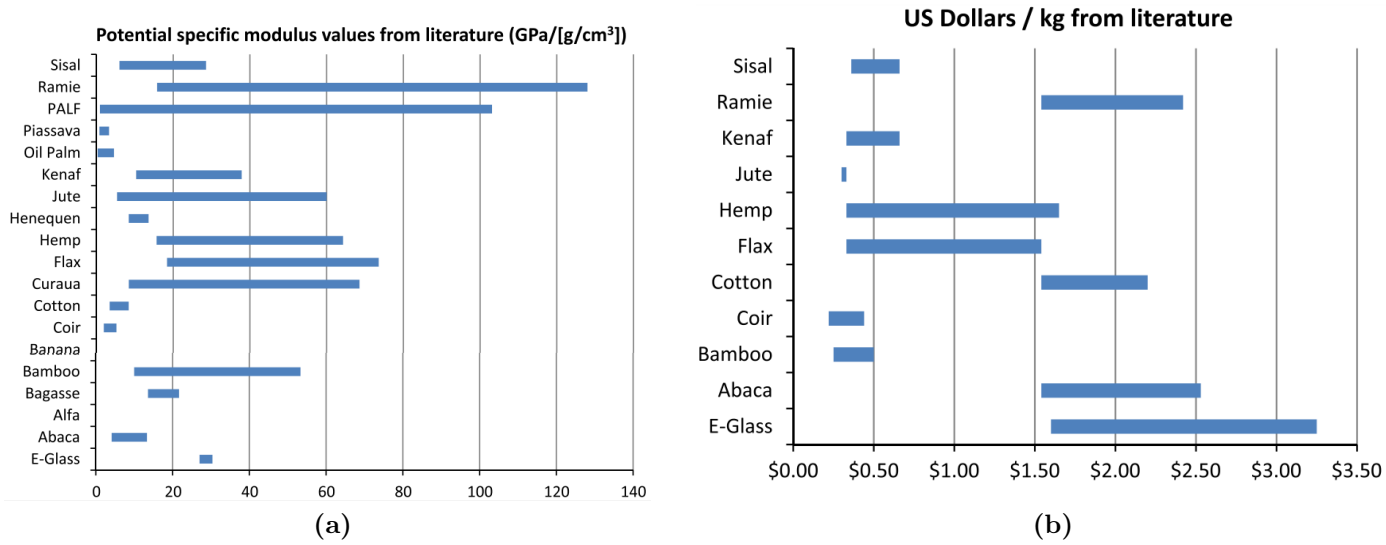


Figure 1.7: (a) Comparison of potential specific modulus, natural fibres and glass fibres; (b) Cost per weight comparison between glass and natural fibres [7]

contributes to a high surface area, and thus improved load transfer in composites. In addition to that, the cost of flax can be significantly lower than that of glass fibres, further increasing its attractiveness for cost-driven applications, such as the automotive industry [35]. Indeed, the mean cost per weight of flax fibres is less than half of glass fibres (see Fig.1.7b). Flax also benefits from good thermal and acoustic insulating properties[5], low risk on health or irritation and low abrasive impact on processing machinery. For these and other reasons discussed over the next sections, the interest on flax fibres as reinforcement for polymer composites has grown over the last two decades [35].

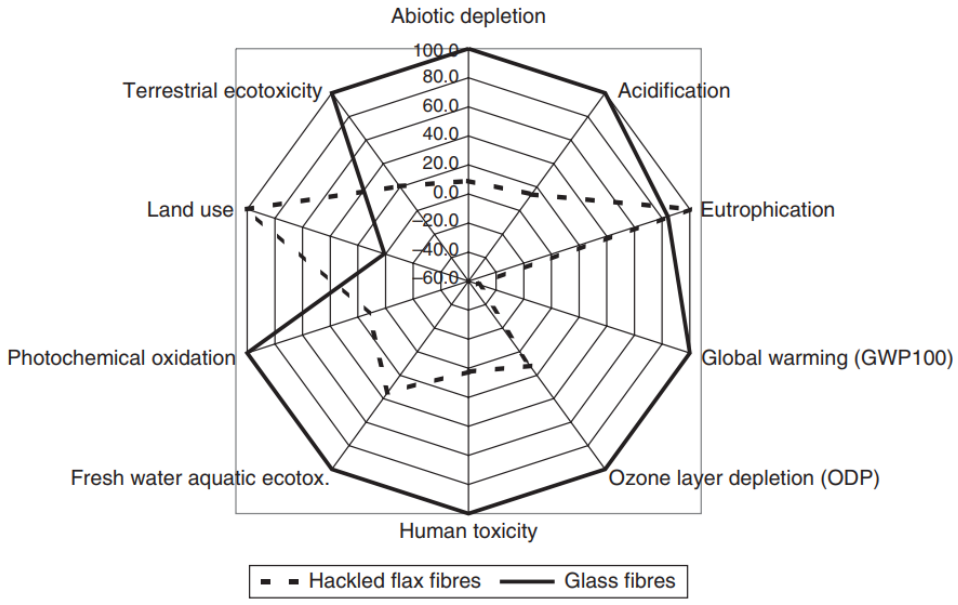


Figure 1.8: Environmental impacts during the production of hackled flax fibres compared to those for glass fibres [8]

[5]From which several of its current commercial applications stem.

1.2.0.1 *Environmental Aspect: Flax v Glass*

Fig. 1.8 is part of a Life Cycle Assessment of hackled flax flax fibres, which were compared to glass fibres using 1 kg of each material as a basis of calculation. Although flax presents negative aspects inherent to its agricultural production, such as land use and eutrophisation due to the use of fertilisers, compared to glass fibres, the production of hackled flax contributes 90% less for depletion of abiotic resources, 88% less for photochemical oxidation and 98% less for human toxicity. Besides that, a major positive factor of flax fibres is its negative contribution for global warming due to CO_2 sequestration (i.e., negative carbon footprint). While the processing of flax is calculated to result in 0.79 $kgCO_2$ per kilogram of fibres produced, the same mass of fibres captures the equivalent of around 1.4 $kgCO_2$ [74] due to photosynthesis during growth. In combination to its low toxicity, this last fact results in a smaller impact on overall CO_2 emissions if thermorecycling of a thermoset matrix is performed [8], which is not the case for glass fibres, whose most adequate end-of-life remains an opened question.

Furthermore, flax production is considerably less energy-demanding than the production of synthetic fibres used for composites reinforcement. While flax requires about 6.5 MJ/kg of energy from extraction to transformation into continuous structural fibres, glass fibres and carbon fibres use up 3.5- and 30-fold more energy, respectively [74, 75].

Altogether, this data clearly shows that, if carbon and, in particular, glass fibres raise environmental concerns, provided it matches or surpassess the properties of the latter, flax fibres can be "strong" solution.

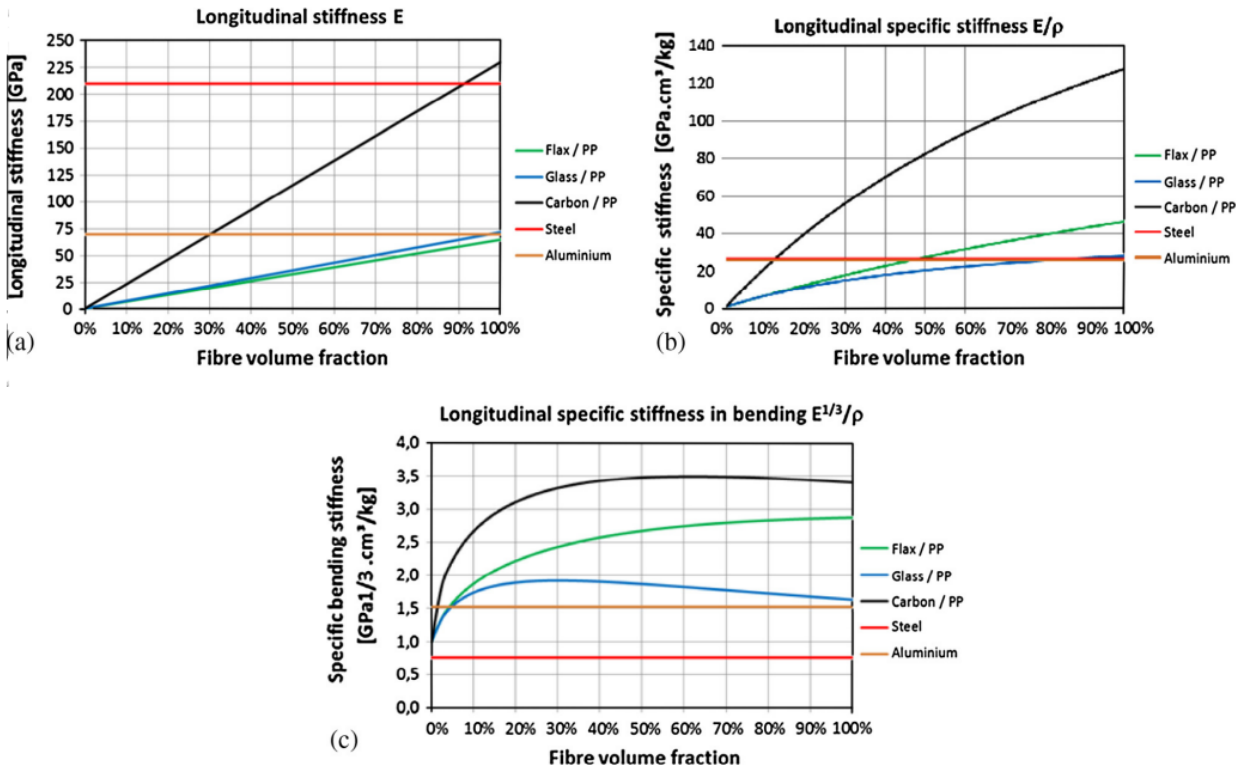


Figure 1.9: The absolute (a) and specific (b in tension, c in plate bending) longitudinal stiffness of flax, glass, carbon fibre UD composites, steel and aluminium as a function of the fibre volume fraction (calculated properties, based on average data) [3].

1.3 Towards High-Performance Environmentally Friendly Composites

Besides the good mechanical properties and its much lower environmental impact, the case for flax fibre composites also benefits from their superior stiffness as compared to glass fibre composites and other structural materials, this; on the other hand, is not seen in the case of specific strength. Using a unidirectional (UD) composite in a polypropylene matrix as a model, whereas the absolute longitudinal stiffness of flax fibres is similar to that of glass for all volume fractions (see Fig. 1.9a), when the lower density of flax is taken into account, its composite properties are shown to be better than glass fibre composites (see Fig. 1.9b). Furthermore, when the bending properties are compared, flax composites specific stiffnesses are shown to be even better, outperforming the average properties of steel, aluminium, glass fibre composites and even approaching that of carbon fibre composites, being only 15-25% lower for volume fractions between 30% and 60% (see FIg. 1.9c).

On the other hand, flax fibre composites strength still requires improved. Differently from stiffness, strength properties behaviour tend to be more complex in composites. First, it is strongly influenced by the reinforcement architecture, which can vary widely (e.g., non-crimp fabric, weave, braid, mat, among others), and thus making general statements so as to compare flax and glass composites may be misleading [76]. Moreover, processing considerably degrades the strength of glass fibres, with a reduction from 3500 MPa to values around 1500 MPa being commonly accepted [77]. Assuming a reduced strength of 1500 MPa for glass fibres after processing, in a cross-ply (0/90), flax composites would present about half of the specific strength expected from glass fibre composites at a volume fraction of 40%, assuming an approximate rule of mixtures [76]. Those value were confirmed experimentally [11]. Contributing to the discrepancy between the flax fibres and composites specific strength, there are the fibre natural character causing mechanical properties and morphology variation, damaging during processing and interface quality (essential for good load transfer) [35]. The last one being the main focus of the present work.



Figure 1.10: Tesla-based EPCS Series. Body works in high-performance, lightweight natural flax fibre composite (powerRibs^{TM} and ampliTex^{TM}). Thanks to the fibre translucency, the roof can have an internal, fully integrated LED screen that shows live-information during races. [9]

1.4 Recent Applications

Natural fibre reinforced composites are finding increasingly more applications. While research is contributing to better understand of their properties, which allows for use in increasingly more technically and mechanically demanding applications, non-technical variables, such as shape and colour, seem to make these materials appealing for design conception [76].

1.4.0.1 Automobile

The performance of automobiles can be improved using composites to reduce their weight while maintaining their mechanical properties. Besides the obvious applications in race cars (see Fig. 1.10), it also reduces fuel consumption, reducing the vehicle emissions and cost of transportation. In this case, flax fibre composites can be used to replace parts made of glass fibres, as well as reinforce polymer parts, such as Bumpers, door trim panels, C-pillar trims, among others [78]. Nonetheless, their main applications as of today are for interior components in cars in less mechanically demanding applications (see Fig. 1.11), with the high variability of flax properties being the main bottle neck limiting use in structural parts [78]. From 1996 to 2010 the German automotive industry increase natural fibre composites use, predominantly flax, from 4000 tonnes to more than 100000 tones [79]. The main reasons for their use in automobiles is the favourable combination of pricing and good mechanical properties [80]. Flax fibres are significantly longer as compared to most natural fibres, which are particularly suitable for complex-shape composite parts [80].

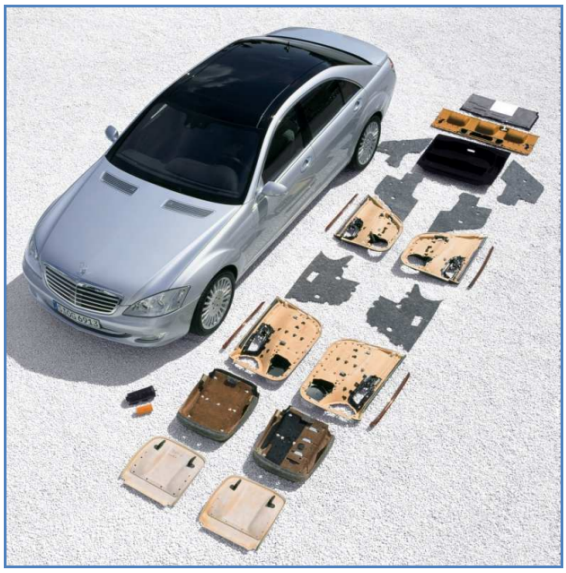


Figure 1.11: Mercedes S class natural fibre reinforced composite parts [10]

1.4.0.2 Sporting Goods

The combination of flax fibres high damping factor and carbon fibres mechanical properties can allow for strong and stiff materials with considerably reduced vibration as compared to composites made only with carbon fibres. This kind of hybrid composite has been used to produce high-performance tennis rackets that reduce the risk of muscular injuries such as tennis elbow. In skis, this improvement in damping capacity provided by flax also allows to enhance precision in manoeuvring. These and other applications are presented in Fig. 1.12.



Figure 1.12: Various applications of flax composites in sporting goods: a) Artengo tennis racket, b) Notox surfboard, c) Caperlan fishing rod, d) ArcWin Archery bow, e) Kang flax ski poles and f) Le Ventoux bamboo-flax bike. [11]

1.4.0.3 Music and Sound

The damping properties, allowing for excellent and controllable acoustics, dimensional stability, ease of processing, strength and tolerance to variations in humidity and temperature; in combination with lightweight, make flax composites interesting for the manufacturing of music instruments that have comparable acoustics, are lighter, maintain tuning for longer, and a more resistant to damages related to daily use when compared to their wood counterparts. Flax composites are also used to produce speakers with better dynamics and homogeneous richer sounds, in this case it is used to absorb vibration providing sound neutrality to the cone. Some examples of applications in music and sound are shown in Fig. 1.13.

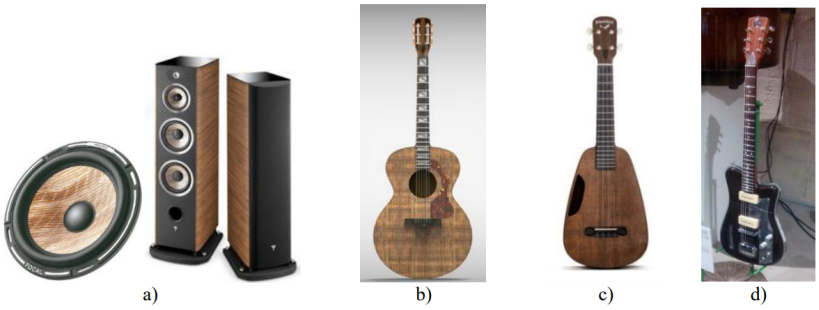


Figure 1.13: a) Aria column speaker 900 and flax cone from FOCAL, b) El Capitan Blackbird Guitar, c) Blackbird flax Ukulele and d) Flax electric Guitar from Depestele. From [11]

1.5 The Present Work

Over the last two decades, advances in the field of natural fibre composites, allowing to better understand and control their properties, the raise of environmental awareness amongst costumers and the need for low-weight, cost-effective materials in industries such as the automobile has contributed to promising projections for the increase in demand of natural fibre composites. Flax fibres present the

best combination of mechanical proprieties, whose specific values are comparable to those of glass fibres. However, the specific strength of composites made with untreated flax is still much lower than that of glass fibre composites, most probably due to poor load transfer. This indicates the need for interface improvement. In the present study, different washing methods and a sizing with an aminosilane compound were investigated as means to improving interfacial compatibility and adhesion. These two factors are essentially controlled by the chemistry and morphology of the interface, which can be described in terms of physicochemical interactions, chemical bonding and mechanical interlocking.

While physicochemical interactions and chemical bonding can be enhanced by surface physical and chemical treatments, trying to improve mechanical interlocking of flax fibres (e.g., by improving surface roughness) is likely to damage the complex and delicate fibre hierarchical structure. In practice, changes in mechanical interlocking are usually a byproduct of physical and chemical treatments. Therefore, the present work focus on the characterisation of physically and chemically treated flax fibres by studying their physicochemical interactions and surface chemical composition, while their effect on the interfacial strength in combination with mechanical interlocking were assessed by interface micromechanical characterisation.

Changes in flax-epoxy physicochemical interactions were investigated using their surface free energies according to the van Oss-Chaudhury-Good acid-base theory. The latter were obtained from Wilhelmy Technique experiments, employed to assess contact angles, which allow for a quantitative measure of solid-liquid molecular interactions, and thus their surface energies.

With the objective of determining the nature and quantity of chemical functionalities contributing to interfacial strength and compatibility, X-ray photoelectric spectroscopy (XPS) analysis was performed on untreated and aminosilane-treated fibres.

Although characterising each of these phenomena is crucial to obtain a correct understanding of the mechanisms contributing to interface quality, isolated, these results may be misleading. Their combined effect can be assessed by studying interface mechanical properties, the ultimate measure of interfacial strength. Microbond tests were conducted to study the impacts of each fibre modification on the interface mechanical properties of flax-epoxy composites at the microscopic level.

Fibre mechanical properties, in combination with those of fibre-matrix interface, determine the reinforcement quality. To complement the characterisation of the studied flax fibres as composite reinforcements, single-fibre tensile tests were performed on untreated elementary fibres, which presented no significant degree of degradation due to storage conditions or handling.

All the results were in good agreement with most of the literature, indicating the success of each experiment. When encountered, divergences with previous works were discussed and possible explanations offered.

According to the approach employed, flax sizing with Bis(trimethoxysilylpropyl)amine was proved to be the only modification effective in improving the practical adhesion between epoxy resin and flax fibres. This improvement was demonstrated to be strongly determined by chemical bonding, rather than physicochemical interactions or mechanical interlocking. Although surface energy analysis suggests that removal of compounds weakly attached to the surface (waxes) occurred during cleaning, micromechanical analysis indicates that washing actually worsen interfacial strength. Even though the root causes of this phenomena may lay in frictional stresses, it could not be assessed by the approach used, remaining an opened question.

Over the next sections first, a *Literature Review*, providing the reader with the theoretical background required to understand the models, techniques and concepts employed in the present document and the state of the art in flax fibres composites is offered; second, the *Materials and Methods* used are described; third, the *Results and Discussion* about what can be derived from them are considered, and finally the *Conclusions* from the entire work and the *Perspectives* to the field stemming from them are presented.

2 Literature Review

2.1 Theoretical Background

2.1.1 Flax Fibres Structure

The flax plant is approximately 80-cm long, presenting a fibrous structure all along its stem [34]. Such structure is hierarchically organised in four different levels, namely, the stem itself, fibre bundles, elementary fibres and elementary fibre components (see Fig. 2.1).

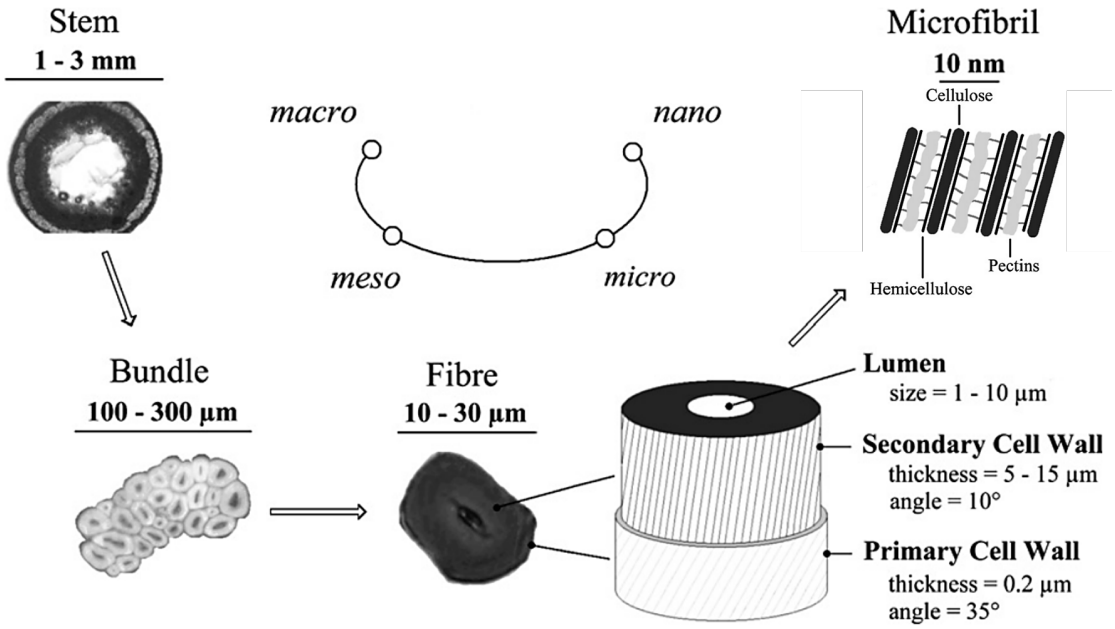


Figure 2.1: Flax structure, from stem to cellulosic fibrils [12]

The stem is made of concentric layers of tissue whose main functions are both to maintain structural and functional integrity, and allow the flux of nutrients and water to the whole plant (see table 2.2 for details). Flax fibres are found in bundles in the plant sclerenchyma, a tissue associated with the phloem, or bast, vessels (in charge of the flux of organic nutrients produced during photosynthesis), reason why they are often called bast fibres (less commonly, phloem fibres). Fibre bundles are located in an intermediate region of the stem cross-section between the bark, composed of cortical tissue and epidermis, and the xylem, or woody tissue, both eliminated during processing [34] (see Fig. 2.1)[50]. The main function of bast fibres is to support bast vessels while strengthening the stem as a whole, they are joined primarily by ionic cross-links formed between galacturonate moieties of pectin molecules in the presence of calcium cations.

Fibre bundles can have from 10 to 40 elementary fibres. The partial separation of such bundles after processing completion results in the so-called technical fibres. This structure can have lengths up to the entire flax stem [81].

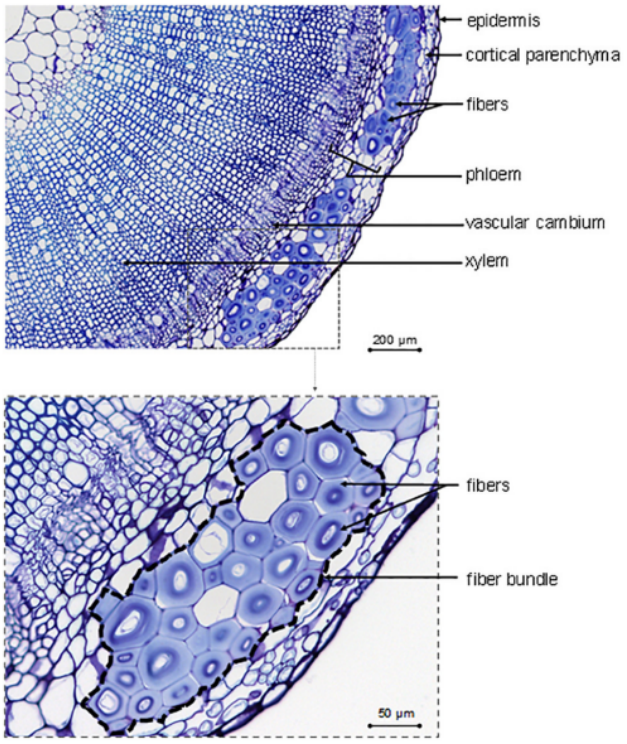


Table 2.1: Description of identifiable tissues and cells on the transverse cross-section in the bottom part of a growing flax stained with toluidine blue [50]

Table 2.2: Main tissues and cell types composing flax stems [50]

Basic tissue system	Tissue	Cell type	Location	Main functions
Dermal	Epidermis		Outermost layer	Protection
Ground	Parenchyma	Parenchyma	Through the stem body	Metabolism
	Sclerenchyma	Fiber	Bundles in phloem	Mechanical support
Vascular	Phloem	Sieve-tube element	Phloem	Food/elaborated sap conduction
		Companion cell	Phloem	Delivery of substances to the sieve-tube element
	Xylem	Vessel element	Xylem	Water and raw sap conduction Mechanical support
		Tracheid	Xylem	Water and raw sap conduction Mechanical support

The elementary fibres themselves are elongated plant cells presenting two concentric cell walls [33] from which the cytoplasm was removed during processing, leaving a central hole called lumen [81]. Although their precise dimensions can vary significantly according to several factors, such as the flax variety and location in the stem, elementary flax fibres usually have diameters from 10 to 30 μm and are 10 to 80 mm-long [12, 81–84]. The outmost cell wall (primary wall) is usually 0.2 μm-thick [85], being mostly composed of pectins and randomly oriented cellulose microfibrils [86, 87]. The primary wall surrounds a secondary wall, the thickest (approximately 10μm-thick), and structurally most important cell wall, which accounts for approximately 80% of the fibre cross-section. It possesses numerous cellulosic microfibrils oriented with a 10° offset with respect to the elementary fibre axis (microfibrillar angle - MFA) [88] embedded in a matrix composed of pectic and hemicellulosic material [33] (see Fig. 2.1). These microfibrils compose 70% of the fibre weight[89], measure a few nanometers wide [34, 81, 90–94] and are the stiffest constituents of the fibre (theoretical tensile modulus of 137 GPa [95]). Their high quantity and arrangement with low MFA when compared to other plant fibres are the main contributors to the outstanding mechanical properties of flax [34].

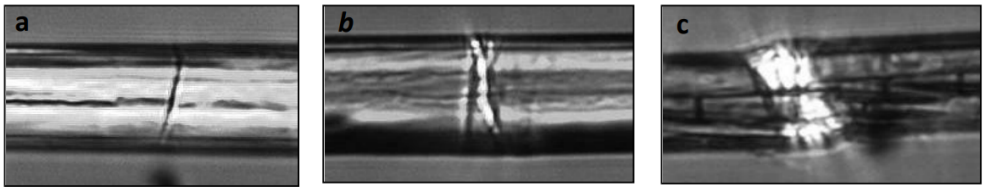


Figure 2.2: Defects on fibres observed by polarised optical microscope. Fibre diameters in all images are ca. 20µm [13]

2.1.1.1 Structure Defects

Defects are mostly introduced during plant growth and mechanical extraction (i.e., during scutching and hackling). These defects can be located either on the surface or the internal structure of the plant cells [14]. Surface defects can be either transverse (so-called kink bands, nodes or dislocations [14]) or longitudinal (microcraks) and are usually observed using optical or scanning electron microscope (SEM) (see Fig. 2.2c and Fig. 2.3). Internal defects occur transversely and are mostly due to a misalignment of the cellulose microfibrils in the amorphous matrix and/or concentration of pectins and hemicelluloses [34]. Being highly crystalline, cellulose microfibrils deviate light, allowing the observation of the internal defects using polarised light optical microscopy (see Figs. 2.2a and 2.2b).

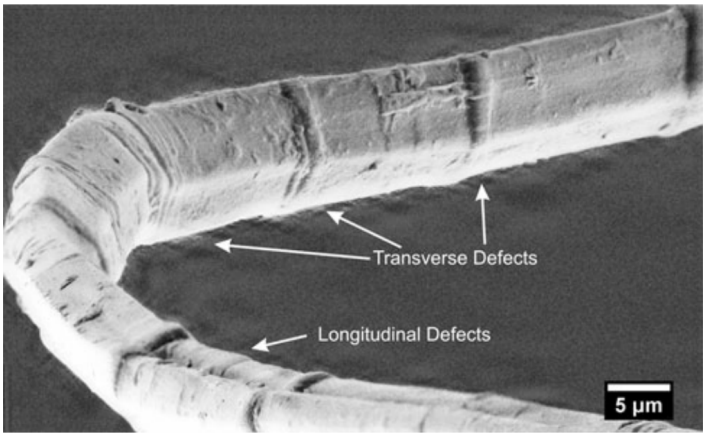


Figure 2.3: Field-emission SEM image of an elementary flax fibre showing transverse defects and longitudinal defects [14]

2.1.2 Flax Fibres Composition

Flax composition can vary considerably according to the source. This variation can be attributed to several factors such as fibre variety, crop year, soil quality, different processing methods, different degrees of maturity and measurement conditions [96]. Table 1.1 summarises some of the results found in the literature for flax fibres composition, whose main constituents, Cellulose, Pectins, Hemicelluloses, Lingn, Waxes and Water, are briefly discussed below.

2.1.2.1 Cellulose

Main constituent of natural fibres, cellulose is a linear polysaccharide composed of D-glucose units linked by β-1,4 glucosidic bonds whose degree of polymerisation is around 8000 [97, 98]. Its linear chain with multiple hydroxyl groups favourably distributed in the space promotes strong and abundant intermolecular hydrogen bonds (see Fig. 2.4), resulting in a highly crystalline structure (60 - 65% crystallinity [99, 100]), which composes the microfibrils, the main structural component of the fibre (theoretical Young's Modulus of 137 GPa [95]). In FRC, hydrogen bonding and polar interactions between cellulose hydroxyl groups and polar resins groups (e.g., epoxide and amino in epoxy resins) are expected to significantly contribute to fibre-resin compatibility and interfacial adhesion.

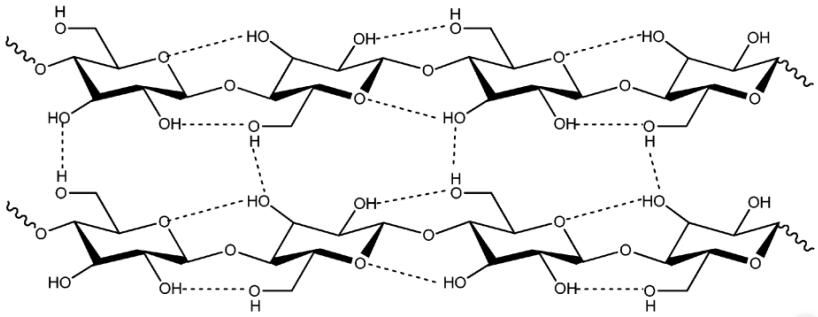


Figure 2.4: Cellulose structure. Inter and Intramolecular hydrogen bonds are presented as dashed lines [15]

2.1.2.2 Pectins

Pectins are the main contributors to cohesion between microfibrils in the secondary wall and especially elementary fibres in the primary wall [101–104]. In terms of chemical structure, pectins are galacturonate-rich complex heteropolysaccharides [105], which form intermolecular ionic cross-links in the presence of divalent cations, notably Ca^{2+} (see Fig. 2.5). Due to its higher concentration in the region between elementary fibres (so-called middle lamella), pectins present a particularly high influence in the interfacial adhesion between natural fibres and the matrix in FRCs.

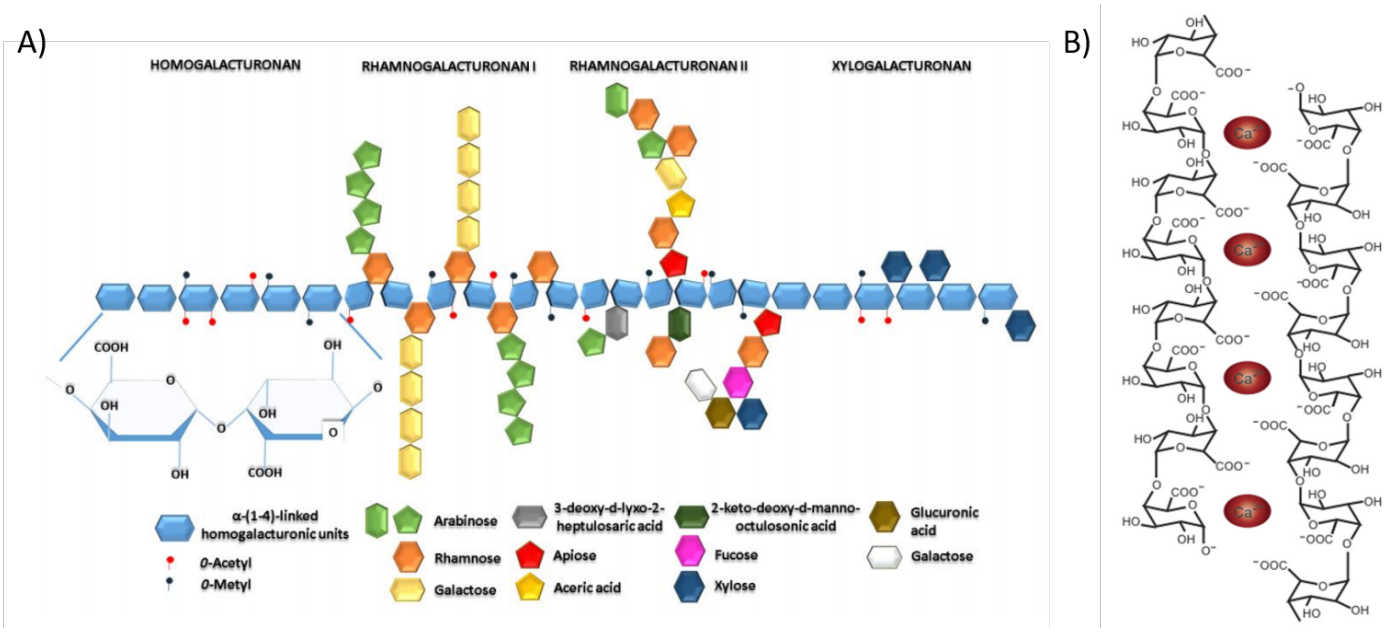


Figure 2.5: A) Schematic structure of pectin, with approximate relative abundance between groups [16]; B) Schematics of an "eggbox" structure consisting of two antiparallel poly-galacturonic acid chains complexed by Ca^{2+} [17]

2.1.2.3 Hemicelluloses

Hemicellulose molecules are strongly bonded to cellulose microfibrils, constituting an interface between the latter and the pectic cement [106]. Due to its high hydrophylicity, hemicellulosic mechanical properties are considerably dependent on the environment relative humidity (RH). As an example, its Young's modulus may vary from 8 GPa to 0.01 GPa as RH is varied from 0 to 1 [107]. As pectin, hemicellulose is a complex heteropolysaccharide that presents a considerable degree of branching (see Fig. 2.6), differently from cellulose molecules. Compared to cellulose, it is a significantly smaller polysaccharide,

containing from 500 to 3000 monosacharide units [108]. Consequently, the presence of hemicelluloses at the interface fibre-resin is mostly detrimental as compared to the presence of cellulose.

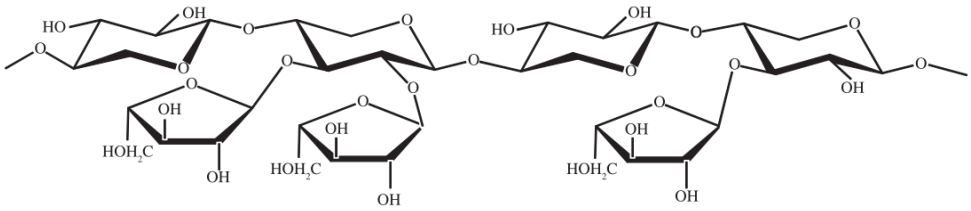


Figure 2.6: Example of a common hemicellulose repeating motif: L-arabino-D-xylane [18]

2.1.2.4 Lignin

Since flax fibres are originary from the phloem, their secondary wall is primarily cellulosic, that is why, differently from other types of natural fibres such as coir and hemp fibres [109], it presents considerably lower lignin content. This biomolecule is mainly found in the middle lamella, surrounding elementary fibres, where, due to its hydrophobicity, it plays a role in preventing water loss [110]. Although its amount is usually not sufficient to significantly influence the interfacial properties as compared other fibre components, the hydrophobic character of lignin is detrimental to the compatibility between natural fibres and polar matrices (such as epoxy resins). In terms of chemical structure, lignin resembles highly cross-linked phenolic resins and is mainly composed of guaiacyl [111].

2.1.2.5 Waxes

Waxes present a significant impact on the interfacial adhesion between fibre and resin. Due to their highly apolar character, resulting in poor interactions with polar cellulose molecules and short chain, they are weakly attached to the elementary fibres surface, constituting a weak link (or weak layer) at FRCs interface. With regards to chemical composition, waxes are a complex mixtures of nonpolar hydrocarbons, alcohols, aldehydes, ketones, esters and carboxylic acids (i.e., lipids). Due to relatively small-chain structures, usually between 29 and 33 carbon atoms [112], these waxes present low boiling point, reason why washing treatments with hot liquids (even in the case of polar liquids) are an effective manner of removing such compounds from the fibre surface. Their function, when on the fibres surface, is primarily plant protection against foreign bodies and water loss [112].

2.1.2.6 Water

The content of water in flax fibres usually varies from 8 to 10 wt.%, it is usually strongly bonded to the pectins hydroxylated groups [106]. Therefore, pectin-rich regions of the fibres (middle lamella and secondary wall) tend to have high water content, which is expected to decrease with the increase in the efficiency of the fibre processing methods in removing the primary wall (separate the bundles of elementary fibres).

2.1.3 Interfacial Compatibility and Adhesion in Natural Fibre Composites

The interfacial compatibility and adhesion in fibre reinforced composites is essentially controlled by the chemistry and morphology of the interface, whose contributions can be described in terms of three main interactions, namely Physicochemical Interactions, which determine fibre-matrix wettability and

compatibility behaviour, and thus their physical adhesion (e.g., van der Waals forces); Chemical Bonding (such as covalent bonds); and Mechanical Interlocking due to surface roughness and interpenetration. In particular cases, other factors such as macromolecular entanglements and interdiffusion can also play role [113]. To achieve an extensive and proper interfacial contact, resulting in a strong interfacial adhesion, a good wettability between fibre and matrix is need, which mainly depends on their surface energy [114]. In addition to that, the physical adhesion mechanisms, determined by the surface energies, will also play an important role in maintaining a stable contact after composite consolidation [115].

The three main contributors to interface adhesion and compatibility are briefly discussed over the next sections.

2.1.3.1 Physicochemical Interactions

At the molecular level, fibre-matrix interactions are determined by the intermolecular interactions between their surface chemical groups, whose overall strength can be characterised by the the work of adhesion, the work required to disjoint a unit area of the fibre matrix interface, thereby creating a unit area of matrix-vacuum and fibre-vacuum interfaces [116]. In its turn, the work of adhesion can be obtained in terms of fibre and matrix surface energies, defined as the sum of different contributions of specific and non-specific intermolecular interactions (e.g., Lifshitz/van der Waals type and Lewis acid-base). A high surface energy of the composite phases contributes to a high work of adhesion, while the matching of its components results in a good interfacial compatibility.

2.1.3.2 Chemical Bonding

While physical interactions at the molecular level mainly depend on the specific and non-specific interactions, chemical bonding is based on primary covalent bonds at the interface [1]. Provided the chemical composition of the fibre and surface are known, it is possible to promote chemical bonding by functionalising the fibre surface with molecules presenting suitable moieties that will chemically bind to the matrix, and vice-versa. Typical chemical bonding at the interface of natural fibres reinforced composites involves hydroxyl groups of cellulose and lignin and functional groups in the matrix [114] (e.g., epoxide and amino in epoxy resin).

2.1.3.3 Mechanical Interlocking

Mechanical interlocking is promoted by roughness and matrix spreading on a fibre surface, resulting in interpenetration of the phases. A highly interpenetration will not only mechanically lock the surfaces, but also increase their total contact area, thereby increasing fibre-matrix adhesion.

2.1.3.4 Assessing Interfacial Compatibility and Adhesion

Physicochemical Interactions and Chemical Bonding can be enhanced by surface physical and chemical treatments. On the other hand, trying to improve mechanical interlocking of flax fibres by improving surface roughness is likely to damage the complex and delicate fibre hierarchical structure. In practice, surface roughness modifications usually take place as a byproduct of physical and chemical treatments [35]. Therefore, the present work focused on the characterisation of physically or chemically treated flax by studying their wettability and surface chemical composition, while the combined effect of the

[1] Further discussion on the components assumed as contributing to physicochemical interactions as opposed to purely chemical is provided in section 2.1.4. This subject has caused great confusion in the literature, with several mistakes being repeatedly published [117], as discussed by C. Rulison [118].

latter and mechanical interlocking on the interface strength were assessed by interface micromechanical characterisation.

2.1.4 Wettability Models and Assessment

As previously discussed, good interfacial adhesion initially requires a good wetting between fibre and matrix, to achieve an extensive and proper interfacial contact. In its turn, the wettability mainly depends on the surface energy of the materials composing the interface [119]. A high surface energy of the composite phases contributes to a strong interface (i.e., high work of adhesion), while the matching of its different components (i.e., matching of intermolecular interactions nature) results in a good interfacial compatibility. These interactions are mainly controlled by the functional groups on the surface both fibre and matrix at the interfacial contact area [119].

Surface energies can be derived from equilibrium contact angles[2], using models such as Owens-Wendt model [121], Zisman plot [122], Fowkes method [123], Schultz model [124] and van Oss model[3] [125]. The first accurate model relating the characteristic ideal contact angle of a liquid droplet (θ) on a solid surface and the surface free energy (γ) of the different phases in equilibrium at the triple line where solid (s), liquid (l), and gaseous (g) phases meet (see Fig. 2.7) was introduced more than two centuries ago by Sir T. Young [126] (Eq. 2.1).

$$\gamma_{sv} = \gamma_{sl} + \gamma_{lv}\cos\theta \tag{2.1}$$

An issue arising from this relationship comes from the fact that only the contact angle (θ) and the liquid-vapour surface energy (γ_{lv}) can be directly assessed. By Introducing the notion of Work of Adhesion (Eq. 2.2), W_A, the balance between the energy consumed to eliminate individual solid-vacuum (s°) and liquid-vapour (sv) surfaces and form a solid-liquid surface (sl) upon droplet deposition [116] (i.e., the work required to separate a solid-liquid surface into individual solid-vacuum and liquid-vapour surfaces) and assuming that the solid-vacuum and solid-vapour surface free energies are approximately equal ($\gamma_{s^\circ} \approx \gamma_{sv}$, i.e., neglecting spreading pressure [127]), the Young-Dupré equation (Eq.2.3) discards both unknowns of Eq.2.1.

$$W_A = \gamma_{s^\circ} + \gamma_{lv} - \gamma_{sl} \tag{2.2}$$

$$W_A = \gamma_{lv}(\cos\theta + 1) \tag{2.3}$$

Similarly, the work of cohesion W_C may be defined as the work required to separate a fictitious surface in the bulk of a single phase (i.e., the work to create a new surface in a single phase) per unit area.

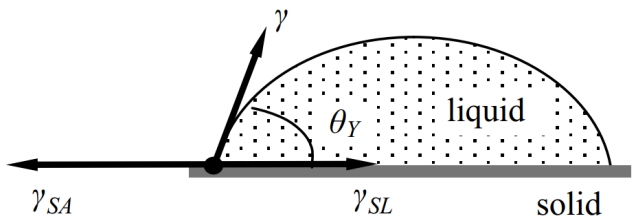


Figure 2.7: Scheme illustrating the Young equation, which relates the characteristic ideal contact angle of a liquid droplet (θ) on a solid surface and the surface free energy (γ) of the different phases in equilibrium at the triple line where solid (s), liquid (l), and gaseous (g) phases meet [19].

[2]In this work, used as a synonym of most stable contact angle [120].

[3]Here used as a synonym of van Oss-Chaudhury-Good acid-base theory

$$W_C = 2\gamma, \quad W_{ll} = 2\gamma_l, \quad W_{ss} = 2\gamma_s \tag{2.4}$$

Berthelot developed further the previous models by assuming that the work of adhesion between solid and liquid (W_{sl})[4], can be obtained as the geometric mean of the work of cohesion of a solid (W_{ss}) and the work of cohesion of a liquid (W_{ll}), Berthelot's hytothesis (Eq. 2.5).

$$W_{sl} = \sqrt{W_{ll}W_{ss}} = 2\sqrt{\gamma_l\gamma_s} \tag{2.5}$$

On the basis of Berthelot's hypothesis, Eq. 2.3 can be modified so as to obtain a relationship between the measurable contact angle and liquid-vapour surface free energy, and the solid vapour free energy.

$$W_{sl} = 2\sqrt{\gamma_{sv}\gamma_{lv}} = \gamma_{lv}(\cos\theta + 1) \tag{2.6}$$

Fowkes then assumed that the surface free energy of a solid or surface tension of a liquid are the sum of independent contributions associated with each possible intermolecular interaction [123].

$$\gamma_{sv} = \gamma_{sv}^{d} + \gamma_{sv}^{p} + \gamma_{sv}^{h} + \gamma_{sv}^{ab} + \gamma_{sv}^{\circ} \tag{2.7}$$

where d, p, h and ab stand for dispersion, polar, hydrogen, and acid-base, respectively and γ° accounts for all remaining interactions. Fowkes than assumed the dispersion component to be due solely to London interactions (induced dipole - induced dipole). Owens and Wendt followed Fowkes pathway and further stated that all the remaining components of the surface free energy could be grouped into a polar component (γ_{sv}^{p}).

$$\gamma_{sv} = \gamma_{sv}^{d} + \gamma_{sv}^{p} \tag{2.8}$$

Using the notion of W_A assuming Berthelot's hypothesis, Eq. 2.8 can be written as,

$$\gamma_{sl} = \gamma_{sv} + \gamma_{lv} - 2\left(\sqrt{\gamma_{sv}^{d}\gamma_{lv}^{d}} + \sqrt{\gamma_{sv}^{p}\gamma_{lv}^{p}}\right) \tag{2.9}$$

Plugging Young's Eq. 2.1 into the previous one and reordering it as a function of the type y = ax + b, Eq. 2.10 can be derived.

$$\frac{\gamma_{lv}(1+\cos\theta)}{2\sqrt{\gamma_{lv}^{d}}} = \sqrt{\gamma_{sv}^{p}}\left(\frac{\gamma_{lv}^{p}}{\gamma_{lv}^{d}}\right) + \sqrt{\gamma_{sv}^{p}} \tag{2.10}$$

As a result, for a set of contact angles data obtained for different test liquids with known surface tension components, from linear regression using Owens-Wendt Equation (Eq. 2.10) it is possible to calculate at once the two unknowns γ_{sv}^{d} and γ_{sv}^{p}.

Fig. 2.8 presents an example of the application of this methodology. Contact angles obtained for the same solid-liquid system from three different approaches are used (MKT, W1 and W2).

Nonetheless, assuming that all non-dispersive components can be grouped into a single component representing alike interactions is a questionable assumption, since this term is suppose to account for rather opposite-character interactions (specific interactions), such as electron donor and electron accepetor interaction (Lewis acid-base theory). To account for the latter case, van Oss [125] introduced a three component-based model in which specific polar interactions are subdivided into acid-like and base-like components, while all the non-specific interactions (Lifshitz/van der Waals type) are grouped in another term.

[4]Hereafter used as a synonym of W_A.

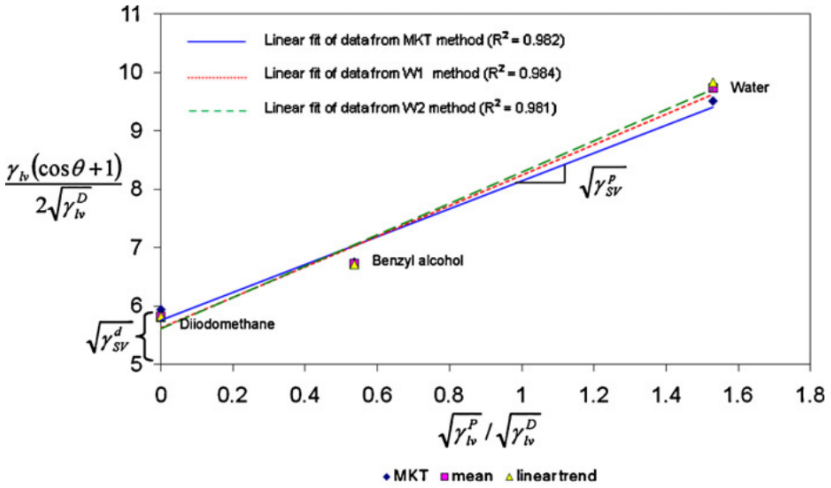


Figure 2.8: Owens-Wendt plot used to estimate the surface energy of coir fibres employing the contact angles obtained from different approaches (Molecular-Kinetic Theory [MKT], mean advancing and receding contact angles in Wilhelmy Balance (W1) and linear trend (W2)). [20]

2.1.4.1 Acid-Base Approach

The acid-base approach (van Oss model) was developed by C. J. van Oss, R. J. Good and M. K. Chaudhury [125]. In this model the solid surface energy γ_{sv} is obtained as the sum of a non-polar component, γ_{sv}^{LW}, which accounts for all the non-specific interactions (Lifshitz/van der Waals type: dispersion [London], induction [Debye] and dipole [Keesom][5]) that a surface is capable of making, and a polar component, γ_{sv}^{AB}, which is described with a higher degree of detail as compared to the Owens-Wednt model, accounting separately for all the electron donating (acid component, γ_{sv}^{+}) and electron accepting (base component, γ_{sv}^{-}) phenomena according to Lewis acid-base theory (see Eq. 2.11).

$$\gamma_{sv}^{tot} = \gamma_{sv}^{LW} + 2\sqrt{\gamma_{sv}^{+}\gamma_{sv}^{-}} \tag{2.11}$$

Where $\gamma^{tot} = \gamma^{LW} + \gamma^{AB}$
For which the work of adhesion can be written as:

$$W_A = \gamma_{lv}(1+\cos\theta) = 2(\gamma_{lv}^{LW}\gamma_{sv}^{LW})^{1/2} + 2(\gamma_{lv}^{-}\gamma_{sv}^{+})^{1/2} + 2(\gamma_{lv}^{+}\gamma_{sv}^{-})^{1/2} \tag{2.12}$$

2.1.4.2 Fibres Surface Free Energy

Applying the van Oss model, the fibre surface energy and its components can be estimated by solving a system of equations with input data from at least three liquids with known surface tension γ_{lv} and respective components γ_{lv}^{LW}, γ_{lv}^{+} and γ_{lv}^{-}, that wet a solid surface resulting in a characteristic contact angle θ.

An advisable approach is to first use a completely dispersive probe (such as Diiodomethane), allowing to initially obtain γ_{sv}^{LW}, followed by monopolar probes with acid or base characters (or at least dominating acid or base components), one of each. C. Della Volpe and S. Siboni [128] report a selection criteria based on the "condition number" of a triplet of probe liquids[6] described as a system $\boldsymbol{Ax}=\boldsymbol{b}$:

[5] In which the dispersion forces are notably dominant - that is why it is always called dispersive.
[6] This approach can be generalised to any system of n≥3 probe liquids.

Table 2.3: Surface energy components of suggested liquids according to C. Della Volpe and S. Siboni scale [51]

Liquid	γ (mJ/m^2)	γ^{LW} (mJ/m^2)	γ^+ (mJ/m^2)	γ^- (mJ/m^2)
Water	72.8	26.25	48.50	11.16
Diiodomethane	50.8	50.80	0.00	0.00
Ethylene Glycol	48.0	33.90	0.97	51.60

$$2\begin{bmatrix}\sqrt{\gamma_{l,1}^{LW}} & \sqrt{\gamma_{l,1}^{-}} & \sqrt{\gamma_{l,1}^{+}}\\ \sqrt{\gamma_{l,2}^{LW}} & \sqrt{\gamma_{l,2}^{-}} & \sqrt{\gamma_{l,2}^{+}}\\ \sqrt{\gamma_{l,3}^{LW}} & \sqrt{\gamma_{l,3}^{-}} & \sqrt{\gamma_{l,3}^{+}}\end{bmatrix}\begin{bmatrix}\sqrt{\gamma_{sv}^{LW}}\\ \sqrt{\gamma_{sv}^{+}}\\ \sqrt{\gamma_{sv}^{-}}\end{bmatrix}=\begin{bmatrix}\gamma_{l,1}(1+\cos\theta_1)\\ \gamma_{l,2}(1+\cos\theta_2)\\ \gamma_{l,3}(1+\cos\theta_3)\end{bmatrix} \tag{2.13}$$

It is expected that a group of liquids that minimises the condition number (cond($\boldsymbol{A}$)) defined as presented in Eq. 2.14 (i.e., a well-conditioned system) will provided the most reliable results[7].

$$\text{cond}(\boldsymbol{A}) = ||\boldsymbol{A}||||\boldsymbol{A}^{-1}|| \tag{2.14}$$

where $||\boldsymbol{A}||$, a matrix norm, is defined as
$||\boldsymbol{A}|| = \sum_{i,j=1}^{3} |\boldsymbol{A}_{i,j}|$

Different scales of liquid surface energy can be used in the van Oss model, from which, the van Oss scale, which assumes the acid and base components of water to be equal ($\gamma^+ = \gamma^- = 25\text{mJ/m}^2$) and the C. Della Volpe and S. Siboni scale, which assumes water to have an acid character ($\gamma^+ = 48\text{mJ/m}^2$ and $\gamma^- = 11.16\text{mJ/m}^2$) seem to be the most used in the literature. Since, better results have been reported when using the latter, it is used in this work [130].

Following the approach used by C. A. Fuentes et al. [26], water, diiodomethane and ethylene glycol are suggested as acid-like probe, completely dispersive probe and base-like probe (see Tab. 2.3). It is reported that this triplet presents a low condition number (5.4) when compared to other triplets found in the literature. Indeed the values reported by C. Della Volpe and S. Siboni [128] for several triplets are all above 5.98.

2.1.4.3 Dynamic Contact Angle Measurements via Wilhelmy Technique

In the Wilhelmy technique applied to fibres dynamic contact angle measurement, the fibre is attached to a beam of an electrobalance and held vertically in a fixed position over the entire measurement, while a beaker containing a probe liquid is raised and lowered via driving platform (further details about this technique are presented in Section 3.2.5.1). The forces detected by the balance while the fibre is scanned in advancing direction at constant velocity are a resultant of the wetting force, sample weight and buoyancy as in Eq. 2.15 (see Fig. 2.9).

$$F_{total} = p\gamma_{lv}\cos\theta + mg + \rho_l gAd \tag{2.15}$$

where F_{total} is the total force measured on the electrobalance, p is the fibre wetted perimeter, γ_{lv} is the liquid surface tension, θ is the contact angle at the three-phase contact line, m is the fibre mass, g is the acceleration of gravity, ρ_l is the liquid density, A is the fibre cross-sectional area and d is the immersion depth (defined as a decreasing value starting from the liquid surface level).

As latter discussed in Section 3.2.5.1, before measuring the contact angle, the fibre sample weight must be measured and set to zero in the balance (this is done automatically in the system used in the

[7]This condition is equivalent to the minimisation of the system output sensitivity to errors in the input [129].

present work). Owning to their high surface area to volume ratio the buoyancy in elementary fibres is negligible for most practical cases [131]. A quick estimate can be done using a typical fibre volume of 1.57×10^{-12} m^3 (using 20 μm as typical diameter and a probe length of 5mm), for which a buoyancy force of ~ 0.01 μN is expected (using an average liquid density of 10^3 kg/m^3), indeed it is negligible when compared to the wetting force, ~ 1 μN. Additionally, due to cross-section variability, trying to account for the buoyancy may actually introduce an additional error in the calculations, rather than eliminating it.

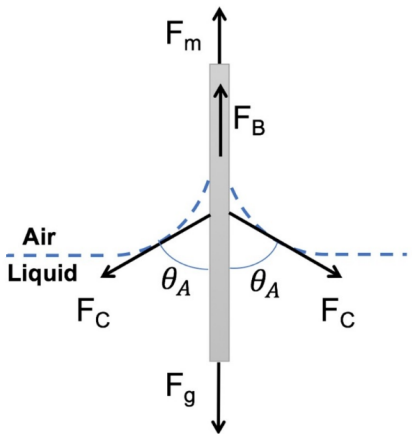


Figure 2.9: Schematic of the force balance diagram model assumed in the Wilhelmy technique method to calculate the advancing dynamic contact angle as the liquid contact line (i.e. solid-liquid-air interface line) moves due to immersion of the fibre into the probe liquid vessel [21]. (Ideal perfectly fat surface).

Error Sources Two important preliminary sources of error in natural fibres dynamic contact angle measurements are the liquid absorption and the fibre perimeter variability[8].

- **Liquid Absorption**
  Natural fibres are known for their high water absorption, especially in the case of technical fibres. A common approach to account for the impacts of liquid absorption is to use the electrobalance of the tensiometer to weigh the fibre before and after the measurements. The absorbed mass is then determined and its effect on the measurements can be supposedly removed [20, 26]. This approach; however, is an over simplification, since water absorption and the consequent swelling of the fibres is a dynamic phenomenon, meaning that both the impact on the local diameter variation and total fibre weight are likely to vary over the experiment. Another method to deal this issue is to work with elementary fibres. As compared to technical fibres, elementary fibres do not present middle lamella, contributing to significantly reduce the void space in the latter case, which is expected to reduce swelling and water absorption. It is acknowledge; however, that this method can be improved by accounting for the swelling in the level of the elementary fibres[9]

- **Fibres Wetted Perimeter and Perimeter Variability**
  Natural fibres are highly anisotropic, presenting diameters that can vary from 10 to 30 μm [12, 81–84]. This variation may deviate the results from the right values to an important degree, as

[8] For more details, see the discussion presented in Section 2.1.4.5

[9] A methodology allowing assessment of elementary fibres swelling has been reported in the literature [132], this analysis would benefit from the use of more detailed surface energy models.

presented by G. Van Gansen et al. [133]. Using hexane (assumed to completely wet the fibre surface due to its low surface tension, γ_{lv} =18.2 mN/m, [10]) it is possible to assess both, the average and local perimeters. For these conditions, extrapolating the measured values at zero depth and subtracting the weight contribution from the results, Eq. 2.15 becomes:

$$F_{measured} = p\gamma_{lv} \tag{2.16}$$

2.1.4.4 *Static Advancing Contact Angles*

The Wilhelmy method allows for Dynamic Contact Angles (DCA) measurements, i.e., the contact angle at a moving wetting line (solid-liquid-vapour triple line). In this case, in addition to the phases surface energies, the measured contact angle is reported to depend on speed and direction of the wetting line displacement [109], being either an advancing contact angle, when the contact line is moving in the sense of wetting the solid, or receding contact angle, when the contact line is moving in the opposite sense (i.e., dewetting the solid). The resulting behaviour presents a sort of hysteresis, which tends to increase with surface roughness and chemical heterogeneity increase (see Fig. 2.10) [11]. Other phenomena contributing to hysteresis are the fluid viscous flow, reorientation of molecules or groups in polar solids [12], transport of molecules from the liquid across the solid surface, either by surface diffusion or else by evaporation, diffusion in the gas phase, and adsorption on the solid, resulting in a gradient of surface free energy density in a region close to the wetting line, affecting the force measured at this point.

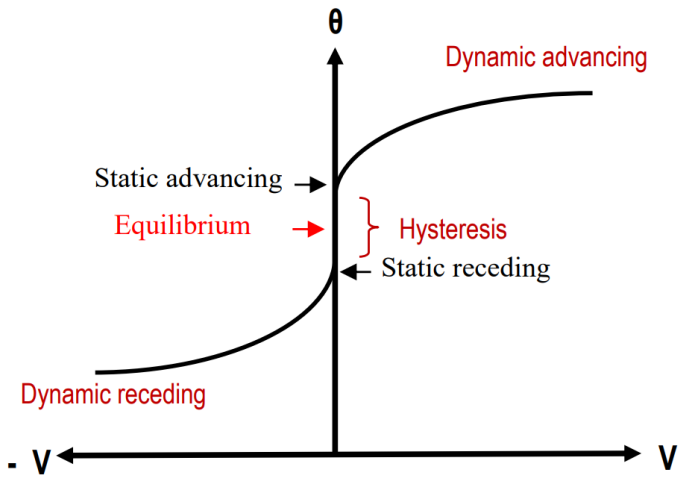


Figure 2.10: Schematic representation of the velocity dependence of the experimentally determined contact angle θ, showing static advancing and receding limits, and the equilibrium angle θ_{eq} (Young's contact angle) [22].

Moreover, in receding mode, the thickness of the liquid vapour adsorbed layer on the solid surface close to the three-phase line will be greater than that observed in advancing mode (if the film is not saturated in the latter case - i.e., equilibrium solid-vapour when the gas phase is saturated with liquid vapour), resulting in different surface concentration gradients, leading to at least a small degree of hysteresis, even in the case of ideally flat surfaces [134] (see Fig. 2.11).

[10] At low advancing velocities this can be confirmed using gold nanocoating [133]

[11] To understand the impact of chemical and surface roughness heterogeneities on the contact angle see the discussion about Cassie-Baxter and Wenzel wetting models presented in the next section

[12] This component in particular is often neglected, though its contribution to histeresis may be dramatic though [134]. A water drop may considerably change the surface while advancing over it, which will lead to altered solid-liquid interactions in receding mode.

Since DCA differs from the equilibrium property of the material, its use as a value to measure the physicochemical interactions, which are by definition related to the thermodynamic (equilibrium) properties of the phases, is questionable. Several models relating DCAs and the referent equilibrium contact angles of a liquid-solid system according to the measurement conditions can be found in the literature. When the advancing and the receding contact angles are well defined, Eq. 2.17 is often used, being the most common approach for smooth homogeneous materials [120].

$$\cos\theta = 0.5\cos\theta_{ad} + 0.5\cos\theta_{re} \tag{2.17}$$

Nonetheless, this approach has no theoretical basis. In his book, *Wetting of Real Surfaces* [19], E. Y. Bormashenko calls this approach "naive" and refers to other models, such as the one developed by R. Tadmor [135], which assumes that the effect of line tension and triple line pinning are interrelated and that wetting line energy contribution "opposes the progress toward an equilibrium contact angle". Eq. 2.18 summarises the mathematical model in terms of advancing θ_{ad} and receding angles θ_{re}.

$$\theta = \arccos\frac{\Gamma_{ad}\cos\theta_{ad} + \Gamma_{re}\cos\theta_{re}}{\Gamma_{ad} + \Gamma_{re}} \tag{2.18}$$

where, $\Gamma_{re} = \left(\frac{\sin^3\theta_{re}}{2-3\cos\theta_{re}+\cos^3\theta_{re}}\right)^{\frac{1}{3}}$; $\Gamma_{ad} = \left(\frac{\sin^3\theta_{ad}}{2-3\cos\theta_{ad}+\cos^3\theta_{ad}}\right)^{\frac{1}{3}}$.

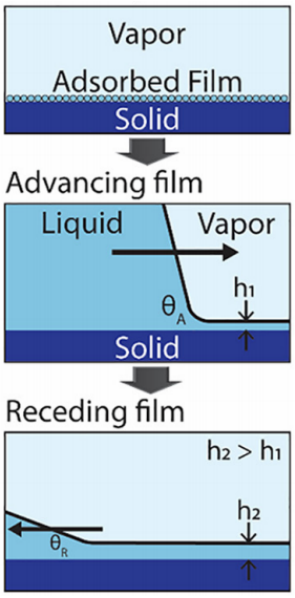


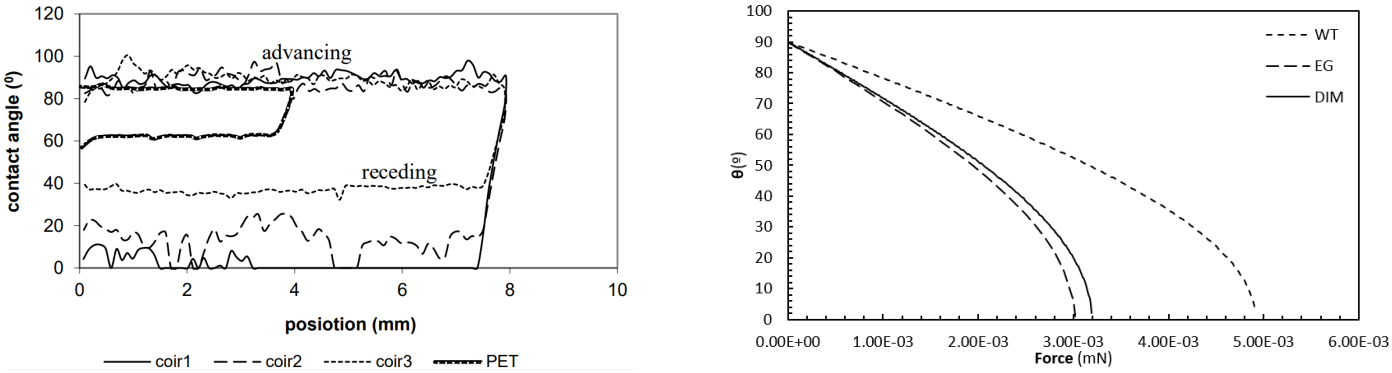
Figure 2.11: Thin liquid film formed during liquid retreat can be thicker from precursor film formed during spreading. Contact angle hysteresis is caused by different disjoining pressure [23]

In the case of natural fibres, due to their notable roughness and chemical heterogeneities, liquids tend to remain in some areas of the fibre in the receding mode after the fibre was deepened in the liquid surface, resulting in a large scatter in the values, which often go to zero (see Fig. 2.12a). To this is added the fact that the DCA relates to the experimental data by a cosine function (Eq. 2.15), which has a higher rate of variation for smaller angles [24], thus higher variations in the outputs are expected in receding mode for the same degree of variation in the force input, as per Fig. 2.12b. A common approach to obtain the static advancing contact angle values from DCA measurements in this case is to use a non-linear regression to fit advancing contact angles obtained at different speeds to the Molecular Kinetic Theory (MKT) [136] (Eq. 2.19).

The MKT models the macroscopic behaviour of the wetting line according to the overall statistics of individual molecular displacements in the triple line. Molecules can either advance with frequency K^+ or recede with frequency K^-. As a result, the net frequency, $K_{net} = K^+ + K^-$, is equal to the wetting line displacement velocity ν. At equilibrium, there is no movement of the wetting line, thus $\nu = K_{net} = 0$ and $K^+ = K^- = K_0$.

$$\nu = 2K_0\lambda\sinh\frac{\lambda^2\gamma_{lv}(\cos\theta_0 - \cos\theta)}{2k_BT} \tag{2.19}$$

where k_B is Boltzmann's constant, T is the Temperature, λ is the characteristic average displacement length of the molecules from one adsorption centre to another and K_0 is the equilibrium rate of molecular displacement. The driving force for the wetting line is assumed to be the out-of-balance surface tension force $\gamma_{lv}(\cos\theta_0 - \cos\theta)$, where θ_0 is the static contact angle, θ is the dynamic contact angle and γ_{lv} is the surface tension of liquid in contact with its equilibrium vapour phase.



(a) (b)

Figure 2.12: (a) Typical dynamic contact angle measurements of coir and PET fibres [24]; (b) Contact angle as a function of the wetting force according to Eq. 2.15 for Water (WT), Ethylene Glycol (EG) and Diiodomethane (DIM). Weight and buoyancy were assumed negligible and the fibre diameter set to an average value of 20 µm

The static advancing contact angles are then derived by fitting the experimental values of DCA obtained at different wetting velocities, $\theta(\nu)$, using the MKT simplified as follows:

$$\nu = \mathrm{Asinh}[\mathrm{B}(\mathrm{C} - \cos\theta)] \tag{2.20}$$

where $\mathrm{A} = 2\mathrm{K}_0\lambda$, $\mathrm{B} = \gamma_{\mathrm{lv}}\lambda^2/2\mathrm{kT}$, and $\mathrm{C} = \cos\theta_0$.

A further complication faced in the present work stems from the fact that flax technical fibres present a high degree of water absorption. To minimise the impacts of this issue, in the present work, measurements had to be performed on elementary flax fibres. Nonetheless, results from successive advancing and receding cycles performed on the same specimen presented a clear and biased variation (i.e., it could not be attributed to the experimental random error), meaning that even a single fibre was probably swelling over the experiments. To reduce this effect, the final measurement protocol per fibre specimens consisted of a single advancing-receding cycle immediately followed by wetted perimeter assessment, which made the use of the MKT impracticable in the available time since several different measurement speeds would have to be used (which means that the measurements would be multiplied by the number of measurement speeds[13]).

2.1.4.4.1 Low-Speed Approach to Equilibrium

Instead of the equilibrium contact angle from a mean of advancing and receding cosines or employing the MKT to obtain the static advancing contact angle, an alternative approach had to be used. As per Fig. 2.10, if the wetting velocity is low enough, kinetic equilibrium is expected to be approached, and the measured advancing contact angles to approach the static advancing contact angle (which still differs from the equilibrium - or most stable - contact angle [120]). Indeed, all the results found in the literature of flax fibres surface energy that employed the Wilhelmy technique used advancing contact angles in their calculations [137–139]. Although some authors seemed to present a certain degree of awareness with respect to the intrinsic bias in the results introduced by this approach [139], none of them tried to evaluate whether the measurement speeds were sufficiently small so as to assume that the measured

[13]Each of the 5 measurements conduced using each of the 3 probe liquids, for each of the 4 types of fibres were performed using different elementary fibres manually isolated (see Appendix A for an estimate of the time it would take if MKT were to be employed).

values were as close as the equipment and calculation methods allowed to the equilibrium. This may be a reflection of an erroneous belief amongst researchers that the advancing contact angle represents the equilibrium contact angle of the lower-free energy areas in heterogeneous surfaces [120]. Some of the implications of using the static advancing contact angle as an approach to equilibrium are:

1. Overestimation of the contact angles leading to lower fibre surface energy components and fibre-matrix work of adhesion as compared to equilibrium (see Eq. 2.13)
2. In polar chemically heterogeneous surfaces, such as flax fibres, the results are prone to be more sensitive to the hydrophobic component [120] (see Fig. 2.13);

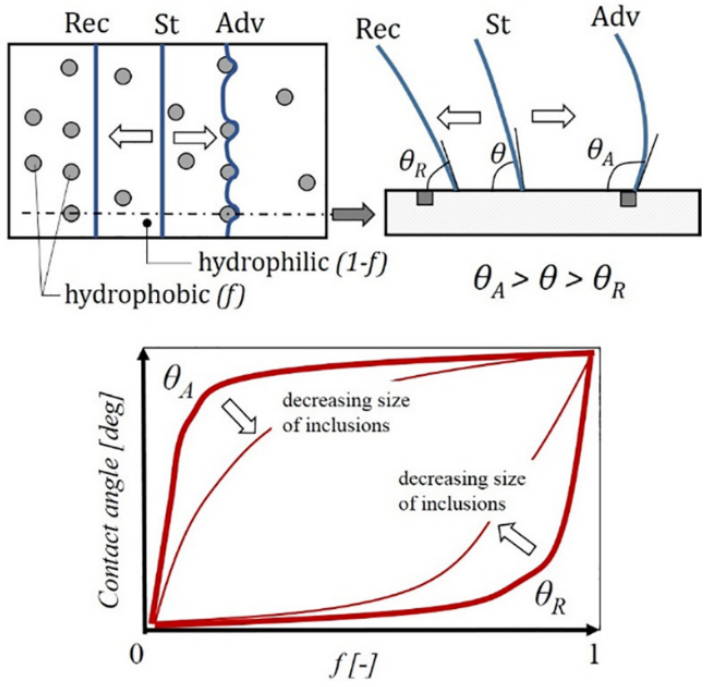


Figure 2.13: Effect of surface heterogeneity on the three-phase contact line and contact angle. The graph presents correlations between advancing and receding contact angles and the fractional area of the solid covered by inclusions (heterogeneity with apolar character). Rec, St, Adv, receding, static and advancing contact lines, respectively; θ_R, θ, θ_A, receding, static and advancing contact angles, respectively

Bearing in mind that these results are likely to underestimate the final components of the surface energy. The present work employes an approach to equilibrium at low wetting velocities so as to approximate the static dynamic contact angles of flax fibres. It is expected that this approach still allows to obtain values that can be used for comparisons between physicochemical interactions of the different types of flax fibres studied and those from similar approaches in the literature, in so far the underestimation for all the fibres is similar.

To assure that the measurements are taken at the closest approach to kinetic equilibrium at each point of the specimen axial direction, the maximum speed that did not cause a measurable difference in the final values of contact angle[14] was determined by successive measurements at increasing speeds, starting from the minimum allowed by the equipment. This approach was assumed to result in kinetic equilibrium for the equipment and calculation methods employed; therefore, allowing for static advancing contact angle calculation.

[14] i.e., the maximum speed that did not cause a measurable increase in the hysteresis between the advancing and receding contact angles for the equipment and calculation methods employed (see Fig. 2.10)

2.1.4.5 Issues Related to Wetting Techniques

Unpredictable, large variation of contact angle values have been observed when untreated natural fibres were studied using wetting techniques [26]. The main issues related to characterisation of natural fibres surface free energy using wetting methods (i.e. Sessile Droplet, Wilhelmy Technique, Washborn method, among others) seem to be:

1. The irregular distribution of topographical and chemical heterogeneities;
2. The presence of macro-topographical irregularities;
3. Liquid Absorption during the experiment.
4. Non-flat surfaces

2.1.4.6 Irregular distribution of topographical and chemical heterogeneities

Surface chemical heterogeneity and micro-topographical heterogeneity (roughness) are common factors affecting the measured contact angles in wetting techniques [26]. To deal with such problems, two simple models are employed:

1. Cassie-Baxter wetting model;
2. Wenzel wetting model.

Cassie-Baxter wetting model: The Cassie-Baxter Wetting Model deals with chemical heterogeneities by assuming that the surface is composed of n chemically different elements randomly distributed (see Fig. 2.14). If each element i of the n elements, which accounts for a fraction f_i of the substrate has characteristic surface tension coefficients $\gamma_{i,sl}$ and $\gamma_{i,sv}$, it can be demonstrated that the apparent contact angle θ^* can be modelled by the following equation:

$$\cos\theta^* = \frac{\sum_{i=1}^{n} f_i(\gamma_{i,sv} - \gamma i, sl)}{\gamma} \tag{2.21}$$

When the surface is composed of only two different of species, this model yields:

$$\cos\theta^* = f_1\cos\theta_1 + f_2\cos\theta_2 \tag{2.22}$$

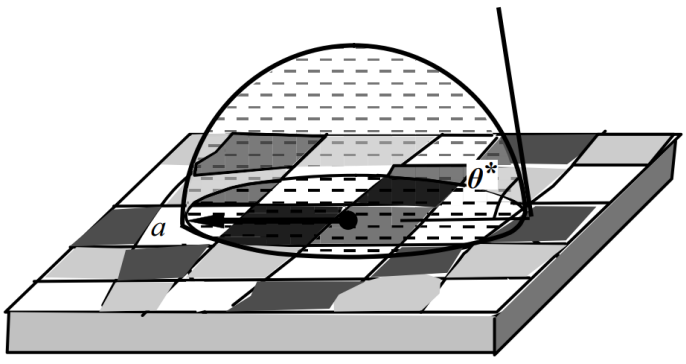


Figure 2.14: Cassie–Baxter wetting of flat chemically heterogeneous surfaces (various grey scale colours correspond to different chemical species) [19]

Wenzel wetting model : Wenzel's Model deals with the wetting of rough (micro-topographical heterogeneities), chemically homogeneous surfaces assuming total penetration of liquid into the surface roughness, leaving no void space between the phases (complete wetting, see Fig. 2.15). In this case, the apparent contact angle, θ^*, is assumed to equal the Young contact angle, θ (contact angle of the smooth surface) corrected by a multiplication factor (r).

$$\cos\theta^* = \mathrm{r}\cos\theta \tag{2.23}$$

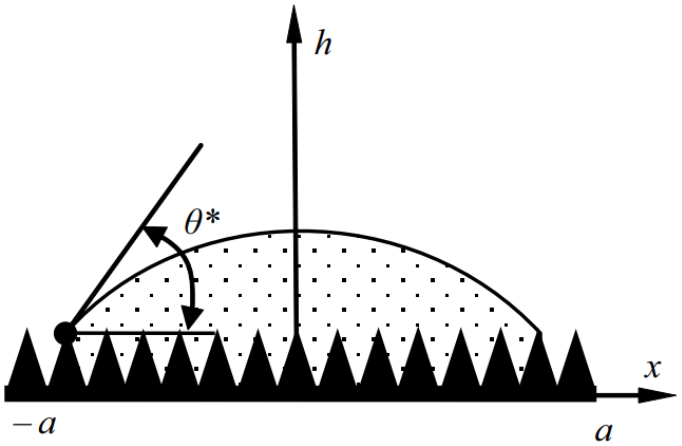


Figure 2.15: Wenzel wetting of a chemically homogeneous rough surface: liquid completely wets the grooves coming representing the surface roughness [19].

Although, the two theories can be easily combined to deal with surfaces presenting both heterogeneities, such as natural fibres, both of them assume regular or constantly distributed heterogeneities along the surface. However, the latter case is far from what is seen in natural fibres, which vary considerable from sample to sample and even in the same sample. A statistically rigorous methodology to accurately measure the contact angles of natural fibres corrected by such models would require several measurements along the axial directions of several fibres, yielding a multidimensional probability distribution dependent on each of the varying parameters introduced by each model. This approach is not suitable for sessile droplet method, since each measurement performed in a given position of the fibre requires an individual assay and, even in the case of Wilhelmy technique and Washburn's method, which allow to "scan" the entire surface in the axial direction over a single assay, the interdependent probability distributions are expected to hinder a meaningful result analysis.

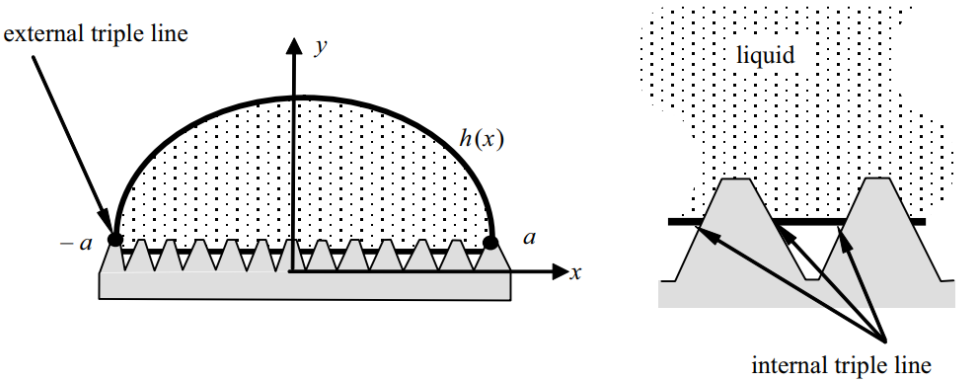


Figure 2.16: Wetting of a substrate built of conical posts. The external and internal triple lines are shown [25].

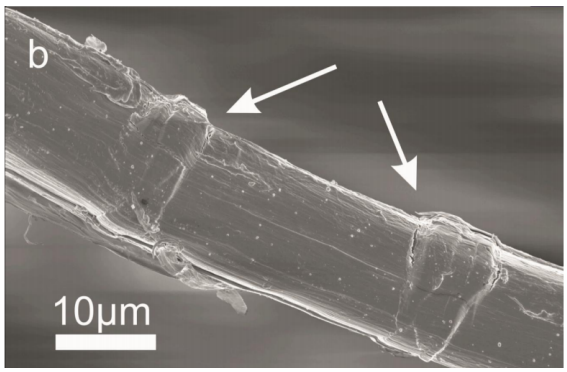


Figure 2.17: SEM micrographs of flax fibres with defect regions. Arrows show the kink bands on flax fibre surfaces [13]

Besides that two additional deviations from each model can make the characterisation even more complicated. When it comes to the Cassie-Baxter model, for each phase, previous knowledge of either their contact angle or surface fraction are required; moreover, chemically complex surfaces have to be treated using Eq. 2.21, which increases the number of parameters to be known prior to the measurement (or obtained from parallel measurements with different well-characterised liquids). The second additional deviation from the models is related to the assumption of total penetration of liquid on the roughness used to derive Wenzel's model, rather than that, a mixed wetting state (see Fig. 2.16) must be employed, dealing with the partial liquid penetration, and consequent remaining air in equilibrium with liquid vapour, as a chemical heterogeneity. Once again, the degree of partial penetration will vary along the fibre axes and from fibre to fibre.

2.1.4.6.1 Macro-topographical irregularities (Waviness)

Another issue identified by C. A. Fuentes et al. [26] while studying bamboo fibres using the Wilhelmy technique was the deviation of the surface tension tensor caused by surface "waviness" (macro-topographical irregularities), which can be understood as topographical irregularities that cannot be completely enclosed by a single droplet.

The Wilhelmy technique allows to obtain the contact angle from the resultant force in the vertical direction using Eq. 2.15 (see Fig. 2.9).

In this case, an accurate measurement relies on the flatness of the fibre surface, such that the contact angle can be defined as the angle between the vertical and the surface tension tensor. However, in natural fibres this is often not the case. Although the impact of micro-topographical heterogeneities on the surface tension tensor direction direction can be neglected (i.e., it does not cause an important deformation on the meniscus), untreated natural fibres often present macro-

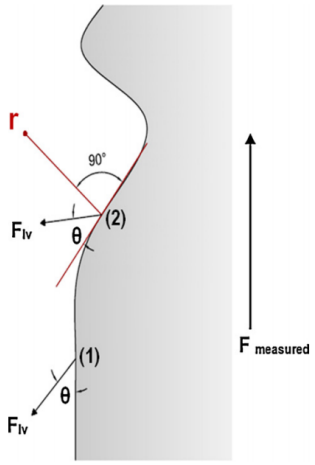


Figure 2.18: The radius of curvature of the fibre surface is constantly changing during the movement of the meniscus over the fibre body, and so the direction of the wetting force, r–curvature radius, F_{lv}–liquid–vapour interfacial force (or wetting force). Position (1): smooth fibre and position (2): fibre with surface irregularities [26]

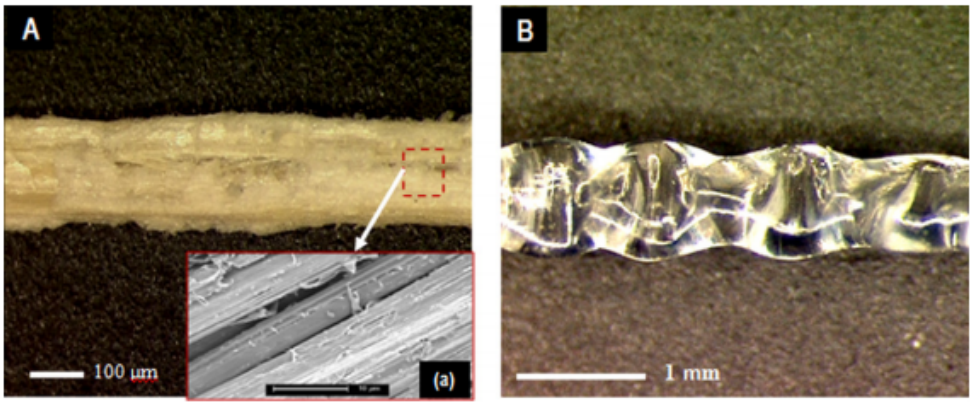


Figure 2.19: (A) Optical microscopy of non-autoclave treated bamboo fibre and SEM image of disjointed elementary fibres, the scale bar in (a) is 10 m. (B) Optical microscopy image of altered PET fibre [26]

irregularities on the surface, such as kink bands (also called "nodes" or "dislocations" [13]), regions presenting accumulation of amorphous pectic and hemicellulosic matrix, which appear oriented perpendicularly to the fibre axis as horizontal bands [34] (see Fig. 2.17, for an schematic view of the fibre structure in this region, see Fig. 2.28). Kink bands are formed due to local bending and compressions during mechanical processing or due to environmental forces during growth [13]. This surface irregularity causes variations of the immediate surface tension tensor direction. The force balance model; however, assumes fibre surface to be vertical, resulting in misleading data (see Fig. 2.18).

C. A. Fuentes et al. [26] report a significant increase of non-treated bamboo fibres contact angle measure by Wilhelmy technique due to such macro-topographical irregularities. To evaluate the importance of such factors, a model of PET fibres was studied (see Fig. 2.19).

2.1.4.6.2 Liquid Absorption

Natural fibres are porous (technical fibres in especial due to the middle lamella) and present high liquid absorption. As previously state, this results in different problems when using wetting techniques, affecting both droplet shape and wetting force measurement.

Droplet shape, used for sessile droplet contact angle measurements, is affected over time by liquid absorption due to solid-liquid surface increase (resulting in changes in the apparent contact angle, as previously discussed when talking about Wenzel's model), changes in the droplet total volume, water spreading along the surface, among other deviations from ideal behaviour [140].

The effects of liquid absorption in wetting force measurements, used in Wilhelmy technique are:

1. Fibre swelling and shrinking, changing the wetted perimeter over time during the experiment and from experiment to experiment [26];
2. Fibre weight changes during the experiment [20, 26];
3. Liquid absorption at the contact line, which can distort the contact angle [26].

2.1.4.6.3 Non-flat Surfaces

Since it can change the final morphology of the droplet, a non-flat surface geometry can hinder sessile droplet measurements. When a droplet is deposed on a fibre surface, two morphologies can be observed, a stable geometry of an axi-symmetric unduloid (barrel) or a metastable geometry of a 'clam-shell' [141], as presented in Fig. 2.20. The axi-symmetric unduloid morphology contact angle is measured by analysing

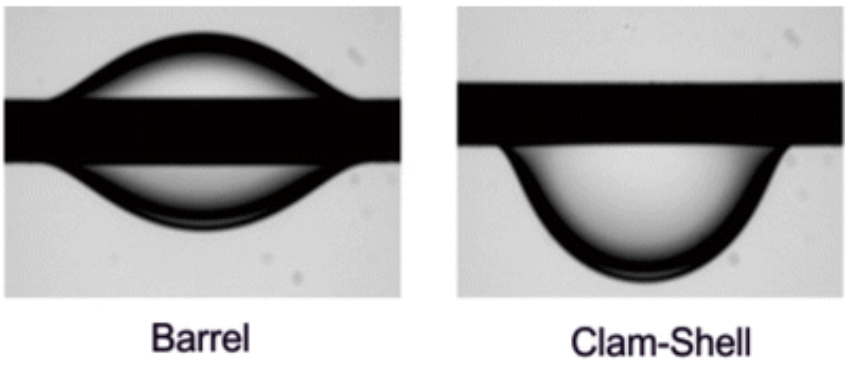


Figure 2.20: Usual morphologies assumed by a droplet wetting a fibre surface [27].

the droplet shape [142]. On the other hand, the clam-shell morphology does not present symmetry for rotations around the fibre axis, which hinders the contact angle measurements using droplet shape [15]. It is a well-known result that the unduloid form prevails when the droplet is large enough relative to the fibre and the contact angle is relatively low [143]. By using a small enough droplet, such that the fibre surface curvature can be neglected with respect to the droplet radius, better measurements can be obtained. This; however, can result in other problems related to the measurement, and droplet deposition. On the other side of the spectrum, a larger droplet volume can be used to promote axi-symmetric unduloid morphology, once again, it can result in problems related to the droplet deposition and, if the droplet radius becomes excessively large, it starts to present deformation due to gravitational effects (the hydrostatic pressure and Laplace's pressure magnitudes become comparable [19]), which can invalidate the measurements.

2.1.4.6.4 Fibre Components Solubilisation

Another issue common to all wetting techniques is the solubilisation of low-molecular-weight non-cellulosic material (mainly pectin, hemicellulose and lignin) in the probe liquids [144]. This issue is expected to have a series of consequences on the measurements, affecting the results and their reproducibility if the same specimen is to be used again, changing the surface properties from advancing to receding mode in dynamic contact angle measurements, and thus the final values of equilibrium contact angle measured and, finally, contaminating the probe liquids, which can significantly influence the subsequent results if those are not constantly changed.

2.1.4.7 Adhesion Optimisation

The selection of the pair fibre-resin that is expected to result in the best interface properties in terms of physicochemical interactions can be obtained by evaluating the Work of Adhesion (W_A), Spreading Coefficient (S), Wetting Tension (ΔF) and Fibre-Resin Interfacial Energy (γ_{sl}). A brief description of each one of this parameters is provided in the next paragraphs.

1. **Work of adhesion:** Work required to disjoint a unit area of the solid-liquid interface, thereby creating a unit area of liquid-vacuum and solid-vacuum interfaces [116]. A high work of adhesion

[15] Since one cannot be completely sure of the droplet alignment by evaluating the recorded images, if the droplet shape is analysed using a picture in which the subsection imaged is not a plane of symmetry, which is most often than not the case, the real contact angle cannot be obtained.

is desirable. In the present sutudy, the work of adhesion is be used as the main parameter to evaluate physicochemical interactions.

$$W_a = \gamma_s + \gamma_{lv} - \gamma_{sl} = \gamma_{lv}(1 + \cos\theta) \tag{2.24}$$

2. **Spreading Coefficient** [16]**:** Work required to prevent spreading by exposing a unit area of solid-vacuum interface while destroying corresponding amounts of solid-liquid and liquid-vacuum interfaces [116]. When the solid is atomically flat, chemically homogeneous and isotropic, insoluble, nonreactive, and nonstretched [17], S can be obtained as follows [145]:

$$S = \gamma_s - (\gamma_{sl} + \gamma_l) \tag{2.25}$$

The desirable outcome, $S > 0$, corresponds to instantaneous spreading.

3. **Wetting Tension:** Work needed against wetting a porous network by eliminating a unit area of solid-liquid interface while exposing a unit area of the solid-vacuum interface [116] (arithmetic mean of W_a and S). Wetting is favoured by $\Delta F > 0$.

$$\Delta F_i = \gamma_s - \gamma_{sl} \tag{2.26}$$

4. **Interfacial Energy:** Reversible work per unit area needed to increase the interfacial surface. As a result, reducing the interfacial energy favour wetting. Using the van Oss model,

$$\gamma_{sl} = \gamma_s^{LW} + \gamma_l^{LW} + 2\left[(\sqrt{\gamma_s^+\gamma_s^-} + \sqrt{\gamma_l^+\gamma_l^-} + \sqrt{\gamma_s^{LW}\gamma_l^{LW}} + \sqrt{\gamma_s^+\gamma_l^-} + \sqrt{\gamma_s^-\gamma_s^+}\right] \tag{2.27}$$

The optimal condition corresponds to the maximum work of adhesion on the region where spontaneous wetting occurs ($S \geq 0$), resulting in maximum wetting tension, ΔF [114].

2.1.5 Interface Mechanical Characterisation

This section presents the theory underlying the microbond test, which is used to study interface mechanical properties at the microscopic level. For more information on the other possible techniques, please refer to section 2.2.2.

2.1.5.1 Technique Choice

Among the most used techniques to study interface mechanical properties of FRC (push out [microindentation], pullout, single fibre fragmentation and microbond), the reasons underlying the choice of microbond (also known as microdroplet debond and highly similar to pullout test [146]) in the present work were [28, 29, 146]:

1. Indication of resin-fibre wetting through the aspect ratio and (approximate) contact angle of droplets (see Fig. 2.21);
2. Also allows the study of debonding mechanisms (see Fig. 2.22);
3. Relatively fast and easy sample preparation and experiments.

[16] Also known as Spreading Parameter [19].

[17] i.e., Specific surface energy and surface tension are equal.

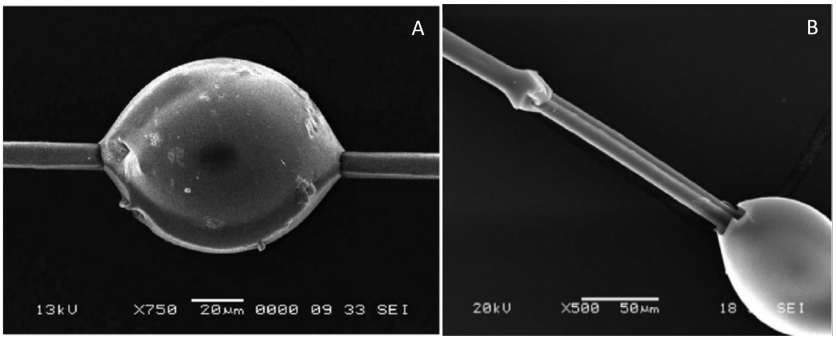


Figure 2.21: (A) PLA microdroplet on single flax fibre [28]; (B) Debonded sample without peeling [29]

2.1.6 Experiment Description and Modelling

The Microbond test consists basically of pulling out a polymer matrix microdroplet, previously deposited on the fibre, at constant deformation rate, while the forces during the measurement are recorded. By monitoring the variation of such force, visual inspection of the sample, among other techniques, it is sometimes possible to determine when interface failure (i.e., debonding) starts to occur. The force at debonding process start (i.e., when a crack starts to propagate on the fibre surface) is called debonding force, F_d, and differs from the maximum recorded force, F_{max}, which is a sum of the interface strength and frictional forces between matrix debonded regions and fibre surface.

A simple and widely used model to assess interface mechanical properties from microbond experiments is the apparent interfacial shear strength (IFSS), τ_{app}, calculated dividing the maximum recorded force (or the debonding force, if directly measurable from the experiment readings) by area of fibre embedded in matrix microdroplet[18] [146]. As latter discussed in Section 2.1.6.2, the apparent IFSS actually depends on the fibre embedded length in the matrix, l, and can only be used to evaluate qualitatively the interfacial bonding strength as a function of the specimen geometry [24, 147].

$$\tau_{app} = \frac{F_{max}}{\pi D l} \tag{2.28}$$

where F_{max} is the peak pullout force, D is the fibre equivalent diameter and l is the embedded length.

To avoid fibre rupture, the pullout force must be maintained below the fibre ultimate tensile strength. This can be controlled by limiting the embedment length below a critical value l_c, estimated using Eq. 2.28, with fibre breaking force F_B calculated with respect to the fibre tensile strength σ_f and mean cross-section diameter D_m, $F_B = \sigma_f \pi D_m^2/4$,

$$l_c = \frac{\sigma_f D_m}{4\tau} \tag{2.29}$$

[18]Hereafter, embedded area.

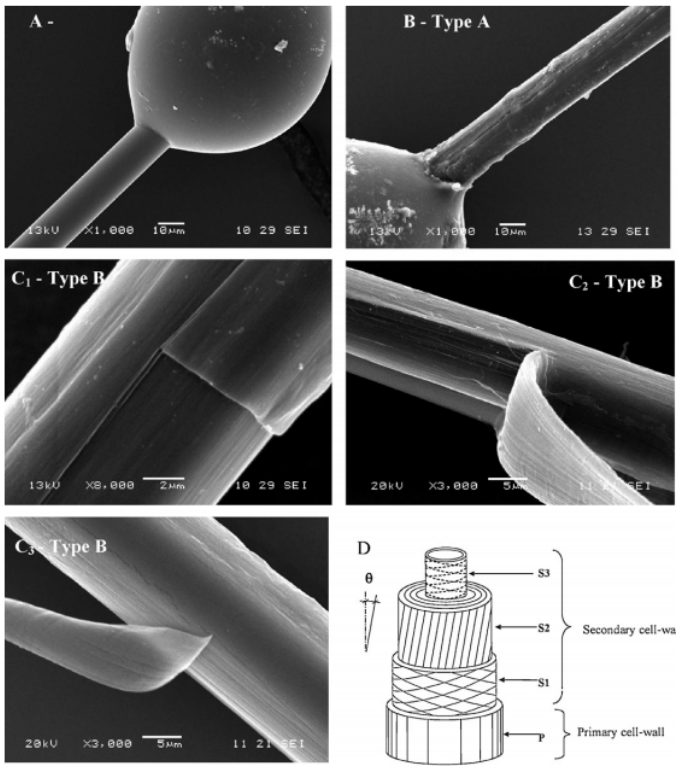


Figure 2.22: Fibre surfaces after microdroplet sliding, glass/PLLA (A), flax/PLLA (type A) (B), flax/PLLA (type B) (C1-C3), (D) schematic diagram of the structure of a flax (Reminder) [28]

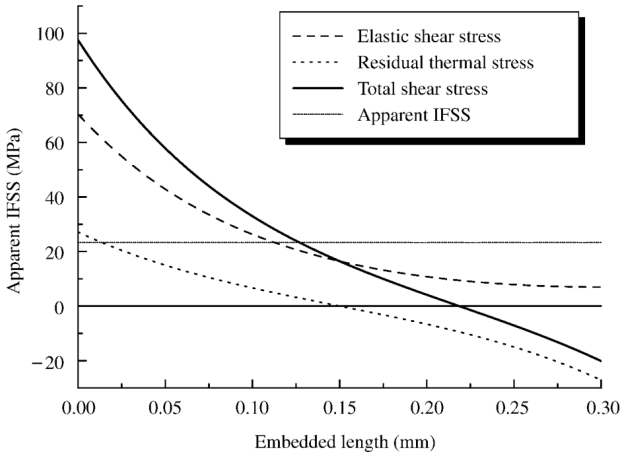


Figure 2.23: Variations of the total interfacial shear stress and its components along the axial coordinate in a microbond or pullout specimen. The horizontal line shows the apparent shear strength value for this specimen [30]

An estimate can be obtained by using the values presented by A. Le Duigou et al. [29] for flax fibres-epoxy resin interface. In this work two varieties of flax fibres were studied, namely Hermes and Electra, both harvested in the Normandy, Northern France, between 2003 and 2007. For Hermes fibres $l_c \cong 293$ μm, while for Electra fibres $l_c \cong 224$ μm. Nonetheless, to assure a great margin of safety, accounting for frictional effects (which cannot be separately considered using τ_{app} [31]), epoxy resin microdroplets with embedment lengths of about 100 μm were used in this study.

As previously mentioned, τ_{app} as calculated by Eq. 2.28, results in a specimen geometry-dependent IFSS, which cannot be used to characterise the interfacial bond strength without accounting for frictional forces. The main parameter affecting the apparent IFSS is the embedded length [30, 148–157]. According to S. F. Zhandarov et al. [30], this dependence is due to both, the mechanism of load transfer at the interface and the residual thermal stresses generated during the curing of the specimen, which result in a complex shear stress distribution pattern along the embedded length. Fig. 2.23 presents how the total interfacial shear stress and its components are expected to vary for a typical specimen in a microbond or pullout test along the fibre axial coordinate, evidencing the intricate shear stress distribution whose value will vary along the embedded length, invalidating the hypothesis used to calculate τ_{app}, simultaneous failure over the entire embedded length. The interface is then assumed to fail locally and gradually through interfacial crack propagation ('unzipping' mechanism) at a critical local shear stress τ_d, which can be confirmed by direct visual observation of crack propagation [158] or by a decrease in the slope of the force-displacement curve, marking the beginning of interfacial debonding process ('kink' point), which can be seen if the equipment employed for measurement is sufficiently stiff and the free end of the fibre is sufficiently short [30], the last factor being related to the friction between the debonded surface and the fibre, which accounts for a further increase in the measured force as a function of the displacement even after crack propagation starts to occur (see Fig. 3.16). Consequently, at interface failure, the shear stress over most of fibre embedded area is less than τ_d, whose value is significantly greater than τ_{app}, as presented by Fig. 2.23.

2.1.6.1 Failure Mode

The different regions of the curve force-displacement in a pullout test, corresponding to different regimes of interfacial debonding, can be seen in Fig. 2.24 [19]. This debonding occurs through interfacial

[19] A similar reasoning can be made for microbond test, except for a constant friction force resulting in a plateau after point D, instead of a decreasing force

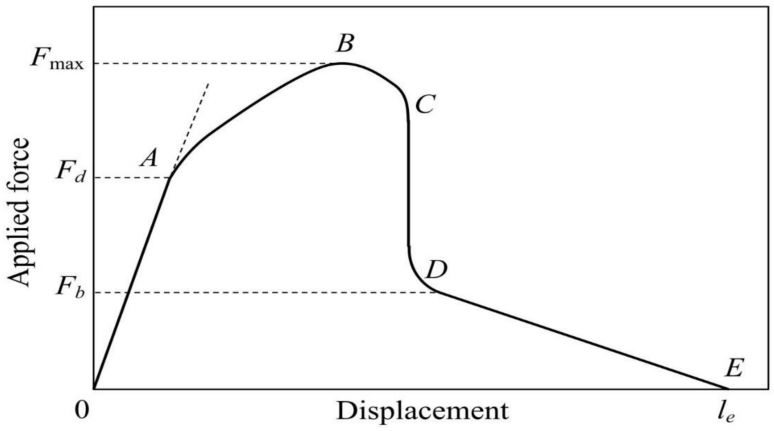


Figure 2.24: An idealised force–displacement curve in the pullout test [31]. A similar behaviour is observed for microbond test, except for a constant friction force resulting in a plateau after point D

crack propagation (unzipping) and, as such, has contributions of adhesion and fibre-matrix friction [31].

1. **First Stage (OA, initial loading):** the fibre displacement is nearly proportional to the applied force (intact interface);

2. **Second Stage (AB, debonding initiation):** the applied force reaches the debonding force ($F = F_d$). As the crack propagates, the friction between the debonded fibre regions and the matrix contribute to the rise until the friction increase no longer compensates for the decrease in fibre-matrix interface (B), from this point further crack propagation results in force decrease.

3. **Third Stage (B-D, debonding instability):** as the interface is decreased an instable point is reached (C) and the remaining embedded area instantly debonds. The force then drops to a smaller value (D), so-called post-debonding force, F_b.

4. **Fourth Stage (DE, remaining segment):** this region presents the frictional interaction between the debonded fibre and the matrix. The decrease of this value represents the fibre exiting the specimen in pullout tests. This is not observed in the microbond case, in which the fibre is expected to stay embedded in the matrix even after interface failure, resulting in a force plateau corresponding to fibre-matrix friction. This plateau extends until the end of the test, presenting a few jumps according to the fibre specimen cross-section variation (see Fig. 3.16)

2.1.6.2 Modelling Interfacial Crack Propagation

Two main approaches are found in the literature to perform a more detailed analysis of the interfacial debonding considering the actual mechanism of interfacial failure, the Stress-Based Model, which associates the interfacial strength to an interfacial stress at which the interface starts to fail [30, 31, 148, 149, 152, 159], and the Energy-Based Model, in which the amount of energy released per unit area during interfacial debonding is determined [31, 160, 161]. By applying such models it is possible to separate the contributions of fibre-matrix bonding and friction.

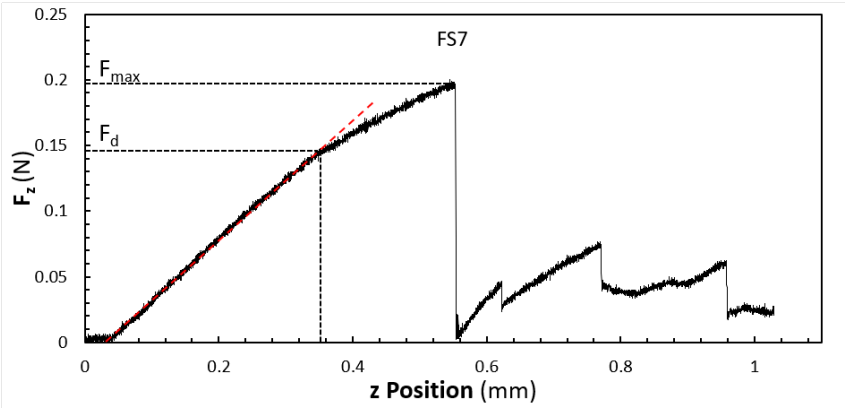


Figure 2.25: Typical Force versus Position curve obtained from microbond tests using Bio-epoxy resin and Flax Fibres. Debonding (F_d) and Maximum (F_{max}) forces are indicated, they correspond respectively to the initial force at which crack propagation starts and the force at the moment in which the sum of the frictional and interfacial adhesion forces are surpassed by the tensile force, resulting in catastrophic failure of remaining bonded surface

Energy-Based Model: Instead of deriving the IFSS, this model is based on determining an interfacial toughness by using fracture mechanics to analyse the interfacial cracking process, more specifically, by solving the system for the energy release rate of a propagating crack [162]. This analysis allows to account for two important features that cannot be captured by a simple analysis using the apparent shear strength, namely, the residual thermal stresses, coming from the different volumetric expansion and shrinkage of fibre and matrix over the processing, and the friction between resin debonded regions and fibre, a significant term, since loading occurs mostly in mode II in microbond (as well as pullout) test [162].

In this model, the analysis begins by simplifying the complex-shape matrix droplet as cylinder with length equal to the embedded fibre length, l, and radius r_m, chosen so as to preserve the total fibre volume fraction within the matrix. By force balance, for a fibre loaded with a stress σ_d at the top of the specimen (see Fig. 2.26), the matrix stress is $-\sigma_d \nu_f/\nu_m$ (where ν_f and ν_m are the fibre and matrix volume fractions). The specimen bottom is assumed to be free of stresses.

For an interfacial debond of length a, as presented in the Fig. **??**, the energy release rate due to debond growth can be equated using Eq. 2.30, which applied a general fracture mechanics method as developed by J. A. Nairn et al. [32].

$$G(a) = \frac{r_f}{2}\left\{C_{33s}\overline{\sigma}^2 + 2D_{3s}\overline{\sigma}\Delta T + \left(\frac{D_3^2}{C_{33}} + \frac{\nu_m(\alpha_T - \alpha_m)^2)}{\nu_f A_0}\right)\Delta T^2 - \left[\frac{\nu_f \sigma_d}{2}\left(\frac{1}{E_A} - \frac{1}{E_m}\right) + D_{3s}\Delta T\right]\left[\frac{2\tau_f}{r_f}C_T(a) - \left(\overline{\sigma} + \frac{2D_3\Delta T}{C_{33}}\right)C'_T(a)\right]\right\} \tag{2.30}$$

where $\overline{\sigma}$ is a reduced stress defined as

$$\overline{\sigma} = \sigma_d - \frac{2\tau_f a}{r_f} - \frac{\sigma_0 E_A}{v_f E_A + v_m E_m} \tag{2.31}$$

For r_f, ν_f, α_T, and E_A equal to the fibre radius, volume fraction, transverse thermal expansion coefficient, and axial modulus; ν_m, α_m, and E_m the matrix volume fraction, transverse thermal expansion coefficient, and modulus; τ_f the friction stress on the debonded regions; $C_T(a)$ a stress-transfer function; and $C_{33s}, D_{3s}, A_0, D_3$, and C_{33} constants depending on the fibre and matrix properties and geometry (see Appendix B for their definition).

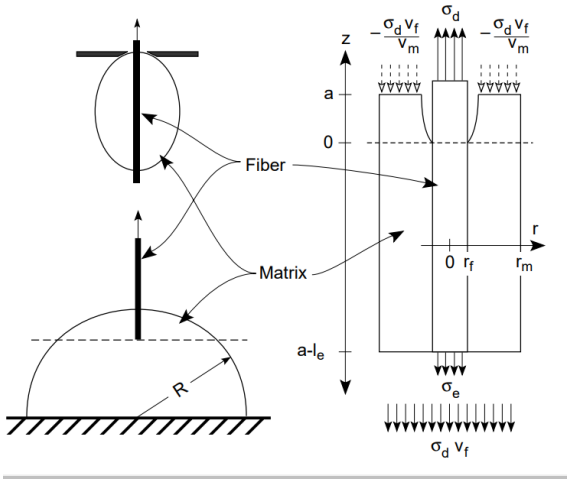


Figure 2.26: The left side shows the microbond (top) and pullout (bottom) specimen geometries. The right side shows the equivalent concentric cylinder model where the embedded length of fiber is in a cylinder of matrix. The fibre in both specimens is loaded with stress σ_d. The "dotted" arrows are the remaining microbond specimen boundary conditions; the solid arrows on the bottom of the specimen are the remaining pullout specimen boundary conditions [32]

$$C_T(a) = \int_0^{l-a} F(z)dz \tag{2.32}$$

F(z) is the solution for axial fibre stress in concentric cylinders of length l – a under unit normal stress on the fibre and corresponding ν_f/ν_m stress on the matrix at z=0 in addition to zero stress on the other end at z = l–a. The function F(z) and $C_T(a)$ can be analytically, numerically or experimentally defined and inserted in Eq. 2.30 to obtain the energy release rate. From shear-lag approach, a simple analytical model can be derived, this approach was shown to be accurate when compared to finite element analysis [32, 163].

$$C_T(a) = \frac{1}{\beta}[\coth\beta(l-a) - \operatorname{csch}\beta(l-a)] \tag{2.33}$$

where β is the shear-lag parameter corrected for finite specimens as defined by Nayfeh [164],

$$\beta^2 = \frac{2}{r_f^2 E_f E_m}\left[\frac{E_f\nu_f + E_m\nu_m}{\frac{\nu_m}{4G_f} + \frac{1}{2G_f}\left(\frac{1}{\nu_m}\ln\frac{1}{\nu_f} - 1 - \frac{\nu_f}{2}\right)}\right] \tag{2.34}$$

for E_f, E_m, G_f and G_m, respectively, the tensile (E) and shear (G) moduli of fibre (f) and matrix (m).

Stress-Based Model: In the stress-based model, the interfacial crack growth process is assumed to be governed by the local shear stress at the interface fibre-matrix at the crack tip, which independent on the crack length (a) [160] and is equal to a critical value τ_d. This critical shear stress (real IFSS) can be used with other parameters of the crack propagation and specimen properties in a matrix-fibre stress transfer model (here represented by f_s) allowing to correlate the applied force and the current crack length a.

$$F = f_s(a, l, \tau_d, \Delta T, ...) \tag{2.35}$$

Besides the difference between the test temperature and the stress-free temperature (ΔT), the crack length, fibre embedded length and IFSS, other factors that may be significant include the interfacial friction and specimen geometric parameters other than its l. A simplification of the specimen geometry similar to the one previously presented in the energy-based model discussion is applied so as to ease the analysis (see Fig. 2.26).

Extensive and detailed development of stress-based models (i.e., f_s functions) can be found in the literature [149, 160, 165]. Since the kink point at which the crack starts to propagate on the fibre surface, marking the debonding force F_d, is constantly difficult to determinate, especially in microbond test, which does not allow for visual determination, a case that has attracted considerable attention in the literature is the calculation of τ_d from F_{max}. As discussed by I. Van de Weyenberg in the only attempt in the literature to apply the stress-based approach to model flax fibres microbond tests [35], none of the approaches developed thus far to separate the frictional forces from the debonding force seems to correctly fit the results in the case of flax fibres microcomposites. Moreover, as latter discussed in section 2.2.3, since the shear-lag theory is employed in both Energy- and Stress-based models, their results are expected to serve only for qualitative analysis, whose advantage over τ_{app} is the uncoupling of fictional stresses.

In the present study, even though a few specimens presented a distinguishable kink point (see Fig. 3.16), allowing direct τ_d calculation from F_d, because of the scarcity of τ_d results available in the literature for comparison and a relatively small number of specimens tested when compared to other studies that employed the stress-based model or energy-based model to natural fibres [22, 24, 35] (mainly due to the difficult isolation of flax fibres), the approach employed by the great majority of the studies on flax fibres composites is followed in the present work, and τ_{app} is used to access the interface micromechanical properties [29, 53, 144, 166–168]. It is important to bear in mind that this approach results in IFSS values that account for both frictional forces and interface strength, and therefore, specimens with higher interface strength, if smoother, may have τ_{app} values lower than those with a weaker but rougher interface [35]. Moreover, specimens with different embedded lengths will tend to present different magnitudes of associated frictional forces. To limit the impact of this last point, care was taken to obtain microdroplet specimens with similar sizes, and thus, their embedded lengths were approximately the same size [20].

Local Interfacial Shear Stress (τ_d): the local interfacial shear stress as a function of the debonding force, F_d, can be obtained based on a shear-lag approach modified for finite specimens, as presented by Zhandarov et al. [31].

$$\tau_d = \frac{F_d \beta}{2\pi r_f} \coth(\beta l) + \tau_T \tanh\frac{\beta l}{2} \tag{2.36}$$

where β and its parameters are defined as previously presented in Eq. 2.34 and τ_T accounts for residual thermal stresses if the specimen is formed at temperatures above the stress-free temperature, which is usually assumed to be equal to the crystallisation temperature of semi-crystalline polymers or glass transition temperature of amorphous polymers (or even the room temperature, if it is above the glass transition temperature).

$$\tau_T = \frac{\beta r_f E_f}{2}(\alpha_f - \alpha_m)\Delta T \tag{2.37}$$

where the parameters follow the same convention previously presented.

[20] Nonetheless, a comparison with values obtained from models developed to calculate τ_d from F_{max} on the basis of the stress-based model may be worth doing, since the theory has been developed after I. Van de Weyenberg's study, see recent publication of Serge F. Zhandarov et al. [31]

Choosing the Best Model Each model tends to emphasise a different aspect of the debonding phenomena, as toughness (characterised by the energy-based model) and ultimate interfacial shear strength (characterised by the stress-based model) follow different laws when the specimen geometry is varied [169]. In accordance with the results obtained by Zhandarov and coworkers [30, 31, 149, 159–161, 169, 170], I. Van de Weyenberg [35] determined that the stress-based model seems to be a better fit. A brief list of the reasons is presented below:

1. Using finite element model (FEA) simulation, it was found by Zhandarov et al. [160] that the energy criterion is best suited for larger embedded lengths with $l > 20\, r_f$ (≈ 200 μm for average-sized elementary flax fibres), when the energy release rate due to debonding is higher and eventually plateaus at a characteristic value for each fibre-matrix system. The stress-based model, on the other hand, yielded better results when l was smaller. As earlier presented in quick estimate obtained from plugging typical values available in the literature for flax fibres tensile strength in Eq. 2.28, l values larger than 220 μm are likely to result in premature fibre break for fibres presenting average geometrical and mechanical properties, making the experiment impractical. That is why most of the droplets used in the present study had $l <$ 200 μm, and thus were expected to be better characterised by an stress-based approach.

2. In another study, Zhandarov and coworkers [170] showed that τ_d values are nearly independent on the fibre diameter, differently from G values. As previously discussed, flax elementary fibres present a wide scatter in diameter values, an thus, using a stress-based model allows to reduce the parameters to account for in the analysis.

3. Finally, results from the energy-based model are dependent on the energy release due to elastic deformation of the fibre length between the droplet and the clamp, which is expected to have a smaller or no impact on τ_d (even though, as later discussed, this value can have an important impact on the fibre tensile properties - refer to section 2.2.3).

Shear-Lag Approach Limitations

However, the validity of the shear-lag model to calculate shear stresses is a reason of considerable debate in the literature. According to J. A. Nairn [171], no matter how detailed the assumptions used

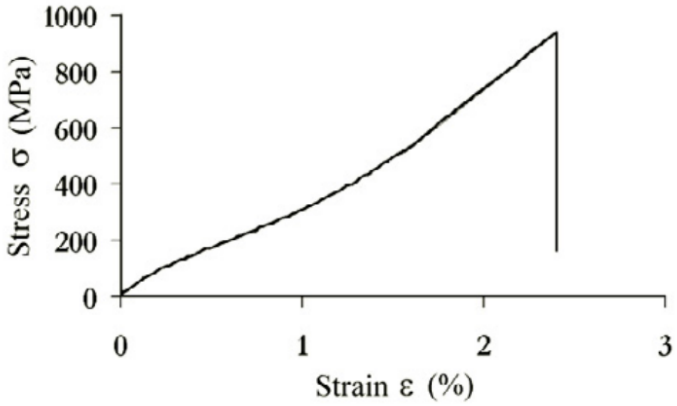


Figure 2.27: Example of a stress-strain curve of an elementary flax fibre. Modified from K. Charlet et al. [33]

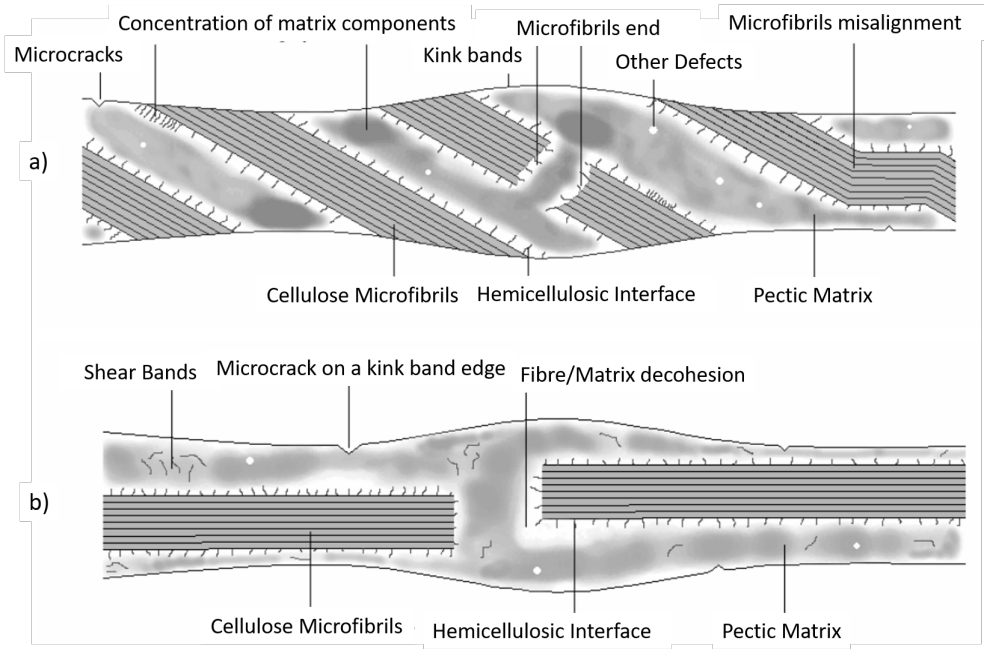


Figure 2.28: Schematics of the main flax fibres secondary wall structural components and defects: a) Under rest condition; b) Under tensile load [34].

to derive the final equations are defined, the results will still be flawed for there is no set of assumption that can escape the fact that the shear-lag stresses are exponential in form while true stress transfer is non-exponential [171]. In addition to that, the standard models in the literature were defined for smooth fibres and consider no variability in the properties along the specimen, which is not the case of natural fibres. Therefore, the results from the stress-based model should be regarded as qualitative, rather than quantitative when applied for flax fibres composites [35][21].

2.1.7 Tensile Properties of Flax Fibres

Due to their complex structure and high variability of properties, flax fibres (and natural fibres in general) present difficult mechanical characterisation. Other issues such as non-elastic mechanical behaviour under tensile stress, non-circular cross-section, presence of defects, ageing, and degradation by microorganisms further increase the imprecision in the final results. Having these problems in mind,

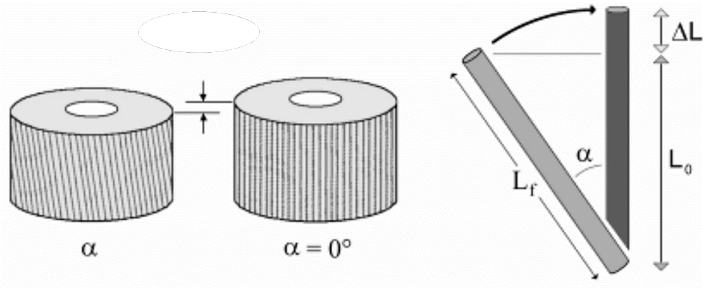


Figure 2.29: Schematic representation of microfibrils alignment with respect to the tensile axis under tensile loading [34]

[21]The same can be said of an Energy-based model that employed shear-lag analysis.

the current sections aims to present a theoretical background on flax fibres tensile properties, focusing on the relation between structural changes under load, and their impacts on mechanical response and failure mechanisms. The current understanding of the factors affecting mechanical properties, as well as a compilation of results found in the literature are provided in section 2.2.3.

2.1.7.1 Structural Changes Under Tensile Stress

A non-linear behaviour is observed in some types of flax fibres (see Fig. 2.27), being particularly common in the case of naturally processed fibres, it is assumed to be associated with the rearrangement of cellulose microfibrils in the fibre cell wall under loading [13, 33, 172]. By assuming progressive alignment of the cellulose microfibrils with the tensile axis, K. Charlet et al. [33] presented a quantitative explanation to the deviation from linear behaviour in flax fibres tensile response. The latter work, also showed that the large scatter of the mechanical properties of flax fibres is not primarily associated with the pronounced cross-section dimensions variation along the stem profiles, but rather to intrinsic variation of properties among specimens typical of natural materials.

Three different tensile deformation regimes can usually be identified in natural fibres stress-strain curves: an initial linear regime, followed by a non-linear regime and a final linear one. In Fig. 2.27, these regimes can be observed from 0 to 0.3 % strain, from 0.3 to 1.5 % strain and from 1.5 % strain until rupture, respectively. By considering the structural composition of the fibres, the current consensus on the tensile properties of natural plant fibres assumes that the first linear region is associated with the global loading of the elementary fibres via deformation of the cell walls. The non-linear regime is interpreted as an elasto-visco-plastic deformation of the fibre, occurring specially in the S2 layer of the secondary cell wall due to the rearrangement of the pectic and hemicellulosic material caused by the alignment of the cellulose microfibrils with the tensile axis [33]. The final linear regime is assumed reflect the elastic mechanical response of the aligned microfibrils.

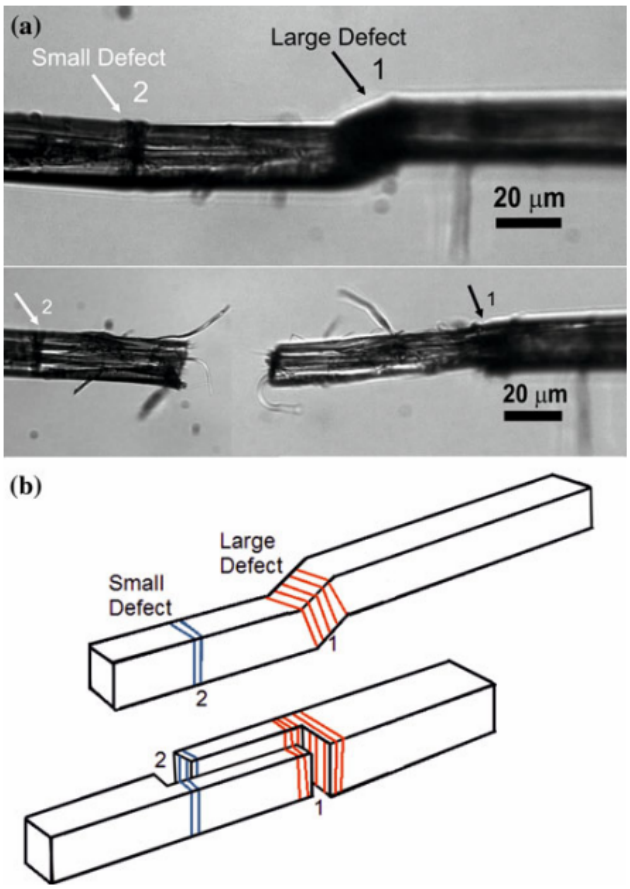


Figure 2.30: Fracture behaviour of a flax fibre showed a by optical microscope images of a fibre before and after fracture and b in a schematic view. The locations of small and large transverse defects are indicated [14]

To further demonstrate the relation between the non-linear regime and the alignment of the microfibrils, K. Charlet et al. present a compelling mathematical argument based on the observed ranges of deformation. Let α be the variation of the microfibrils angle defined with respect to the tensile axis (twist angle), then the total deformation of the fibres due to the alignment of the microfibrils is given by Eq. 2.38, which can be related to the true strain in the limit of small deformations by Eq. 2.39 (see Fig. 2.29).

$$\Delta L = L - L_0 = L_0 \left(\frac{1}{\cos\alpha} - 1 \right) \tag{2.38}$$

$$\epsilon = \ln \left(1 + \frac{\Delta L}{L_0} \right) = -\ln(\cos\alpha) \tag{2.39}$$

An $\alpha \approx 9°$ is obtained when a typical non-linear regime from 0.3% to 1.5% strain ($\epsilon_{n-l} = 1.2\%$) is assumed. By using actual values coming from tensile tests of elementary fibres, the obtained twist angles were consistently within the range reported for flax fibres, mainly obtained by XRD analysis [22].

2.1.7.2 Failure Mechanism

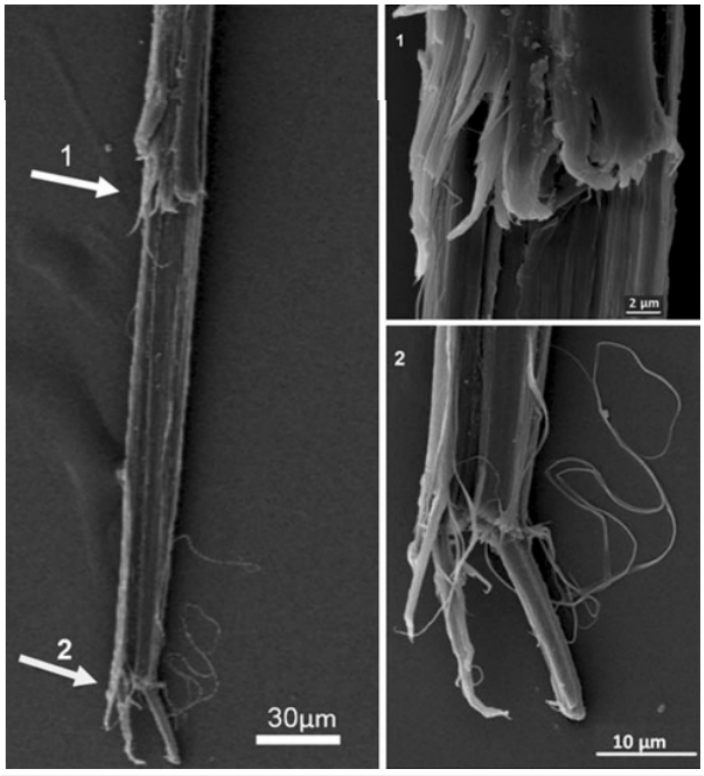


Figure 2.31: Scanning electron microscope image of a large fracture zone in a single flax fibre. Magnified views (1 and 2) are presented to highlight the longitudinal cracks along the fibre, and the formed microfibrillar units at the inner layers at both fractured ends [14]

In situ Environmental Scanning Electron Microscopy (ESEM), Acoustic Emission (AE), among other techniques have been applied to study the failure mechanism of elementary and technical flax fibres loaded in tensile mode [39, 173, 174]. According most recent accepted mechanism, confirmed by ESEM experiments, failure initiates by widening of cracks in the primary cell wall. This is followed by a separation between primary and secondary walls and plastic deformation of the secondary wall fibrils until failure [173]. While the primary cell wall was shown to failure in a brittle fashion, the secondary wall presents a more complex mechanism. As discussed in the previous section, when the structure is subjected to a tensile load, the microfibrils tend to rearrange parallelly to the tensile axis, this causes the rupture of their bonds with amorphous matrix, and creates shear bands [34] (Fig. 2.28 schematically presents the the secondary wall structure under rest and tensile load). It reflects a weaker lateral strength relative to tensile strength, confirmed by a lower compressive strength when compared to tensile strength (1200 MPa and 1500-1800 MPa [175]), which eventually leads to failure by microfibrills separation due to interfibrillar crack growth (see Fig.).

Fig. 2.30a presents one example of elementary fibre fracture surface. According to the analysis made by M. Aslan et al. [14], it is believed that the crack propagation started at a kink band (large defect) where it propagated transversely and continued longitudinally, reaching an internal defect (small defect) where it began to propagate in the transverse direction again until, reaching the surface, which led to failure (Fig.2.30b presents a schematic view of the fracture surface). In Fig. 2.31 it is possible to see the aligned microfibrils in the fracture surface, once again, it seems that transverse crack propagation occurred in the locations indicated by the arrows, while longitudinal propagation occurred between them.

[22] Which can be performed thanks to the crystalline character of the cellulose microfibrils.

2.2 State of the Art

The present chapter briefly discusses previous results found in the literature for FRC. Although greater attention is paid to works on flax fibres that used similar approaches to the ones employed in the present study, in special those in which epoxy resin was used as matrix, whenever relevant, studies using different techniques and investigating different systems are mentioned. The main objective is to complement chapter 2.1, providing the reader with enough information to not only understand the results and discussion presented in the next chapters, but also where the present work is situated in terms of the current progress towards the development of reliable and high-performance commercial flax fibres composites.

2.2.1 Physicochemical Interactions

As previously discussed, good interfacial adhesion is directly related to the fibre-matrix wetting quality, which mainly depends on the physicochemical interactions between the two phases. Fibre-matrix adhesion is primarily governed by surface energies [176]. However, few studies presenting a direct assessment of this property can be found in the literature on flax fibres reinforced composites [137–139, 144, 177–184]. These studies can be divided into those that used wetting techniques, obtaining the surface energy from the contact angles measured between the solid and different probe liquids [137–139, 144, 177, 178, 184], and those that used non-wetting techniques, obtaining the fibre surface energy and its components using a different principle [179–183]. The theory underlying wetting techniques has already been briefly stated in Section 2.1.4, a discussion about the results obtained by these methods, the obstacles in their comparison, an attempt to put them into perspective, and a reminder or description of the techniques are presented in section 2.2.1.1. Non-wet techniques (Inverse Gas Chromatography (IGC) [180, 182, 183] and Atomic Force Microscope (AFM) [179]) have their working principle briefly explained so as to provide the reader with a basis to comprehend the results available in the literature, this is followed by an analysis of the results yielded from their use. Table 2.4 summarises flax fibres surface energy values available in the literature divided by technique and model/method used to interpret the results.

2.2.1.1 Wetting Techniques

Obstacles to Comparison

Although all the techniques were shown to provide reasonably consistent results, reproducibility is still a major concern [176]. A diverse set of issues impacting the measurement techniques, such as surface roughness, porous character of natural fibres and several others mentioned in section 2.1.4.5 added of the composition variation due to several factors, such as retting technique, variety, origin, among others [185], considerably increase not only the batch-to-batch variability, but also the variability within the specimens from the same batch [23]. Another issue may arise from the fact that the probe liquids used may partially dissolve some of the non-cellulosic components on the fibre surface [186]. Moreover, a concern that has been raised in the specific literature about surface energy assessment over the past years is the use of "questionable contact angle measurement methodologies" [120], mainly due to the lack of sufficient training and sample surface preparation, and wrong results interpretation [187]. As a result, the reported works often fail to provide the necessary information allowing for reproducibility [120].

[23] Even along the same specimen

Table 2.4: Summary of flax fibres surface energy values available in the literature divided by technique employed and model/method used to interpreter the results (Owens - Wendt - Rabel - Kaelble [OWRK]; Good - van Oss - Chaudhury [GvOC]; Johnson–Kendall–Roberts [JKR]).

Technique (Model/Method)	Variety (Origin)	Retting Technique	γ_c mJ/m^2	γ_{sv} mJ/m^2	$\gamma_{sv}^d;\gamma_{sv}^{LW}$ mJ/m^2	$\gamma^P;\gamma_{sv}^{AB}$ mJ/m^2	γ_{sv}^+ mJ/m^2	γ_{sv}^- mJ/m^2	References/Publication
Sessile Drop (OWRK/ Static Drop Shape Analysis)	Viking (Normandie [FR])	Dew Retting	—	62.5 (±1.7)	26.6 (±0.6)	35.9 (±1.1)	—	—	[144]/2006
Sessile Drop (GvOC/ Static Drop Shape Analysis)	Viking (Normandie [FR])	Dew Retting	—	61.43	36.68	23.23	3.01	43	
Wilhelmy Technique (OWRK)	— (—)	Dew Retting	—	25.5 - 36	2.67 - 10.82	14.7 - 33.3	—	—	[137]/1999
	— (Finland)	Dew Retting	—	43.5	23.5	20	—	—	[138]/2003
Wilhelmy Technique (GvOC)	— (Belgium/Northern France)	Dew Retting	—	35.2 (±2.1)	28.5 (±1.5)	6.63 (±2.38)	0.67 (±0.47)	16.7 (±1.5)	[139]/2019
Washburn (Zisman Plot)	— (Belgium)	Dew Retting	33.6 (±0.3)	—	—	—	—	—	[177]/2007
	— (Poland)	Dew Retting	35.5 (±1.0)	—	—	—	—	—	[184]/2003
Floating Test (OWRK-Wu)	— (—)	Dew Retting	—	28.5	27.8	0.7	—	—	[178]/1993
	— (—)	Warm-Water Retting	—	32.5	31.3	1.2	—	—	
AFM (JKR)	Prairie Grande (Manitoba [CA])	Enzime Retting	—	—	32.9 (±2.1)	—	—	—	[179]/2018
IGC (Gutmann's Concept/ Dorrys-Gray)	Netherlands	Dew Retting	—	—	43.78	—	—	—	[180]/2002
	— (—)	Dew Retting	—	—	34.9	—	—	—	[181]/2008
	— (Elizabeth Port [ZA])	—	—	—	51.37	—	—	—	[182]/2011
IGC (GvOC)	— (Manitoba [CA])	—	—	46.1 (45.3 - 49.4)	39.1 (38.6 - 41.0)	6.9 (6.6 - 8.3)	—	—	[183]/2017

As a consequence of the above mentioned facts, it is often difficult to compare the values of flax fibres surface free energy from different sources. When doing so, it is advisable, first of all to evaluate whether the considered studies meet the recommendations for correct contact angle assessment presented in the specialised literature [120, 187, 188]. The validity of studies that fail to meet such recommendations as a source of information for comparison is to be questioned. Additionally, classification of the fibres according to the different factors that may lead to composition variation is also advised since these are expected to result in different surface chemistry and, consequently, different surface energy. Table 2.4 is an attempt towards this goal.

2.2.1.1.1 Sessile Droplet Results

When sessile drop technique is used, two different general approaches may be employed, either the droplet is deposited on a flattened solid surface composed of fibre fabrics or compacted table of ground fibres [189] or it is directly deposited on a single fibre (which is usually and elementary fibre) [144][24]. In the first the measurement is strongly influenced by capillarity resulting in liquid absorption and imbibition. Acera Fernández et al. [189] used this method in a more qualitative fashion to evaluate

[24]In the literature, the drop-on-fibre technique is often isolated in a category of its own. However, in the present work, the choice was made so as to group both it as a subset of the sessile droplet technique with the intent of facilitating the understanding of someone that may not be well-familiarised with fibres surface energy assessment.

the changes in the hydrophilic/hydrophobic character of flax fibre fabrics treated using different solvent extraction methods. After deposition, the volume of the droplets was found to be approximately stable for about 10 s, allowing a first determination of an apparent contact angle using various probe liquids that was correlated to the hydrophilic/hydrophobic character of the fibres. In addition to that, the kinetics of absorption was used as a second indication of hydrophilic character change. As the authors acknowledge, these results have to be view with precaution in a more qualitative fashion, since other factors such as the surface texture and topography may influence the water contact angle measurements in this case. No values of surface energy were extracted from these results; however, it may provide a quick qualitative means of assessing the effects of fibre treatments on interface adhesion assessment, if there exists previous knowledge of the hydrophilic/hydrophobic character of the matrices to be used.

Another approach used in sessile droplet is the so-called drop-on-fibre technique [186]. As opposed to the previous case, this approach allows for quantification of surface energy components from static contact angles assessed by studying the geometry of a droplet deposited on an elementary fibre, an example of mathematical model used in this case is presented in Appendix C. Baley and coworkers [144] used drop-on-fibre technique to obtain the surface free energy components of flax fibres. The probe liquids were chosen so as to minimise the solubilisation of fibre surface components. Both the Owens-Wendt and van Oss models where used to decomposed the surface energy values. As it can be seen in table 2.4, this work presents by far the highest total surface energies, this may be a consequence of the use of static contact angles instead of trying to assess the advancing and receding angles separately. In this case, instead of a global energy minimum, in which the most stable contact angle would be measured [120], the results may actually be related to a local energy minimum within the hysteresis range (i.e., metastable) [190]. When using the drop-on-fibre method, due to the difficult control over the shape of the droplet, trying to simulate advancing and receding conditions may be a considerably difficult task, trying to tilt the fibre in which the drop was deposited would invalidate the fitting models usually used, developed for symmetrical morphologies[25]. Although it is not possible to categorically state that these results are flawed, its static contact angles are most probably related to a metastable condition closer to a receding condition, which led to smaller contact angles and resulting higher apparent surface energies[26]. In their favour, C. Baley et al. argue that their angles are close to those usually reported for cellulose fibres [191]. Notwithstanding this argument, the surface energy values found in the literature for the so-called cellulose fibres [191, 192] are notably higher than those observed for the most common natural fibres used as composites reinforcement [186]. Indeed, although cellulose is the main component of plant fibres, it is mostly present in their bulk, while non-cellulosic components can be present in large quantities at the fibre surface [186]; hence, comparing flax surface energy values with cellulose fibres is a questionable approach.

Wilhelmy Technique

K. Van de Velde and P. Kiekens [137] studied the surface energy of four different types of flax fibres using Wilhelmy technique and applying Owens-Wendt model to treat the results. In their work, both the advancing and receding contact angles were obtained, with hysteresis ranging from 20° to 70°. As usual, some of the receding angles obtained in this work were null. Besides roughness and chemical heterogeneity, an additional contribution to the high hysteresis values in this study may be due to the relatively high measurement speeds ($\sim$ 1.2 mm/min). Even though K. Van de Velde and P. Kiekens call

[25] Appendix C presents a brief development on the issues one may face when trying to perform drop-on-fibre measurements.

[26] This may be related to the transition between clamshell and barrel morphologies after droplet deposition, investigations on this subject were not found in the literature.

the attention to the importance of hysteresis characterisation, advancing angles were used to calculate the surface energy components and work of adhesion. This factor is likely to have led to underestimated results. Indeed, when compared to other values presented in table 2.4, these are amongst the smallest ones. When compared to the other studies that employed Owens-Wendt model, K. Van de Velde and P. Kiekens are the only to obtain a dominantly polar character. Moreover, their dispersive component, except for a single type of fibre, was no more than 4 mJ/m^2. An explanation to such a disparity may be provided by the fact that, when polar probe liquids are used (only water and Ethylene glycol were used for measurements in this work), the advancing contact angles tend rise to high values and plateau quickly with the increase in hydrophobic character (or fraction of hydrophobic inclusions, as in Fig. 2.13) of a hydrophilic surface [120] (see Fig. 2.13).

G. Cantero et al. [138] used Wilhelmy technique to study one type of flax technical fibres coming from Finland based on the Owens-Wendt model. No further information was provided on the type of contact angle used in the calculations; nonetheless, having in mind that obtaining receding contact angles of flax is seldom possible and that the angles reported are compatible with advancing values obtained by Wilhelmy technique reported in other works on flax [137, 139], it is likely that those values correspond to advancing contact angles. The presentation and analysis of the results follows a more qualitative approach, limited to showing bars charts and considerations on the relative variation of components. Overall, the surface energy components were intermediate when compared to other works. The main particularity of these is the fact that the dispersive and polar components accounted for almost half of the total each. However, due to the aforementioned uncertainties, these results have to be considered with precaution.

W. Woigk et al. [139] studied technical flax fibres from commercial wet spun UD-woven fabrics [27] using Wilhelmy Technique [28]. These technical fibres were tested in advancing and receding mode at a wetting speed of 1.5 mm/min, a comparatively high value. As expected, surface heterogeneity made impracticable to obtain receding contact angles and, similar to what was done in K. Van de Velde and P. Kiekens [137], all calculations were performed using the advancing values, with all the consequences previously discussed (i.e., overestimation of contact angles). The van Oss model was used to decomposed the fibre surface energy.

When compared to the other values, the total surface free energy obtained in this work is intermediate to low. As it was the case for most of the works, the fibre presented a dominant non-specific character. When compared to the values obtained by c. Baley et al. [144], although the same general trend is seen, with a dominant non-specific component presenting relatively high basic and acid components (for comparison, see [186, 193]), both, specific and non-specific components obtained by the latter are considerably higher. On one hand, as previously discussed, the values obtained by C. Baley and coworkers come from static contact angles, which, in this particular case, seem to be between the most stable and the static receding contact angles, resulting in higher surface energies, W. Woigk et al.; on the other hand, used advancing angles for their calculations, which is expect to result in the opposite behaviour, leading to underestimated surface free energy values.

As compared to K. Van de Velde and P. Kiekens [137], in spite of also using advancing contact angles in their calculations, W. Woigk and coworkers did not observed the dominant non-specific components. Care has to be taken here since two different models with different assumptions on the decomposition of the surface energy components were used.

An additional, argument supporting the results obtained by W. Woigk et al. is built on the basis of a surface chemical analysis made by XPS. The different components of the C1s peak (see section 3.2.4)

[27] Same provider described in section **??**.

[28] Same equipmet described in section 3.2.5.1.

were related to the physical interactions of the fibres, following an approach similar to other works in the literature [194–197]. The C1 peaks were related to non-specific interactions, while C2, C3 and C4 were related to specific interactions. In their work, C1 accounted for about 70% of C1s, which reasonably correlates to the distribution between specific and non-specific components obtained (see table 2.4).

Overall, these results seem to corroborate that the correct treatment of data from such Wilhelmy technique experiments on flax fibres is a nontrivial step, leading to considerable differences in the results. The machines used to measure flax fibres wetting force must have compatible sensitivities $\sim$1 μN [29]. As a result, provided the fibres are rigid enough to avoid bending when immersed in the probe liquids [198], even with a sturdy environmental isolation, tiny perturbations, such as air flow due to machine parts movement may add a significant amount of noise to the results [47].

Washburn's Technique The Washburn's analysis obtains contact angles from capillary rise measurements [176]. It is based on the modelling of an upwards liquid flow in a packed fibre bed, assuming laminar flow of probe liquid through a constant cylindrical pore geometry under negligible gravitational effects (usually assumed between the first 10 to 60 s of capillary rise [176]). This is made on the basis of a combination between the Laplace equation and Hagen-Poisueille equation for steady flow conditions. The main criticisms to this technique are based on its low reproducibility, which stems from significant difficult packed fibre column reproduction, resulting in poorly defined effective pore radii [176]. Measurements with packed non-fibrous modified flax columns, such as flax pulp [138] can be found in the literature, such values were not included in the present discussion since it is questionable whether they really probe the fibres surface and, as previously discussed, the bulk composition may be significantly different. Moreover, liquid-fibres interactions may result in swelling, changing the effective pore radii during the experiments [199].

The Washburn equation relates the mass gained by the fibres column (m) with capillary constant K, associety to its pores geometry, over a time (t) due to capillary rise of a liquid with surface tension γ_{lv} and density ρ that wets the fibres with contact angle θ:

$$\frac{\mathrm{m}^2}{\mathrm{t}} \cdot \frac{\eta}{\rho^2} = \mathrm{K}\gamma_{\mathrm{lv}} \cos\theta \tag{2.40}$$

This technique requires data from a large set of probe liquids presenting surface tensions over a broad range of values. The fibre surface tension is then obtained from a Zisman Plot, in this method the the critical surface tension is obtained, γ_{c}, which refers to the maximum measured liquid wetting rate (i.e., γ_{c} can be thought as the surface tension of an imaginary liquid with maximum value so as to present complete fibre wetting or that "just wets the fibre surface completely" [177]) (see Eq. 2.41).

$$\gamma_{\mathrm{c}} = \lim_{\theta \to 0^\circ} \gamma_{\mathrm{lv}} \cos\theta = \gamma_{\mathrm{sv}} - \gamma_{\mathrm{sv}} \tag{2.41}$$

In this case, when the same conditions assumed in Eq. 2.6 hold, introducing γ_{c}=γ_{lv} in Eq. 2.6 leads to:

$$2\sqrt{\gamma_{\mathrm{c}}\gamma_{\mathrm{sv}}} = 2\gamma_{\mathrm{c}} \Leftrightarrow \gamma_{\mathrm{c}} = \gamma_{\mathrm{sv}} \tag{2.42}$$

Since the properties are measured while the solid is being wetted, the contact angles thus obtained are advancing ones and can be determined if K is known [176], which is often not the case [177]. Therefore, once again, precaution when evaluating these results must be taken.

[29] The current work employed a tensiometer at sensitivity $\sim 1\mu$g

Alexis Baltazar-y-Jimenez and Alexander Bismarck [177], determined the γ_c of Belgian dew-retted flax fibres, by Washburn method using a standard sample holder (Krüss GmbH, Hamburg, Germany) in which a controlled mass of flax fibres were inserted. This study obtained $\gamma_c = 34$ mJ/m^2, a value considerably close to that obtained by I. Aranberri-Askargorta et al. [184], $\gamma_c = 35.5$ mJ/m^2. The latter was performed on dew-retted flax fibres coming from Poland. An interesting result from the study of I. Aranberri-Askargorta and coworkers was the evaluation of the surface tension variation by post-treating the fibres with more sophisticated separation processes after dew retting, such as Ultrasond technique and Steam Explosion, which are known for increasing the removal of waxes and the fibres individualisation [184], fibres thus obtained presented average values of $\gamma_c = 36.2$ mJ/m^2 and $\gamma_c = 38.7$ mJ/m^2, respectively, approaching the value obtained for cellulose fibre using the same method $\gamma_c = 40.3$ mJ/m^2.

When compared to other results in the literature, the values obtained from Washburn's Technique are intermediate. Nevertheless, the validity of such comparisons is questionable since capillary rise is not widely accepted as a means to determine the surface tension of fibres [199], the solid surface energy is obtained from an approximation from the critical surface tension, and the measurements are taken only in advancing mode.

Floating Mode

This method is based on testing pieces of fibre with known size and density against less dense binary liquids mixtures whose surface tensions can be varied over the experiment by changing the mixture proportion. By determining the point of transition between floating and sinking (i.e., the point at which the gravitational forces can be counteracted by interfacial forces), assuming that the fibres have a cilindrical shape and the gravitational effects are negligible, it can be shown that this transition takes place at $\theta \approx 0^\circ$ when the liquid surface tension is equal to the critical surface tension γ_c. If the spreading pressure is assumed negligible, then, as previously discussed, this value equals γ_{sv}. Some concerns related to this technique are stem from the solubilisation of the fibre surface components on the probe liquids and all the factors affecting wetting line geometry, such as water absorption. According to the authors, this method has the advantages of obtaining results without need of extrapolations since the point where $\theta = 0^\circ$ is measured directly, they also state that wetting line equilibrium is stablised at microscopic level, and thus it is not influenced by macroscopic roughness, which, as previously discussed in section 2.1.4.5, results in an important impact on contact angles.

J. M. van Hazendonk et al. [178] used the floating method to study 0.5 cm-long pieces of vacuum-dried flax technical fibres extracted by different degrees of both dew and warm-water retting[30]. Part of those fibres had their non-cellulosic surface components removed by different chemical treatments with increasing degrees of harshness so as to obtain a final specimen whose surface composition (measured in terms of Glucose/Neutral sugars, Lignin and Uronic Acid mass fraction) approached 100% cellulose content. Using polar and apolar liquid mixtures, fibres surface energy was decomposed in polar and apolar components according to Owens-Wendt model. In their study, the results were compared to those of the different surface components of flax fibres (except for pectins) found in the literature. Non-treated specimens retted to a normal degree presented a strong dispersive character, showing values of dispersive and polar components comparable to waxes ($\gamma_{sv}^p \approx 26.5$ mJ/m^2 and $\gamma_{sv}^p \approx 0$ mJ/m^2) [200], those specimens presented a small polar component, which the authors associated to more polar fatty substances, such as triglycerides and phospholipids (a questionable affirmation, since it is widely accepted in the literature, and confirmed by SEM micrographs, [13] that those compounds only partially cover the

[30] values presented in table 2.4 correspond to "normal" retting degree for both dew and warm-water retting

fibre surface). The differences in the values between the different retting degrees were found to be small with warm-watter retting reaching higher values for both disperse and polar components. Extraction of fatty acids caused a significant increase in surface energy (γ_{sv}^{p} ≈37.6 mJ/m^2 and γ_{sv}^{p} ≈ 2.7 mJ/m^2), resulting in a surface mainly composed of cellulose, pectins, and hemicellulose, a subsequent removal of pectins further raised the values (γ_{sv}^{p} ≈ 45.3 mJ/m^2 and γ_{sv}^{p} ≈ 3.4 mJ/m^2), this surface is expected to be mainly composed of cellulose, hemicelluloses and lignin, both values were in agreement with the literature for those components [178], except pectin, whose values were not found. The final fibres were composed of 83wt.% cellulose, with other carbohydrates, lignin and uronic acid accounting for less than 4wt.%, its surface energy was significantly higher than that obtained for the other specimens, notably its polar component, (γ_{sv}^{p} ≈ 50 mJ/m^2 and γ_{sv}^{p} ≈ 10.5 mJ/m^2). When compared to the literature values for cellulose surface tension, only highly oriented cellulose fibres presented comparably high values of dispersive component [201]. The polar component was significantly lower than those found in the literature

Overall, the total surface energies obtained by this method were intermediate when compared to other results for flax fibres. The dispersive components were relatively low, but comparable, to other studies that employed Owens-Wendt model. The polar components, on the other hand, were remarkably low (even after chemical treatments). Another issue comes from the fact that no other study trying to reproduce these results was found.

2.2.1.2 Non-Wetting Techniques

Inverse Gas Chromatography (IGC)

In IGC, differently from wetting methods, the surface free enthalpy of natural fibres and its different components are directly obtained, without need for contact angle measurements. It is a particularly useful technique when measuring surface free enthalpy of irregular, chemically heterogeneous and non-flat surfaces, as it is the case of natural fibres [202]. Additionally, differently from most of the wetting techniques, it considerably facilitates the measurements since technical fibres, instead of the tiny and difficult to handle elementary fibres, can be used for the measurements without the issues caused by swelling [186, 202].

The term *inverse* indicates that the material of interest is placed in a chromatographic column and its interactions with selected, pure test solutes are studied [203] (in contrast to what is done in Gas Chromatography, in which a mixture of different compounds is separated due to different elution times, resulting from different interactions with the column packing material). An experiment of IGC consists of introduction of vapour pulses or frontal injections of adsorbates (also known as solutes or probes) of known surface energy components, in a chromatographic column filled with the analyte (adsorbent - fibres). The retention time and shape of a chromatographic peak are affected by the nature and magnitude of interactions between the adsorbate and adsorbent, which allows to deduce the properties of the latter.

In a pulse experiment, a controlled amount of probe molecule is injected as a pulse, which is transported by the mobile phase (carrier gas, usually an inert gas) through the system to the column with the solid sample. After adsorption and desorption have occurred inside the column a resultant peak (chromatogram) is obtained. The most common method in this case is the so-called infinite dilution IGC, in which a near zero surface coverage of the analyte is obtained; hence, it is assumed that only the adsorption of isolated probe molecules on the solid surface is analysed, allowing to neglect lateral interactions between adsorbed molecules. A criticism to this approach is that adsorption only occurs on the most energetic sites of the solid surface; thus, all the results obtained refer to these particular

sites, their is based on the assumption that the most energetic sites of adsorption of the fibre and matrix surfaces play the most important role in determining the level of physicochemical interactions.

An alternative approach is the frontal injection technique. In this case, the probe molecules are added continuously to the carrier gas and the chromatogram shows a breakthrough curve. Due to the continuous nature of this technique, equilibrium can be assumed throughout the entire experiment, while pulse chromatography requires the assumption of a fast equilibrium approach. Whether or not a pulse experiment represents (quasi-)equilibrium values depends strongly on the carrier gas flow rate, with a lower flow rate being more likely to result in equilibrium, this; however, leads to longer experiments and broader peaks (which may reduce the accuracy of the retention time determination). In this case, it is advisable to repeat the experiment at different flow rates so as to determine the optimum using Van Deemter equation, which relates height equivalent to a theoretical plate (HETP) of a chromatographic column to the various flow and kinetic parameters which cause peak broadening [204].

The free enthalpy of adsorption ΔG°_{ads} is related to the net retention volume V_N of the probe by an Arrhenius relationship:

$$-\Delta G^{\circ}_{ads} = RT\ln V_N + C \tag{2.43}$$

where C is the De Boer or Kemball/Rideal constant [205, 206] (which depends on the reference states and experimental conditions). The free enthalpy of adsorption can be related to the surface properties of the solid and the probes by the work of adhesion:

$$-\Delta G^{\circ}_{ads} = -(\Delta G^{LW}_{ads} + \Delta G^{AB}_{ads}) = aNW^{LW}_{A} - \Delta G^{AB}_{ads} \tag{2.44}$$

where ΔG^{LW}_{ads} and ΔG^{AB}_{ads} correspond, respectively to the non-specific and specific interactions (as previously discussed in Section 2.1.4.1); N is he Avogadro's number; a is the specific surface area of one adsorbed probe molecule; and W^{LW}_{A} is the reversible work of adhesion corresponding to apolar interactions, which can be written according to Eq. 2.5 as follows:

$$W^{LW}_{A} = 2\sqrt{\gamma^{LW}_{s}\gamma^{LW}_{l}} \tag{2.45}$$

where γ^{LW}_{s} and γ^{LW}_{l} are non-specific components of the solid and liquid (or liquid and fibre for this matter) surface energy, respectively.

By using purely dispersive probes, such as n-alkanes, whose ΔG^{AB}_{ads} is null and γ^{LW}_{l} and a are known, the slope of the straight line $\Delta G_{ads}{}^{\circ}$ ($RT\ln V_N$) v $a\sqrt{\gamma^{LW}_{l}}$ allows to calculate the dispersive component γ^{LW}_{s} of the solid surface energy.

The specific free enthalpy of adsorption (ΔG^{AB}_{ads}) is usually treated through the lenses of Lewis acid-base interactions, via two different models, either applying Gutmann's semi-empirical scale [207] ([180–182]) or the van Oss model [125] ([183]).

The Gutmann's semi-empirical scale [207] describes the probe molecules in terms of acceptor (AN, dimensionless) and donor (DN, $KJmol^{-1}$) numbers, which, as their name imply, are related to the ability of a molecule to attract or release electrons, respectively. The analyte (fibre), in its turn, is described in terms K_a and K_b, respectively, acid and base characteristic parameters. These parameters are then related to ΔG^{AB}_{ads} as follows [208, 209]:

$$\Delta G^{AB}_{ads} = K_a DN + K_b AN \tag{2.46}$$

$$\frac{-\Delta G^{AB}_{ads}}{AN} = K_a \frac{DN}{AN} + K_b \tag{2.47}$$

Hence, K_a (dimensionless) and K_b (in $kJmol^{-1}$) are respectively the slope and the y-intercept term of $-\Delta G_{ads}^{AB}/AN = f(DN/AN)$. Since these results cannot be directly compare to the ones obtained in the present work, only the dispersive term of the surface energy are presented in IGC results. Moreover, due to their large scatter (usually 10-20%), the validity of these parameters is is still a matter of debate [210].

Although not common, van Oss model can also be applied to decompose ΔG_{ads}^{AB} [211]. In this case,

$$\Delta G_{s,l}^{AB} = -2(\gamma_{sv}^{+}\gamma_{l}^{-})^{1/2} - 2(\gamma_{sv}^{-}\gamma_{l}^{+})^{1/2} \tag{2.48}$$

The dispersive and Lifshitz-van der Waals components obtained by IGC were the highest ones among the considered techniques. This stems from the widely accept fact that, when infinite dilution IGC is used, the small amount of probe molecules introduced in the column will preferentially interact with the highest energy sites of the surface [181, 202]. A. Legras et al. [183] obtained the different components of the surface energy according to the acid-base theory. Even though their values of dispersive component obeyed the trend of the other IGC measurements, being higher than those from other techniques, the component accounting for the specific interactions was considerably close to the results obtained by W. Woigk et al. [139], which may indicate that the Lewis interactions present less influence of sites energy gradient, either due to less energy variability or due to a higher range of energies probed for these sites.

Atomic Force Microscope (AFM)

The use of AFM to assess the surface energy of flax fibres is significantly more recent when compared to the other techniques. The literature on this method includes a single result on flax fibres [179] and few other results on cellulosic fibres [211, 212]. Besides being a unusual work in terms of technique used, this study also use an unconventional retting method, based on an enzymatic treatment (the complete processing method, fibre variety and isolation and specimen preparation are carefully presented in the original paper).

This technique is based on measurements of the adhesion force F_A between an oscillating microscopic tip with variable radius (R_P) (such as the $2R_P$=51.6 nm n-type silicon-made tip used in the work on flax [179]) and the substrate (fibre). In short, F_A can be extracted from the force required to separate the tip and the substrate at their closest position, where short range van der Waals interactions take place (so-called, pull-off force). This force can then be related to the work of adhesion W_A either by the Johnson-Kendall-Roberts (JKR) (Eq. 2.49) [213] or the Derjaguin–Muller–Toporov (DMT) (Eq. 2.50) [214] contact mechanics models.

$$F_A = 2\pi R_p W_A; \tag{2.49}$$

$$F_A = \frac{3}{2}\pi R_p W_A \tag{2.50}$$

Assuming that the interactions between the fibre surface and silicon tip will be purely dispersive, the dispersive component of the fibre surface energy can be obtained assuming W_A to be as follows.

$$S = 2\sqrt{\gamma_{sv}^{d}\gamma_{tv}^{d}} \tag{2.51}$$

where γ_{tv}^{d} is the tip surface free energy. This kind of measurement could further benefit from the use of Chemical force microscopy (CFM), which would allow for the determination of surface energy components other than the dispersive by carefully tailoring the chemistry of the tip used [211].

Since it allows punctual measurements, this technique is expected to better characterise the surface heterogeneity and roughness of natural fibres [215]. However, because the tip chemistry is not well-defined in this approach (which is not the case in CFM), its results are often considered "more qualitative" [211]. Whether or not this is the case and having in mind the obstacles to comparison of values from different studies previously discussed, the measured value $\gamma_{sv}^{d} = 32.9 \pm 2.1$ mJ/m^2 mostly lies in between the high ones obtained from IGC and those from wetting techniques. Studies employing CFM on flax fibres using a methodology similar to that employed by C. J. Bastidas [211] may allow for detailed characterisation of flax fibres heterogeneities. Additionally, results thus obtained may allow for the determination of Cassie-Baxter and Wenzel's models parameters, eventually enabling more accurate equilibrium contact angles assessment and surface energy determination from wetting methods, which could be compared to those obtained from CFM.

Perspectives

The best methodology to study flax fibres surface energy, allowing to properly consider the adhesion fibre-matrix in FRCs, is still to be determined. Although significant differences between the values of each study are observed, each one of them seem to find a different argument in the literature to claim their validity. Employing wetting techniques incurs a series of issues that obstruct data analysis and comparison, making experiments time-consuming to perform. Flax, in especial, has the additional hurdles of high water absorption and swelling, requiring the use of elementary fibres in most of the cases, which are significantly delicate and almost invisible to the naked eyes; thus, difficult to handle. Although, non-wetting approaches may be a suitable option to avoid these issues, results still present a considerable variability when different studies are compared, again, this could be related to the lack of standardisation of the fibres and absence of well-established experiment conditions hindering reproducibility. Applying a multicomponent decomposition to fibre surface free energy values obtained from non-wetting techniques, instead of simple dispersive component determination, is still needed if these methods are to be used in composites interface design [183], requiring a more sophisticate approach, such as using Chemical Force Microscopy with suitable tip chemistries instead of simple AFM. In spite of the lack of agreement on the best technique, standardisation of the fibres and a careful description of the experimental conditions and assumptions used in the data treatment are needed. The correct understanding of the adhesion mechanisms coming from reliable results of fibres surface energy would allow for more sophisticate simulation, design and optimisation of natural fibre reinforced composites.

2.2.2 Interface Mechanical Characterisation

As previously discussed, three main parameters that determine the interface quality are physico-chemical interactions, chemical bonding and mechanical interlocking. Although the characterisation of each of these phenomena is crucial to obtain a correct understanding of the mechanisms that improve interface quality, isolated, their results may be misleading. Therefore, it is essential to complement the study of those three parameters with an assessment of interface mechanical properties if the effect of a fibre treatment on compatibility and adhesion is to be assessed.

FRC interface mechanics can be assessed in three different scales, namely:

1. **Nanoscopic**: by testing microstrains and stresses locally at the fibre-matrix interface. As a result, microscopic-scale phenomena, such as mechanical interlocking, will not be accounted for. Nanoscopic interface strength can be obtained using techniques such as Raman Spectroscopy [216],

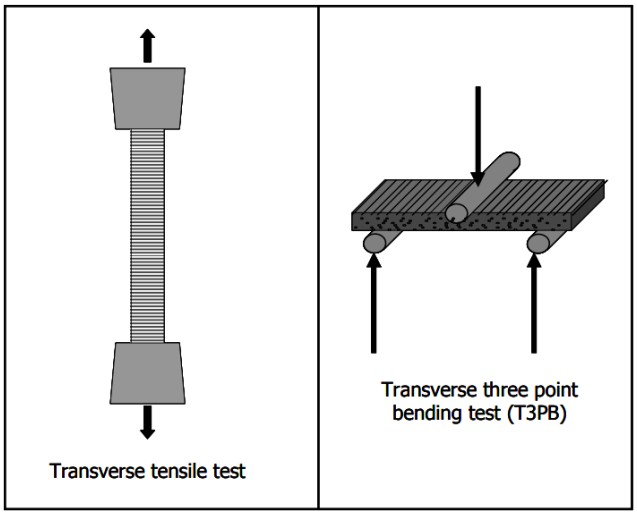


Figure 2.32: Schematic representation of the transverse tensile test and the transverse three point bending test (transverse 3PBT) on unidirectional (UD) composites [35]

nanoindentation, nano-scratch tests, nano-mechanical imaging techniques, among others [186][31];

2. **Microscopic**: at the microscopic level, physicochemical interactions and chemical bonding are added of mechanical interlocking. As briefly mentioned in section 2.1.5, some of the micromechanical interface characterisation used for FRC are push-out (microindentation), pullout, single fibre fragmentation and microbond.

3. **Macroscopic**: indirect determination of the interfacial adhesion by studying off-axis loading [217]. The most common macroscopic techniques used to assess interface strength in natural fibres composites are transverse tensile and bending tests and short-beam shear test.

Natural fibres reinforced composites are usually characterised using Micro or Macroscopic techniques [35]. The advantages, disadvantages and results obtained from such techniques are discussed below. The main objective of this discussion is to determine the best technique to be used in the present work and compile results for latter comparison. Studies whose results present greater relevance for the present work are described in greater detail.

2.2.2.1 Macromechanical Techniques

The most common approaches for assessing the mechanical performance of composites interfaces are based on fast and straightforward static mechanical analysis at the macroscopic scale. By using test samples (generally unidirectional [UD] composites) with controlled shape and dimensions, usually imposed by standards, certain loading condition and corresponding failure modes can be induced so as to highlight the impact of the interface on the mechanical properties and reduce that of the fibres and matrix [186] (i.e., no intrinsic interfacial property is measured). Consequently, such measurements do not allow for direct assessment of intrinsic interfacial properties, but obtain it within the context of certain loading conditions, nature of the induced stresses and composite microstructure, which tend to vary considerably in different studies, hindering their comparison, usually done in a more qualitative than quantitative fashion.

[31] All these require exhaustive polishing of the material to reduce surface roughness

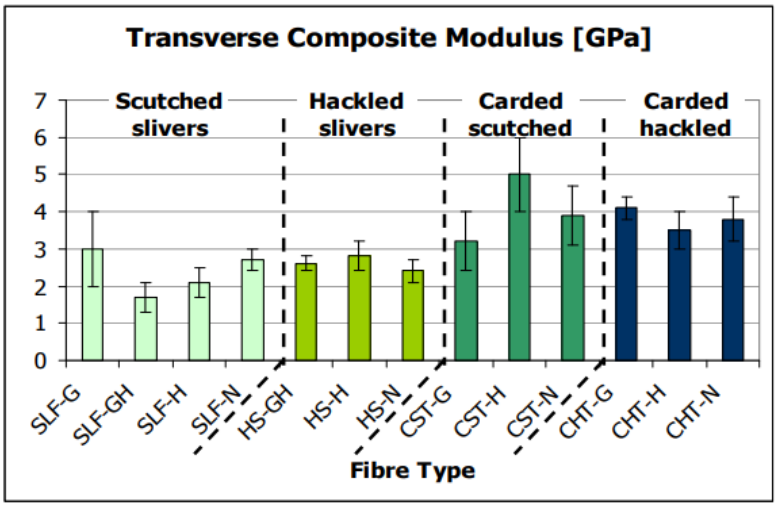


Figure 2.33: Tensile strength in transverse direction of UD flax/epoxy composites (v_f=40 vol%). The data are grouped per processing step of the flax reinforcement: S-Scutched; H-Hackled; C-Carded. Different fibre types are used as reinforcement: L-Long; S-Slivers; T-Tow;. Fibres with different degrees of retting were used: G-Green; GH-Green Half Retted; N-Normal Retted [35]

2.2.2.1.1 Transverse Tensile and Bending Tests

The mechanical behaviour of UD composites loaded in transverse direction is predominantly determined by the matrix and interface properties, hence it can be used to characterise interface quality [113]. In this case, the ultimate strength of the UD samples, measured either in tensile or flexural (bending) mode (see Fig. 2.32), is related to the interface strength. To investigate the influence of interfacial adhesion on the composites strength, the efficiency factor of the longitudinal strength, the ratio of the experimental longitudinal strength to the ideal value calculated using the rule of mixtures, is usually calculated [193].

Even though tensile mode specimens preparation and tests are straightforward and do not require a considerable amount of time, their results are considerably influenced by imperfections in the sample, which may cause underestimation of the interface properties. Flexural mode setup allows for smaller gauge lengths, reducing the probability of critical defects in the tested length, leading to better results [35]. Moreover, to assure that the recorded values are characteristic of the interface and not of individual phases, it is important to study the fracture surfaces. In the ideal case, the fibres at the fracture surface will be free of matrix [193]. Additionally, stress concentration at the loading nose may cause compressive failure, which does not have a straightforward relation with interface mechanical properties [35].

In natural fibres composites, transverse mechanical tests are mostly used as a technique for fast screening of interface quality and additional validation of micromechanical tests. As previously discussed, their main limitations are the presence of structural imperfections (voids, micro-cracks or surface irregularities) resulting from processing, which may influence the result to an important degree. Even when flexural mode is used, reducing the gauge length, and hence the probability of critical defects, techniques to inspect the specimens for defects are mostly limited to visual inspection and post-processing treatments, such as polishing, which result in an important degree of human error. Moreover, the final specimens will always be influenced by the mould used in their fabrication. Therefore, the results should be interpreted with care [35].

I. Van de Weyenberg [35] studied the influence of flax fibre (Arianne variety harvested in 1996 in Alveringem, Belgium) processing and chemical treatment with an aminosilane sizing on the interface

properties of a composites based on epoxy resin (HM 533, E=2.9 GPa and σ_u=50 MPa) using transverse tensile and flexural tests. The results for fibres with different degrees of retting at different processing stages were obtained in tensile mode. The tensile strengths varied from 3 to 12 MPa (considerably below the matrix tensile strength) for specimens made with 40 vol.% (see Fig. 2.33), indicating a positive result of the processing steps, which is attributed to a higher degree of fibres weak areas removal and a better resin impregnation. The degree of retting [32] presented no explicit correlation with the transverse strength, according to the author, the slight tendency to an improvement with the degree of retting observed in the case of scutched flax (long fibre and short carded fibre) as opposed to hackled flax may be an indication that the latter present a higher degree of impurities, which are removed during retting, those impurities are expected to influence the interface properties of the composites. The results have to be considered with a significant degree of precaution, since imperfections in the specimens are likely to be reducing their final properties.

In the same work I. Van de Weyenberg also studied aminosilane (aminoethylaminopropyltrimethoxy) sized flax epoxy composites, now performing transverse 3PBT measurements. Even though the relative error in the results is significantly high, reaching ca. 24% in certain cases (see Fig. 2.34), there seems to be a slight increase in interfacial strength due to the treatment. When the same tests were conducted using microbond technique (presented in section 2.1.5), a weak, but positive correlation was obtained between the bond strength, τ_d (IFSS, see section 2.1.6.1), and the transverse flexural strength, with a correlation coefficient of 0.6409, was obtained (see Fig. 2.35). The three outline specimens correspond to mild silanisation treatments. According to the author, an explanation for their out-of-trend behaviour may be an additional curing step at high temperature used to manufacture the transverse 3PBT specimen manufacturing, but not the microbond specimen, which may have led continuation of siloxane curing whose reaction completion could not be attained due to the mild conditions, such unreacted layer woruld act rather as a weak interface in the microbond specimen.

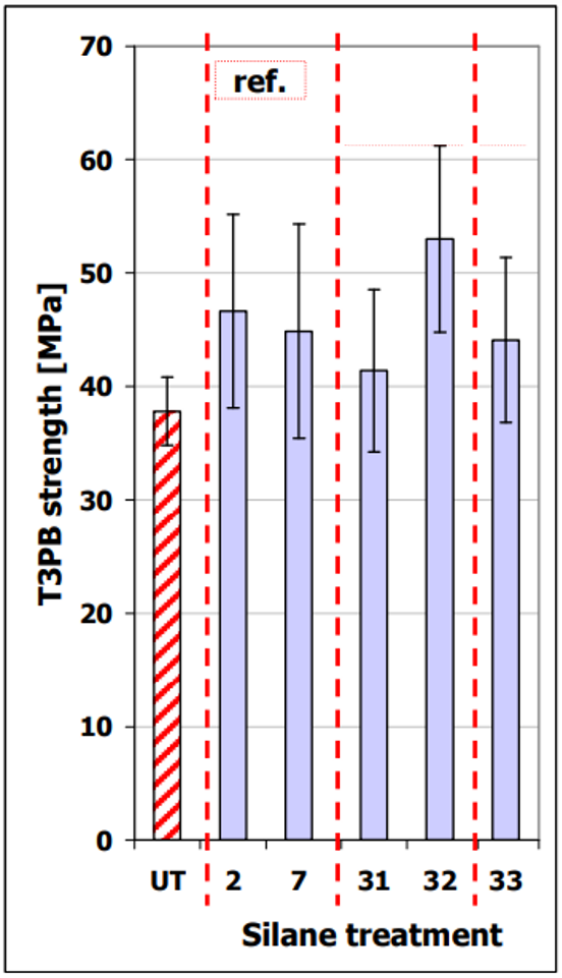


Figure 2.34: The transverse three point bending strength for several flax/epoxy systems. For the specimens code, please refer to Fig. 2.35. Only optimal results are presented. For details about the procedure and the complete set of results, please refer to the source. Modified from [35]

To complement the analysis, the fracture surfaces were also studied. Remainders of matrix material were observed on specimens that presented a higher flexural strength (i.e., matrix failure, Fig. 2.36a), while low flexural strength was correlated to clean fibre surfaces (i.e., interface failure, Fig. 2.36b). Once again, a good agreement with the results obtained by transverse 3PBT was proved.

[32] Green fibres correspond to non-retted straws that had their husks removed by rippling), half-retted and normal retted

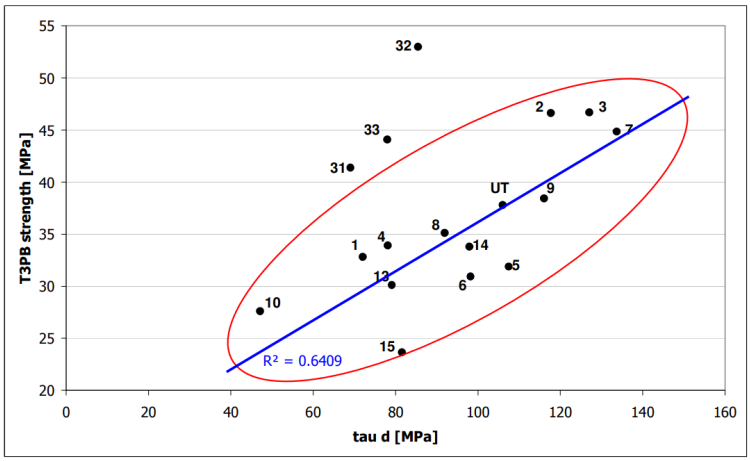


Figure 2.35: Comparison between the interfacial shear strength, obtained from a stress-based approach similar to that presented in section 2.1.6.2, added of an experimental frictional stress (constant stress observed after debonding) (X-axis), and the transverse flexural composite strength, measured by three point bending (Y-axis). A positive correlation between both data series can be noticed, with a correlation coefficient of 0.6409. Different numbers refer to modified silanisation treatment. UT symbolises the untreated fibre. Specimens 2 and 7 are identical and underwent the standard treatment, Specimens 31 and 32 are also identical and underwent the same treatment with slightly modified parameters (ethanol silane solution instead of water/acetone and 50 °C instead of 105 °C after silane-curing step). 33 correspond to a specimen that underwent the same treatment as 31 and 33, but was not degreased. For details about the procedure and the complete set of results, please refer to the source. Modified from [35].

Fibre failure either due to cell wall removal (Fig. 2.36b) or fibres splitting (2.36d) occurred in both cases, this highlights the need for internal fibre adhesion improvement, which may be as detrimental as poor interface strength. The author states not to be completely aware of the root causes of the overall bad performance of this treatment, which are most probably related to a bad coupling between the sizing and the fibres since the chemistry matrix-sizing is well-understood and controlled for the similar case of glass fibres. Overall, transverse 3PBT seems to be in good agreement with other results and indicates no or small impact of the aminosilane treatment, as performed by I. Van de Weyenberg, on the interface strength.

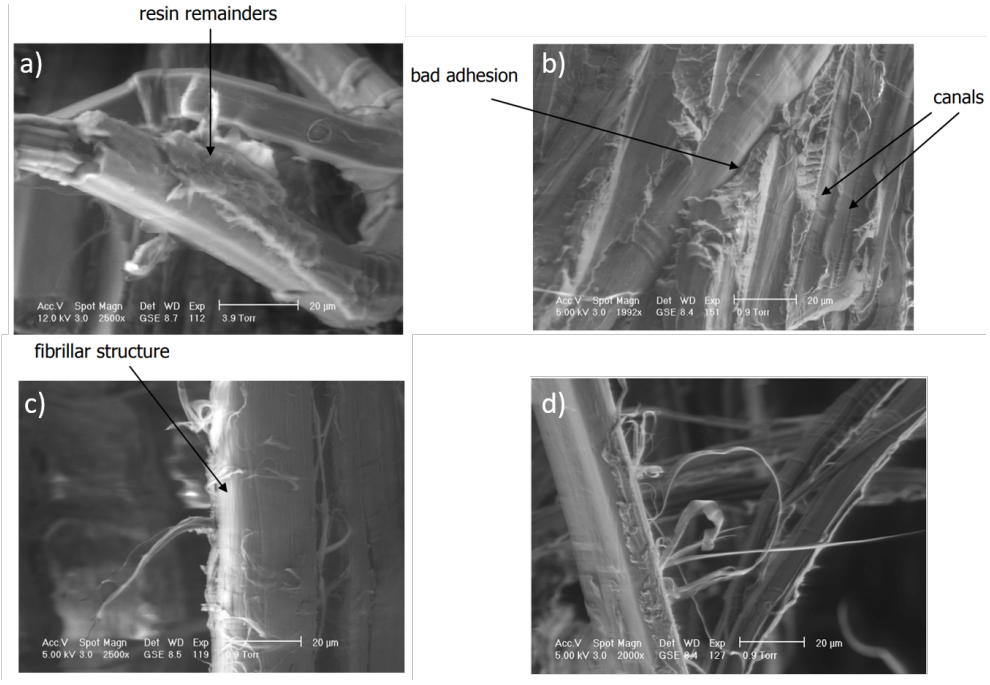
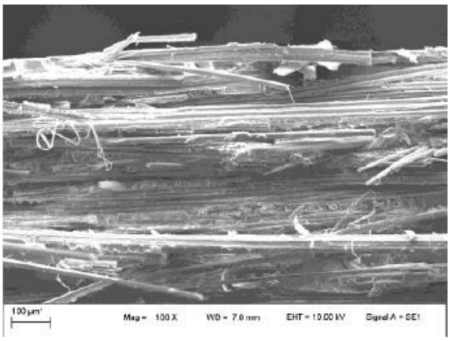


Figure 2.36: Transverse 3PBT failure surfaces showing the correlation between high flexural strength specimens and matrix failure, leaving resin remainders on the surface of the fibres a), poor flexural strength specimens and interface failure, resulting in a clean fibre surface and clean and smooth matrix surface in places from which the fibres were removed (canals); moreover, a gap can be seen between the matrix and a still embedded fibre, further indicating bad adhesion. b) In both cases, poor internal fibre adhesion caused either out cell wall decohesion, revealing aligned microfibrils structure c) or fibre splitting in longitudinal direction d). Modified from [35].

Notwithstanding Van de Weyenberg's results, using transverse 3PBT to study the interface quality of UD flax-epoxy composites after the fibres were sized using an aminosilane compound (3-aminopropyltrimethoxy silane), T. Chi [218] observed a significant improvement in IFSS. Indeed, composites made using the silane-sized fibres presented a transverse strength of 17 MPa, value that was more than the double of that obtained using non-treated fibres, 8 MPa.

L. Q. N. Tran et al. [52] also studied the interfacial adhesion of flax fibres (long fibres for composite-



Flax/PLA

Table 2.5: Typical SEM images of the fracture surface of flax fibre composites in transverse 3PBT [52]

Table 2.6: Work of adhesion, interfacial energy, transverse strength and efficiency factor of longitudinal strength of different fiber-matrix systems

Composite	W_A (m^J/m^2)	Interfacial energy (m^J/m^2)	Transverse strength (MPa)	Efficiency factor of longitudinal strength
U-Flax/PLA	83.7	0.1	19.2± 1.6	0.77
A-Flax/PLA	84.7	0.6	22.1± 6.7	0.82

making applications, Lineo - Belgium) composites, using a bio-based Polylactic acid (PLA) as matrix. In order to remove waxes and other fatty substances from the surface of untreated fibres a treatment using an alkali solution (NaOH 3% aqueous solution) followed by de-ionised water washing and vacuum drying at 90 °C for 2h was applied to part of the fibres. 3PBT specimens were tested in longitudinal and transverse directions so as to assess interface adhesion. Surface energy (measured by Contact Angle using the Wilhelmy technique) and SEM study of the failure surface were employed in parallel. Results are summarised in table 2.6 and Fig. 2.5. Even though the standard deviation associated with the results was considerably high, the transverse flexural strength seems to indicate an increase in interfacial adhesion in the treated specimen from 19.2 ±1.6 MPa to 22.1 ± 6.7 MPa. Measurements in the longitudinal direction also indicate interface quality improvement, with an increase of the efficiency factor of longitudinal strength from 0.77 to 0.82. Finally, the results from surface energy assessment corroborate those obtained from 3PBT, with improvements in work of adhesion and interfacial energy, which was correlated to an increase in the polar component and decrease in the dispersive component of the fibres (expected behaviour for waxes removal - refer to section 2.2.1). Fractographs of transverse 3PBT specimens presented fibres with clean surface, indicating that the results are representative of the interface strength. According to the author, the improvements are probably linked to a pure physical adhesion improvement, considering that no chemical bonding between the surfaces is expected to take place. Once again, the 3PBT presented a good agreement with the additional experiments.

To be added: [219]

2.2.2.1.2 Short-Beam Shear Test

Short-beam shear test is basically a 3PBT in which the specimen has a low span-to-thickness ratio (typically 4 to 5 [186]) so as to induce interlaminar failure due to shear stresses, rather than tensile failure. The shear stress at break (interlaminar failure) of a short-beam shear test specimen, interlaminar shear strength (ILSS), is mostly dependent on the matrix and interface mechanical properties and can be used to characterise the interface strength.

As transverse 3PBT it can be used as a quick and simple method of interface quality characterisation. As a test for fibre composites interfacial strength, short-beam shear test is less dependent of specimen imperfections than 3PBT [220]. Just as in 3PBT, interfacial failure must be certified by fractography and only results obtained using the same matrix system at the same fraction of fibres can be compared

among them to evaluate interface strength.

An interesting result from short-beam shear tests was obtained by H. Bos [41] in study comparing composites based on epoxy resin (Ampreg 20, cure with ultraslow hardener, 100:30 (w/w)) filled with 50 wt.% of untreated flax fibres (warm-water retted from the Netherlands) to those obtained at the same weight fraction for viscose fibres (semi-synthetic fibres whose composition is approximately 90% regenerated cellulose.), both prepared at room temperature via pultrusion. A ILSS of 15.4±0.4 MPa was obtained for flax, which was less than half that obtained for viscose, 39.6±0.6 MPa, even though the flax fibres used in the experiments presented a tensile strength approximately 30% higher than the tested viscose fibres. This result clearly presents the impact of interface quality on the properties of fibre reinforce composites, without which the potential of the reinforcement cannot be fully explored. After dewaxing by ethanol extraction, this difference felt to 25.4±05 MPa against 37.8±0.9 MPa for viscose fibres, showing how detrimental the weak waxy layer on the surface of untreated flax fibres can be to composites properties.

ILSS is widely accepted as a method to assess natural fibres reinforced composites interface quality; however, its main disadvantages, similarly to transverse 3PBT, lay on the high experimental conditions-dependence of the results, even for similar fibre-matrix systems. For instance, C. Campana et al. [221] obtained ILSS values around 23.02±1.62 MPa using epoxy resin (DER 332, IPDA hardner 80:20 (wt/wt)) and 30wt.% untreated flax fibres prepared by vacuum infusion, while S. Sathish, also studying epoxy-untreated flax composites prepared by compression moulding obtained results around 3 MPa.

2.2.2.2 Micromechanical Techniques

Differently from the previous methods, micromechanical techniques allow for direct assessment of intrinsic interface properties, enabling straightforward comparison between different studies. As previously mentioned, these properties are a combination of the physicochemical interactions, chemical bonding and mechanical interlocking. As trade-offs, great care is required in the manufacturing of complex and delicate samples, and results analysis demands less straightforward models.

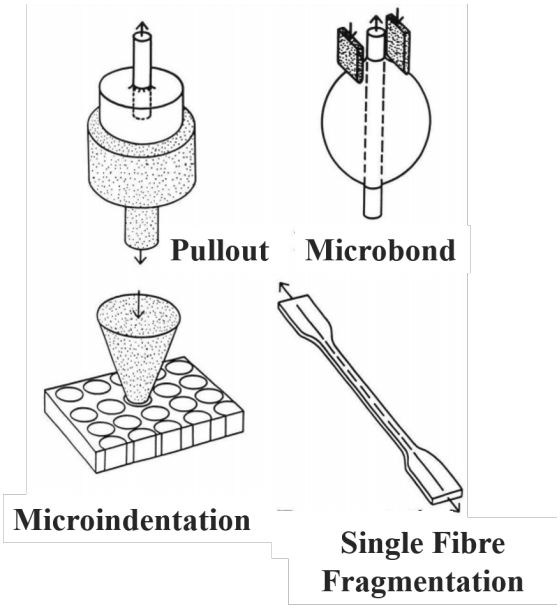


Figure 2.37: Schematic representation of different micromechanical tests for interface characterisation. Modified from [36].

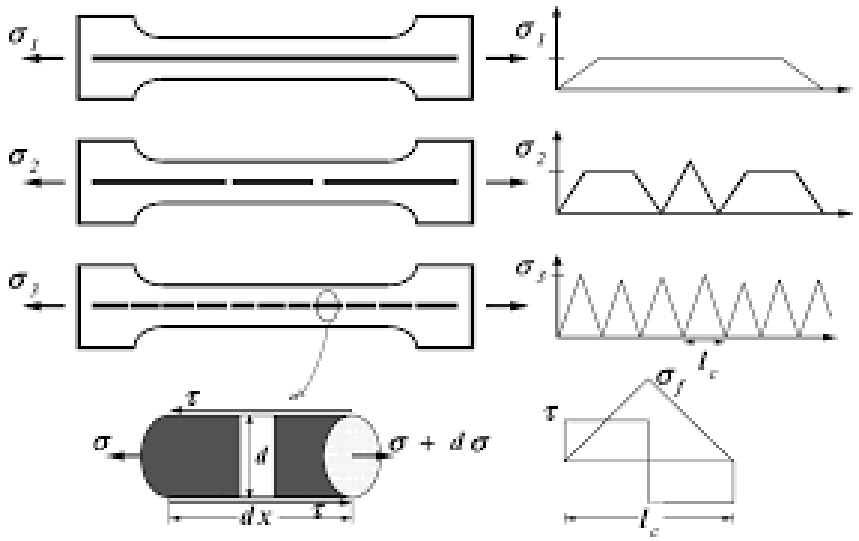


Figure 2.38: Specimen with increasing number of fibre breaks due to increased strain levels in the matrix. Right: Stress in fibre as function of position for the respective matrix strain levels. Zero stress corresponds to a position with a fibre break [37]

2.2.2.2.1 Pullout Test

Similar to the microbond test, the classic pullout is based on tensile loading of technical or elementary fibres embedded in a (fixed) polymer matrix with defined embedded length (see Fig. 2.37). According to the fibre tensile properties, this embedded length is varied so as to have interfacial failure, rather than fibre failure.

The force required to initiate debond and than pullout of the fibre are recorded and treated using models similar to those presented in section 2.1.5. Classic pull ou results in hard embedded length and alignment control when applied to fibres with diameters in the range of a few microns, reason microbond is almost always preferred to classic pullout.

2.2.2.2.2 Single Fibre Fragmentation Test

The IFSS of a fibre-matrix system can also be obtained using single fibre fragmentation test. Each test specimen for the single fragmentation test consists of one fibre encapsulated in a chosen polymer matrix, usually, dogbone-shaped (see Fig. 2.38). Elongating the specimens in a tensile tester results in fibre breakage. This experiment is done under light microscope so that the fragmentation process can be observed in-situ. The fibre inside the resin breaks into increasingly smaller fragments at locations where the fibre's axial stress reaches its tensile strength. This requires a resin system with a sufficiently higher strain-to-failure than the fibre's. When the fibre breaks, the tensile stress at the fracture location reduces to zero. Due to the constant shear in the matrix, the tensile stress in the fibre increases roughly linearly from its ends to a plateau in longer fragments. The higher the axial strain, the more fractures will be caused in the fibre, but, as the fragments length become too short to transfer enough stress into the fibre to cause further breakage, the number of fragments plateaus (see Fig. 2.38). Fibres can break along their length away from the ends by a critical length characteristic of their ultimate tensile strength. If the fragments length exceeds 2 times the critical length, the process repeats itself by the same mechanism. Once all the broken pieces are reduced to less than twice the critical length, further elongation of the test specimen will not cause a tensile stress transferable to the fibres; hence, no further

fragmentation can take place after this point. The final fibres fragments length distribution can be related to the interfacial shear strength [37], e.g., using elementary shear-lag analysis (e.q. 2.52)[33]

$$\tau = \frac{r_f \sigma_u}{l_c} \tag{2.52}$$

where σ_u is the fibre tensile strength and l_c is the critical length.

This test requires previous knowledge of the fibres tensile strength at the critical length, usually obtained from single fibre tensile tests on specimens of different gauge lengths, allowing to extrapolate the tensile strength at critical length by statistical methods, such as Weibull distribution [35].

The main concerns when using single fibre fragmentation test to study natural fibres are the possible damages and structural modifications caused by specimen preparation, and fibre splitting, which can render results interpretation complex.

Studying the effect of isostatic polypropylene matrix transcrystalinity on dew-retted flax fibres from the Netherlands, N. E. Zafeiropoulos, C. A. Baillie and F. L. Matthews [222] obtained IFSS values varying from 12 to 23 MPa (as calculated from Eq. 2.52) and critical lengths varying from 1185 μm to 711 μm according to the specimen processing conditions. Having in mind their specificities, these results seem to be in good agreement with the range of values obtained in works employing microbond. Comprehensive results were obtained by A. Stamboulis, C. Baillie and E. Schully [223] studying different thermoplastic matrices-flax fibre composites, their results was comprised between 5.6 MPa, for low density polyethylene (LDPE), and 18 MPa, for high density polyethylene, for flax-PP composites an IFSS of 17.3 was obtained in this study (in good agreement with the previous study).

Also using single fibre fragmentation, R. Joffe, J. Andersons and L. Wallstrom/ [224] studied composites made using elementary enzyme-retted flax fibres from Finland and different thermoset matrices. The IFSS values obtained in this work were 33±7 MPa when an epoxy matrix was used, 28±11 MPa for vinylester and 13±2 MPa for polyester. Additionally a treatment to improve interfacial adhesion using maleic anhydride was tested, the treatment resulted in a decrease in the final IFSS to 24±3 MPa. When compared to other IFSS values from microbond test experiments in the literature, which are usually comprised between 13 MPa and 23 MPa [29, 168, 225], the results obtained in the latter study seem to be slightly high.

2.2.2.2.3 Microindentation

Also referred to as push-out, microdebond [34] or simply indentation test, microindentation is based on the indention setups developed for microhardness tests in metals. Basically, the test consists of indenting fibres in a UD composite and record the force required to debond initiation (push-in test) or complete interface failure (push-through test) (see Fig. 2.37). In both cases, the IFSS can be obtained from the debonding force.

Microindentation allows to test specimens obtained from cuts perpendicular to the fibres direction. Fibres embedded length can be controlled by polishing the specimens and varies according to the type of microindentation test (it is usually in the tens of microns for push-through test), this step can damage the specimen, significantly influencing the results [226].

Since natural fibres tend to fail by split under compressive load, this kind of test is not suitable for flax fibres composite. Additionally, fibre bundles interface is prone to fail during polishing if a thin

[33] This analysis is often criticised for over simplifying the problem (refer to N.E. Zafeiropoulos, C.A. Baillie and F.L. Matthews [222]).

[34] Not be be confused with microbond

Table 2.7: Compilation of IFSS values available in the literature for various systems Flax-Epoxy Resin. Typical Glass Fibres-Epoxy Resin and Regenerated Cellulose(Lyocell)-Epoxy Resin IFSS values are presented for comparison.

Fibre type	**Variety (Origin)**	**Retting Technique**	**Resin (Type-Trade name)**	**IFSS (MPa)** Apparent	**IFSS (MPa)** Stress-Based▲	**IFSS (MPa)** Linear Regression	**References/Publication**
Glass	—	—	Epoxy (DGEBA-Epolam2020)	29.3 (±2.4)	—	—	[144]/2006
Lyocell*	—	—	Epoxy (EPOTUF,37-127)	14.8 (±3.2)	—	—	[227]/2012
Flax	Melina (Picardie [FR])	Dew Retting	Bio-Epoxy (DGEBA-SuperSap)	11.9 (±4.1)	—	11.8	[53]/2014
	Melina (Picardie [FR])	Dew Retting	Epoxy (DGEBA-Epolam 2020)	20.4 (±4.0)	—	20.1	[53]/2014
	Melina (Picardie [FR])	Dew Retting	Bio-Epoxy (DGEBA-Greenpoxy 55)	17.0 (±5.0)	—	16.4	[53]/2014
	Melina (Picardie [FR])	Dew Retting	Bio-Epoxy (DGEBA-Epobiox STR 100)	28.5 (±6.4)	—	25.4	[53]/2014
	Electra (Normandy [FR])	Dew Retting	Epoxy (DGEBA-Epolam2020)	13.2 (±3.2)	—	—	[29]/2012
	Marilyn (Normandy [FR])	Dew Retted	Epoxy (DGEBA-Epolam2020)	17 (±4)	—	—	[168]/2015
	Viking (Normandy [FR])	Dew Retting	Epoxy (DGEBA-Epolam2015)	22.7	—	—	[144]/2006
	Hermes (Normandy [FR])	Dew Retting	Epoxy (DGEBA-Epolam2020)	22.5 (±1.5)	—	—	[29]/2012
	Hermes (Normandy [FR])	Dew Retting	Epoxy (DGEBA-Epolam2020)	22.3 (±2.1)	—	—	[167]/2013
	— (Harbin [CN])	—	Epoxy (DGEBF-NPEF-170)	23.6 (±3.5)	—	—	[166]/2016
	Arianne (Alveringem [BE])	Dew Retting	Epoxy (DGEBA-HM 533)	23 (±7)	106	—	[35]/2005

∗ Regernerated Cellulose

▲ Stress-Based Model Empolying Shear-Lag analysis

specimen (few tens of microns) is needed, as it is the case for push-through test. Except for the attempts made in the present work, which were stopped in the polishing step after several failures in the attempts to achieving the correct thickness without destroying the sample, no studies testing flax fibre composites using microindentation could be found in the literature.

2.2.2.2.4 Microbond Test

In the present study the microbond test was used. The current section aims to present and discuss some relevant results in the literature of flax fibres composites obtained using microbond test with focus on epoxy resin matrices. Table 2.7 summarises the microbond results as of today in the literature for flax-epoxy resin composites.

Carbohydrates such as hemicellulose, pectin and notably cellulose, and other polyhydroxilated molecules, such as lignin, are the main structural components of natural fibres. As demonstrated by surface energy studies [200], when the weakly attached waxy layer is removed from the fibres surface, it acquires a notable polar character, consequently, tends to present stronger interfaces when used as reinforcement in composites made of polar matrices, such as epoxy resins. The typical IFSS values obtained for this two kinds of matrices highlight this fact. A. Stamboulis, C. Baillie and E. Schulz [223], while studying the interface of flax fibres composites made with various apolar thermoplastic matricess obtained IFSS values comprised between 5.6 MPa for low density polyethylene (LDPE) and 18 MPa for high density polyethylene (HDPE), range that is below the great majority of interfacial shear strengths obtained in studies using epoxy as matrix available in the literature, as per table 2.7.

Most IFSS results obtained for flax-epoxy systems available in the literature concentrate around 23

MPa. Although results from systems composed of French flax made with DGEBA Epolam 2020 epoxy resin resin may dominate the publications, which may introduce a bias in the data, independent works using Belgian and Chinese flax fibres and different epoxy resins seem to confirm this trend. It is notable; however, that two varieties of fibres (Electra and Marilyn), even when retted likewise, seem to present lower interface strengths when used as reinforcement for DGEBA - Epolam 2020 resin. Noticing this fact, A. le Duigou et al. [29] studied Electra and Hermes fibres, whose IFSS values are 13.2±3.2 MPa and 22.5±1.5 MPa, respectively. Using Laser Confocal microscopy and SEM, it was proved that Electra fibres present a slightly thicker resin penetration layer and a rougher surface, which usually correlate to a better interface adhesion. The different behaviour seems to stem from a difference in biochemical composition. A micro-volume chemical analysis in an approximately 2 μm-depth surface layer indicated considerable changes in biochemical composition, in spite of not presenting significant surface chemistry differences up to 10 nm-depth, as observed using XPS. This result highlights the existence of a complex interface between matrix and fibre, and indicates that assuming its area and chemistry equal to that of the surface at the small depths probed by XPS (about 10 nm [228]) may result in underestimation of the specimens real properties. Additionally, the importance of indicating fibres variety and origin is highlighted.

L. Marrot et al. [53] studied composite systems based on flax fibres (Dew-retted Melina flax from Picardie, France) and different bio-based epoxy resins using microbond technique (see Melina fibres results in table 2.7). According to the authors, the main contributors to adhesion between flax and both bio- and petrochemical-based resins were hydrogen boding and van der Waals interactions between fibre hydroxyls and epoxy resin epoxide groups and frequently amino groups, depending on the hardener used. In this study, in addition to the usual apparent interfacial shear strength calculated using Eq. 2.28, which is expected to change according to the drop embedded length due to friction between matrix debonded surface and the fibre (see discussion in section 2.1.5), a second value was calculated from a linear regression of the curve apparent IFSS as a function embedded length, which is expected to reduce the impact of friction stress. Such approach resulted in regression with coefficients of determination ranging from 0.65 to 0.82 and did not resulted in statistically different outcomes, which is expected to be an indication of low frictional stresses impact on the results[35]. Regarding the absolute values of IFSS obtained for bio-based resins, significantly different behaviours were obtained. Such systems resulted in both the greatest and the smallest apprarent IFSS values, 28.5±6.4 MPa and 11.9±4.1 MPa. According to the author, the root cause to this difference was mostly the nature of the hardener used. While the highest IFSS system was cured using a polyamine hardener (similar to that usually used for petrochemical-based DGEBA-Epolam 2020), the lowest IFSS system was cured using a polyamide hardener, even though both are expected to contribute to hydrogen bonding, polyamide hardeners are known for a lower reactivity, yielding final materials with poorer mechanical properties, which may have a negative impact on the fibre-matrix adhesion (e.g., by improving matrix failure as opposed to interface failure[36]). Indeed, the stiffness and strength of the bio-based epoxy resins were found to correlate with the measured values of IFSS. Overall, this work highlights that bio-epoxy resins may be as good or even better than petrochemical-based resins in terms of practical adhesion with flax fibres, which seems to be importantly affected by type of hardener chosen, often neglected when comparing micrbond results.

A. Lefeuvre et al. [168] investigated the role of the main cell-wall polysaccharide-constituents on the internal cohesion between cell-wall layers by performing successive solvent extractions with increasing degrees of harshness so as to gradually remove fibre components. Microbond experiments in a system flax (Dew-retted Marylin from Normandy, France) - epoxy (DGEBA - Epolam2020) resin were

[35]Embedded lengths smaller than 200 μm were used.

[36]The authors do not present a detailed discussion about this particular point.

Table 2.8: Apparent IFSS calculated for flax fibres that underwent extraction increasingly removing the polysaccharides in their structure [53]

Extracted Components	IFSS (MPa)	Peeling (%)
Untreated	17^{a} (± 4)	8.3
Cortical Residues	17^{a} (± 4)	33.3
Middle Lamella Pectins	15^{bc} (± 2)	29.6
Elementary Fibre Matrix Pectins	15^{bc} (± 2)	57.1
Structural Hemicelluloses and Pectins*	16^{ac} (± 4)	15.0

* molecules interacting with cellulose microfibrils
a,b and c indicate statistically different groups

performed so as to assess whether the removal of fibre compounds would cause internal fragilisation, which could be related to an increased occurrence of pilling (for typical pilled fibre surface in microbond test, see Fig. 2.22 C1-C3). First the fibres were cleaned from cortical tissue, then remaining middle lamella pectin was removed, this was followed by the removal of pectins from the fibre matrix and then structuring hemicelluloses and pectins (molecules interacting with cellulose microfibrils). The remaining fibre consisted basically of cellulose and a small percentage of lignin of Klason (a highly stable mixture of modified biomolecules), see table 2.8. The differently treated specimens presented no significant difference in IFSS, whose average varied from 15 MPa to 17 MPa, additionally, with the exception of the fibres that underwent all the treatments, an increasing degree of pilling was observed, indicating fibre fragilisation. On the other hand, J. M. van Hazendonk et al. [178] performed similar extraction processes and observed significant increase in both dispersive and polar components of flax after each treatment, which is expected to improve the interface strength between flax and epoxy resin (this study is further discussed in section 2.2.1). A. Lefeuvre et al. and J. M. van Hazendonk et al. results suggest that the effect of physicochemical interactions improvement may not result in a stronger adhesion between the composite phases if fragilisation takes place. Indeed, as previously discussed in section 2.2.2.1.1, when phenomena such as pilling take place, the actual interface strength being measured is that between the different fibre components, rather than the fibre-matrix interface. According A. Lefeuvre and coworkers the reduction in pilling for the specimen that underwent all the chemical treatments was probably due to hydrogen bonding between cellulose microfibrils after rearrangement in a more compact structure.

As previously discussed in section 2.1.6.2, although more complex, the values of IFSS from the stress-based model are still qualitative ones when applied to natural fibres composites. I. Van de Weyenberg [35] carried out the single study that can be found in the literature trying to apply the stress-based model to characterise flax fibres-epoxy composites interface strength from microbond tests. As no direct determination of the debonding force was possible from the measurement readings, several attempts to decouple the maximum recorded force from the frictional forces were tried. A semi-empirical approach using the frictional forces from the plots after interface failure was judged to be the best fit, yielding the most reasonable results, still, the absolute values were considered significantly high, being 106 MPa for untreated fibres and reaching 133.7 MPa for silane treated fibres [35]. In spite of this concern, such qualitative method allowed to demonstrate the smoothing of flax fibres due to silanisation, factor that may have contributed to the inefficiency of this treatment in increasing the interfacial strength to a significant extent. It was concluded that friction plays an important role in the debonding process to the extent that frictional stress can equal the bond strength of flax-epoxy composites.

Table 2.9: Factors affecting the mechanical properties of flax fibres. Modified from [54]

Plant Growth	Variety, Cultivation, Origin, Fibre Location in the Stem, Climate (e.g., rainfall and temperatures during growth)
Harvesting Stage	Fibre Ripeness, which affects: cell wall thickness, coarseness of fibres, adhesion between fibres and surrounding structure, size and shape of lumen, porosity, and microfibril angle
Fibre Extraction Stage	Decortication Process, Retting Method, Separating Conditions
Supply Stage	Transportation Conditions, Storage Conditions, Age of Fibres
Measurement Conditions	Crosshead Displacement Rate, Gauge Length, Moisture, Temperature, Specimen Cross-Section Variability
Surface Treatment	Chemical treatment, Upgrading Treatment, Water Treatment, Drying Treatment, among others.

2.2.3 Tensile Properties

Flax fibres mechanical properties are no exception when it comes to variability. It was shown that a wide variety of parameters related to flax growth and location from which the fibres are extracted from the stems can result in significant changes in the their mechanical properties [12, 54, 56]. Different processing methods, testing conditions and a multitude of other factors further increase this phenomena [54], some of them presented in table 2.9. As a consequence, a broad range of values has been reported in the literature (see table 2.10), which is an important hurdle to reliable design of flax fibres composites reinforcements. It is expected that the understating and isolation of the main contributors to fibre mechanical properties variation, some of them discussed below, and development of more adequate measurement techniques (as per section 2.2.3.1) will allow a more precise mechanical characterisation, improving the reliability of flax fibre composites for structural applications.

Table 2.10: Tensile properties of elementary and technical flax fibres [13]

Flax fibre type	Method	**Gauge** Length	**Average** Strength	**Young's** Modulus	**Failure** Strain	References
	Green retted	5	678 ± 216	—	—	[229]
	Dew retted	5	906 ± 246	—	—	[229]
	Dew retted	8	621 ± 295	52 ± 18	1.3 ± 0.6	[230]
	Enzyme retted	9	591 ± 250	57 ± 22	1.4 ± 0.9	[231]
Elementary fibres	Enzyme retted	5	750 ± 650	89 ± 35	—	[232]
	Scutched	5	732 ±-	—	—	[35]
	Hackled	3	1522 ± 400	—	—	[175]
	Hackled	10	945 ± 190	57 ± 35	2.0 ± 0.4	[12]
	—	10	1339 ± 486	54 ± 15	3.3 ± 0.8	[172]
	—	10	722 ±-	—	—	[233]
Technical	—	—	690 ± 345	28 ±—	2.9 ± 0.3	[234]
fibres	—	20	613 ± 442	—	—	[39]

Flax fibres present a highly hydrophilic character, which is mostly associated with the hydrophilicity of their structural components, mostly polyhydroxilated carbohydrate molecules (refer to section 2.1.2).

Table 2.11: Tensile properties of untreated and chemically treated technical flax fibres. Treatment agents: Anhydride (MA), acetic anhydride (Ac), silane (Si), ethanedial (glyoxal), 3-aminopropyltriethoxysilane (APS) and dimethyloldihydroxyethylene urea (DMDHEU) [38, 55]

	Breaking strength (MPa)	Breaking strain (%)	Young's modulus (GPa)	Bundle diameter (lm)	Number of fibres tested	Reference
Untreated	300 ± 100	1.1 ± 0.4	30 ± 11	84 ± 20	23	
MA	185 ± 60	1.2 ± 0.3	18 ± 5	88 ± 14	24	
Ac	185 ± 85	0.8 ± 0.2	24 ± 10	77 ± 16	21	[38]
Si	555 ± 210	1.6 ± 0.6	40 ± 13	79 ± 13	22	
S	245 ± 95	1.1 ± 0.4	28 ± 9	85 ± 17	21	
Untreated	457 ± 94	1.59 ± 0.35	41.6 ±2.3	—	—	
Glyoxal 3 wt%	635.1 ± 99.4	1.17 ± 0.20	57.3 ±2.9	—	—	
APS	587.8 ± 105.1	1.42 ± 0.3	41.8 ±3.5	—	—	[55]
DMDHEU	454.7 ± 147.9	1.33 ± 0.39	37.7 ±3.0	—	—	

As a result, the environmental relative humidity (RH) will have an important impact on flax fibres mechanical properties. An increase in RH from 30% to 90% was found to result in a decrease of approximately 35% and 19% in the static and dynamic tensile moduli of flax, respectively [235]. In conjunct with a significant degree of porosity, flax pronounced hydrophilicity is responsible for a high moisture absorption and consequent poor dimensional stability, which plays a significant role in changing their mechanical properties [54].

In flax reinforced composites, it is common to treat the fibres surface to increase the compatibility and strength at the fibre-matrix interface, such treatments can have an important impact on the final properties of the specimens, which may not compensate the increase in adhesion. Alix et al. [38] treated flax fibres (Hermes variety from a 2004-crop cultivated in Normandy, France) using four different standard chemical treatments that consisted of fibres surfaces functionalisation with maleic anhydride (MA), acetic anhydride (Ac), silane (Si)[37] and styrene (S). As presented in table 2.11, the treatments caused a reduction in stiffness and toughness, except for Si-treated fibres, which seemed to have increased the mechanical properties. According to the authors, the significant increase in tensile mechanical properties in the Si-treated specimens may be due to silane compound grafting in between microfibrils, where it would act as a binding agent (cross-linking of microfribrils). Due to the high error associated to the values and the use of fibre bundles instead of elementary fibres, caution has to be taken in

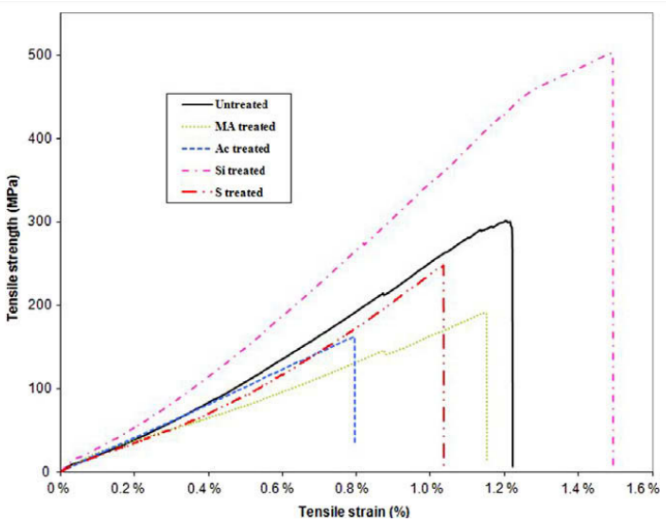


Figure 2.39: Tensile strength-strain curves for untreated and treated flax fibres [38]

[37] More specifically, γ-methacryloxypropyltrimethoxysilane

Table 2.12: Tensile properties of flax fibres according to their location in the stem [12, 56]

Location	Number of tested fibres	Diameter (lm)	Young's modulus (GPa)	Strength (MPa)	Ultimate strain (%)
Top[a]	36	19.0 ± 3.5	59.1 ± 17.5	1129 ± 390	1.9 ± 0.4
Middle[a]	37	19.6 ± 6.7	68.2 ± 35.8	1454 ± 835	2.3 ± 0.6
Bottom[a]	31	20.1 ± 4.1	46.9 ± 15.8	755 ± 384	1.6 ± 0.5
Top[b]	57	21.5 ± 5.3	51 ± 22	753 ± 353	1.8 ± 0.7
Middle[b]	45	21.3 ± 6.3	57 ± 29	865 ± 413	1.8 ± 0.7
Bottom[b]	59	21.3 ± 6.3	51 ± 26	783 ± 347	2.0 ± 0.9

The considered gauge length was 10 mm.
[a] Fibres from Hermes variety.
[b] Fibres from Agatha variety.

this analysis; moreover, in this work, Si-treated fibres were the only ones not to be dried before the experiments. Fig. 2.39 shows typical tensile curves obtained for treated and non-treated fibre bundles. Since their general behaviour is similar, a small impact on the structure of the bundles is expected from these chemical treatments.

D. Perremans et al. [55] also studied the impact of chemical treatments on tensile properties of technical flax fibres. Three different treatments aiming to cross-link the amorphous components in the middle lamella with high diffusivity monomers were tested, namely, ethanedial (glyoxal), 3-aminopropyltriethoxysilane (APS, an aminated silane compound similar to the one used in the present work) and dimethyloldihydroxyethylene urea (DMDHEU). Results were summarised in table 2.11. While APS and DMDHEU were found to have no significant impact on the stiffness of untreated technical fibres, Glyoxal was found to significantly stiffen the specimens, reaching values comparable to elementary fibres stiffness (see tables 2.12 and 2.13). When it comes to strength, only Glyoxal and APS had significant, positive impacts. All the treatments, in particular Glyoxal, seemed to have decreased fibres ductility. It is believed that a condensation reaction between hydrolysed Glyoxal and the hydroxyls from the pectin and hemicellulose molecules, creating cross-links in the amorphous matrix between elementary fibres (APS and DMDHEU moities are expected to have decreased reactivity towards hydroxyls as compared to hydrated aldehydes). Both theories were confirmed using FTIR, XPS and C^13NMR in parallel to study the changes in surface chemistry due to the treatments.

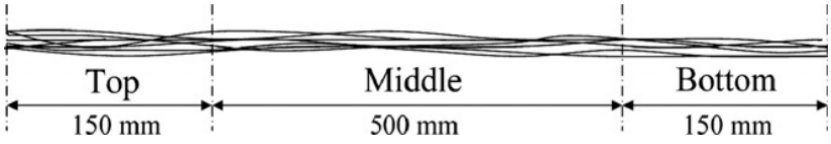


Figure 2.40: Definition of the three locations from which fibres were extracted from oriented tows [12].

In addition to that, flax fibres composition and geometry are expected to vary along the plant longitudinal direction. Charlet et al. [12, 56] studied the mechanical properties of flax fibres (dew-retted, mechanically-extracted Hermes fibres from a 2002-crop [12] and Agatha fibres from a 2003-crop [56], both from Normandy, France) taken from the middle of tows with known growth direction that were divided into three different zones (see Fig. 2.40). According to the authors, this corresponds to similar zones in the stems. Middle fibres were found to have the best tensile properties as well as the highest content of cellulose (see table 2.12). Charlet and coworkers related this change in properties to weather variations over the plant development and the porosity of the different regions of the stem[38].

[38] A reader wanting to understand more about the possible correlations between plant growth and tensile properties is

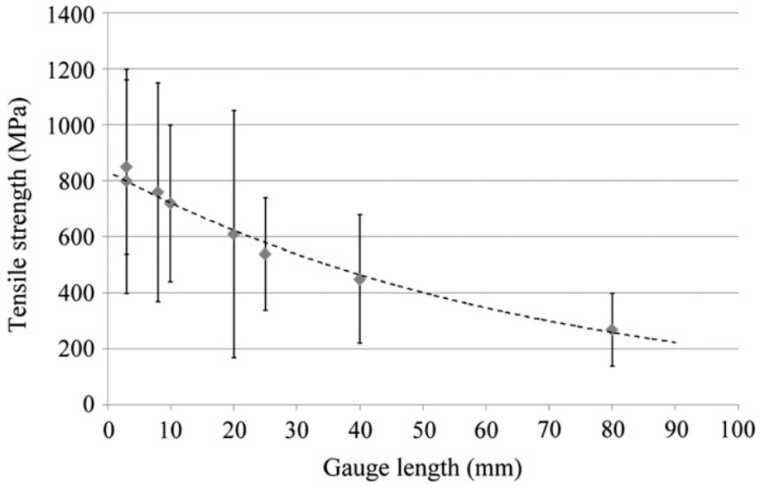


Figure 2.41: Tensile strength of flax bundles as a function of gauge length (the dotted line is an approximation). Compilation from different studies [39–41]. From [42].

Even though a considerable number of elementary fibres specimens with a short gauge length (10mm) were used in this study, the large error with respect to the difference between the properties of specimens from different zones requires caution when evaluating these findings.

The chosen gauge length was also found to impact the mechanical properties of flax (see Fig. 2.41). A higher gauge length is expected to be detrimental for the tensile strength for two main reasons: first, as it is the case for other materials, the amount of defects [39] increase in the tested length as the gauge length is increased; second, for clamp lengths larger than the elementary fibre length, failure is expected to occur in the middle lamella due to shear failure of the relatively weak pectic cement [175]. Regarding this latter aspect, K. Charlet et al. [42] studied the interfacial strength of a specimen composed of two elementary fibres tested in tensile mode. The mean value obtained for this property was 2.9 MPa, which is two to seven times lower than the interfacial shear strength between flax fibres and the most common matrices (see table **??**). This finding agrees with the disparity between the recorded tensile properties of fibre bundles and elementary fibres, with the latter being usually two to four times stronger than the former. Supporting the statement of K. Charlet et al., F Coroller and coworkers [167] studied the effect of fibres individualisation on tensile failure of flax-epoxy unidirectional composites; although no impact on the Young's modulus values was observed, the tensile strength was proved to be dependent on the fibre individualisation. It highlights the importance of isolating the fibres as much as possible from the bundles when making composite materials, as a means of increasing the area of stronger fibre-matrix as opposed to weaker fibre-fibre interface [42].

I. Pillin and coworkers [43] studied the tensile properties of different varieties of flax fibres, which were further subdivided into two groups, oleaginous fibres (cultivated for its omega 3-rich seeds) and textile fibres (the ones usually used for composites applications), refer to Fig 2.42. Appreciable differences between the varieties were observed, especially in specific tensile strength. These results highlight the importance of stating the fibre variety when studies on flax for composites reinforcements are carried out. Although oleaginous fibres were found to have lower mechanical properties when compared to textile, phenomena that is attributed to a lower content of cellulose, both presented competitive mechanical properties when compared to glass fibres.

The effect of water washing and drying cycles on tensile properties were studied by le Duigou et

referred to the original works [12, 56]

[39] for a discussion about the defects found in flax fibres, refer to section 2.1.1.1 and Fig. 2.28)

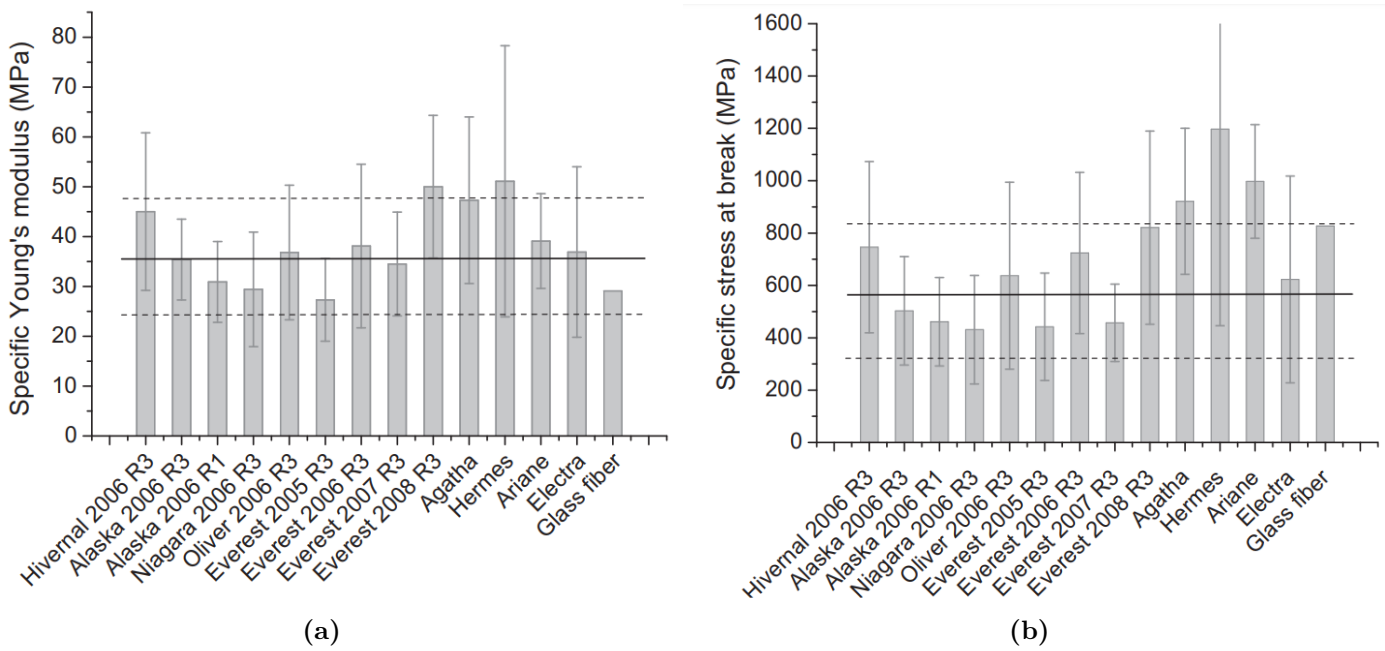


Figure 2.42: a) Specific Young's modulus for each flax sample as compared to glass fibres; b) Specific stress at break for each flax sample as compared to glass fibres. In both cases, the solid line represents average values for oleaginous flax and dash lines their standard deviation [43].

al. [28]. Hermes flax fibres cultivated in Northern France were immersed in distilled water at 23 °C for 72 h aiming to clean the surface. In another treatment a drying cycle at 105 °C during 14 h was performed. Both processes were followed by an 8-days ageing period at 23°C under RH = 50%. The water washing was fount to have no affect on the stiffness, but resulted in a decrease in the tensile strength and elongation at break of 15% and 18%, respectively. The drying cycle, on the other hand, was found to significantly decrease tensile modulus, strength and elongation at break by 20%, 45 % and 33%, respectively.

2.2.3.1 A New Approach

In spite of the compatible mechanical properties, the large variation in its mechanical properties has been long considered one of the main obstacles to employing flax fibres in high-end applications [11]. Notwithstanding that, it has recently been proved that, replacing single fibre tensile test by impregnated fibre bundle test (IFBT), method in which fibres mechanical properties are back-calculated from the tensile properties of unidirectional composite specimens loaded in the fibre direction using

Table 2.13: Elementary flax fibre properties vs back-calculated technical fibre properties. E_{f1}: Stiffness calculated between 0% and 0.1% strain; E_{f2}: Stiffness calculated between 0.3% and 0.5% strain; $\sigma_{f,u}$: Tensile strength [11]

	E_{f1} (GPa)	E_{f2} (GPa)	$\sigma_{f,u}$ (Mpa)
Elementary fibre test	57.0±13	44.5±14	791±319
Back-calculated from IFBT	59.8±2.4	40.8±3.5	527±138

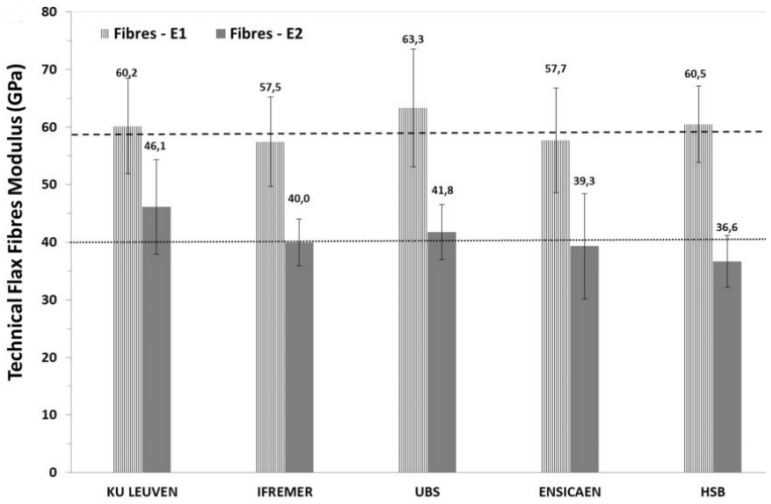


Figure 2.43: Back-calculated technical flax fibres tensile obtained by different laboratories using IFBT for the same batch of fibres. Dotted horizontal lines (E1 and E2) represent the average values, as calculated by fitting the rule-of-mixtures equation through all the experimental data [11]

straightforward micromechanical equations (such as rule of mixture) [40], flax fibres stiffness can be back-calculated with a considerably low scatter, comparable to that obtained for glass fibres. This conclusion came from a parallel study on flax fibres from the same batch tested using IFBT[41] by five independent laboratories [236][42], which obtained fibres stiffness values presenting no statistically significant difference (95% confidence interval-ANOVA, Tukey's grouping method), see Fig. 2.43.

The much lower scatter in the values obtained by IFBT as compared to single fibre tensile test (see table 2.13) are a logical result. As opposed to the latter, which requires a substantial amount of work in the preparation of a single specimen (see sections 3.2.1 and 3.2.7), resulting in seldom more than a few tens of specimens tested by each study, IFBT allows for simultaneous test of a few tens of technical fibres; hence, a few hundreds of elementary fibre by specimen tested [11]. Therefore, each data point from IFBT corresponds to the average properties of more fibres than usually tested in an entire study using single fibre tensile test.

The small difference in the mean stiffness obtained from both methods is another argument in favour of IFBT. The greater difference observed in the case of tensile modulus calculated between 0.3% and 0.5% strain (E_{f2}), case in which IFBT back-calculated stiffness is about 10% lower, is credited to slip of elementary fibres over each other inside the technical fibres, embedded in the IFBT-samples due to the lower mechanical properties of the pectic cement. As it is the case in the difference between tensile tests carried out using fibre bundles and elementary fibres, the impact of pectins mechanical properties on the results is expected to be detrimental, in agreement with what was observed. Moreover, not all elementary fibres are likely to be well bonded to the matrix (particularly those at the technical fibre interior), resulting in a less efficient stress transfer to them, especially at higher strains [11].

Such a high improvement in the precision of flax mechanical properties will allow to design composites with increasing reliability. This is an important step towards applying natural fibres composites to industries with tight tolerance specifications, such as the aerospace, as well as increasing the number of important structural applications in automobiles.

[40] A well-established method in the assessment of carbon and glass fibres mechanical properties
[41] Adapted from ISO 10618:2004
[42] at KULeuven, UBS, IFREMER, HBS, ENSICAEN [236]

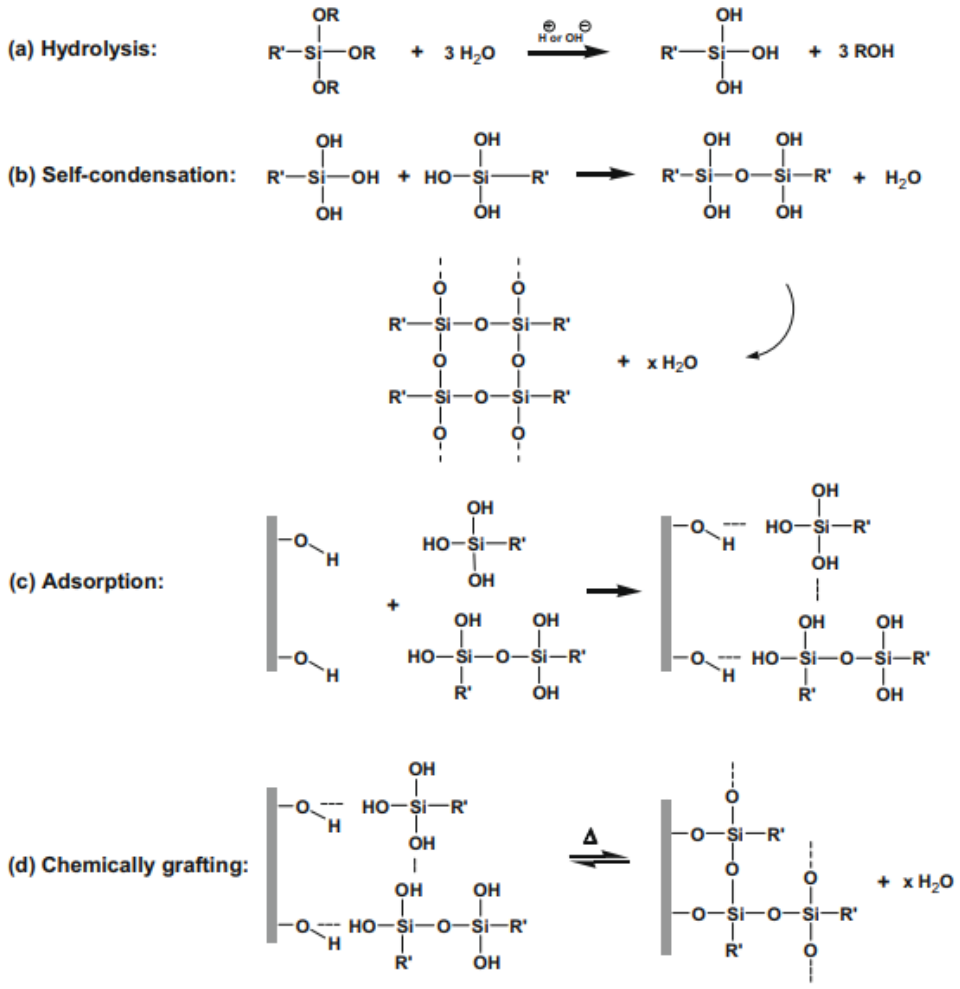


Figure 2.44: Reactions taking place in the sizing treatment: a) Catalysed hydrolysis of silane monomers forming Silanol groups (-Si-OH); b) Undesirable Self-Condensation of Silanols reducing the available sizing acitve sites and reducing the molecule diffusivity (acidic pH can be used to accelerate hydrolysis rate while slowing down self condensation [44]); c) Physical Adsorption of Silanol groups to Hydroxyl groups on the surface of natural fibres by hydrogen bonding (surface coating) and/or in the cell walls (cell wall bulking)

2.2.4 Silanisation

A class of compounds widely used to treat the surface of fibres used to produce FRC is the silane coupling agents [237]. Such agents, which have long been used to treat glass fibres, contain hydrolysable Alkoxyl group OR' that can be converted into Hydroxyl in aqueous medium, being subsequently adsorbed to Hydroxyls groups from the carbohydrates on the surface of the fibres and eventually reacting with the latter under correct heating conditions (see Fig. 2.45). According to the chemistry of the matrix, the R group in the silane compound molecule can be chosen so a to cross-link both phases[43]. Although the chosen R groups can have properties diametrically opposed according to the properties of the matrix (e.g., hydrophilic amino compounds for epoxy matrices or hydrophobic hydrocarbon chains for PP), those compounds are usually grouped together when the composite is considered from the point of view of the fibres since the Silane group determines how effective the grafting reaction will be. Such coating process is often called "sizing" treatment and the compound used in this coating process, "size" or

[43]or at least increase the physicochemical interactions by changing the fibre surface polarity and creating an interpenetrating network when an apolar matrix is used.

"sizing" agent.

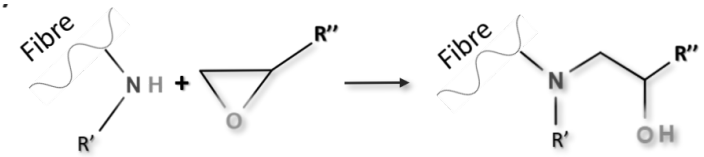


Figure 2.45: Reaction between an amino group from the sizing and epoxide group from the epoxy resin (most common Epoxy matrix - Aminosilane coupling agent reaction)

Aminosilanes, especially γ–aminopropyltriethoxysilane (APS), are the most common silane-coupling agents used as sizing in natural fibres applications for both thermoplastics and thermoset polar matrices [44]. In the present work, Bis(trimethoxysilylpropyl)amine (see Fig. 3.1b) was used, this bis-silane (silane coupling agent with two silane heads) may lead to a thicker and more homogeneous coating when compared to mono-silanes, such as APS [238] due to the formation of a polysiloxane network on the surface of the fibre. On the other hand, polysiloxane formation due to self-condensation (see Fig. 2.45b) may be detrimental to molecular diffusion in the fibre cell wall [44] (as discussed below). The reaction between the amino group and the epoxide funcitonalities of epoxy is presented in a generic fashion in Fig. 2.45.

Studies on natural fibres have found a positive correlation between silane-based modifications and improvement of thermal stability and moisture resistance of natural fibres and their composites, even when hydrophilic-backbone aminosilanes were used as sizing for polar matrices [239–241] [44]. In the latter case, the main mechanism is usually the impregnation of the fibres cell walls with small silane molecules capable of diffusing through it, reducing the size of the cell wall nano-pores where water molecules would usually penetrate (bulking treatment) [44][45].

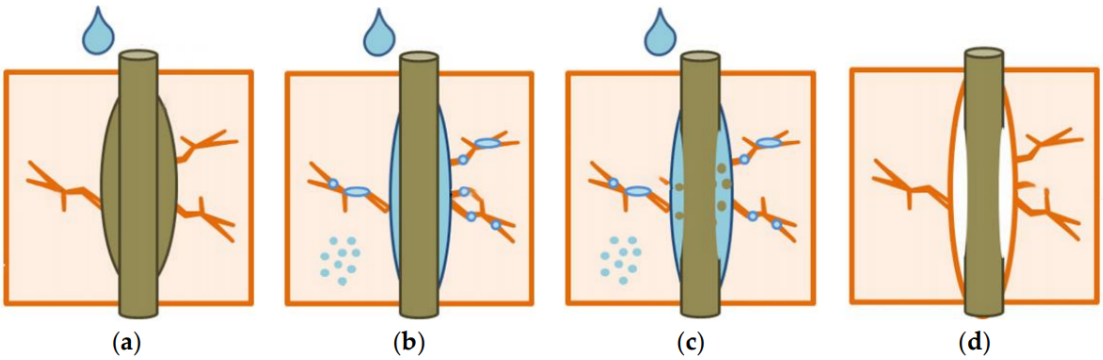


Figure 2.46: The degradation of interfacial adhesion due to moisture absorption: (a) development of micro-cracks due to expansion of swollen fibre, (b) water molecules diffused in the bulk matrix flow along the fibre–matrix interface, (c) water-soluble components leach from fibre, (d) ultimate matrix–fibre debonding takes place [45]. Copied modified from [46].

Trying to improve the hygroscopic properties of flax fibres so as to reduce moisture sorption and its consequent dimensional changes, which can significantly damage natural fibre reinforced composites

[44] As expected, in the latter case the moisture resistance increase will be much lower as compared to the hydrophobic backbones used for apolar matrices

[45] Bis-silanes may also work based on a different principle [242]

interfaces [243] (see Fig. 2.46), B. Fathi et al. [244] studied a composite system based on a bio-epoxy resin (SuperSap CLR resin & CLH hardener) and flax fibres whose surfaces were primed using TEMPO reagent[46]-mediated oxidation and then treated with an aminosilane coupling agent, which showed improved interfacial adhesion and reduction in water absorption. When the fibres were treated using γ-glycidoxypropyltrimethoxy-silane, improvements in tensile properties were also reported [38, 55].

Studying a system jute fibres-epoxy (40vol.%), Gassan and Blendzki [245] observed an increase of 27% and 15% in the composite stiffness and fatigue strength, respectively. The treatment also improved the critical load for damage initiation and resulted in a slower damage propagation [245]. In the work of J. George, J. Ivens and I. Verpoest [240], flax fibres used as reinforcement for epoxy resin (HM 533) were treated with 3-aminopropyltriethoxysilane, resulting in an increase in tensile strength from 53.4 MPa to 62.54 MPa, in tensile modulus from 7.86 GPa to 9.83 GPa and a decrease in impact strength from 10.47 kJ/m^2 to 8.65 kJ/m^2. P.J. Herrera-Franco and A. Valadez-Gonzalez [246] observed similar improvements in a henequen/HDPE system.

I. Van de Weyenberg [35], on the other hand, observed no significant increase in the interface strength of a system based on flax fibres-epoxy resin after the fibres were treated using aminoethylaminopropyl-trimethoxy silane, as assessed by transverse 3PBT and microbond tests. Notwithstanding Van de Weyenberg's, using transverse 3PBT to study the the interface quality of flax-epoxy composites after the fibres were sized using an aminosilane compound (3-aminopropyl-trimethoxy), T. Chi [218] observed a significant improvement. Indeed, composites made using the silane-sized fibres presented a transverse strength around 17 MPa, value that was more than double of that obtained using non-treated fibres, 8 MPa[47].

[46] 2,2,6,6-tetramethylpiperidine-1-oxy radical

[47] Due to the relevance of such studies to the present work, further discussion can be found in section 2.2.2

3 Experimental Section

3.1 Materials

3.1.1 Flax Fibres

Non-crimp UD flax fabrics (ampliTex ® UD type 5057) fabrics with an areal weight of 150±7.5 g/m^2 and fibres of nominal linear density of 300 tex oriented at 0° were provided by Bcomp® (Fribourg, Switzerland) [247]. According to the provider these UD fabrics are compatible with infusion-based processes (vacuum infusion, RTM), wet layup, bladder inflation moulding (BIM) and compression moulding. As-recieved sample is presented in Fig. 3.1a.



(a) **(b)**

Figure 3.1: a) As-received UD sample composed of untreated technical fibres, its entire length (not shown in the figure) is about 1m; b) Silane compound used as surface sizing agent

Part of the fibres were treated with Bis(trimethoxysilylpropyl)amine (see Fig. 3.1b) by CENTEXBEL-VKC. It is expected that this compound, when functionalised on the fibres surface, will react with the resin, cross-linking both phases (see Fig. 2.45), improving the mechanical properties and positively affecting the thermal stability and moisture resistance of the final material. The literature about the effect of this treatment on flax fibre reinforced composites and reaction mechanisms is discussed in section **??**.

3.1.2 Bio-Epoxy Resin

In the present work, SR InfuGreen 810 (Green Epoxy systems for Injection and Infusion) from Sicomin Technical Systems [57], a DGEBA epoxy resin with 38% of carbon from plant origin[1] was used. It is specially formulated for resin transfer processes, such as injection or infusion, having low viscosity at ambient temperature. The resin was cured using a polyamine hardener, SD 4771 Ultra-Slow (Sicomin

[1]The bio-based carbon content is certified by Carbon-14 measurements (ASTM D6866 or XP CEN/TS 16640) as a function of the carbon origin contained in the epoxy molecule.

Technical Systems), with weight fraction of 1 part of hardeners to 4 parts of resin. The system was cured during 24 h at room temperature and under atmospheric pressure.

Table 3.1 summarises the mechanical properties of a typical cast SR InfuGreen 810 obtained using SD 4771 Ultra-Slow as hardener using and a curing cycle of AT + 16h at 60°C [57].

Table 3.1: Mechanical properties and Glass Transition Temperature (T_g) of a typical cast SR InfuGreen 810 obtained using SD 4771 Ultra-Slow as hardener and curing cycle: AT + 16h at 60°C [57].

Property	(Unit)	*SR InfuGreen* 810 / SD 4771
Tension		
Modulus of elasticity	(GPa)	3.1
Maximum Resistance	(MPa)	74
Resistance at Break	(Mpa)	68
Ultimate Tensile Strain	(%)	4.2
Strain at Break	(%)	5.1
Flexion		
Modulus of elasticity	(GPa)	3.0
Maximum Resistance	(MPa)	116
Ultimate Tensile Strain	(%)	5.4
Strain at Break	(%)	7.4
Shear Strength		
Maximum Resistance	(MPa)	47
Compressive		
Compressive Yield Strength	(MPa)	100
Offset Compressive Yield	(%)	12.8
Impact Choc Charpy		
Resilience	(kJ/m^2)	83
Glass Transition		
T_{g1}	(°C)	84

3.2 Methods

3.2.1 Elementary Fibres Isolation

As previously discussed, flax fibres present a complex hierarchical structure. Consequently, it is important to correctly choose the hierarchical level at which the properties measured will present the lowest deviations from ideal behaviour according to the measurement technique employed. In the current work, elementary fibres were chosen for most of the experiments with the objective of limiting the impacts of the middle lamella and its components on the final results (e.g., liquid absorption and reduction of mechanical properties by slipping of elementary fibre over each other in the bundle), and reduce the radial geometrical anysotropy, facilitating cross-sectional area approximation for single fibre tensile test and embedded length/area determination for microbond test from longitudinal profile micrographs. Additionally, elementary fibres were used in the cleaning treatments so as to ensure that their surface was effectively assessed by the washing liquids, which is usually not the case for fibres in the innermost parts of bundles.

The protocol followed for elementary fibres isolation is briefly summarised below:

1. Technical fibres were removed from as-received samples;

2. With the naked eyes, smaller bundles were separated from the technical fibres using tweezers up to the point that no disjoint sections between fibres in the bundle could be seen. The final specimens from this step usually consisted of bundles containing 1 to 4 elementary fibres;

3. Bundles from the previous step were further separated with the aid of a stereo microscope, which allowed to identify disjoint sections where the fibre could be separated. After this step, the specimens were usually elementary fibres, which were kept between microscope slides;

4. Optical microscopy in transmission mode was then used so as to discard all non-elementary fibres specimens remaining from the previous step.

To prevent contamination of the specimens, gloves were always used.

3.2.2 Tensile Test and Microbond Specimens Preparation

Except for microdroplet deposition, in the case of microbond specimens, and gauge length measurement, in the case of tensile test specimens, both had similar preparation steps, consisting of placement in paper support and diameter measurement. The following sections briefly describe how those samples were prepared. When pertinent, a briefly discussion about the assumptions and limitations of the techniques is presented.

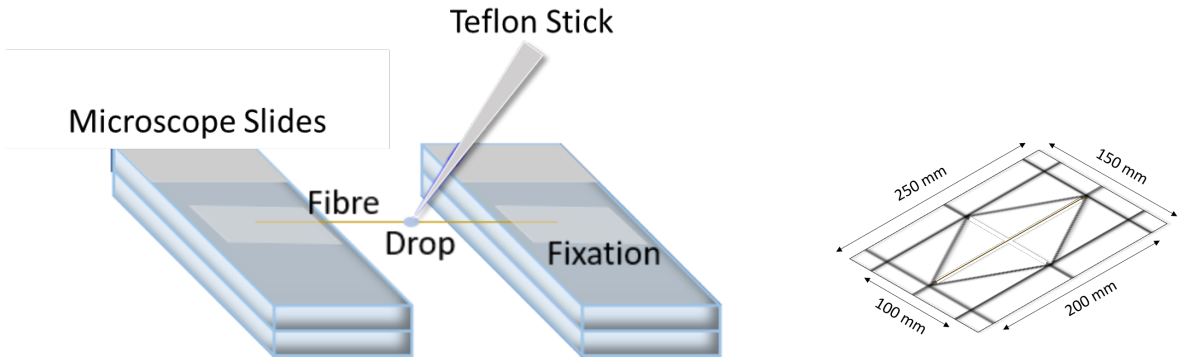


Figure 3.2: a) Schematics of microdroplet deposition setup, composed of microscope slides as supports and a fixed elementary fibre with microdroplet deposited using a Teflon stick. b) Schematics of the tensile and microbond tests specimen support. It was used to facilitate fibres handling and fixation in the equipment. Dimensions of support for elementary are presented

3.2.2.1 Microdroplet Deposition

In the particular case of microbond specimens, epoxy resin microdroplets were deposited and cured on elementary fibres. Fig. 3.2a presents the tools used to perform the deposition. The protocol followed is briefly summarised below:

1. Using a stereo microscope and tweezers, several elementary fibres (isolated as presented in section 3.2.1) had their ends fixed to parallel microscope slides using scotch tape (see Fig. 3.2a);

2. Microdroplets of uncured resin previously mixed with harder presenting axial length below 200 μm (see section section 2.1.5) were deposited on the fibres using a small Teflon stick;

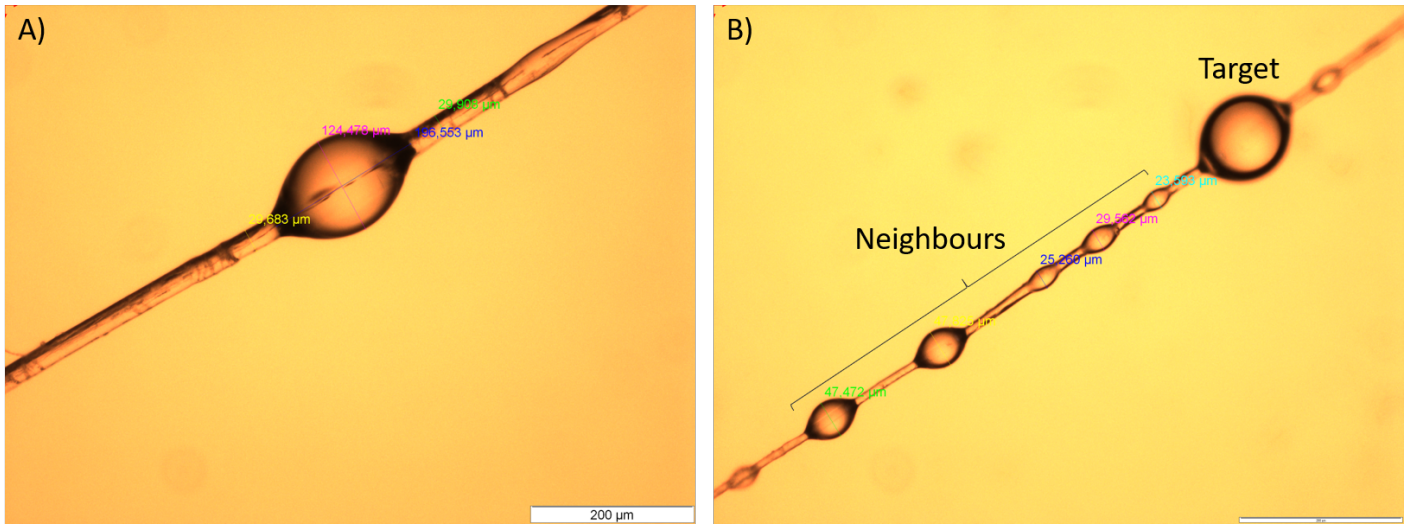


Figure 3.3: Microbond specimen characteristic dimensions measurement: A) Typical specimen presenting characteristic dimensions; B) Typical specimen presenting small-diameter "neighbours" (their diameter was taken into account when determining the distance between support knives, see section 3.2.6), Scale bar: 200 µm

3. The specimens were left to cure at room temperature and under atmospheric pressure for 24h;

After resin curing (see Fig. 3.3A), these specimens were placed on paper supports and had their characteristic dimensions measured as presented in the next sections.

3.2.2.2 Placement in Support

To facilitate handling without damaging the specimens, keep the specimen straight, and assure good clamping, simple elementary fibres or elementary fibres with cured microdroplets, both presenting longer than 2 mm, were glued to paper supports (based on ASTM D3379 - 75 [248], see Fig. 3.2b) using acrylic glue (superglue) so as to obtain a straight specimen, whose gauge length was approximately 2 mm. This is a widely used procedure in the field of (natural) fibre reinforcements mechanical test [13, 28, 249–258]. Great care was taken in correctly aligning the fibres with the largest diagonal of the diamond in the paper support so as to avoid parasitic forces in the transverse plane during tensile loading. Additional tensile tests were carried out using fibre bundles for comparative purposes, the only parameter changed in the whole preparation process in this case was the gauge length, set to approximately 4 mm.

3.2.2.3 Cross-section Measurement

The determination of flax fibres cross-sectional area is an important step, whose assumptions may considerably affect the final results. Simplified cylindrical geometries whose dimensions are defined as the mean values obtained from longitudinal micrographs are usually employed when determining the cross-sectional area for mechanical tests. M. Aslan [13] demonstrated that, on average, this assumption can lead to 39% lower tensile strengths when compare to those obtained using the true cross-sectional area, which is neither a perfect circle (often being described as a hexagon [90][2]) nor a continuous area (due to the lumen in its centre). In addition to that, as proved by K. Charlet et al. [12], the characteristic radial dimension of the fibres can vary two to threefold within a few millimetres in the stem [12]. In spite of that, except when surface characterisation by Wilhelmy Method is carried out and liquids assumed to

[2]Also a questionable approximation [13].

completely wet the fibre surface (e.g., using hexane) can be used to the measure wetted perimeter, there seem to be no easy alternative when the fibres must be used in isolation for tensile and microbond tests. Having this in mind, the present study will employ the cylindrical approximation and the cross-section diameters will be determined from longitudinal micrographs of the elementary fibres.

The protocol followed for elementary fibres approximate diameter determination from longitudinal micrographs is briefly summarised below:

1. Fibre specimens glued to paper supports, as described in the previous section, were placed between two microscope slides so as keep the entire specimen approximately in the same plane;

2. With an optical microscope (Olympus AX70) in bright-field [3], transmission mode, using magnifications of 5 and 10 times, several measurements of the specimens characteristic dimensions were taken from longitudinal micrographs. Microbond and Tensile test required different characteristic dimensions to be measured:

- **Microbond**: Target Droplet axial length (i.e., fibre embedded length) and diameter, and fibre mean embedded diameter, obtained as the arithmetic mean of the diameters before and after droplet (Fig. 3.3 A)) were measured. Small-diameter droplets formed close to the target droplet were frequently observed, in this case, their diameters were measured to correctly grip the final specimen (Fig. 3.3 B)).

- **Tensile Test**: Fibres diameters were measured in five different locations equally spaced along the specimen so as to obtain a mean value and a standard deviation (see Fig. 3.4 for illustration a similar protocol applied to a bundle of fibres).

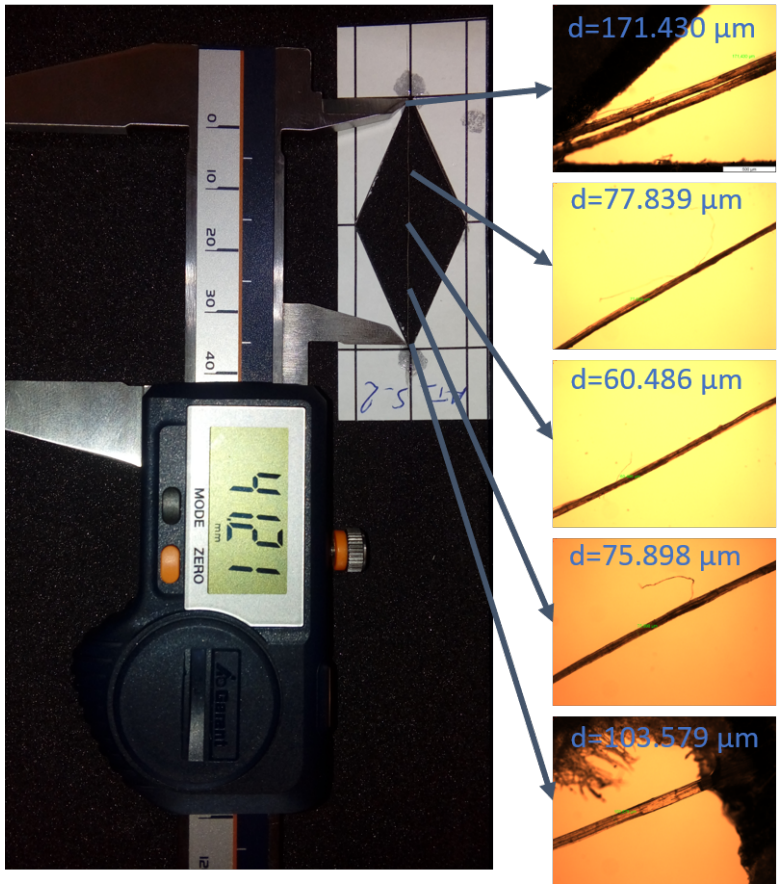


Figure 3.4: Measurement of Gauge length and Diameter of Fibres Bundle Tensile Test Specimen

After cross-section measurement, microbond specimens were ready for experiment, tensile test specimens, on the other hand, had their gauge length measured as an additional step.

3.2.2.4 Gauge Length Measurement

In the particular case of tensile test specimens, after placement in paper support and diameter measurement according to the aforementioned protocols, the gauge length between the glue points was measured using a caliper. Fig. 3.4 shows typical measurements for fibres bundle specimens[4].

[3] Eventually in dark field to highlight fibres boundaries, helping to identify bundles of two well-attached fibres

[4] Tested only for comparative purposes.

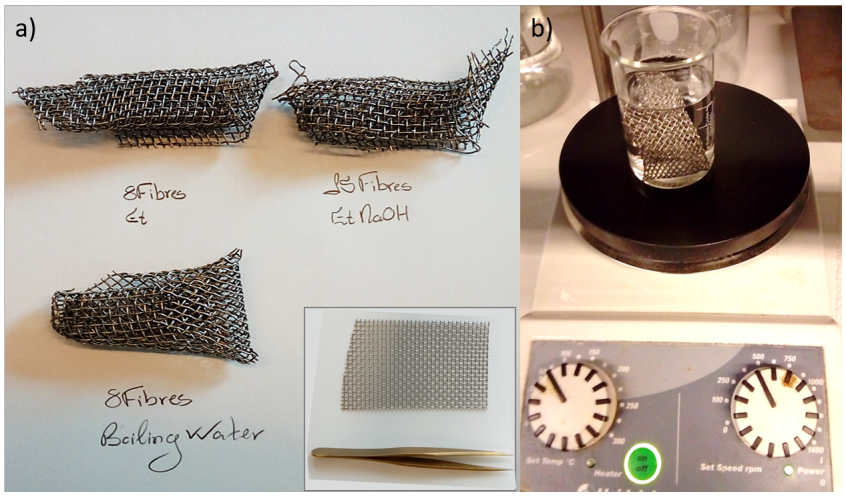


Figure 3.5: Cleaning methods and chemical treatments apparatus: a) Caged fibres. The inset shows the stainless steel mesh used to hold the fibres during the treatment; b) Caged fibres in a beaker with cleaning liquid in a hot plate

3.2.3 Elementary Fibres Cleaning

Flax fibres are known for having significant amount of waxy compounds weakly attached to the surface of elementary fibres [13, 34, 189, 259]. These compounds present a high surface free energy, coming mainly from a high dispersive component [178], consequently, their contribution to physicochemical interactions can induce results that indicate a high interfacial adhesion, a misleading conclusion. Additionally, cleaning also targets the removal of low molecular weight material present in the middle lamella (between cell walls), mainly composed of heterosides, notably pectin and hemicellulose [13, 189, 189, 259**?**]), increase elementary fibres individualisation, increasing resin impregnation and physicochemical interactions between epoxy resin and cellulose [189]. However, since the cellulose microfibrils, the main structural component of elementary fibres, are also held together by such compounds, their excessive removal may cause significant weakening, which may not be compensated by the improvement in fibres dispersion and physicochemical interactions [28, 144, 189, 260].

In the present work, two cleaning (i.e., washing) of methods were tested. In both cases elementary fibres carefully isolated under stereo microscope from technical fibres were caged in a thin stainless steel mesh and immersed in beakers containing continuous agitated deionised water or ethanol held at temperatures of 100°C and 75°C, respectively, for two hours (see Fig. 3.5), the product of such cleaning procedures was then rinsed using deionised water at room temperature and transferred to a desiccator at room temperature and 1 atm pressure, where it was stored until use.

3.2.3.1 Boiling Deionised Water Cleaning

This procedure is based on the boiling water cleaning methodology proposed by Bourmaud et al. [260] [5]. This procedure was developed with the aim of implementing an environmentally friendly treatment for the technical fibres in order to improve interfacial adhesion by removing undesired compounds from their surface and ease fibre-bundle separation and extraction of elementary fibres while preserving their mechanical properties. Although a small percentage of the elementary fibres structural pectin may have been removed, making the fibres sightly more brittle and less stiff in average, this cleaning method was proved to be effective in removing undesired middle-lamella compounds. A decrease in the elementary

[5] An increase in the treatment time was added in cases in which these fibres did not underwent tensile testing

fibres diameter was also observed, which can be understood as a further confirmation of the middle-lamella carbohydrates extraction.

Elementary fibres caged in a thin stainless steel mesh were immersed in deionised water under continuous agitation for 2h in a beaker (see Fig. 3.5b). The product was rinsed with distilled water until the liquid extracts were completely clear. The elementary fibres thus cleaned were store in a desiccator at ambient pressure and temperature.

When a significant amount of technical fibres was treated by the same method, it was observed that, even though the water used to treat the fibres had turned into a yellowish colour, the rising water still presented extracts, which were less than those observed in the cleaning method using hot ethanol. This can be interpreted as an evidence of the effectiveness of the treatment.

3.2.3.2 Hot Ethanol Cleaning

This procedure is based on the first step of the solvent extraction treatments proposed by J. Acera Fernández et al. [189], an adaptation of the standard Tappi T264, which utilises Ethanol and benzene to extract waxes, fats, some resins, and possibly some portions of wood gums from wood material and is originally employed when posterior chemical analysis of the remainder compounds are to be performed. In their work, the authors report that the extracts from flax fibres using this treatment consisted mainly of lipophilic compounds, resulting in higher fibre yarn linear and areal densities, and avoiding fibres degradation, mainly due to excessive removal of pectin cement, usually observed when using harsh chemical treatments (e.g. NaOH solution extraction [189]).

Elementary fibres caged in a thin stainless steel mesh were immersed in a beaker containing approximately 100 ml of ethanol 99 vol.% Euro Denatured (1:1:1) provided by VWR Chemicals, at 75 °C under constant agitation for 2 h. The product was rinsed with distilled water until the liquid extracts were completely clear. The elementary fibres thus cleaned were store in a desiccator at ambient pressure and temperature.

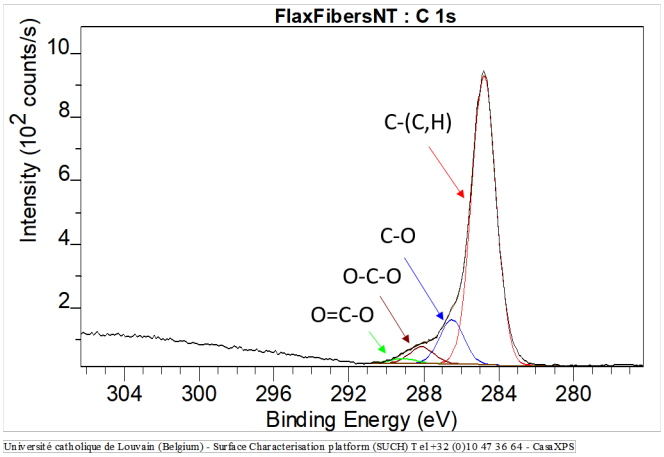


Figure 3.6: C 1s spectra, decomposed into four components C1–C4 for Unmodified Flax Fibres.

3.2.4 Surface Chemical Analysis

The physicochemical interactions and chemical bonding of fibre-matrix are determined by the surface chemistry of both phases. Differently from the polymeric matrix, a homogeneous material whose surface composition is approximately that of the bulk material, which is known, natural fibre are chemically

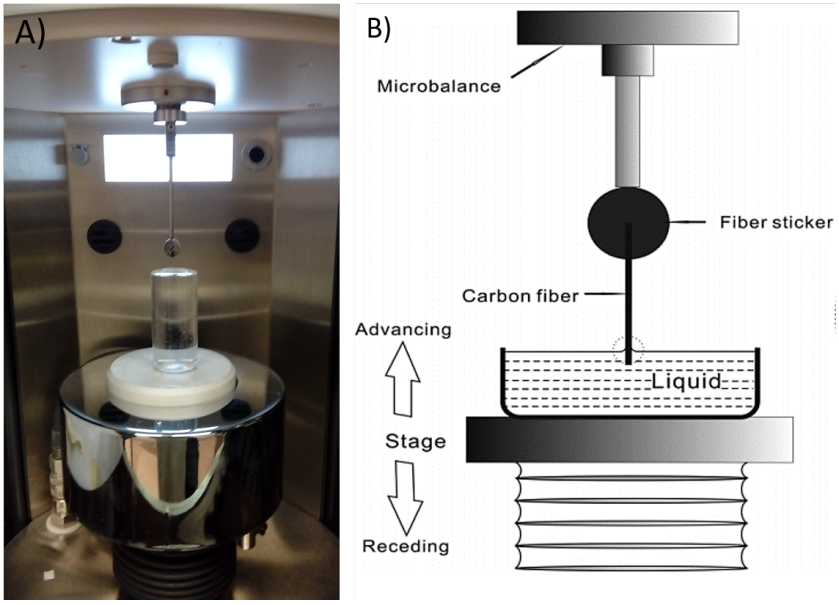


Figure 3.7: A) 1μg-resolution Kruss tensiometer K100 SF, B) Schematic drawing of the K100 SF tensiometer indicating each component [47]

anisotropic, requiring surface sensitive analysis methods in order to determine the nature and quantity of chemical functionalities contributing to interface strength and compatibility.

X-ray photoelectric spectroscopy (XPS,aka Electron Spectroscopy for Chemical Analysis [ESCA]) has proved to be one of the most useful tools for surface characterisation of natural fibres [193], allowing quantitative elemental composition and functional groups determination with typical probed depths of about 10 nm [228]. XPS working principle is governed by the photoelectric effect, basically, the sample is irradiated with X-rays, resulting in ejection of electrons from a small depth near to the surface, whose energy analysis provides a spectrum with characteristic discrete peaks corresponding to their binding energy, which is a function of the chemical identity and bonds of the parent atom. In this work, untreated and aminosilane treated technical fibres were studied using a Surface Science Instruments SSX100/206 spectrometer equipped with a monochromatic and micro-focused AlKα X-ray beam.

The following sequence of spectra was recorded: survey spectrum, C_{1s}, O_{1s}, N_{1s}, Si_{2p}, Ca2p, Zn_{2p} and C_{1s} again to check the charge compensation stability with time and the absence of sample degradation. To set the binding energy, the C-(C,H) component of C_{1s} was fixed to 284.8 eV. Data treatment was performed with the CasaXPS program (Casa Software Ltd, UK). Molar fractions were calculated using peak areas normalised on the basis of acquisition parameters after linear background subtraction, and consideration of experimental sensitivity factors provided by the manufacturer. C_{1s} spectra were decomposed with a Gaussian/Lorentzian(70/30) product function, by constraining the FWHMs of all components to be equal.

Figure 3.6 presents a typical result of XPS analysis for Unmodified Flax Fibres obtain in the present study. The different peaks of the C 1s spectra and its decomposed components are identified.

3.2.5 Wilhelmy Technique

3.2.5.1 Dynamic Contact Angle Measurements

The surface energy of flax fibres decomposed according to the van Oss model [125] was calculated from their static advancing contact angles with various liquids measured using the Wilhelmy Technique. Those

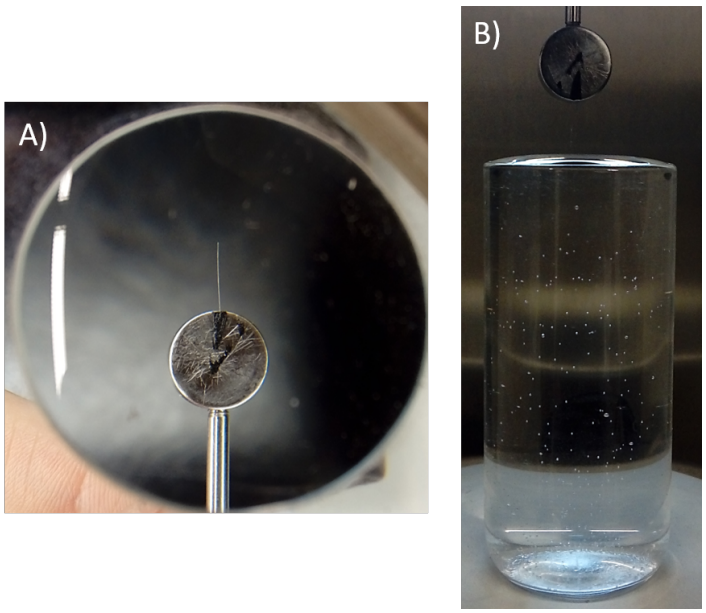


Figure 3.8: A) Detail of Wilhelmy Balance Fibre Specimen mounted on tensiometer holder; B) Detail of Fibre Specimen placed in the close vicinity of the test liquid surface before measurement is started

values allowed to characterise flax-epoxy physicochemical interactions. For more about the theory behind this approach and critical presentation of literature on flax fibres reinforced composites physicochemical interactions assessment, the reader is referred to sections 2.1.4 and 2.2.1.

Contact angle measurements of untreated, aminosilane treated, water-washed and ethanol-washed elementary flax fibres isolated according to the protocol presented in section 3.2.1 were performed using a Krüs K100 tensiometer with resolution set to 1 μg weight (See Fig. 3.7). Fibre samples were attached to the beam of an electrobalance taking great care to avoid parasitic forces in the transverse plane by ensuring axial alignment with the balance beam, and to have a free length as close as possible to the maximum immersion depth set (see Fig. 3.8 A)). The latter factor allows to have a stiff sample capable of overcoming the liquid surface tension without bending [198]. Ensuring a strong attachment between the fibre specimen and the balance beam is also an important factor to prevent bending.

A maximum immersion depth of 5.5 mm was set. To measure the displacement of the specimen, the machine sets as reference its initial position (stage initial position, see Fig. 3.7A) when the measurement is started plus a 1-mm displacement farther away from the balance beam, meaning that the maximum probed length when a 5.5 mm immersion depth is set would be about 4.5 mm. Therefore, to obtain the largest possible probed fibre length, the specimens were placed as close as possible to the probe liquid surface before the measurements started, taking care to avoid contact, which would invalidate the measurements. In practice, the maximum probed lengths were around 3.5 mm.

Measurements were taken at low wetting speeds so as to approach kinetic equilibrium at each point of the specimen axial direction. The maximum speed that did not cause a measurable difference in the final values of contact angle[6], 0.5 mm/s (value set to carried out the experiments), was determined by performing successive measurements at increasing speeds, starting from the minimum allowed by the equipment 0.1 mm/s. This approach was assumed to result in kinetic equilibrium for the equipment and calculation methods employed; therefore, allowing for static advancing contact angle calculation. Furthermore, successive cycles performed using the same specimen indicated a time-dependent change

[6]i.e., the maximum speed that did not cause a measurable increase in the hysteresis between the advancing and receding contact angles for the equipment and calculation methods employed (see Fig. 2.10)

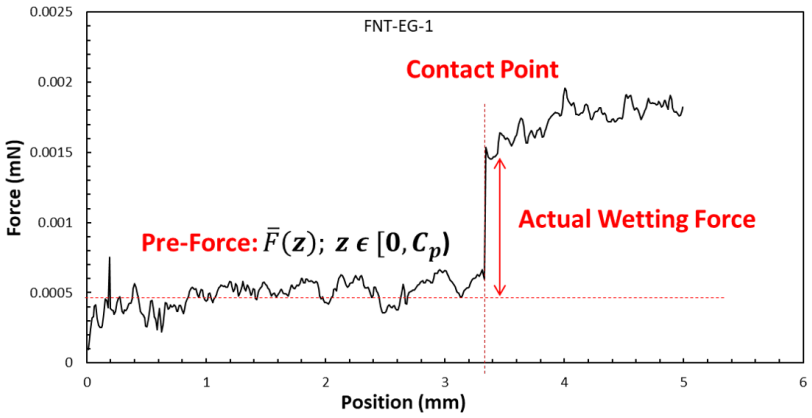


Figure 3.9: Typical Force versus Position result obtained for Flax Fibres when the device sensitivity is set to its minimum (1 µg). The force measured before the contact point (pre-force) is attribute environmental interference and must be subtracted from the values after contact point (corresponding to a jump in the curve, which is related to the wetting force) [47]. Results from untreated fibres tested using ethylene glycol.

in the measured properties. To minimise the impact this phenomena could have on the final results, the fibres were changed at each new cycle.

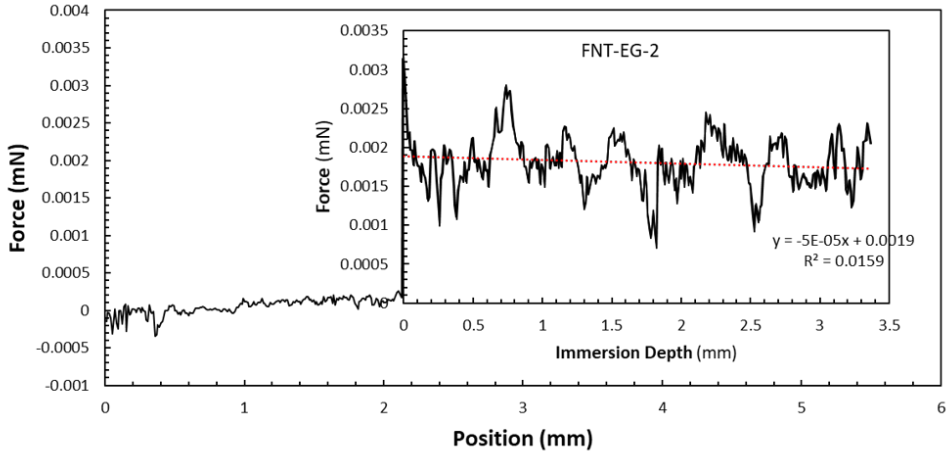


Figure 3.10: Illustration of the raw force data treatment procedure. The curve presented in the inset had the pre-force subtracted and contact-point set to zero. Results from untreated fibres tested using ethylene glycol.

At least three probe liquids are required to perform the measurements so as to obtain the three components of the fibre surface energy according to the van Oss model. Among the available triplets, that with the lowest condition number, water, diiodomethane and ethylene glycol, (see Tab. 2.3), was chosen so as to minimise the system output sensitivity to errors in the input (see section 2.1.4.2). All probe liquids used in the present work were analytical grade (ultrapure water: 18.2 Ω cm resistivity, diiodomethane 99%: Acros, and ethylene glycol 99%: Sigma–Aldrich). C. A. Fuentes et al. [26] reported that this triplet presents a low condition number (5.4) when compared to other triplets commonly found in the literature. Indeed the values reported by C. Della Volpe and S. Siboni [128] for several triplets are all above 5.98. Additionally, hexane was used to determine the wetted perimeter as described in section 2.1.4.3, procedure that was carried out immediately after the contact angle measurement so as to assess the sample dimensions as close as possible to that of the wet fibre. This was performed in advancing

mode using higher wetting speeds, 1 mm/s, sufficiently low to ensure kinetic equilibrium.

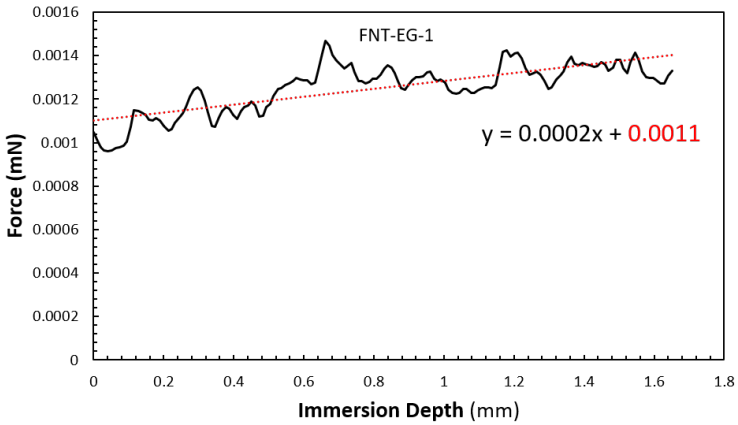


Figure 3.11: Typical Wetting Force versus Immersion Depth curve for Flax Fibres using hexane as probe liquid. The force at zero immersion, obtained by linear regression, is used to calculate the wetted perimeter, which is then employed in the subsequent contact angle calculations.

3.2.5.2 Data Treatment

Fig. 3.9 shows a typical raw data plot of force as a function of position obtained for elementary flax fibres. As discussed in the previous section, although the maximal immersion depth was set to 5.5 mm the fibre probed length was around 3.5 mm, and thus an initial region of at least 2 mm in which no fibre wetting took place was observed for all the specimens. However, due to the low magnitude of the wetting force, a high sensitivity had to be set and even before fibre-liquid contact, an approximately constant pre-force was measured (indicated in Fig. 3.9), phenomena usually observed in this kind of experiments, whose origins are still unknown [7][47]. It was demonstrated by S. Qiu et al. [47] that the actual wetting force can be obtained by subtracting the pre-force from the values acquired after contact point (see Fig. 3.9). In the present work, an approach similar to that suggested by Qiu et al. [47] was followed, assuming that the pre-force was the average of force values before contact point, which subtracted from all the data-points. Additionally, the position referential was set on the probe liquid surface by setting the contact point to zero. The raw data treatment procedure is illustrated in Fig. 3.10, the inset curve corresponds to the values used in the final calculations. The same treatment was applied to the raw data obtained for wetted perimeter determination. Although the linear regression in this curve was not used to calculate the contact angles, it allows for a quick visual estimation of the final results, provided it is approximately horizontal. For each probe liquid, 5 specimens of each fibre type were tested using a data sampling of 0.01 mm^{-}1 and probed length of approximately 3.5 mm, resulting in approximately 1750 valid force data-points per fibre-liquid pair that were average in the calculate each of the three fibre-liquid characteristic contact angles according to Eq. 2.15 and the assumptions discussed in section 2.1.4.3. Those contact angles were then treated according to the van Oss model [125] so as to obtain a dispersive, electron donor and electron acceptor surface free energy components characteristic of each fibre type surface, the theory behind these calculations is extensively discussed in section 2.1.4.2. Surface energy components from the contact angles were calculated using Surften 4.3, a program for calculation of acid-base solid surface free energy components by Professor C. Della Volpe [261], using the scale developed by C. Della Volpe and S. Siboni [51, 262].

[7]Most probably related to environmental perturbation, such as air flow due to liquid vessel holder movement [47].

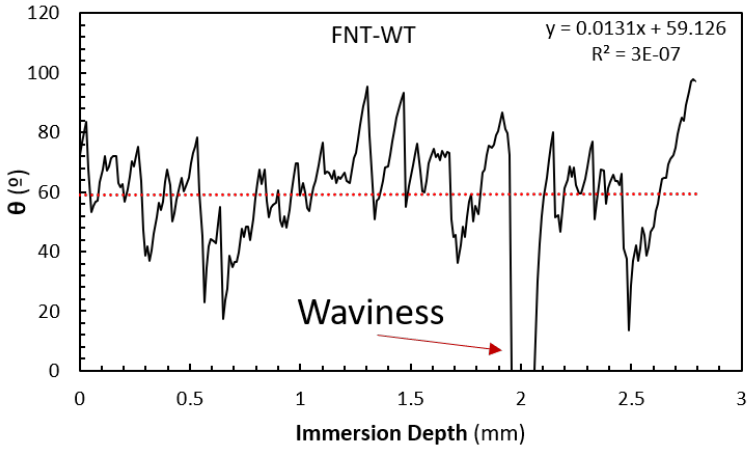


Figure 3.12: Typical contact angle curve presenting waviness signature (sudden drop to $\theta = 0°$). Results from untreated fibres tested using water.

Treated force values for measurements using hexane as probe liquid were used to calculate the wetted perimeter. In this case, since $\theta_{\text{hexane}} \approx 0°$, all deviations of the mean force from a constant value were attributed to non-wetting phenomena (e.g., buoyancy). Following the approach of Qiu et al. [47], these non-wetting contributions were eliminated by taking the force values at zero immersion depth from linear regression (for more details on this assumption, the reader is referred to section 2.1.4.3), see Fig. 3.11. These force values were then introduced in Eq. 2.16 to calculate the wetted perimeter of each specimen.

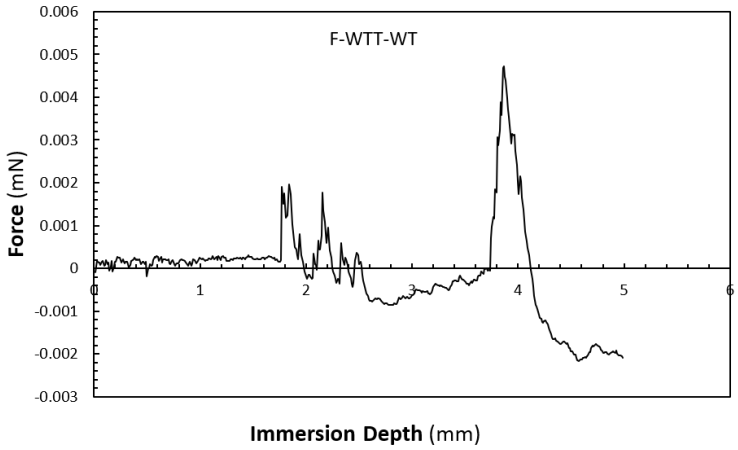


Figure 3.13: Typical raw data force curve presenting bending signature (negative-force regions followed, or not, by sudden peaks). Results from water-washed fibres tested using water.

3.2.5.3 Conditions for Data Elimination

In sections 2.1.4.3 and 2.1.4.5 several possible error sources and their consequences on the measurements were discussed. Although it is not always possible to eliminate all sources of error in the measurements, some of them result in a characteristic effect on the readings. Two of the most characteristic non-ideal behaviours detected were waviness (see section 2.15 for details) and fibre bending due to insufficient fibre specimen stiffness (see section 3.2.5.1). The fingerprint of waviness is a sudden

peak or valley in the force readings, Fig. 3.12 depicts a typical contact angle curve presenting waviness, resulting in a sudden drop to $\theta = 0°$. Fibre beding resulted in complete invalidation of the results with characteristic negative-force regions (see Fig 3.13). Waviness and Bending characteristic readings were used as criterion to discard specimens.

3.2.6 Microbond Test

3.2.6.1 Setup Description and Protocol

The microbond test was performed to assess the interfacial shear strength of flax-epoxy microcomposites. Untreated, aminosilane treated, water-washed and ethanol-washed elementary fibres (isolated as per section 3.2.1) were used in the manufacturing of microcomposite samples composed of a single microdrolet deposed in an elementary fibre glued to a standard paper support, as described in detail in section 3.2.2. The setup used to perform the experiments was adapted from the work of S. Safi et al. [48], it is presented in Fig. 3.14A and schematically represented in Fig. 3.14B. Below, the protocol followed to perform the experiments is briefly presented.

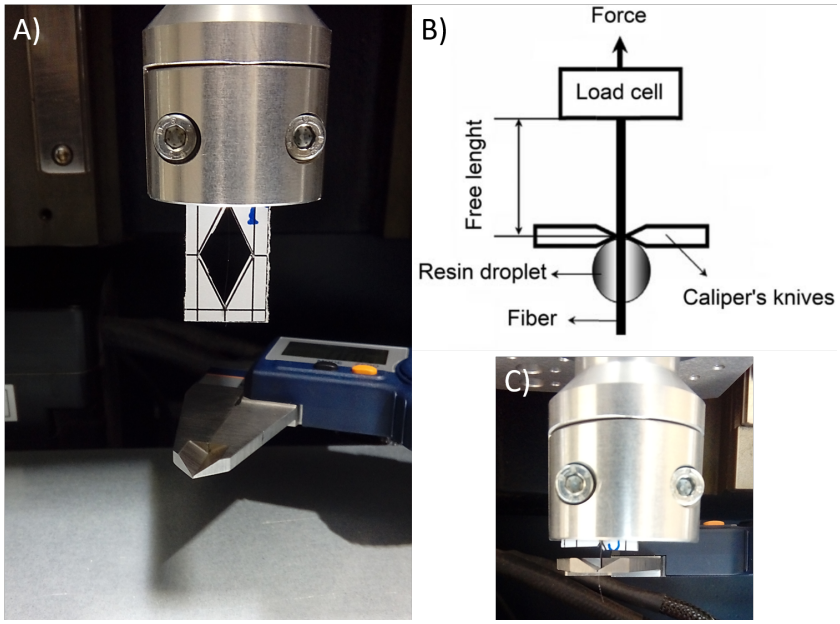


Figure 3.14: Gripped Microbond Specimen: A) Elementary fibre with deposited microdroplet placed in paper support; B) schematic representation of a microbond test setup with identified components [48] C) Microdroplet held by caliper. Caliper's knives gap was adjusted for each specimen according to the measured fibre diameter

1. The paper specimen was attached to a 1 - 10 N load cell (calibrated for forces ∼100 mN) of a Bruker's Universal Mechanical Tester (UMT) (see Fig. 3.17A) using a clamp;
2. the inferior part of the paper support and the fibre next to the inferior glue point (below the droplet) were cut. To grip the droplet, a caliper is used;
3. The free fibre is then positioned in between the caliper's knives, such that the knives were above the target droplet (see Fig. 3.14C). The distance between the knives was then set to 10 µm larger than the measured fibre diameter or the largest neighbour droplet, it was equal or smaller 60 µm for all tested samples. This ensured that the target droplet, rather than a neighbour or the fibre itself were griped by mistake.

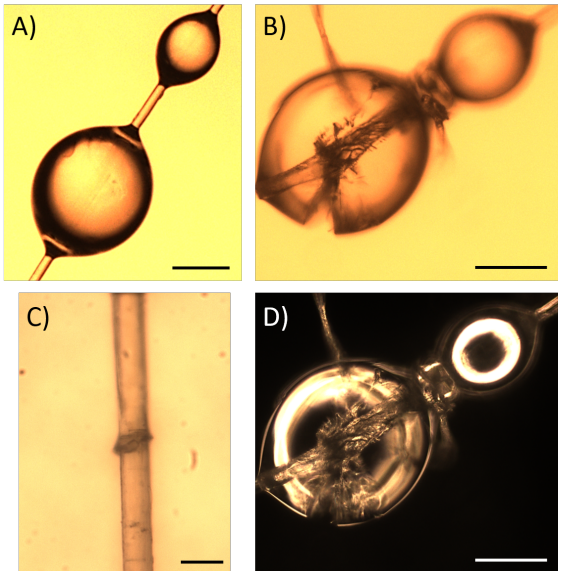


Figure 3.15: Optical Micrographs of Microbond specimen: A) Before experiment (Bright Field, Scale Bar 100 µm); B) After experiment (Bright Field, Scale Bar 100 µm); B) After experiment (Bright Field, Scale Bar 100µm); C) After experiment, broken droplet meniscus and debonded region in the fibre (Bright Field, Scale Bar 25 µm); D) After experiment, highlighting broken interface inside drop (Dark Field Field, Scale Bar 100 µm).

4. The crosshead was then moved up so as to have the droplet just below the caliper's knives;

5. The experiment was then carried out in tensile mode using a displacement rate of 0.017 mm/s ($\approx$ 1 mm/min). Once the droplet interface failed, the specimen was removed from the equipment and stored for further analysis using optical microscope (see Fig. 3.15).

The tests resulted in one of the two possible outcomes:

- **Interface Failure**: Force displacement curve presented an increase and sudden drop followed by a region with non-zero force values, composed of smaller receptions of the previous behaviour if

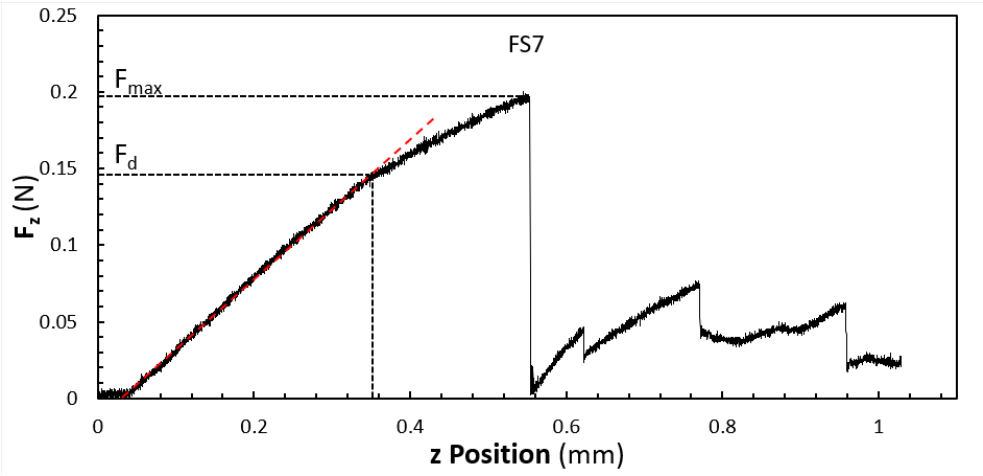


Figure 3.16: Typical Force versus Position curve obtained from microbond tests using Bio-epoxy resin and Flax Fibres. Debonding (F_d) and Maximum (F_{max}) are indicated, they correspond respectively to the initial force at which crack propagation starts and the force at the moment in which the sum of the friction and interfacial adhesion forces are surpassed by the tensile force, resulting in catastrophic failure of remaining bonded surface

there were smaller-diameter neighbours (see Fig. 3.16) or constant, corresponding to the frictional forces. Results presenting this behaviour were accepted

- **Fibre Failure**: Force displacement curve presented an increase and sudden drop to zero, remaining constant. Results presenting this behaviour were rejected.

3.2.6.2 Data Treatment

As extensively discussed in section 2.1.5, the apparent interfacial shear strength was used to assess surface energy, this value was calculated as the ratio of the maximum recorded force,F_{max}, to the approximate fibre embedded area, πlD, (Eq. 2.28). The fibre-resin interface area (embedded area) was approximated as the product πlD, using the specimen embedded length, l, and fibre mean embedded diameter, D, both measured as per section 3.2.2. F_{max} was taken directly from the experiment readings (see Fig. 3.16).

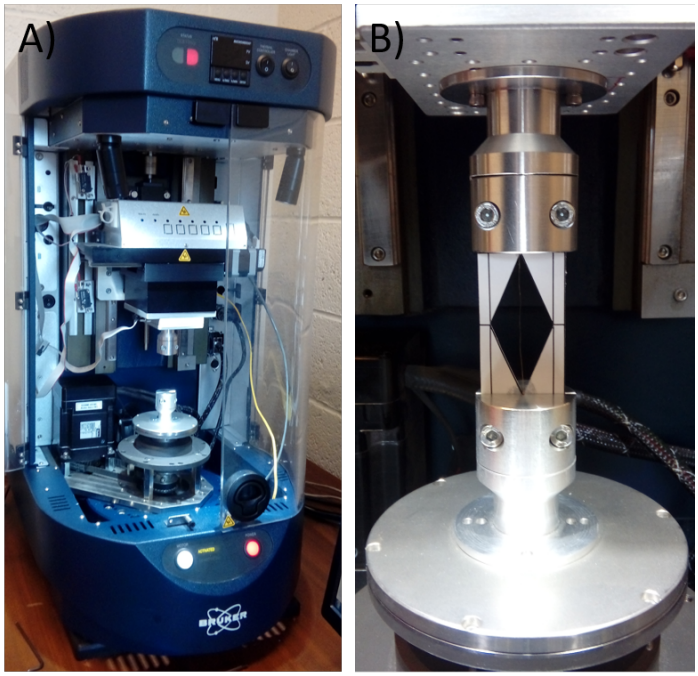


Figure 3.17: A) Bruker's Universal Mechanical Tester (UMT) - machine used for Microbond and Tensile Tests. B) Gripped Tensile Test Specimen

3.2.7 Tensile Test

3.2.7.1 Setup Description and Protocol

Fibre mechanical properties, in combination with fibre-matrix interface strength and area, determine the quality of the reinforcement. To complement the characterisation of the studied flax fibres as composites reinforcements, tensile tests were performed so as to determine their mechanical properties. Following the standard for determination of tensile properties of elementary flax fibres for plastic composites (NF T25-501-2 [263]), widely used in the literature [264–267], the Young's Modulus of untreated elementary fibres specimens whose dimensions were previously measured (refer to section 3.2.2) were determined from tensile tests performed using a Bruker's Universal Mechanical Tester (UMT) (3.17A)

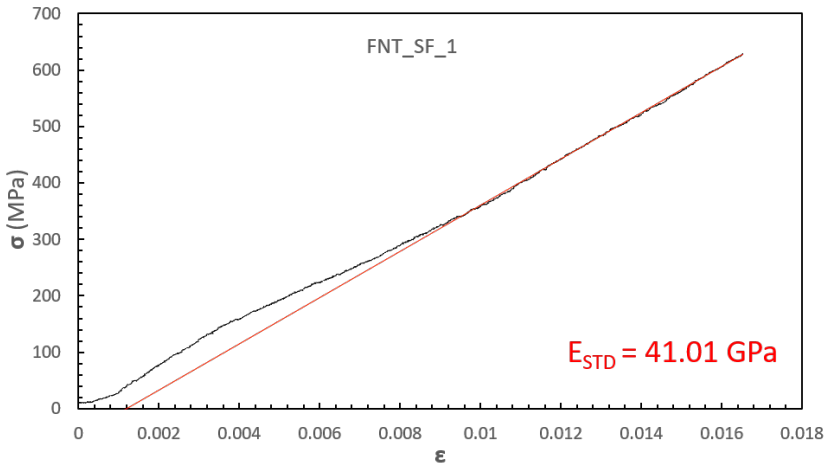


Figure 3.18: Typical curve strain-stress for non-(pre)strained elementary flax fibres. The Young's Modulus is obtained from the slope of the linear region according to the Standard for determination of tensile properties of elementary flax fibres NF T25-501-2

equipped with a 1 - 10 N load cell (calibrated for forces $\sim$ 10 mN), with displacement rate defined as 0.017 mm/s ($\approx$ 1mm/min). A brief summary of the protocol followed is presented below:

1. Elementary fibre specimens glued to paper supports prepared as per section 3.2.2 (see Fig. 3.2b) were clamped in the equipment as presented in Fig. 3.17B. Clamping was made on the glue point of the paper specimen, ensuring the that gauge length tested equalled that previously measured in section 3.2.2. Great care was taken to align the fibre specimen with the axial direction of the crosshead by meticulously centring its ends in the clamps, this allowed to avoid parasitic forces in the transverse plane.

2. The paper support was cut in its middle on both sides, freeing the fibre specimen, now sustained due to clamping;

3. The measurement was started and once the fibre failed data-acquisition was stopped. Fibre failure was determined visually and confirmed by the drop to zero in the recorded tensile force.

4. The specimens were removed from the equipment and store for subsequent study using optical microscope.

3.2.7.2 Data Treatment

Using the specimen dimensions, previously measured according to protocol described in section 3.2.2, in accordance with the standard NF T25-501-2, the raw data, measured as Force-Position, was converted into specimen Strain-Stress, whose typical behaviour for the elementary fibres studied in the current work is presented in Fig. 3.18. Data Treatment for extraction of tensile properties was also obtained according to NF T25-501-2, this standard assumes that the fibre Young's modulus is determined as the slope of the stress–strain curve before rupture, red line in Fig. 3.18. Fibre tensile strength and strain at break were taken as the coordinates of the last point in the curve strain-stress.

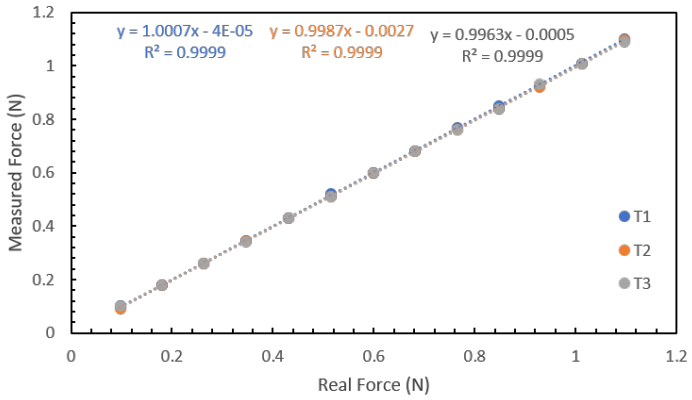


Figure 3.19: Load cell calibration curve for force values from 0.1 N to 1 N using standard specimens whose weight was assessed with $\sim$ 1 mN precision. Correlation was demonstrated to the 4th decimal digit of the coefficient of determination three times.

3.2.7.3 Calibration and Experimental Error

Prior to executing the experiments, the load cell was calibrated to force values from 0.1 N to 1 N using standard specimens whose weight was assessed with $\sim$ 1 mN precision. Fig. 3.19 presents a curve of Measured Force as a function of the Real Force determined by the total weight of the specimens clamped to the equipment. The objective of this procedure was to assure that the load cell, whose specifications are for 1 to 10 N forces could still be used to assess forces one order of magnitude below this range in a reliable fashion[8], typical order of magnitude and tensile and microbond experiments. Correlation was demonstrated to the 4th decimal digit of the coefficient of determination, meaning that the equipment is sufficiently sensitive and accurate to the experiments.

Since the specimens deformation was measured according to the crosshead displacements (it is not practical to attach bulky gauge extensiometers to the fibres), and the equipment cannot be considered perfectly rigid, the effective deformations measured were expected to be influenced by the machine compliance. Because tensile testing was performed only as a quick assessment of the fibres mechanical behaviour, used only for qualitative comparative purposes, rather than precise quantification, compliance was not accounted for. Basically, when the system is assumed to have only elastic deformation due to the loading, the assembly equipment-fibre can be thought as an association of springs in series, whose measurements will account for the resultant spring constant, which is lower than the fibre specimen spring constant (or Young's Modulus for that matter[9]); accordingly, the measured deformation is smaller than the fibre deformation. A reader wanting to further understand the impacts of this assumption and how to account for it is referred to Appendix D.

[8]It is common place in the literature to report just the maximum force value allowed by the load cell, which does not completely characterise its valid range of operation.

[9]$E=k\frac{L_0}{A}$, where A is the cross-sectional area, L_0 the initial length and k the spring constant of the fibre specimen

4 Results and Discussion

4.1 Chemical Analysis

With the objective of determining the nature and quantity of chemical functionalities on the fibre surface contributing to interfacial strength and compatibility with epoxy resins of known composition, X-ray photoelectric spectroscopy (XPS) analysis was performed on untreated and aminosilane-treated fibres. In this section, XPS analysis results are mainly described and explained. These results are then further employed in subsequent sections so as to draw more conclusions, particular in parallel with the results from Physicochemical Interactions in section 4.2.

Table 4.1: XPS analysis of Untreated and Silane-Treated Flax Technical Fibres presenting Elemental Surface Atomic Fraction (s.at.%) and Binding Energy (B.E. - eV) by bond. Silane-Treated Fibres were analysed twice in different locations proving chemical heterogeneity.

Type	Reading	$Zn_{2p_{3/2}}$	O_{1s}	N_{1s}	$Ca_{2p_{3/2}}$	C_{1s}					Si_{2p}		
						O=C-O	C=O, O-C-O	C-(O,N)	C-(C,H)	C tot.	SiO_2	Si-O-C	Si tot.
Untreated	B.E. (eV)	1022.1	532.5	400.1	347.4	289.2	288.1	286.5	284.8	80.378	102.1	—	1.142
	s.at.%	0.254	16.615	0.808	0.802	1.132	3.742	9.963	65.541		1.142	—	
Silane-Treated 1	B.E. (eV)	1022.0	532.9	400.0	347.4	288.7	287.8	286.5	284.8	68.976	102.4	101.1	1.624
	s.at.%	0.138	27.453	1.16	0.648	2.301	5.035	22.445	39.195		0.874	0.75	
Silane-Treated 2	B.E. (eV)	1022.1	532.5	400.0	347.4	288.9	287.9	286.4	284.8	69.097	102.1	101.1	1.555
	s.at.%	0.08	27.134	1.538	0.596	1.321	5.571	21.449	40.756		0.788	0.767	

Zinc: The amount of Zn detected is close to the detection limit (0.1%), especially in the case of silane treated fibres, even though, it was an expected element at the surface of plants. Zn is a common and important element in plants metabolism, in which it is usually found in its ionic form engaging in low molecular weight complexes, storage metalloproteins, free ions and insoluble structures associated with the cell walls. Zn's strong tendency to form tetrahedral complexes with N-, O- and S- is what underlies most of its metabolic functions in plants [268].

Oxygen: Although O is the second most abundant element, its chemical shifts are relatively small, which hinders 1s decomposition. A common approach in plant fibres surface chemistry analysis is to perform an O balance so as to estimate the relative concentration of their different main biochemical compounds, whose ratio O/C is well known. However, this is an approach mostly used for lignin-rich fibres since lignin, differently from carbohydrates such as cellulose, hemicellulose and pectins, has carbons that are not bonded to oxygen and a distinct O/C ratio. Flax is a cellulose-rich fibre, rather than a lignin-rich one, whose surface is rich in pectin, hemicellulose, and cellulose, all polyhydroxylated macromolecules with similar composition, although their O to C ratio is slightly different, the absence of the distinct carbons C-(C,H), present in lignin, hinders the estimation of the compounds fraction on the fibre surface by Oxygen balance with Carbon. It is possible to observe an increase in the fraction of oxygen after the treatment, this was an expected result, since the sizing used presents 6 Si-O-CH_3 functionalities that, after hydration to silanol (Si-OH), can react with the hydroxyls on the surface of the fibres.

Nitrogen: N is notably present as a component of the plants amino acids. Additionally, it can be found in the form of nitrates in minerals extracted from the soil. Its increase in the sized fibres is a clear indication of the sizing agent, Bis(trimethozysilylpropyl)amine (see Fig. 3.1b), presence.

Calcium: Ca is another common compound found in plants. It comes either from minerals (e.g., silicates) or, most importantly, from pectates, more specifically in ionic crosslinks joining two pectin molecules via ionic interactions with carboxylates moieties from galacturonates (see fig. 2.5).

Carbon: The C1s characteristic readings were decomposed in 4 components with the same full width at half maximum (FWHM).

1. The peak at B.E.≈284.8 eV corresponds to the shift for non-oxidised forms of carbon[1];
2. at B.E.≈286.6 eV, the peak evidencing carbon bonded to a single more electronegative element, such as C-N and C-O (i.e., degree of oxidation +1), is observed;
3. at B.E.≈288 eV, the peak referent to C^{+2} is seen. This peak is mostly related to O-C-O or C=O bonded carbon atoms;
4. at B.E.≈289 eV, C^{+3}, usually referent to O=C-O carbon species, can also be noticed.

Flax Fibres are mostly composed of the carbohydrates present in the secondary and primary phloem sclerenchyma cell walls, well-known for being polyhydroxylated molecules. As expected, the most common forms of carbon in these polysaccharides are C-C, C-H and C-O, as observed in the results. Nonetheless, other forms can come from multiple sources, such as the lipids in waxes and pectates.

The treatment with a silane compound, results in an observable decrease of the relative amount of C-C and C-O with respect to C-O, C-N and C^{+2}-species, which is, once again, consistent with the chemical structure of the sizing agent (see Fig. 3.1b).

Silicon: Finally, Si2p presents, or not, two components according to specimen analysed. In untreated and treated fibres, the peak at chemical shift B.E. ≈ 102 eV is observed. This peak is attributed to an 'intrinsic' form of Si in the fibres. As it is well-known, Si is an atom seldom, or not found, in biochemical reactions [2], that is why this 'intrinsic' Si most probably comes from minerals in the form of silicates. In silane-treated fibres though, a second peak at B.E.≈101 eV, which befits Si as it is found in the sizing agents (Si-O-C) is observed. This further confirms and allows to characterise the bonds resulting from the sizing treatment.

4.2 Physicochemical Interactions

Physicochemical interactions between flax fibres and epoxy resin were assessed using the Wilhelmy Technique, allowing to obtain the contact angles between the different surfaces analysed and a series of liquids, which were used to obtain their surface free energy components according to the van Oss model. All the theory, their assumptions and limitations, relevant results in the literature and the protocols followed to perform the experiments were discussed in sections 2.1.4, 3.2.5 and 2.2.1. In this section, the results obtained for untreated fibres (NT), aminosilane treated fibres (S), water-washed (WTT) fibres and ethanol-washed (EtT) fibres are presented and briefly described, compared with those in the literature (in special to studies that have used similar methods and models), and finally a rationalisation of these values is attempted on the basis of surface chemistry results and additional information about flax fibres surface available in the literature.

[1] C-H and C-C are respectively reduced and non-oxidised carbon forms in biochemistry.

[2] For an interesting discussion on the topic, see how the Nobel-Laureate Francis Arnold and her research group at Caltech 'convinced' cells to 'bring Silicon to life' [269]

Table 4.2: Surface Energy components of Natural fibres submitted to different treatments (NT: Untreated; S: Silane-Treated; EtT: Ethanol-Washed and WTT: Water-Washed Fibres) according to the van Oss model (γ^{LW} : Lifshitz–van der Waals, γ^{+} : Acid or Electron Acceptor, γ^{-} : Basic or Electron Donor, γ^{AB} : Acid-Base or Lewis-like, γ^{Total} : Total surface free energy components) using the Wilhlemy Technique with three probe liquids (WT: Water; EG: Ethylene Glycol; DIM: Diiodomethane) to characterise the fibres contact angle θ. The Work of Adhesion (W_A) is calculated using the surface free energy components of a DGEBA-base system [58], similar to the one used in the present work.

	Van Oss Components (mN/m)					θ (°)			
Fibre Type	γ^{LW}	γ^{+}	γ^{-}	γ^{AB}	γ^{Total}	WT	EG	DIM	W_A (mJ/m^2)
S	23.056	0.041	7.777	1.135	24.191	76.627	70.110	69.673	62.479
WTT	25.006	0.252	3.737	1.942	26.948	82.926	63.716	66.222	64.870
EtT	26.108	0.116	5.476	1.592	27.700	78.373	64.060	64.292	66.049
NT	26.807	0.429	9.652	4.071	30.877	67.248	54.575	63.073	69.642
DGEBA-Epoxy Resin	35.1	0.68	5.85	3.989	39.089				

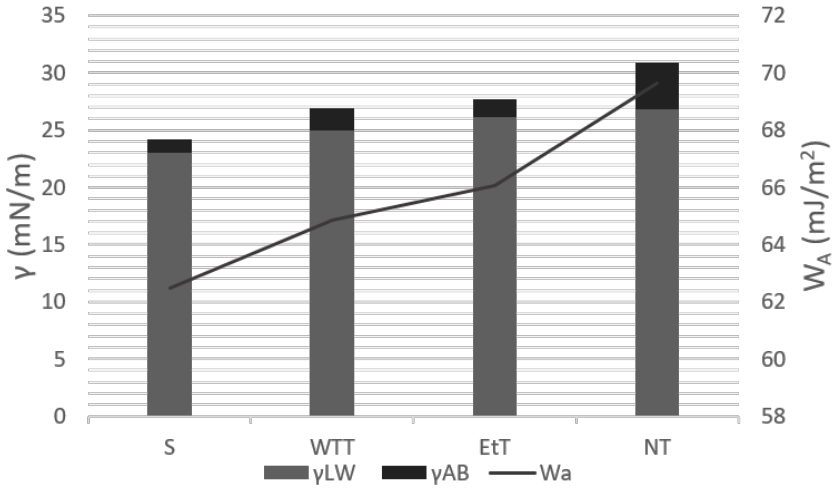


Figure 4.1: Total Surface Free Energy divided in acid-base (AB) and Lifshitz van der Waals (LW) components, and respective work of Adhesion with Epoxy Resin with properties presented in table 4.2 for NT:Untreated; S: Silane-Treated; EtT: Ethanol-Washed and WTT: Water-Washed Fibres

4.2.1 Surface Energy Results Presentation

Table 4.2 presents the contact angles of the different pairs fibre-probe liquid and the surface free energy components calculated from these angles according to the van Oss model, using the acid-base scale for liquids developed by C. Della Volpe and S. Silboni [51] (see table 2.3). Except for S fibres, water (WT) seems to present the highest contact angle, and ethylene glycol (EG) the lowest, a reasonable result, knowing that water has the highest surface free energy and ethylene glycol the smallest (see table 2.3). The explanation to the contrasting behaviour of S fibres is its much smaller acid component, which weakens its interactions with the notably basic ethylene glycol. In terms of absolute values, the range of advancing contact angles obtained is in good agreement with those in similar studies [137–139].

A more precise evaluation of the surface physicochemical interactions can be done considering the surface free energy components. Cleaned and treated fibres all present a decrease in dispersive component with respect to NT fibres. In EtT fibres and WTT fibres, this behaviour is mostly expected to stem from the removal of the undesirable surface waxes (which are weakly attached to the fibre surface, contributing

Table 4.3: Dispersive (W_A^d) and Acid-Base (W_A^{AB}) components to the total work of adhesion of Ethylene-washed (EtT) and Water-washed (WTT) fibres

Fibre-Resin	$W_A^d = 2\sqrt{\gamma_f^d \gamma_m^d}$	$W_A^{AB} = 2\sqrt{\gamma_f^+ \gamma_m^-} + 2\sqrt{\gamma_f^- \gamma_m^+}$	W_A
EtT-Epoxy (mJ/m^2)	60.543	5.505	66.049
WTT-Epoxy (mJ/m^2)	59.252	5.618	64.870
Δ(Et – WTT) (mJ/m^2)	1.291	-0.113	1.178

to a lower interfacial adhesion), the main objective of such cleaning procedures. Accordingly, the water washing protocol is expected to be more efficient in its main end. Nonetheless, when EtT and WTT specimens work of adhesion with epoxy is considered, it appears that the physicochemical interactions would contribute to a stronger adhesion in composites made with the former type of fibre. Although the cleanings procedures had an important impact on fibre acid and base components, overall, their specific interactions (see γ^{AB}) are similar and cannot explain the difference in W_A, rather than that, this phenomena is mostly due to the difference in dispersive components. This fact can be put in evidence calculating the dispersive and acid-base contributions to the work of adhesion for each specimen (see table 4.3), indeed, the acid-base component of the work of adhesion is actually higher for the WTT fibres, contributing to even out the final values, instead of increasing the difference. Since it is known that the removal of waxy components and consequent reduction of the dispersive component is a positive outcome to fibre-matrix adhesion since waxes are poorly attached to the surface, creating a weak layer, it is likely that EtT fibres surface, which appears to be better in terms of physicochemical interactions, is actually worse due to the higher presence of waxes. This hypothesis is tested assessing the interfaces micromechamical properties (see section 4.3). In addition to that, the decrease in the acid-base components was an expected phenomena mainly due to removal of remaining middle lamella pectins from the fibre surface and, depending on the harshness of the cleaning, hemicelluloses and pectins composing the elementary fibres amorphous matrix [189, 260]. Even though the cleaning methods were chosen among the less harsh available in the literature, hemicelluloses and pectins from the elementary fibres matrix may have been removed, case in which a reduction in the fibre-matrix interface adhesion is expected to occur due to reduction of the fibre internal cohesion, promoting pilling [168] (previously discussed in section 2.2.2).

Aminosilane-treated fibres also presented a reduction in γ^{LW}. This was expected since the first step of this chemical treatment is a degreasing, so as to prime the fibre surface, I. de Weyenberg [35] report a typical procedure in which a mixture of hexane/ethylacetate is used. In this case; however, the additional contribution of the aminosilane compound grafted to the surface of the fibres is expected to result in a significant impact on the surface energy components. Indeed, as discussed in section 2.2.1.1.1, a typical approach employed in the literature is to relate the functional groups on the fibres surface to the specific and non-specific components of the surface energy [194–197]. By XPS analysis, a common practice is to use the relative surface atomic fractions and the decomposition of C1s peaks [3], assuming that the relative portion of C-[C,H] in C1s is related to the aliphatic and aromatic carbons, which engage in Lifshitz-Van Der Waals interactions, while C-[O,N], O-C-O and C=O, and C≡O would be representative of the specific interactions [139]. Most probably due to the particularities of the aminosilane chemistry, having Si and N atoms contributing to the the final interactions, part by chemical bonding, part by hydrogen bonding, this approach does not hold true in the present work (as per values presented in table 4.1) so that the surface energy components do not relate in a straightforward fashion to the fraction

[3] In the case of fibres presenting a high degree of lignin (fibres from the plant xylem), which is not the case of flax, the characteristic O/C fractions can be linked to the amount of lignin and cellulose.

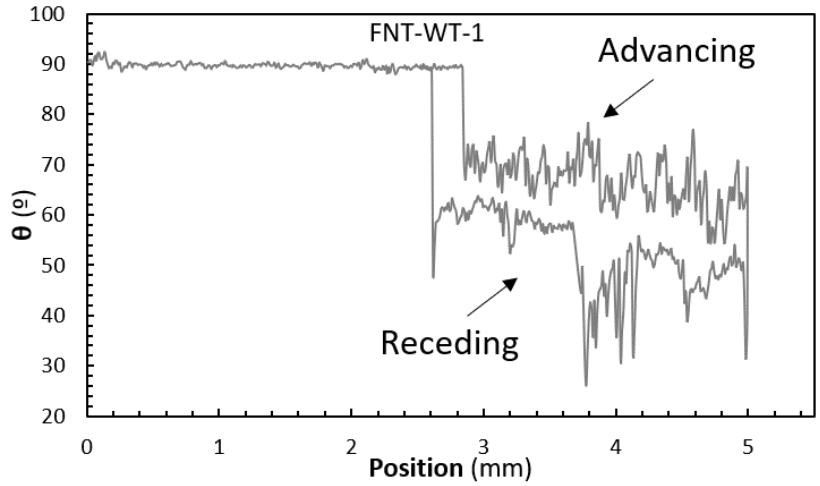


Figure 4.2: Example of non-usual results presenting non-zero receding angles. Obtained from untreated fibres using water as probe liquid.

of the different components in C1s decomposition, which would lead to a 43% polar character, while the actual value is only 4.6% (assuming it to be $\gamma^{AB}/\gamma^{Total}$). Untreated fibres; on the other hand, present a reasonable agreement between the components of C1s peaks and the values obtained from contact angles. While the latter indicate a surface whose acid-base character accounts for 13% of the interactions at the surface, XPS indicates an 18% polar surface. A corollary from these results is that the low work of adhesion obtained for aminosilane-treated fibres when compared to the compared to the other specimens (see Fig. 4.1) may not be the most representative of the practical fibre-matrix adhesion, case in which chemical bonding would be expected to be the dominant contributor. This proposition will be tested using the results from microbond specimens results.

4.2.2 Critical Comparison with the Literature

The surface energy values obtained in the present work seem to follow the general trend of results in the literature, with dominant non-specific interactions (see table 2.4), particularly the works of K. Van de Velde and P. Kiekens [137] and W. Woigk et al. [139] using Wilhelmy plate and advancing contact angles to assess surface energy, the latter employing the van Oss model and the study of J. M. Van Hazendonk et al. [178] using Floating test. These works are discussed and compared in section 2.2.1.

A major limitation of the Wilhelmy Technique applied to flax fibres is the impracticability of receding contact angle measurements, often droping to zero due to a series of factors, such as surface roughness and the cosine dependence of the final values (see section 2.1.4.3). The use of advancing contact angles to calculate surface energy leads to underestimation of the final values, since these angles will often be higher than the true equilibrium contact angles (most stable contact angles [120]), even in the approach to kinetic equilibrium at low wetting velocities, or using the molecular kinetic theory, cases in which the static advancing contact angles are determined (see Fig. 2.12a). This is most probably the reason the present work seems to particularly agree with studies that also used the Wilhelmy technique [137, 139], whose results are amongst the lowest in the literature. Nevertheless, in rare cases, receding contact angles were obtained in the present study (see Fig. 4.2), K. Van de Velde and P. Kiekens [137] also report receding contact angles measurements. Since these results could not be treated in a statistically significant fashion and were likely to result in misleading conclusions, as in K. Van de Velde and P. Kiekens work, these values were not treated. It may be worth to further investigate these particular

cases, whose results usually fit in a reasonable range. However, this is out of the scope of the present work.

A particularly good agreement was obtained with the results of W. Woigk et al. [139], whose experimental conditions, probe liquids, equipment and fibres provider were identical as the ones used in the the present work. Nonetheless, W. Woigk et al. tested technical fibres rather than elementary fibres. As a result, a higher content of pectins from the middle lamella and a higher liquid absorption are likely to have affected their results. When compared to waxes, pectins have a higher disperse and polar components (see table 4.4), which is in good agreement with the differences between their results and the ones obtained in the present work (see table 2.4). The effect on the wetting line deflection due to liquid absorption is a more complex phenomena, whose impacts are difficult to predict.

Table 4.4: Polar and dispersive components of some of main biomolecules contributing to flax surface energy according to various sources

Material	Method - Model	γ^{d} (mJ/m2)	γ^{p} (mJ/m2)	Reference
Cellulose	CAA—geometric mean	27.5 (±1.5)	41 (±2.9)	[191]
Cellulose	CAA—harmonic mean	26.5 (±1.1)	43.0 (±2.4)	[191]
Cellulose	IGC—finite concentration	43.4	—	[144]
Hemicellulose	CAA—geometric mean	35.3–39.5	—	[201]
Lignin	Fowkes plot	40	—	[201]
Pectin	CAA—geometric mean	31.7	3.50	[270]
Waxes	CAA—geometric mean	26.5	0	[144]

Curiously, the results obtained using a peculiar technique, Floating test, by J. M, Van de Hazendonk et al. [178] also present a relatively good agreement with the current work. The impacts of washing treatments with similar objectives and wahing liquids on the fibres; however, differs from that observed in the present work. As an example, their extraction of fatty acids using ethanol, which is expected to have a similar impact as the cleaning method performed in the present with work hot ethanol, resulted in fibres with γ_{sv}^{p} ≈37.6 mJ/m^2 and γ_{sv}^{p} ≈ 2.7 mJ/m^2, with higher rather than lower total surface energy, presenting an increase of approximately 6 mJ/m^2 as opposed to our results, that were about 3 mJ/m^2 lower than untreated fibres. Even though, it is important to highlight that J. M, Van de Hazendonk et al. employed a considerably harsher 6 h-extraction using Soxhlet apparatus; moreover, their results are in good agreement with what is expected from a surface mainly composed of Pectin, Hemicellulose and Lignin, as per table 4.4. Therefore, if these results are correct, the hypothesis of the lower efficiency of waxy compounds removal in EtT fibres when compared to WTT is also expected to hold true, and overall, both water- and ethylene-washing are expected to result in a rather poor surface degreasing, which may be compensated by higher mechanical properties due to better structural integrity with respect to J. M, Van de Hazendonk et al. specimens. This fact remains to be further studied. Unfortunately, no reproduction of the floating test applied to flax fibres could be found in the literature.

IGC has become increasingly common in studies of surface energy analysis. Even though a few issues related to this technique may still remain to be solved, the complicate handling of elementary fibres and the incertitude in the equilibrium approach are much less problematic (see discussion in section 2.2.1.1.1). The only result in the literature found to apply IGC in combination with the van Oss method, and thus allowing for comparison with the present work, was provided by A. Legras and coworkers **??** recently. Both, their Lifshitz-van der Waals (γ_{sv}^{LW} ≈ 39.1 mJ/m^2) and Acid-Base (γ_{sv}^{AB} ≈ 6.9 mJ/m^2) surface free energy are greater than those obtained in the present work. Nonetheless, the relative contribution of the different components to the total surface energy is in good agreement, with a 15% acid-base character

??, compared to a 13% acid-base character here obtained (see table 4.2). Bearing in mind that our results were obtained using advancing contact angles and that this is expected to underestimate the surface free energy, the results of A. Legras et al. seem a good candidate to what would be expected if the most stable contact angles were used to calculate the surface energy components of the specimens studied in the present work.

Other results presented in table 2.4, such as those of C. Baley et al. [144] and G. Cantero and coworkers [138], had higher values and no particular correlation with our results. A discussion about these and other works reported in the literature of flax fibres surface energy is provided in an overview offered in section 2.2.1.

4.2.3 Partial Conclusion

Bearing in mind the limitations of using static advancing contact angles rather than the most stable contact angles to the calculation of the surface free energy components, the present results seem to be reasonable and are in good agreement with similar works in the literature; moreover, the general trends observed in most of the remaining works were found to correlate with ours, further indicating successful experiments. Additionally, there are indications of a better waxes removal when employing water washing rather than ethylene washing, in this case, lower mechanical properties are expected in specimens undergoing the latter cleaning method, even though their work of adhesion suggests a stronger interface. Another question remaining to be investigated is whether chemical bonding in aminosilane treated fibres will compensate for its lower work of adhesion, case in which an IFSS higher or similar to that of other specimens is expected.

4.3 Interface Mechanical Properties

A typical force-displacement curve obtained from microbond test is shown in Figure 6.9. A first indication of the interface quality is given by the average or apparent interfacial shear strength, τ_{app}, and can be calculated as $\tau_{app} = \frac{F_{max}}{\pi D l}$. This formula implies a uniform shear stress distribution along the total embedded length, and will therefore give only a rough estimation of the interface strength. However, it still allows a quick, qualitative comparison between fibre-matrix systems [35]. As previously discussed in section 2.2.2, even a more sophisticate mathematical analysis using stress-based or energy-based models results in qualitative results, since shear-lag theory is applied in the derivation of the final equations. As discussed by I. de Weyenberg [35], an additional issue of those approaches stems from the fact that their assumptions is not completely adequeta to natural fibres, its properties variability and surface roughness. Trying to apply the stress-based model, I. de Weyenberg was able to obtain only partial indications of the phenomenon contributing to interfacial adhesion in the fibres studied in her work. Therefore, following the most commonly used approach to study flax-epoxy micromechanical interface properties [29, 53, 144, 166–168], the apparent interfacial shear strength, τ_{app}, will be used in this section. The main disadvantage of τ_{app} is the impossibility of removing the frictional contributions to the interfacial strength, it means that a rougher or larger fibre surface will tend to present higher τ_{app}. The latter factor was minimised by employing microdrolpets with approximately equal embedded lengths. However, since it was done visually, it is still likely that surfaces presenting larger areas will have their τ_{app} increased by the contribution of frictional stresses. The use of this method; however, allows to compare the results obtained in the present work with those the literature, which would not be possible otherwise. The theory behind all the different methods, namely apparent interfacial shear

strength, stress-based model and energy-based model, has been extensively developed in section 2.2.2, a more detailed argumentation so as to why τ_{app}.

The present work focused on the characterisation of physically or chemically treated flax by studying their wettability and surface chemical composition, while the combined effect of the latter and mechanical interlocking on the interface strength were assessed by interface micromechanical characterisation, particularly, the microbond test. Over the next sections, the results obtained are presented and critically discussed, the hypotheses stated in previous sections are tested, a comparison with the values available in the literature is then presented and finally conclusions and perspectives are offered.

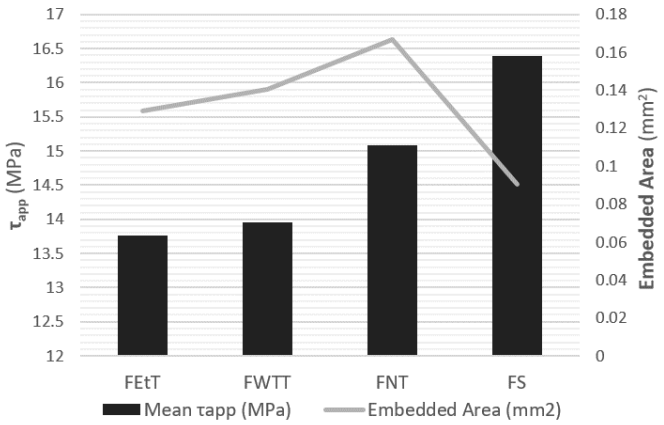


Figure 4.3: Apparent IFSS from Microbond test for NT: Untreated; S: Silane-Treated; EtT: Ethanol-Washed and WTT: Water-Washed Fibres (F).

Table 4.5: Mean Apparent IFSS and Embedded length from various Microbond test specimens for NT: Untreated; S: Silane Treated; EtT: Ethanol Washed and WTT: Water Washed Fibres (F).

Fibre Type	Embedded Area (mm^2)	τ_{app} ± SD (MPa)
FEtT	0.1292	13.76±1.80
FWTT	0.1403	13.95±1.73
FNT	0.1667	15.08±1.21
FS	0.0906	16.39±0.60

4.3.1 Interface Mechanical Properties Results Presentation

Table 4.5 presents the results obtained for the different chemically treated or cleaned fibre specimens, Fig. 4.3 presents the same results graphically so as to facilitate visualisation and comparison of possible trends in the results. It is observed that S fibres presented both, the smallest embedded area and highest τ_{app}, followed by NT fibres, whose embedded area is the highest one. Wate- treated and ethylene-treated presented rather similar τ_{app}, with the former having a slightly higher mean value, the same trend was observed in their embedded areas. This indicates the efficacy of aminosilane treatment in increasing the practical adhesion in flax-epoxy composites. On the other hand, washing the fibres did not result in an improvement in terms of τ_{app} with respect to NT fibres.

Comparing these results with those of section 4.2, some interesting conclusions can be drawn. First, as expected, practical adhesion in S fibres is shown to depend strongly on chemical bonding rather than

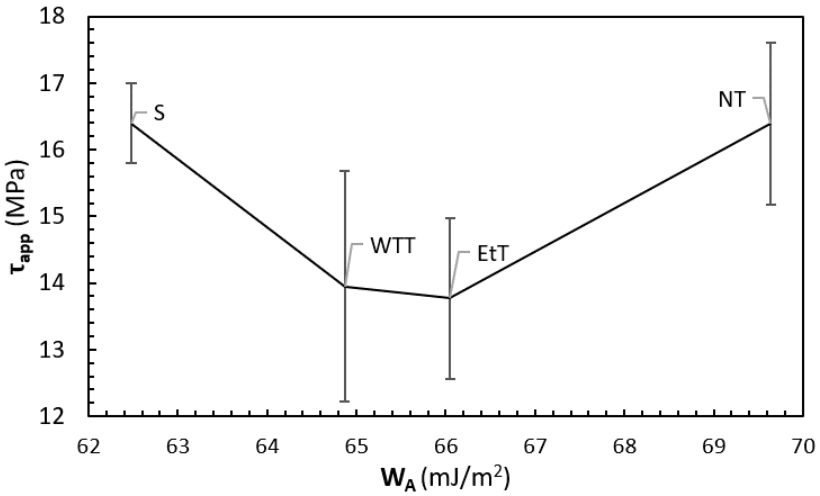


Figure 4.4: Apparent IFSS as a function of Work of Adhesion NT: Untreated; S: Silane Treated; EtT: Ethanol Washed and WTT: Water Washed Fibres (F).

physicochemical interactions. While these fibres were found to present the poorest physicochemical interactions, as assessed by the work of adhesion, their IFSS is the best amongst the specimens (see Fig.4.4). Hypotheses of contributions from mechanical interlocking due to roughness modifications are not likely to hold true since these fibres presented the smallest embedded length, which is expected decrease the contribution of the frictional stresses when compared to the other fibres. Furthermore, silane treated fibres were found to be smoother than untreated fibres [35].

Equally contradicting the findings obtained in terms of physicochemical interactions, WTT fibres presented a higher (mean) τ_{app} when compared to EtT fibres, confirming a higher efficiency in waxes removal by WTT. Although the evidence in the literature strengthens this conclusion (as previously discussed), the rather small difference in the values (0.19 MPa), when put in perspective with their standard deviations, must be seen with a high degree of precaution. Indeed statistically significant difference may be observed. Due to the need of a great number of tested samples to properly assess a statistically significant difference, it could not be not used in the current results. Additionally, the embedded area of WTT fibres is larger than that of EtT, which may indicate a higher contribution of frictional stresses to τ_{app} values in the former, resulting in misleading conclusions. For a better assessment of this difference, it is suggested the test of a greater number of specimens so as to perform statistical analysis and the use of direct roughness assessment techniques, such as AFM (which may still be misleading, due to resin impregnation [29], as previously discussed in section 2.2.2). In addition to that, fibre fragilisation causing increased pilling, as observed by A. Lefeuvre et al. [168], is not likely to have occurred in the present case, due to the low harshness of the cleaning methods used, as indicated in the literature [189, 260]. Furthermore, micrographs of debonded surface (see Fig. 3.15) indicated fibres-matrix interface failure, rather than matrix failure or internal fibre decohesion. The larger embedded areas of untreated fibres causing a higher degree of frictional stresses may be a possible explanation for the difference in apparent IFSS of WTT and EtT fibres. In the only study available in the literature of flax-epoxy composites in which the decomposition of frictional and interfacial bonding forces was performed, I. Van de Weyenberg [35] proved that the former may contribute to a significant extent in the final results. As previously discussed, the results of τ_{d} and τ_{app} for aminosilane-treated and untreated flax using approximately equal embedded areas may lead to opposing conclusions due to the lower roughness of the former when compared to the latter caused by the silanisation treatment.

4.3.2 Critical Comparison with the Literature

Overall, the range of values obtained in the present study for flax-epoxy systems, from 13.76±1.80 MPa to 16.39±0.6 MPa, are in good agreement with the literature, from 11.9±4.1 MPa to 28.5±6.4 MPa, presented in table 2.7. In particular, the results of L. Marrot et al.[53] studying Melina flax from Picardie (11.9 MPa), A. Lefeuvre [168] on Marylin flax from Normandy (17±4 MPa), and A. le Duigou et al. [29] (13.2 MPa ±3.2 MPa), investigating Electra flax, also from Normandy. All these fibres were harvested in France, dew-retted, and have IFSS values below the mean in the literature 20 MPa.

A particularly good agreement was obtained with the results of L. Marrot et al. [53] on untreated flax fibres bio-epoxy resins, especially values obtained using a resin system composed of DGEBA-Greenepoxy 55 and a polyamine hardener (τ_{app}=17 MPa). This epoxy system, obtained from the same provider, differs from the one used in the present work only in bio-carbon content (55±2%, against 38% in the current work). The apparent IFSS of other bio-based and a petrochemical-based epoxy resins with different hardeners was also studied, it was shown that polyamine hardeners contribute to higher values, when compared to polyamides and aliphatic amines, which can be linked to better mechanical properties of the cured resin and increase in amino groups capable of establishing hydrogen bonds with hydroxyls in the fibre surface, potentially reacting with them. In aminosilane-treated fibres, whose interfacial strength was proved to depend mostly on chemical bonding, amino groups from the hardener are expected to react with free silanol moieties in the sizing. Indeed the sizing used in the present work is a bis-aminosilane (see Fig. 3.1b), which promotes the increase of the free-silanol moieties remaining from the sizing process as opposed to widely used mono-aminosilane, such as APS. The lower content of polyamine hardener here employed, 1:4 against 1:3 in L. Marrot et al. may have contributed to a lower IFSS in the present study. Nevertheless, a high scatter of values was observed in the former work, with a standard deviation of 5 MPa, meaning that their values a essentially equal to ours, whose means differs only by 1.9 MPa. In addition to that, a good correlation between these properties and the interface mechanical properties assessed at macroscopic level was also observed, which remains to be studied in the flax-epoxy systems studied in the present work (methods for macromechancial characterisation of interfaces in composites were presented in section 2.2.2). These and the additional results provided by L. Marrot et al.[53], show promising IFSS results, indicating that bio-based epoxy resins reinforced with flax fibres have comparable or greater values than those obtained for petrochemical based resins.

4.3.3 Partial Conclusion

In this section the results of microbond tests performed on NT, S, EtT and WTT fibres were presented and analysed based on similar studies available in the literature. The values were in good agreement with other works, in particular with results on similar bio-based epoxy, case in which the choice of hardener was identified as an important factor, changing the fraction of amino groups contributing to hydrogen bonding, and potentially chemical bonding with hydroxyl groups in the fibre surface. This is even more critical in the case of aminosilane-treated fibres, once silanol groups remaining from sizing in the present work may have an important contribution to the practical adhesion by reacting with both, amino and epoxide groups in the resin, in addition to reactions between epoxide groups from the resin and amino groups from the sizing. This suggests that resin-hardener fraction may also be optimised for compatibility and interfacial adhesion.

Furthermore, questions that remained opened from section 4.2 were addressed. It was proved that the main contributor to S fibres practical adhesion is chemical bonding. In spite of presenting the poorest work of adhesion and a smaller contribution from frictional stresses due to small embedded area, these fibres presented the highest apparent IFSS amongst the specimens. The microbond sample of untreated

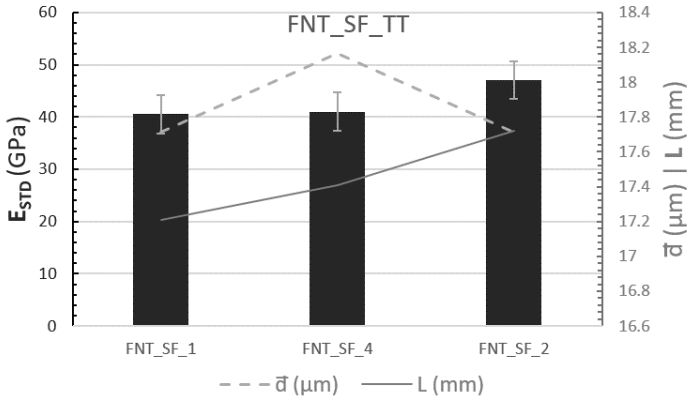


Figure 4.5: Summary of the Young's Modulus values obtained as determined by the Standard NF T25-501-2 from tensile tests performed on three untreated elementary flax fibres

Table 4.6: Summary of the tensile test results performed on untreated elementary flax fibres

	$\overline{\mathrm{d}}$ **(µm)**	**L (mm)**	$\mathrm{E_{STD}}$ **(GPa)**	σ_u **(MPa)**	ϵ
Average	17.9±0.3	17.5±0.3	42.9±3.6	771±118	0.021±0.003

fibres had the highest embedded area, which is likely to have increased its τ_{app} due to higher frictional stresses, an AFM characterisation would be an effective way of quantitatively test for this hypothesis. Moreover, EtT and WTT fibres were found to have the lowest IFSS. Fibre fragilisation causing internal failure would be a possible explanation to this phenomena. However, evidence in the literature suggests otherwise [189, 260]. Another possible explanation could stem from a lower contribution of frictional stresses on τ_{app} due to the smaller embedded areas of the specimens as compared to untreated fibres. This could be assessed either controlling the specimens embedded area in a more precise fashion (rather than the simple visual inspection used in the current study), for instance, by using high-precision goniometers. Another possible way of assessing this hypothesis would be to test specimens with vairous embedded lengths and observe how their IFSS varies, so as to evaluate the contribution of frictional stresses to the variation of the total value.

Finally, it could not be proved whether the higher work of adhesion of EtT fibres was due to a lower efficiency in surface waxes removal. Although the mean values of IFSS suggest it, their high scatter relatively to the difference between the means does not allow to confirm a statistically significant difference. This can be tested in several different ways, for instance, by measuring weight variation and assessing the composition of the extracts from the cleaning process.

Overall, the good agreement with the literature seems to indicate the success of the microbond experiments performed in the present work. Although the analysis of τ_{app} allowed to prove some hypotheses from previous sections, there still are open questions since the impossibility of separating the frictional contributions from the final results limited the conclusions. In spite of that, it was possible to prove the efficacy of the aminosilane sizing in improving practical adhesion, which is expected to result in a better in-service load transfer.

4.4 Tensile Properties

Fibres mechanical properties, in combination with fibre-matrix interface strength and area, determine the quality of the reinforcement. To complement the characterisation of the studied flax fibres as composites reinforcements, tensile tests, whose results are presented in table 4.6, were performed on untreated elementary fibres. By comparing the values here obtained with the literature presented in table 2.10, it is possible to observed that, although the tensile strength, 771±118 MPa, and elongation at break, 0.021±0.003, are in good accordance, the Young's modulus here assessed, 42.9±3.6 GPa, seems to be slightly lower, this is mostly probably due to the system compliance, which was not accounted for since mechanical tests were not employed with quantitative purposes, but rather as a quick assessment of the specimen mechanical behaviour. Therefore, the strain at break is likely to be overestimated. However, the measured values still hold reasonable, similar to half of the four values of strain at break reported in table 2.10. Nevertheless, it remains speculative and a multitude of conditions that cannot be accounted for in the present study may have led to this outcome, such as the exact conditions of the extraction process, climate conditions experienced by the crop from which the specimens were harvested, relative humidity during tests, among others. Additionally, Tensile Modulus values closer to the ones obtained here were measured by K. Charlet et al. [12] when studying Hermes elementary flax fibres extracted from the stem bottom (see 2.12). Overall, the measurements were considered successful and the fibre properties within acceptable values, which was considered as an indication of no significant degree of degradation due to storage conditions or handling of the specimens.

5 Conclusion and Perspectives

5.1 Silanisation Effect

The effects of amino silane functionalisation in the interfacial strength of composites flax-epoxy resin was a matter of controversy in the literature, with opposing results published for similar experimental conditions. The present work proved that aminosilane functionalisation using Bis(trimethoxysilylpropyl)amine, a molecule that has two silane heads in opposing ends of a linear carbon backbone with a central secondary amine, is effective in improving the practical adhesion between epoxy resin and flax fibres and that this improvement is, as expected, strongly determined by chemical bonding, rather than physhicochemical interactions or mechanical interlocking. Indeed, aminosilane-treated flax fibres microcomposites presented the best apparent interfacial shear strength of all the different types of specimens as assessed by microbond test, in spite of having the smallest embedded area, which was expected to reduce the frictional contributions to the apparent interfacial shear strength, and the poorest work of adhesion, as per surface energies calculated from contact angles obtained using Wilhelmy technique, which seemed not to correlate with the predictions obtained from XPS analysis. Indeed, the latter indicates a surface whose physicochemical interactions are almost equally divided between specific and non-specific, whilst a minor contribution of 5% from specific interactions were observed from contact angle measurements. The explanation to this divergence may be twofold:

- First, the analysis of peaks decomposition based solely on C1s may be flawed since it is well known that amino groups will have a significant contribution to physicochemical interactions. So will the silane groups; nonetheless, their contribution is a much more intricate one, since they are expected to be found in different converting states on the fibre surface (bonded to hydroxyls, hydrated, bonded to other sizing molecules or free at the surface);

- Second, surface energies obtained in the present work tend to be underestimated, since static advancing contact angles were used instead of the most stable contact angles, which could not be assessed by Wilhelmy Technique for flax fibres due to the impossibility of measuring receding contact angles;

Although this analysis is likely to benefit from further decomposition of nitrogen peaks, it may actually worsen the disparity between the two results. Rather than that, a surface energy calculated from equilibrium properties is likely to improve the agreement between the two methods. On the other hand, XPS analysis was efficient in showing the fingerprint of aminosilane molecules on the surface of treated fibres, with a considerable increase in the content of oxygen and nitrogen, decrease in total carbon content (especially bonded to hydrogen or other carbon atom), and the presence of a new peak with distinct binding energy for silicon atoms matching that characteristic of a silicon atom from silane functional groups. Surface roughness augmentation due to the treatments causing an increase in mechanical interlocking is likely not the case as the literature indicates. A possible way of testing this last point is to perform experiments with specimens of controlled embedded area, observing how it affects the final τ_{app} values. Any variation observed in such conditions are expected to stem from the frictional contributions since interface bond strength is not dependent on the specimen dimensions.

5.2 Ethylene and Water Washing Effect

Contrary to what was expected, the cleaning techniques were not found to improve the mechanical properties of the interface, as per apparent IFSS measurements. Indeed, those specimens, were found to present smaller work of adhesion with epoxy resin when compared to untreated fibres, fact that was expected to stem mostly from the removal of waxes and consequent reduction of their dispersive character, which, differently from the case of aminosilane-treated fibres would not be compensated by an increase in chemical bonding since there was no evidence pointing to that. Nonetheless, it is known that the presence of this waxy layer, which is weakly attached to the surface, is mostly detrimental to the interface quality. Although fragilisation of fibres may have occurred, increasing internal decohesion, and thus causing IFSS reduction, the literature indicates otherwise. Another possible explanation to this fact may arise from the contribution of frictional stresses in increasing the apparent IFSS of untreated flax, whose microbond specimens had larger embedded area, thereby were expected to present a higher contribution of frictional forces to τ_{app}.

Similarly, due to an apparent higher waxes extraction, suggested by a higher decrease in dispersive component, water-treated fibres were expected to present better IFSS as compared to EtT. Although IFSS means corroborate this hypothesis, their difference and relative high standard deviation do not allow to confirm statically significant difference between the samples.

It is a well-accepted in the literature that surface waxes extraction should be beneficial for interfacial compatibility and adhesion. Not being confirmed by the experiments carried out in the present work, this indicates the need to further investigate how the washing protocols used are modifying fibres composition. This could be done by a simple weight analysis, comparing the fibres prior and after cleaning, followed by chemical analysis of the extracts, allowing to identify the components extracted from the surface and efficiency of the extractions. If an important content of biomolecules related to structural functions is observed in the extracts, fragilisation may be occurring, case in which tensile tests and fractography of microbond specimens could be used as quick assessment methods, once degradation in mechanical properties and increasing in pilling during debonding are expected to be observe.

5.2.1 Tensile Properties

The values obtained in the present work shown to be good agreement with the literature. Therefore, the measurements were considered successful and fibres properties within acceptable values, which was considered as an indication of no significant degradation due to storage conditions or handling of the specimens, an important conclusion, since those factor may significantly decrease the properties of the final reinforcement.

5.2.1.1 Perspectives

It was proved that the equipment and methodology used for this test in the present work are reliable ones. On the basis of the discussion provided in Appendix D, it should be straightforward to assess the system compliance. Preparing the specimens for experiments, on the other hand; remains a laborious task, which took several valuable hours of work in the present study. The main reason for that is the complex isolation and handling of flax elementary fibres. Therefore, rather than insisting in this approach, which requires an unreasonable amount of specimens, and thus time to reduce the standard deviation observed to smaller values, other measurements that have proven to be more efficient in testing a much higher amount of fibres at once is indicated. Particularly the impregnated fibre bundle test,

which was found to allow for rather good reproducibility and test of a considerably higher amount of samples at once, significantly decreasing the scatter in the results.

5.3 Overall Perspectives

As the results of the present work indicate, there still is a lack of consensus on the best method to treat flax fibres surface so as to optimise the mechanical properties of the final composite. Although it is a truism that interface micromechenical properties and wettability analysis are important for the quality of the reinforcement, an approach to fibre treatments optimisation solely at the microscale may be misleading, provided other factors such as the impact of fibres mechanical properties and degree of individualisation, which do not play an important role at the micro-level, may actually dominate the reinforcement quality at the macroscopic scale. Therefore, a multiscale characterisation is suggested, allowing to assess the combined effects of the various factors playing a role in the reinforcement quality improvement due to fibres modification, amongst which changes in fibres mechanical properties, degree of individualisation and interface quality, the latter being subdivided into physicochemical interactions, chemical bonding and mechanical interlocking contributions.

The findings in the present work also indicate that chemical bonding may be significantly more effective in improving interface quality. This fact stems from the pre-existing compatibility of fibres and epoxy surfaces (both polar) and the much stronger character of primary bonds. It suggests that the optimisation of sizing, mostly the interactions between sizing molecules and fibres surface and impacts on resin impregnation, may be a much more efficient way of improving interface adhesion and compatibility when compared to the other options. Although the development of an entire new sizing may be cost-prohibitive at the present stage of natural fibres composites development, mostly used for less mechanically demanding applications, sizing optimisation can benefit from methods and compounds developed for glass fibres. Indeed, aminosilane treatments similar to those used in glass fibres were proved to be promising for flax; nonetheless, there seem to be no consensus on the best aminosilane compound to be used, the correct adaptation of the sizing process and the concentration of silane solution used, these are most probably the root causes of the divergent conclusions in the literature. This indicates that further efforts in developing an aminosilane treatment optimised for flax fibres-epoxy composites may contribute a significant extent in improving their interface quality, an important step towards the complete realisation of flax fibres potential as composites reinforcements.

Bibliography

[1] G Pabst. *Köhler's Medizinal-Pflanzen*. Hugo Brmühler, 1887.

[2] The Metropolitan Museum of Art. Mummy bandage from tutankhamun's embalming cache. `https://www.metmuseum.org/toah/works-of-art/09.184.797/`, year=2000–2019.

[3] Frederic Reux and Ignaas Verpoest. *Flax and hemp fibres: a natural solution for the composite industry*. JEC Composites, 2014.

[4] CELC Master of Linen and Hemp. Linen transformation steps. `http://www.mastersoflinen.com/eng/lin/8-de-la-graine-a-la-fibre__`, 2017.

[5] G Schnegelsberg. Was ist hanf? ein beitrag zur begrifflichen klärung. *Die Renaissance der heimischen Faserpflanzen*, pages 205–215, 1996.

[6] Alain Bourmaud, Johnny Beaugrand, Darshil U Shah, Vincent Placet, and Christophe Baley. Towards the design of high-performance plant fibre composites: How can we best define the diversity and specificities of plant cell walls? *Progress in Materials Science*, 2018.

[7] David B Dittenber and Hota VS GangaRao. Critical review of recent publications on use of natural composites in infrastructure. *Composites Part A: Applied Science and Manufacturing*, 43(8):1419–1429, 2012.

[8] Antoine Le Duigou, Peter Davies, and Christophe Baley. Environmental impact analysis of the production of flax fibres to be used as composite material reinforcement. *Journal of biobased materials and bioenergy*, 5(1):153–165, 2011.

[9] Natural fibre company Bcomp. Flax composites applications. {http://www.bcomp.ch/en/products/automotive, 2017.

[10] Andrzej K Bledzki, Omar Faruk, and Volker E Sperber. Cars from bio-fibres. *Macromolecular Materials and Engineering*, 291(5):449–457, 2006.

[11] Farida Bensadoun. In-service behaviour of flax fibre reinforced composites for high performance applications, 2016.

[12] K Charlet, Christophe Baley, C Morvan, JP Jernot, M Gomina, and J Bréard. Characteristics of hermès flax fibres as a function of their location in the stem and properties of the derived unidirectional composites. *Composites Part A: Applied Science and Manufacturing*, 38(8):1912–1921, 2007.

[13] Mustafa Aslan, Bent F Sørensen, and Bo Madsen. *Characterisation of Flax Fibres and Flax Fibre Composites. Being cellulose based sources of materials*. DTU Wind Energy, 2012.

[14] Mustafa Aslan, Gary Chinga-Carrasco, Bent F Sørensen, and Bo Madsen. Strength variability of single flax fibres. *Journal of materials science*, 46(19):6344–6354, 2011.

[15] Hui Wang, Gabriela Gurau, and Robin D Rogers. Ionic liquid processing of cellulose. *Chemical Society Reviews*, 41(4):1519–1537, 2012.

[16] Priscilla Albuquerque, Luana CBB Coelho, José A Teixeira, and Maria G Carneiro-da Cunha. Approaches in biotechnological applications of natural polymers. *AIMS Molecular Science*, 3(3):386–425, 2016.

[17] Herman Höfte, Alexis Peaucelle, and Siobhan Braybrook. Cell wall mechanics and growth control in plants: the role of pectins revisited. *Frontiers in plant science*, 3:121, 2012.

[18] Thomas Heinze, H Barsett, A Ebringerová, SE Harding, T Heinze, Z Hromadkova, C Muzzarelli, RAA Muzzarelli, BS Paulsen, and OA El Seoud. Polysaccharides i: Structure, characterisation and use. 2005.

[19] Edward Yu Bormashenko. *Wetting of real surfaces*, volume 19. Walter de Gruyter GmbH & Co KG, 2018.

[20] L. Q.N. Tran, C. A. Fuentes, C. Dupont-Gillain, A. W. Van Vuure, and I. Verpoest. Wetting analysis and surface characterisation of coir fibres used as reinforcement for composites. *Colloids and Surfaces A: Physicochemical and Engineering Aspects*, 377(1-3):251–260, 2011.

[21] Alireza Mohammad Karim and H Pirouz Kavehpour. Effect of viscous force on dynamic contact angle measurement using wilhelmy plate method. *Colloids and Surfaces A: Physicochemical and Engineering Aspects*, 548:54–60, 2018.

[22] Carlos Fuentes Rojas. Interfacial adhesion in natural and synthetic fibre composites: a physical-chemical-mechanical approach (grensvlakhechting in natuurlijke en synthetische vezel composieten: een fysisch-chemisch-mechanische methodiek). 2014.

[23] Jaroslaw W Drelich. Contact angles: from past mistakes to new developments through liquid-solid adhesion measurements. *Advances in colloid and interface science*, 2019.

[24] Le Quan Ngoc Tran. Polymer composite materials based on coconut fibres (polymeercomposietmaterialen op basis van kokosvezels). 2013.

[25] Edward Bormashenko. General equation describing wetting of rough surfaces. *Journal of colloid and interface science*, 360(1):317–319, 2011.

[26] CA Fuentes, LQN Tran, C Dupont-Gillain, W Vanderlinden, S De Feyter, AW Van Vuure, and I Verpoest. Wetting behaviour and surface properties of technical bamboo fibres. *Colloids and Surfaces A: Physicochemical and Engineering Aspects*, 380(1-3):89–99, 2011.

[27] HB Eral, JM Oh, et al. Contact angle hysteresis: a review of fundamentals and applications. *Colloid and polymer science*, 291(2):247–260, 2013.

[28] Antoine Le Duigou, Alain Bourmaud, Eric Balnois, Peter Davies, and Christophe Baley. Improving the interfacial properties between flax fibres and plla by a water fibre treatment and drying cycle. *Industrial Crops and Products*, 39:31–39, 2012.

[29] Antoine Le Duigou, Antoine Kervoelen, Adélaïde Le Grand, Michel Nardin, and Christophe Baley. Interfacial properties of flax fibre–epoxy resin systems: existence of a complex interphase. *Composites Science and Technology*, 100:152–157, 2014.

[30] Serge F Zhandarov, Edith Mäder, and Oleg R Yurkevich. Indirect estimation of fiber/polymer bond strength and interfacial friction from maximum load values recorded in the microbond and pull-out tests. part i: local bond strength. *Journal of Adhesion Science and Technology*, 16(9):1171–1200, 2002.

[31] Serge Zhandarov, Edith Mäder, and Uwe Gohs. Why should the "alternative" method of estimating local interfacial shear strength in a pull-out test be preferred to other methods? *Materials*, 11(12):2406, 2018.

[32] John A Nairn, Chun-Hsin Liu, David-A Mendels, and Serge Zhandarov. Fracture mechanics analysis of the single-fiber pull-out test and the microbond test including the effects of friction and thermal stresses. In *Proceeding 16th annual technology conference of the american society of composites*. Citeseer, 2001.

[33] K Charlet, S Eve, JP Jernot, M Gomina, and J Breard. Tensile deformation of a flax fiber. *Procedia Engineering*, 1(1):233–236, 2009.

[34] Karine Charlet. *Contribution à l'étude de composites unidirectionnels renforcés par des fibres de lin: relation entre la microstructure de la fibre et ses propriétés mécaniques*. PhD thesis, Université de Caen/Basse-Normandie, 2008.

[35] I Van de Weyenberg. Flax fibres as reinforcement for epoxy composites. *Katholieke Universiteit Leuven*, 2005.

[36] MR Piggott. The single-fibre pull-out method: its advantages, interpretation and experimental realization. *Composite Interfaces*, 1(3):211–223, 1993.

[37] Stefanie Feih, Karen Wonsyld, Daniel Minzari, Peter Westermann, and Hans Lilholt. Testing procedure for the single fiber fragmentation test. *Riso National Laboratory, Riso*, 2004.

[38] S Alix, E Philippe, A Bessadok, L Lebrun, C Morvan, and S Marais. Effect of chemical treatments on water sorption and mechanical properties of flax fibres. *Bioresource Technology*, 100(20):4742–4749, 2009.

[39] G Romhany, J Karger-Kocsis, and T Czigany. Tensile fracture and failure behavior of technical flax fibers. *Journal of Applied Polymer Science*, 90(13):3638–3645, 2003.

[40] A Stamboulis, CA Baillie, SK Garkhail, HGH Van Melick, and T Peijs. Environmental durability of flax fibres and their composites based on polypropylene matrix. *Applied composite materials*, 7(5-6):273–294, 2000.

[41] Harriëtte Louise Bos. *The potential of flax fibres as reinforcement for composite materials*. Technische Universiteit Eindhoven Eindhoven, 2004.

[42] Karine Charlet and Alexis Béakou. Mechanical properties of interfaces within a flax bundle–part i: Experimental analysis. *International Journal of Adhesion and Adhesives*, 31(8):875–881, 2011.

[43] Isabelle Pillin, Antoine Kervoelen, Alain Bourmaud, Jérémy Goimard, Nicolas Montrelay, and Christophe Baley. Could oleaginous flax fibers be used as reinforcement for polymers? *Industrial Crops and Products*, 34(3):1556–1563, 2011.

[44] Yanjun Xie, Callum AS Hill, Zefang Xiao, Holger Militz, and Carsten Mai. Silane coupling agents used for natural fiber/polymer composites: A review. *Composites Part A: Applied Science and Manufacturing*, 41(7):806–819, 2010.

[45] ZN Azwa, BF Yousif, AC Manalo, and W Karunasena. A review on the degradability of polymeric composites based on natural fibres. *Materials & Design*, 47:424–442, 2013.

[46] Ahmad Y Al-Maharma and Naser Al-Huniti. Critical review of the parameters affecting the effectiveness of moisture absorption treatments used for natural composites. *Journal of Composites Science*, 3(1):27, 2019.

[47] Si Qiu, Carlos A Fuentes, Dongxing Zhang, Aart Willem Van Vuure, and David Seveno. Wettability of a single carbon fiber. *Langmuir*, 32(38):9697–9705, 2016.

[48] Somayeh Safi, Ali Zadhoush, and Mahmood Masoomi. Evaluation of interfacial properties of the silane blend sized glass fiber–epoxy composite by the microdroplet test. *Journal of Composite Materials*, 51(11):1573–1581, 2017.

[49] Hüseyin Burak Eral, Jolet de Ruiter, Riëlle de Ruiter, Jung Min Oh, Ciro Semprebon, Martin Brinkmann, and Frieder Mugele. Drops on functional fibers: from barrels to clamshells and back. *Soft Matter*, 7(11):5138–5143, 2011.

[50] Camille Goudenhooft, Alain Bourmaud, and Christophe Baley. Flax (linum usitatissimum l.) fibers for composite reinforcement: exploring the link between plant growth, cell walls development and fiber properties. *Frontiers in plant science*, 10:411, 2019.

[51] C Della Volpe and S Siboni. Acid–base surface free energies of solids and the definition of scales in the good–van oss–chaudhury theory. *Journal of Adhesion Science and Technology*, 14(2):235–272, 2000.

[52] LQN Tran, XW Yuan, D Bhattacharyya, C Fuentes, AW Van Vuure, and I Verpoest. Fiber-matrix interfacial adhesion in natural fiber composites. *International Journal of Modern Physics B*, 29(10n11):1540018, 2015.

[53] L Marrot, Alain Bourmaud, P Bono, and Christophe Baley. Multi-scale study of the adhesion between flax fibers and biobased thermoset matrices. *Materials & Design (1980-2015)*, 62:47–56, 2014.

[54] Libo Yan, Nawawi Chouw, and Krishnan Jayaraman. Flax fibre and its composites–a review. *Composites Part B: Engineering*, 56:296–317, 2014.

[55] Dieter Perremans, Kevin Hendrickx, Ignace Verpoest, and AW Van Vuure. Effect of chemical treatments on the mechanical properties of technical flax fibres with emphasis on stiffness improvement. *Composites Science and Technology*, 160:216–223, 2018.

[56] K Charlet, JP Jernot, M Gomina, J Bréard, C Morvan, and Christophe Baley. Influence of an agatha flax fibre location in a stem on its mechanical, chemical and morphological properties. *Composites Science and Technology*, 69(9):1399–1403, 2009.

[57] Sicomin Technical Systems. Sr infugreen 810, *Green Epoxy systems for Injection and Infusion*. `http://www.sicomin.com/datasheets/product-pdf1167.pdf`, 2017.

[58] SA Page, JC Berg, and J-AE Månson. Characterization of epoxy resin surface energetics. *Journal of adhesion science and technology*, 15(2):153–170, 2001.

[59] Alister D Muir and Neil D Westcott. *Flax: the genus Linum*. CRC press, 2003.

[60] CELC Master of Linen and Hemp. Linen history, *A Brief History*. `http://www.mastersoflinen.com/eng/breves`, 2017.

[61] Louise Quillien. Flax and linen in the first millennium babylonia bc: The origins, craft industry and uses of a remarkable textile. *Prehistoric, Ancient Near Eastern and Aegean Textiles and Dress*, pages 271–96, 2014.

[62] M Xavier MASSET, Madame Émilie GARRIGUES-SANTIN, and Docteur en Pharmacie. *De la fibre végétale à la fibre textile*. PhD thesis, 2008.

[63] Gomaa Abdel-Maksoud and Abdel-Rahman El-Amin. A review on the materials used during the mummification processes in ancient egypt. *Mediterranean Archaeology & Archaeometry*, 11(2), 2011.

[64] Neil Puckett. *The phoenician trade network: tracing a Mediterranean exchange system*. PhD thesis, 2012.

[65] Dr.G.Ramakrishnan A.S.Aishwarya Anand. A critical review of hemp and linen fibres. `https://www.chemarc.com/content/article/a-critical-review-of-hemp-and-linen-fibres/5c74d45ae7a25515d561eb06`, 2019.

[66] LIBECO Belgiuan Linen. Linen in flanders, a tradition of excellence. `https://www.libeco.com/en/about-linen/linen-in-flanders.aspx`.

[67] Pratima Bajpai. *Xylanolytic enzymes*. Academic Press, 2014.

[68] WJM Meijer, N Vertregt, B Rutgers, and M Van de Waart. The pectin content as a measure of the retting and rettability of flax. *Industrial Crops and Products*, 4(4):273–284, 1995.

[69] Bodil Engberg Pallesen. The quality of combine-harvested fibre flax for industrials purposes depends on the degree of retting. *Industrial crops and products*, 5(1):65–78, 1996.

[70] RW Kessler, U Becker, R Kohler, and B Goth. Steam explosion of flax—a superior technique for upgrading fibre value. *Biomass and Bioenergy*, 14(3):237–249, 1998.

[71] Compositeslab. History of composites.

[72] Shiro Kobayashi and Klaus Müllen. *Encyclopedia of polymeric nanomaterials*. Springer Heidelberg, 2015.

[73] Brian Thomas, Denis J Murphy, and Brian G Murray. *Encyclopedia of applied plant sciences*. Academic Press, 2016.

[74] Martha Barth and Michael Carus. Carbon footprint and sustainability of different natural fibres for biocomposites and insulation material. *Hürth: Nova-Institute. Available online at: http://eiha. org/media/2017/01/15-04-Carbon-Footprint-of-Natural-Fibres-nova1. pdf (Accessed Sept 5, 2017)*, 2015.

[75] Young S Song, Jae R Youn, and Timothy G Gutowski. Life cycle energy analysis of fiber-reinforced composites. *Composites Part A: Applied Science and Manufacturing*, 40(8):1257–1265, 2009.

[76] Lut Pil, Farida Bensadoun, Julie Pariset, and Ignaas Verpoest. Why are designers fascinated by flax and hemp fibre composites? *Composites Part A: Applied Science and Manufacturing*, 83:193–205, 2016.

[77] David W Dwight. Glass fiber reinforcements. 2000.

[78] Furqan Ahmad, Heung Soap Choi, and Myung Kyun Park. A review: natural fiber composites selection in view of mechanical, light weight, and economic properties. *Macromolecular materials and engineering*, 300(1):10–24, 2015.

[79] WJ Evans, DH Isaac, BC Suddell, and A Crosky. Natural fibres and their composites: A global perspective. In *Proceedings of the... Risø International Symposium on Materials Science*, pages 1–14, 2002.

[80] Torulf Nilsson. Micro mechanical modelling of natural fibres for composite materials. 2006.

[81] K Charlet, JP Jernot, S Eve, M Gomina, and J Bréard. Multi-scale morphological characterisation of flax: From the stem to the fibrils. *Carbohydrate Polymers*, 82(1):54–61, 2010.

[82] Violette Bossuyt. *Etude de la structure et des propriétés mécaniques de la fibre de lin*. PhD thesis, 1941.

[83] Roger M Rowell. Characterization and factors effecting fiber properties. *Natural polymers and agrofibers based composites*, 2000.

[84] Frederick T Wallenberger and Norman Weston. *Natural fibers, plastics and composites*. Springer Science & Business Media, 2003.

[85] JP Thiéry. Mise en évidence des polysaccharides sur coupes fines en microscopie électronique. *J microsc*, 6:987–1018, 1967.

[86] Christopher T Brett and Keith W Waldron. *Physiology and biochemistry of plant cell walls*, volume 2. Springer Science & Business Media, 1996.

[87] Torulf Nilsson and Per Johan Gustafsson. Influence of dislocations and plasticity on the tensile behaviour of flax and hemp fibres. *Composites Part A: Applied Science and Manufacturing*, 38(7):1722–1728, 2007.

[88] HH Wang, JG Drummond, SM Reath, K Hunt, and PA Watson. An improved fibril angle measurement method for wood fibres. *Wood Science and Technology*, 34(6):493–503, 2001.

[89] SK Batra. Handbook of fiber chemistry—other long vegetable fibers. *Lewin M, Pearce EM*, 1998.

[90] Christophe Baley. Analysis of the flax fibres tensile behaviour and analysis of the tensile stiffness increase. *Composites Part A: Applied Science and Manufacturing*, 33(7):939–948, 2002.

[91] SJ Eichhorn, CA Baillie, N Zafeiropoulos, LY Mwaikambo, MP Ansell, A Dufresne, KM Entwistle, PJ Herrera-Franco, GC Escamilla, L Groom, et al. Current international research into cellulosic fibres and composites. *Journal of materials Science*, 36(9):2107–2131, 2001.

[92] Minoru Fujita and Hiroshi Harada. Ultrastructure and formation of wood cell wall. *Wood and cellulosic chemistry*, pages 1–49, 2000.

[93] JWS Hearle. The structure and mechanical properties of fibres. *Journal of the Textile Institute Proceedings*, 53(8):P449–P464, 1962.

[94] P Näslund, R Vuong, H Chanzy, and JC Jésior. Diffraction contrast transmission electron microscopy on flax fiber ultrathin cross sections. *Textile Research Journal*, 58(7):414–417, 1988.

[95] Ichiro Sakurada, Yasuhiko Nukushina, and Taisuke Ito. Experimental determination of the elastic modulus of crystalline regions in oriented polymers. *Journal of Polymer Science*, 57(165):651–660, 1962.

[96] Yongli Zhang, Yan Li, Hao Ma, and Tao Yu. Tensile and interfacial properties of unidirectional flax/glass fiber reinforced hybrid composites. *Composites Science and Technology*, 88:172–177, 2013.

[97] Erich E Treiber. *Die Chemie der Pflanzenzellwand: ein Beitrag zur Morphologie, Physik, Chemie und Technologie der Cellulose und ihrer Begleiter*. Springer-Verlag, 2013.

[98] DAI Goring and TE Timell. Molecular weight of native celluloses. *Tappi*, 45(6):454–460, 1962.

[99] Helena Lennholm, Tomas Larsson, and Tommy Iversen. Determination of cellulose iα and iβ in lignocellulosic materials. *Carbohydrate Research*, 261(1):119–131, 1994.

[100] HP Fink, E Walenta, and J Kunze. The structure of natural cellulosic fibres-part 2. the supermolecular structure of bast fibres and their changes by mercerization as revealed by x-ray diffraction and c-13-nmr-spectroscopy. *Papier*, 53(9):534–542, 1999.

[101] Christine Andème-Onzighi, Raynald Girault, Isabelle His, Claudine Morvan, and Azeddine Driouich. Immunocytochemical characterization of early-developing flax fiber cell walls. *Protoplasma*, 213(3-4):235–245, 2000.

[102] Isabelle His, Christine Andeme-Onzighi, Claudine Morvan, and Azeddine Driouich. Microscopic studies on mature flax fibers embedded in lr white: immunogold localization of cell wall matrix polysaccharides. *Journal of Histochemistry & Cytochemistry*, 49(12):1525–1535, 2001.

[103] A Jauneau, A Cabin-Flaman, M-C Verdus, C Ripoll, and M Thellier. Involvement of calcium in the inhibition of endopolygalacturonase activity in epidermis cell wall of linum usitatissimum. *Plant physiology and biochemistry*, 32(6):839–846, 1994.

[104] ALAIN Jauneau, CLAUDINE Morvan, FABRICE Lefebvre, MAURICE Demarty, CAMILLE Ripoll, and MICHEL Thellier. Differential extractability of calcium and pectic substances in different wall regions of epicotyl cells in young flax plants. *Journal of Histochemistry & Cytochemistry*, 40(8):1183–1189, 1992.

[105] Subhash K Batra. Other long vegetable fibers: abaca, banana, sisal, henequen, flax, ramie, hemp, sunn, and coir. In *Handbook of fiber chemistry*, pages 464–531. CRC Press, 2006.

[106] Christophe Baley, Claudine Morvan, and Yves Grohens. Influence of the absorbed water on the tensile strength of flax fibers. In *Macromolecular Symposia*, volume 222, pages 195–202. Wiley Online Library, 2005.

[107] WJ Cousins. Young's modulus of hemicellulose as related to moisture content. *Wood science and technology*, 12(3):161–167, 1978.

[108] Lorna J Gibson. The hierarchical structure and mechanics of plant materials. *Journal of the royal society interface*, 9(76):2749–2766, 2012.

[109] Le Quan Ngoc Tran, CA Fuentes, C Dupont-Gillain, AW Van Vuure, and I Verpoest. Wetting analysis and surface characterisation of coir fibres used as reinforcement for composites. *Colloids and Surfaces A: Physicochemical and Engineering Aspects*, 377(1-3):251–260, 2011.

[110] Kevin T Hodgson and John C Berg. Dynamic wettability properties of single wood pulp fibers and their relationship to absorbency. *Wood and fiber Science*, 20(1):3–17, 2007.

[111] TA Gorshkova, VV Salnikov, NM Pogodina, SB Chemikosova, E Vulanov Yablokova, AV Ulanov, MV Ageeva, JEG Van Dam, and VV Lozovaya. Composition and distribution of cell wall phenolic compounds in flax (linum usitatissimum l.) stem tissues. *Annals of Botany*, 85(4):477–486, 2000.

[112] David S Seigler. *Plant secondary metabolism*. Springer Science & Business Media, 2012.

[113] Jang-Kyo Kim and Yiu-Wing Mai. *Engineered interfaces in fiber reinforced composites*. Elsevier, 1998.

[114] LQN Tran, Carlos Fuentes Rojas, Ignace Verpoest, Van Vuure, and Aart Willem. Interfacial compatibility and adhesion in natural fiber composites. 2015.

[115] Le Quan Ngoc Tran, CA Fuentes, Christine Dupont-Gillain, AW Van Vuure, and I Verpoest. Understanding the interfacial compatibility and adhesion of natural coir fibre thermoplastic composites. *Composites Science and Technology*, 80:23–30, 2013.

[116] John Berg. *Wettability*. CRC Press, 1993.

[117] audiodella volp. So you want to measure surface energy. *Charlotte NC (cf. p. 99)*, 1999.

[118] Emilio Marcus de Castro Lobato. *Determination of surface free energies and aspect ratio of talc*. PhD thesis, Virginia Tech, 2004.

[119] L Q N Tran, C A Fuentes, A W Van Vuure, I Verpoest, and Katholieke Universiteit Leuven. Investigating the interfacial compatibility and adhesion of coir fibre composites. *Materials Engineering*, pages 1–5.

[120] Jaroslaw W Drelich, Ludmila Boinovich, Emil Chibowski, Claudio Della Volpe, Lucyna Hołysz, Abraham Marmur, and Stefano Siboni. Contact angles: History of over 200 years of open questions. *Surface Innovations*, pages 1–25, 2019.

[121] D K Owens. Estimation of the Surface Free Energy of Polymers. *Journal of Applied Polymer Science*, 13:1741–1747, 1969.

[122] W Adu Zisman. Relation of the equilibrium contact angle to liquid and solid constitution. *Advan. Chem. Ser.*, 43:1–51, 1964.

[123] Frederick M Fowkes. Attractive forces at interfaces. *Industrial & Engineering Chemistry*, 56(12):40–52, 1964.

[124] Jacques Schultz, Kazuo Tsutsumi, and Jean-Baptiste Donnet. Surface properties of high-energy solids: Ii. determination of the nondispersive component of the surface free energy of mica and its energy of adhesion to polar liquids. *Journal of Colloid and Interface Science*, 59(2):277–282, 1977.

[125] CJ Van Oss, RJ Good, and MK Chaudhury. The role of van der waals forces and hydrogen bonds in "hydrophobic interactions" between biopolymers and low energy surfaces. *Journal of colloid and Interface Science*, 111(2):378–390, 1986.

[126] Thomas Young. Iii. an essay on the cohesion of fluids. *Philosophical transactions of the royal society of London*, (95):65–87, 1805.

[127] Malcolm E Schrader. Spreading pressure in the young equation and intermolecular force theory. *Langmuir*, 9(8):1959–1961, 1993.

[128] C Della Volpe and S Siboni. Some reflections on acid–base solid surface free energy theories. *Journal of Colloid and Interface Science*, 195(1):121–136, 1997.

[129] David A Belsley, Edwin Kuh, and Roy E Welsch. Detecting and assessing collinearity. *Regression diagnostics: Identifying influential data and sources of collinearity*, pages 85–191, 1980.

[130] Ming Weng and Qing Shen. Effect of liquid surface tension data on the validity and accuracy of solid surface tension components and parameters in the application of the van oss–chaudhury–good approach. *Journal of Adhesion Science and Technology*, 28(22-23):2248–2268, 2014.

[131] Bryan B Sauer and William G Kampert. Influence of viscosity on forced and spontaneous spreading: Wilhelmy fiber studies including practical methods for rapid viscosity measurement. *Journal of colloid and interface science*, 199(1):28–37, 1998.

[132] Monica Francesca Pucci, Pierre-Jacques Liotier, David Seveno, Carlos Fuentes, Aart Van Vuure, and Sylvain Drapier. Wetting and swelling property modifications of elementary flax fibres and their effects on the liquid composite molding process. *Composites Part A: Applied Science and Manufacturing*, 97:31–40, 2017.

[133] Gregory Van Gansen, Dieter Perremans, Carlos Fuentes, Aart Willem van Vuure, and David Seveno. Surface Characterization of Natural Fibers. Do's and Don'ts. *Fiber Society 2014 Fall Conference, Philadelphia (USA)*, (February 2015), 2014.

[134] Robert J Good. Contact angle, wetting, and adhesion: a critical review. *Journal of adhesion science and technology*, 6(12):1269–1302, 1992.

[135] Rafael Tadmor. Line energy and the relation between advancing, receding, and young contact angles. *Langmuir*, 20(18):7659–7664, 2004.

[136] T.D Blake and J.M Haynes. Kinetics of liquidliquid displacement. *Journal of Colloid and Interface Science*, 30(3):421–423, jul 1969.

[137] Kathleen Van de Velde and Paul Kiekens. Wettability of natural fibres used as reinforcement for composites. *Die Angewandte Makromolekulare Chemie*, 272(1):87–93, 1999.

[138] Guillermo Cantero, Aitor Arbelaiz, Rodrigo Llano-Ponte, and Iñaki Mondragon. Effects of fibre treatment on wettability and mechanical behaviour of flax/polypropylene composites. *Composites science and technology*, 63(9):1247–1254, 2003.

[139] W Woigk, CA Fuentes, J Rion, D Hegemann, AW van Vuure, C Dransfeld, and Kunal Masania. Interface properties and their effect on the mechanical performance of flax fibre thermoplastic composites. *Composites Part A: Applied Science and Manufacturing*, 2019.

[140] Omid Arjmandi-Tash, Nina M Kovalchuk, Anna Trybala, Igor V Kuchin, and Victor Starov. Kinetics of wetting and spreading of droplets over various substrates. *Langmuir*, 33(18):4367–4385, 2017.

[141] André Walliser. *Caractérisation des interactions liquide-fibre élementaire par mouillage*. PhD thesis, Mulhouse, 1992.

[142] X-F Wu and Yuris A Dzenis. Droplet on a fiber: geometrical shape and contact angle. *Acta mechanica*, 185(3-4):215–225, 2006.

[143] M Connor, PH Harding, J-AE Manson, and JC Berg. Influence of the fiber surface properties on the mechanical strength of unidirectional fiber composites. *Journal of adhesion science and technology*, 9(7):983–1004, 1995.

[144] Christophe Baley, Frederic Busnel, Yves Grohens, and Olivier Sire. Influence of chemical treatments on surface properties and adhesion of flax fibre–polyester resin. *Composites Part A: Applied Science and Manufacturing*, 37(10):1626–1637, 2006.

[145] Pierre-Gilles De Gennes, Françoise Brochard-Wyart, and David Quéré. *Capillarity and wetting phenomena: drops, bubbles, pearls, waves*. Springer Science & Business Media, 2013.

[146] Bernard Miller, Pierre Muri, and Ludwig Rebenfeld. A microbond method for determination of the shear strength of a fiber/resin interface. *Composites Science and Technology*, 28(1):17–32, 1987.

[147] A Hampe and Ch Marotzke. Adhesion of polymers to reinforcing fibres. *Polymer international*, 28(4):313–318, 1992.

[148] G Desarmot and J-P Favre. Advances in pull-out testing and data analysis. *Composites Science and Technology*, 42(1-3):151–187, 1991.

[149] Serge F Zhandarov and Elena V Pisanova. The local bond strength and its determination by fragmentation and pull-out tests. *Composites Science and Technology*, 57(8):957–964, 1997.

[150] MR Piggott. The interface in carbon fibre composites. *Carbon*, 27(5):657–662, 1989.

[151] MR Piggott. Why interface testing by single-fibre methods can be misleading. *Composites Science and Technology*, 57(8):965–974, 1997.

[152] IUliia Arkadevna Gorbatkina and IUliia Arkad'evna Gorbatkina. *Adhesive strength in fibre-polymer systems*. Ellis Horwood, 1992.

[153] MH Auvray, P Chéneau-Henry, FH Leroy, and JP Favre. Pull-out testing of carbon/bismaleimide systems in the temperature range 20–250° c. *Composites*, 25(7):776–780, 1994.

[154] N Takeda, DY Song, K Nakat, and T Shioya. The effect of fiber surface treatment on the micro-fracture progress in glass fiber/nylon 6 composites. *Composite Interfaces*, 2(2):143–155, 1994.

[155] E Pisanova, V Dutschk, and B Lauke. Work of adhesion and local bond strength in glass fibre-thermoplastic polymer systems. *Journal of adhesion science and technology*, 12(3):305–322, 1998.

[156] MR Piggott and MM Reboredo. The durability of kevlar-epoxy interfaces. *Composite Interfaces*, 2(6):457–471, 1994.

[157] HL Cox. The elasticity and strength of paper and other fibrous materials. *British journal of applied physics*, 3(3):72, 1952.

[158] Andreas Hampe and Christian Marotzke. The energy release rate of the fiber/polymer matrix interface: measurement and theoretical analysis. *Journal of Reinforced Plastics and Composites*, 16(4):341–352, 1997.

[159] Serge Zhandarov, Elena Pisanova, and Edith Mäder. Is there any contradiction between the stress and energy failure criteria in micromechanical tests? part iii. experimental observation of crack propagation in the microbond test. *Journal of adhesion science and technology*, 19(8):679–704, 2005.

[160] S Zhandarov, E Pisanova, and E Mäder. Is there any contradiction between the stress and energy failure criteria in micromechanical tests? part ii. crack propagation: Effect of friction on force-displacement curves. *Composite Interfaces*, 7(3):149–175, 2000.

[161] Serge Zhandarov and Edith Mäder. Indirect estimation of fiber/polymer bond strength and interfacial friction from maximum load values recorded in the microbond and pull-out tests. part ii: Critical energy release rate. *Journal of adhesion science and technology*, 17(7):967–980, 2003.

[162] JOHN A Nairn. Fracture mechanics of the microbond and pull-out tests. *Nairn JA. Moore DR, editors. The application of fracture mechanics to polymers, adhesives and*, 20:213–8.

[163] Chun-Hsin Liu and John A Nairn. Analytical and experimental methods for a fracture mechanics interpretation of the microbond test including the effects of friction and thermal stresses. *International journal of adhesion and adhesives*, 19(1):59–70, 1999.

[164] Adnan H Nayfeh. Thermomechanically induced interfacial stresses in fibrous composites. *Fibre Science and Technology*, 10(3):195–209, 1977.

[165] S Zhandarov, E Pisanova, and K Schneider. Fiber-stretching test: a new technique for characterizing the fiber–matrix interface using direct observation of crack initiation and propagation. *Journal of Adhesion Science and Technology*, 14(3):381–398, 2000.

[166] Anu Ajith, Guijun Xian, Hui Li, Zajna Sherief, and Sabu Thomas. Surface grafting of flax fibres with hydrous zirconia nanoparticles and the effects on the tensile and bonding properties. *Journal of Composite Materials*, 50(5):627–635, 2016.

[167] Guillaume Coroller, Anaële Lefeuvre, Antoine Le Duigou, Alain Bourmaud, Gilles Ausias, Thierry Gaudry, and Christophe Baley. Effect of flax fibres individualisation on tensile failure of flax/epoxy unidirectional composite. *Composites Part A: Applied Science and Manufacturing*, 51:62–70, 2013.

[168] Anaële Lefeuvre, Antoine Le Duigou, Alain Bourmaud, Antoine Kervoelen, Claudine Morvan, and Christophe Baley. Analysis of the role of the main constitutive polysaccharides in the flax fibre mechanical behaviour. *Industrial Crops and Products*, 76:1039–1048, 2015.

[169] S Zhandarov, E Pisanova, and B Lauke. Is there any contradiction between the stress and energy failure criteria in micromechanical tests? part i. crack initiation: stress-controlled or energy-controlled? *Composite Interfaces*, 5(5):387–404, 1997.

[170] S Zhandarov, E Pisanova, E Mäder, and JA Nairn. Investigation of load transfer between the fiber and the matrix in pull-out tests with fibers having different diameters. *Journal of adhesion science and technology*, 15(2):205–222, 2001.

[171] John A Nairn. On the use of shear-lag methods for analysis of stress transfer in unidirectional composites. *Mechanics of Materials*, 26(2):63–80, 1997.

[172] C Baley. Influence of kink bands on the tensile strength of flax fibers. *Journal of materials science*, 39(1):331–334, 2004.

[173] HL Bos and AM Donald. In situ esem study of the deformation of elementary flax fibres. *Journal of materials science*, 34(13):3029–3034, 1999.

[174] Gábor Romhány, József Karger-Kocsis, and Tibor Czigány. Tensile fracture and failure behavior of thermoplastic starch with unidirectional and cross-ply flax fiber reinforcements. *Macromolecular Materials and Engineering*, 288(9):699–707, 2003.

[175] HL Bos, MJA Van Den Oever, and OCJJ Peters. Tensile and compressive properties of flax fibres for natural fibre reinforced composites. *Journal of Materials Science*, 37(8):1683–1692, 2002.

[176] Jerry YY Heng, Duncan F Pearse, Frank Thielmann, Thomas Lampke, and Alexander Bismarck. Methods to determine surface energies of natural fibres: a review. *Composite Interfaces*, 14(7-9):581–604, 2007.

[177] Alexis Baltazar-y Jimenez and Alexander Bismarck. Wetting behaviour, moisture up-take and electrokinetic properties of lignocellulosic fibres. *Cellulose*, 14(2):115–127, 2007.

[178] JM Van Hazendonk, JC Van der Putten, JTF Keurentjes, and A Prins. A simple experimental method for the measurement of the surface tension of cellulosic fibres and its relation with chemical composition. *Colloids and Surfaces A: Physicochemical and Engineering Aspects*, 81:251–261, 1993.

[179] Shabbir Ahmed, Xinnan Wang, Kai Li, and Chad A Ulven. Investigation on the surface free energy of a single flax fiber through adhesion measurement by atomic force microscopy. *Journal of Composite Materials*, 52(23):3233–3239, 2018.

[180] NE Zafeiropoulos, DR Williams, CA Baillie, and FL Matthews. Engineering and characterisation of the interface in flax fibre/polypropylene composite materials. part i. development and investigation of surface treatments. *Composites Part A: Applied Science and Manufacturing*, 33(8):1083–1093, 2002.

[181] Ryan H Mills, Douglas J Gardner, and Rupert Wimmer. Inverse gas chromatography for determining the dispersive surface free energy and acid–base interactions of sheet molding compound—part ii 14 ligno-cellulosic fiber types for possible composite reinforcement. *Journal of Applied Polymer Science*, 110(6):3880–3888, 2008.

[182] N Cordeiro, C Gouveia, and M Jacob John. Investigation of surface properties of physico-chemically modified natural fibres using inverse gas chromatography. *Industrial crops and products*, 33(1):108–115, 2011.

[183] A Legras, A Kondor, M Alcock, MT Heitzmann, and RW Truss. Inverse gas chromatography for natural fibre characterisation: dispersive and acid-base distribution profiles of the surface energy. *Cellulose*, 24(11):4691–4700, 2017.

[184] Ibon Aranberri-Askargorta, Thomas Lampke, and Alexander Bismarck. Wetting behavior of flax fibers as reinforcement for polypropylene. *Journal of colloid and interface science*, 263(2):580–589, 2003.

[185] Danny E Akin. Chemistry of plant fibres. *Industrial applications of natural fibres: Structure, properties and technical applications*, pages 13–22, 2010.

[186] Nicolas Le Moigne, Belkacem Otazaghine, Stéphane Corn, Hélène Angellier-Coussy, and Anne Bergeret. *Surfaces and Interfaces in Natural Fibre Reinforced Composites: Fundamentals, Modifications and Characterization*. Springer, 2018.

[187] Jaroslaw Drelich and Abraham Marmur. Physics and applications of superhydrophobic and superhydrophilic surfaces and coatings. *Surface Innovations*, 2(4):211–227, 2014.

[188] C Della Volpe and S Siboni. Use, abuse, misuse and proper use of contact angles: a critical review. *Reviews of Adhesion and Adhesives*, 3(4):365–385, 2015.

[189] J Acera Fernández, N Le Moigne, AS Caro-Bretelle, R El Hage, A Le Duc, M Lozachmeur, P Bono, and A Bergeret. Role of flax cell wall components on the microstructure and transverse mechanical behaviour of flax fabrics reinforced epoxy biocomposites. *Industrial Crops and Products*, 85:93–108, 2016.

[190] Tommi Huhtamäki, Xuelin Tian, Juuso T Korhonen, and Robin HA Ras. Surface-wetting characterization using contact-angle measurements. *Nature protocols*, 13(7):1521, 2018.

[191] Bo S Westerlind and John C Berg. Surface energy of untreated and surface-modified cellulose fibers. *Journal of Applied Polymer Science*, 36(3):523–534, 1988.

[192] M Abdelmouleh, S Boufi, MN Belgacem, AP Duarte, A Ben Salah, and A Gandini. Modification of cellulosic fibres with functionalised silanes: development of surface properties. *International Journal of Adhesion and Adhesives*, 24(1):43–54, 2004.

[193] Raul DSG Campilho. *Natural fiber composites*. CRC Press, 2015.

[194] Qing Shen, Pasi Mikkola, and Jarl B Rosenholm. Quantitative characterization of the subsurface acid–base properties of wood by xps and fowkes theory. *Colloids and Surfaces A: Physicochemical and Engineering Aspects*, 145(1-3):235–241, 1998.

[195] CA Fuentes, Gitte Brughmans, LQN Tran, C Dupont-Gillain, Ignace Verpoest, and AW Van Vuure. Mechanical behaviour and practical adhesion at a bamboo composite interface: Physical adhesion and mechanical interlocking. *Composites Science and Technology*, 109:40–47, 2015.

[196] Frederick M Fowkes. Quantitative characterization of the acid-base properties of solvents, polymers, and inorganic surfaces. *Journal of adhesion science and technology*, 4(1):669–691, 1990.

[197] L Lavielle, J Schultz, and K Nakajima. Acid–base surface properties of modified poly (ethylene terephthalate) films and gelatin: Relationship to adhesion. *Journal of applied polymer science*, 42(10):2825–2831, 1991.

[198] Claudio Della Volpe and Stefano Siboni. The wilhelmy method: a critical and practical review. *Surface Innovations*, 6(3):120–132, 2018.

[199] Sheldon Q Shi and Douglas J Gardner. A new model to determine contact angles on swelling polymer particles by the column wicking method. *Journal of Adhesion Science and Technology*, 14(2):301–314, 2000.

[200] FE Bartell and HH Zuidema. Wetting characteristics of solids of low surface tension such as talc, waxes and resins. *Journal of the American Chemical Society*, 58(8):1449–1454, 1936.

[201] P Luner and M Sandell. The wetting of cellulose and wood hemicelluloses. In *Journal of Polymer Science Part C: Polymer Symposia*, volume 28, pages 115–142. Wiley Online Library, 1969.

[202] José AF Gamelas. The surface properties of cellulose and lignocellulosic materials assessed by inverse gas chromatography: a review. *Cellulose*, 20(6):2675–2693, 2013.

[203] Adam Voelkel, Beata Strzemiecka, Katarzyna Adamska, and Kasylda Milczewska. Inverse gas chromatography as a source of physiochemical data. *Journal of Chromatography A*, 1216(10):1551–1566, 2009.

[204] Frank Thielmann. Introduction into the characterisation of porous materials by inverse gas chromatography. *Journal of chromatography A*, 1037(1-2):115–123, 2004.

[205] JH De Boer. The dynamic character of chemisorptions, 1953.

[206] Charles Kemball and Eric Keightley Rideal. The adsorption of vapours on mercury. i. non-polar substances. *Proceedings of the Royal Society of London. Series A. Mathematical and Physical Sciences*, 187(1008):53–73, 1946.

[207] V Gutmann. The donor-acceptor approach to molecular interactions. 1978.

[208] Viktor Gutmann. *Donor-Acceptor Approach to Molecular Interactions*. Plenum Press, 1978.

[209] Adam Voelkel. Inverse gas chromatography: characterization of polymers, fibers, modified silicas, and surfactants. *Critical Reviews in Analytical Chemistry*, 22(5):411–439, 1991.

[210] M Nardin and J Schultz. Relationship between fibre-matrix adhesion and the interfacial shear strength in polymer-based composites. *Composite Interfaces*, 1(2):177–192, 1993.

[211] Juan C Bastidas, Richard Venditti, Joel Pawlak, Richard Gilbert, Stefan Zauscher, and John F Kadla. Chemical force microscopy of cellulosic fibers. *Carbohydrate polymers*, 62(4):369–378, 2005.

[212] Sergei N Magonov and Darrell H Reneker. Characterization of polymer surfaces with atomic force microscopy. *Annual Review of Materials Science*, 27(1):175–222, 1997.

[213] Kenneth Langstreth Johnson, Kevin Kendall, and AD Roberts. Surface energy and the contact of elastic solids. *Proceedings of the royal society of London. A. mathematical and physical sciences*, 324(1558):301–313, 1971.

[214] Boris V Derjaguin, Vladimir M Muller, and Yu P Toporov. Effect of contact deformations on the adhesion of particles. *Journal of Colloid and interface science*, 53(2):314–326, 1975.

[215] Alexis Pietak, Sandra Korte, Emelyn Tan, Alison Downard, and Mark P Staiger. Atomic force microscopy characterization of the surface wettability of natural fibres. *Applied surface science*, 253(7):3627–3635, 2007.

[216] SJ Eichhorn and RJ Young. Deformation micromechanics of natural cellulose fibre networks and composites. *Composites science and technology*, 63(9):1225–1230, 2003.

[217] Antoine Le Duigou, Peter Davies, and Christophe Baley. Interfacial bonding of flax fibre/poly (l-lactide) bio-composites. *Composites Science and technology*, 70(2):231–239, 2010.

[218] T Truong Chi. The effects of chemical treatment on the mechanical properties of flax fibre reinforced epoxy composites. *Eupoco thesis, Department of Metallurgy and Materials Engineering, Katholieke Universiteit Leuven*, 2000.

[219] S Huo, A Thapa, and CA Ulven. Effect of surface treatments on interfacial properties of flax fiber-reinforced composites. *Advanced Composite Materials*, 22(2):109–121, 2013.

[220] Donald F Adams, Todd R King, and Donald M Blackketter. Evaluation of the transverse flexure test method for composite materials. *Composites Science and Technology*, 39(4):341–353, 1990.

[221] Charlotte Campana, Romain Leger, Rodolphe Sonnier, Laurent Ferry, and Patrick Ienny. Effect of post curing temperature on mechanical properties of a flax fiber reinforced epoxy composite. *Composites Part A: Applied Science and Manufacturing*, 107:171–179, 2018.

[222] NE Zafeiropoulos, CA Baillie, and FL Matthews. A study of transcrystallinity and its effect on the interface in flax fibre reinforced composite materials. *Composites Part A: Applied Science and Manufacturing*, 32(3-4):525–543, 2001.

[223] A Stamboulis, C Baillie, and E Schulz. Interfacial characterisation of flax fibre-thermoplastic polymer composites by the pull-out test. *Die Angewandte Makromolekulare Chemie*, 272(1):117–120, 1999.

[224] Roberts Joffe, J Andersons, and Lennart Wallström. Interfacial shear strength of flax fiber/thermoset polymers estimated by fiber fragmentation tests. *Journal of materials Science*, 40(9):2721–2722, 2005.

[225] Antoine Le Duigou, Peter Davies, and Christophe Baley. Exploring durability of interfaces in flax fibre/epoxy micro-composites. *Composites Part A: Applied science and manufacturing*, 48:121–128, 2013.

[226] MM Desaeger. An integrated theoretical and experimental study of the fibre-matrix interface in carbon-epoxy composites. 1995.

[227] Ramesh-Babu Adusumalli, Moritz Reifferscheid, Hedda K Weber, Thomas Roeder, Herbert Sixta, and Wolfgang Gindl. Shear strength of the lyocell fiber/polymer matrix interface evaluated with the microbond technique. *Journal of Composite Materials*, 46(3):359–367, 2012.

[228] CEZAR-DORU Radu, PAUL Kiekens, and J Verschuren. Surface modification of textiles by plasma treatments. *Surface characteristics of fibers and textiles*, pages 203–218, 2001.

[229] NE Zafeiropoulos and CA Baillie. A study of the effect of surface treatments on the tensile strength of flax fibres: Part ii. application of weibull statistics. *Composites Part A: Applied Science and Manufacturing*, 38(2):629–638, 2007.

[230] Joseph R Davis. *Tensile testing*. ASM international, 2004.

[231] Wei Hu, Minh-Tan Ton-That, Florence Perrin-Sarazin, and Johanne Denault. An improved method for single fiber tensile test of natural fibers. *Polymer Engineering & Science*, 50(4):819–825, 2010.

[232] Roberts Joffe, Jānis Andersons, and Lennart Wallström. Strength and adhesion characteristics of elementary flax fibres with different surface treatments. *Composites Part A: Applied Science and Manufacturing*, 34(7):603–612, 2003.

[233] Janis Andersons, E Spārniņš, and Roberts Joffe. Uniformity of filament strength within a flax fiber batch. *Journal of materials science*, 44(2):685–687, 2009.

[234] MK Sridhar, G Basavarajappa, SG Kasturi, and N Balasubramanian. Evaluation of jute as a reinforcement in composites. 1982.

[235] Gary C Davies and David M Bruce. Effect of environmental relative humidity and damage on the tensile properties of flax and nettle fibers. *Textile Research Journal*, 68(9):623–629, 1998.

[236] Farida Bensadoun, Ignace Verpoest, Joris Baets, J Müssig, N Graupner, P Davies, M Gomina, A Kervoelen, and C Baley. Impregnated fibre bundle test for natural fibres used in composites. *Journal of Reinforced Plastics and Composites*, 36(13):942–957, 2017.

[237] Kash L Mittal. Silanes and other coupling agents, volume 3. 2004.

[238] AM Cabral, RG Duarte, MF Montemor, and MGS Ferreira. A comparative study on the corrosion resistance of aa2024-t3 substrates pre-treated with different silane solutions: Composition of the films formed. *Progress in Organic Coatings*, 54(4):322–331, 2005.

[239] B Singh, M Gupta, and Anchal Verma. Influence of fiber surface treatment on the properties of sisal-polyester composites. *Polymer Composites*, 17(6):910–918, 1996.

[240] J George and I Verpoest, J Ivens. Mechanical properties of flax fibre reinforced epoxy composites. *Die Angewandte Makromolekulare Chemie*, 272(1):41–45, 1999.

[241] ETN Bisanda and Martin P Ansell. The effect of silane treatment on the mechanical and physical properties of sisal-epoxy composites. *Composites Science and Technology*, 41(2):165–178, 1991.

[242] Dale W Schaefer, Yimin Wang, and Tammy L Metroke. Metal-protective films based on mixed silane coupling agents. *Silanes and Other Coupling Agents*, 5:243, 2009.

[243] Manju Kumari Thakur, Raju Kumar Gupta, and Vijay Kumar Thakur. Surface modification of cellulose using silane coupling agent. *Carbohydrate polymers*, 111:849–855, 2014.

[244] Babak Fathi, Mohammadreza Foruzanmehr, Saïd Elkoun, and Mathieu Robert. Novel approach for silane treatment of flax fiber to improve the interfacial adhesion in flax/bio epoxy composites. *Journal of Composite Materials*, page 0021998318824643, 2019.

[245] Jochen Gassan and Andrzej K Bledzki. Effect of cyclic moisture absorption desorption on the mechanical properties of silanized jute-epoxy composites. *Polymer Composites*, 20(4):604–611, 1999.

[246] PJ Herrera-Franco and A Valadez-Gonzalez. Mechanical properties of continuous natural fibre-reinforced polymer composites. *Composites Part A: applied science and manufacturing*, 35(3):339–345, 2004.

[247] Natural fibre company Bcomp. amplitex ud fabric, art. no. 5057. `http://www.bcomp.ch/media/amplitex_5057.pdf`, 2017.

[248] Anon ASTM et al. Standard test method for tensile strength and young's modulus for high-modulus single-filament materials, 1989.

[249] Edgars Sparnins. *Mechanical properties of flax fibers and their composites*. PhD thesis, Luleå tekniska universitet, 2009.

[250] Prasanna Kumar Ilankeeran, Preetamkumar M Mohite, and Sudhir Kamle. Axial tensile testing of single fibres. *Modern Mechanical Engineering*, 2(04):151, 2012.

[251] Luiz Claudio Pardini and Luis Guilherme Borzani Manhani. Influence of the testing gage length on the strength, young's modulus and weibull modulus of carbon fibres and glass fibres. *Materials research*, 5(4):411–420, 2002.

[252] Douglas E Turek. On the tensile testing of high modulus polymers and the compliance correction. *Polymer Engineering & Science*, 33(6):328–333, 1993.

[253] Soo-Keun Kang, Deok-Bo Lee, and Nak-Sam Choi. Fiber/epoxy interfacial shear strength measured by the microdroplet test. *Composites Science and Technology*, 69(2):245–251, 2009.

[254] Suhara Panthapulakkal and Mohini Sain. Agro-residue reinforced high-density polyethylene composites: Fiber characterization and analysis of composite properties. *Composites Part A: Applied Science and Manufacturing*, 38(6):1445–1454, 2007.

[255] S Alix, J Goimard, C Morvan, and C Baley. Prospects about cellulosic fibres extracted from a linseed winter variety of flax (oliver). *Pectins and pectinases*, pages 87–96, 2009.

[256] S Alix, L Lebrun, S Marais, E Philippe, Alain Bourmaud, Christophe Baley, and C Morvan. Pectinase treatments on technical fibres of flax: effects on water sorption and mechanical properties. *Carbohydrate polymers*, 87(1):177–185, 2012.

[257] Igor Maria De Rosa, Josè Maria Kenny, Debora Puglia, Carlo Santulli, and Fabrizio Sarasini. Tensile behavior of new zealand flax (phormium tenax) fibers. *Journal of Reinforced Plastics and Composites*, 29(23):3450–3454, 2010.

[258] Anaële Lefeuvre, Alain Bourmaud, Claudine Morvan, and Christophe Baley. Tensile properties of elementary fibres of flax and glass: Analysis of reproducibility and scattering. *Materials Letters*, 130:289–291, 2014.

[259] Christian Stevens. *Industrial applications of natural fibres: structure, properties and technical applications*, volume 10. John Wiley & Sons, 2010.

[260] Alain Bourmaud, Claudine Morvan, and Christophe Baley. Importance of fiber preparation to optimize the surface and mechanical properties of unitary flax fiber. *Industrial Crops and Products*, 32(3):662–667, 2010.

[261] C Della Volpe and S Stefano. Calculations of acid-base surface tension components (surften 4.3).

[262] C Della Volpe, D Maniglio, M Brugnara, S Siboni, and M Morra. The solid surface free energy calculation: I. in defense of the multicomponent approach. *Journal of Colloid and Interface Science*, 271(2):434–453, 2004.

[263] Reinforcement fibres - Flax fibres for plastics composites - Part 2 : determination of tensile properties of elementary fibres - Fibres de renfort. Standard, AFNOR, Cedex, FR, 2015.

[264] Marianne Gibaud, Alain Bourmaud, and Christophe Baley. Understanding the lodging stability of green flax stems; the importance of morphology and fibre stiffness. *Biosystems Engineering*, 137:9–21.

[265] Christophe Baley and Alain Bourmaud. Average tensile properties of french elementary flax fibers. *Materials letters*, 122:159–161, 2014.

[266] Clément Gourier, Antoine Le Duigou, Alain Bourmaud, and Christophe Baley. Mechanical analysis of elementary flax fibre tensile properties after different thermal cycles. *Composites Part A: Applied science and manufacturing*, 64:159–166, 2014.

[267] Anaële Lefeuvre, Alain Bourmaud, Laurent Lebrun, Claudine Morvan, and Christophe Baley. A study of the yearly reproducibility of flax fiber tensile properties. *Industrial crops and products*, 50:400–407, 2013.

[268] Tsonko Tsonev and Fernando Jose Cebola Lidon. Zinc in plants-an overview. *Emirates Journal of Food & Agriculture (EJFA)*, 24(4), 2012.

[269] SB Jennifer Kan, Russell D Lewis, Kai Chen, and Frances H Arnold. Directed evolution of cytochrome c for carbon–silicon bond formation: Bringing silicon to life. *Science*, 354(6315):1048–1051, 2016.

[270] Luanda Chaves Lins, Valeria Bugatti, Sébastien Livi, and Giuliana Gorrasi. Phosphonium ionic liquid as interfacial agent of layered double hydroxide: Application to a pectin matrix. *Carbohydrate polymers*, 182:142–148, 2018.

[271] BJ Carroll. The accurate measurement of contact angle, phase contact areas, drop volume, and laplace excess pressure in drop-on-fiber systems. *Journal of colloid and interface science*, 57(3):488–495, 1976.

[272] Chunyang Jiang, Xin Zhang, Jingna Zhao, Jingyun Zou, and Xiaohua Zhang. Evaluating the system compliance in testing carbon nanotube fibers. *arXiv preprint arXiv:1706.00755*, 2017.

6 Appendix A: MKT Impracticability

As mentioned in Section 2.1.4.4, it was impracticable to use MKT in the present work, the main reason being the time constrain of this project whose ambitions did not stop in the physicochemical component of the fibre-matrix adherence. A brief approximate calculation can evidence this fact:

1. minimum 5 (measurements for each liquid) × 3 (liquids) × 4 (different types of fibres): minimum 60 specimens;

2. minimum 60 (contact angles measurements) + 60 (wetted perimenter measurements): minimum 120 measurements.

3. Specimens had to be changed after each cycle (advancing/receding + wetted perimeter measurement) since, due to swelling, different cycle in the same specimen resulted in different results (see Section 2.1.4.5):

   (a) Difficult handling of elementary fibres and alignment of specimen in the holder. Elementary fibre fixation in the holder: ~ 5 min/specimen ($t_{step} = 300$ min);

   (b) Change the holder with placed fibre and position the fibre in the vicinity of the probe liquid between experiments: ~ 2 min/specimen (not accounting for probe liquid change; $t_{step} = 120$ min)

   (c) Each specimen corresponds to one isolated elementary fibre. Elementary fibre isolation: ~ 10 min/specimen ($t_{step} = 600$ min)

4. Significantly low measurement velocities were used so as to approach the static advancing contact angle (see Fig. 2.10): 0.5mm/min

   (a) 5 mm of each specimen were probed so as to have enough statistical data to account for properties variation along the axis: (10 min advancing + 10 minutes receding)/specimen ($t_{step} \approx 900$min, roughly half of the receding parts of the experiments were stopped at an early stage since their results would not be valuable [see Section 2.1.4.4]).

   (b) 5 mm of each specimen were measured at 1mm/min displacement rate in advancing mode only were probed for wetted perimeter determination: 5 min/specimen ($t_{step} = 300$ min)

   (c) Total time for 1 measurement velocity not accounting for specimen change, machine setup and other minor time losses: ~ 37 h/measurementvelocity

   (d) The minimum, but by no means sufficient, number of different measurement speeds that allows to use the MKT is 3: minimum ~ 111 h (i.e., minimum 14 complete 8h-work days).

   (e) This could easily result in months of complete days of experiments. This was not practicable due the following reasons:

      i. Other experiments such as fibres mechanical tests, microbond, chemical analysis and a few other trials that were not included in the present manuscript had to be performed in parallel;

ii. The equipment (tensiometer, whose access was kindly provided by Dr C.A. Fuentes and his group in KULeuven) availability had to respected, and only 2 working days could be booked each week. Which means that, even working the entire day 7 weeks would be required to complete the measurements (in case all the data resulted in valid information).

Static advancing contact angles were aimed for instead.

7 Appendix B: Energy-Based Equation Coefficients

$$v_f A_0 = \frac{v_m (1 - \nu_T)}{E_T} + \frac{v_f (1 - \nu_m)}{E_m} + \frac{1 + \nu_m}{E_m} \tag{7.1}$$

$$C_{33s} = \frac{1}{2}\left(\frac{1}{E_A} + \frac{v_f}{v_m E_m}\right) \tag{7.2}$$

$$C_{33} = C_{33s} - \frac{v_m A_3^2}{v_f A_0} \tag{7.3}$$

$$D_{3s} = \frac{1}{2}(\alpha_A - \alpha_m) \tag{7.4}$$

$$D_3 = D_{3s} - \frac{v_m A_3}{v_f A_0}[\alpha_T - \alpha_m] \tag{7.5}$$

8 Appendix C: An Approach to Drop-on-Fibre Measurements

Several mathematical models can be used to fit the shape of a droplet on a fibre. Here the mathematical treatment suggested by X.-F. Wu and Y. A. Dzenis [142] is presented, it can be used to assess the contact angle in Drop-on-Fibre Systems in which an axisymmetrical unduloid (also called barrel) morphology is assumed, instead of clamshell (see Fig. 8.1).

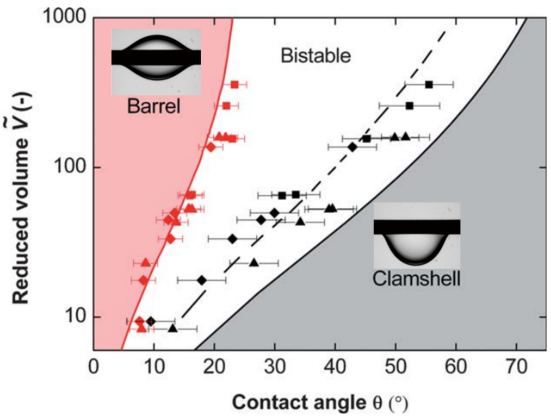


Figure 8.1: Morphology diagram of millimetre-sized drops on fibres as a function of contact angle θ and reduced volume $\tilde{V}$. Black and red symbols indicate the experimentally observed barrel-to-clamshell (θ_{c1}) and clamshell-to-barrel (θ_{c2}) transitions, respectively. Symbol shapes indicate different fibre diameters: (■) 0.2, (▲) 0.3, and (♦) 0.5 mm. The solid lines indicate the numerically determined stability limit of the clamshell (upper red) and the (coinciding) analytically and numerically determined stability limit of the barrel (lower black). The dashed line indicates the condition of equal absolute energy of both states [49].

1 - The Axisymmetrical Unduloid Morphology

H. Burak Eral et al. [49] used electrowetting-functionalised fibres with tunable wettability to study the effect of the parameters that determine which morphology will be seen upon drop deposition on fibres in the case in which the drop diameter is small enough (i.e., drop has small enough volume, V) so that the gravity effects are negligible and the fibre is a symmetrical cylinder with radius r (Fig. 8.1 summarises the findings). For a reduced volume defined as $\tilde{V} = V/r^3$, it can be seen that a barrel morphology is promoted by increasing the drop volume (paying attention to avoid large volumes that could result in a hydrostatic pressure not being negligible with respect to the Laplace pressure [1]), diminishing the fibre diameter and increasing the fibre surface wettability. Although the clamshell morphology is a more common outcome (as its larger area in the diagram indicates), the bistable region should not be forgotten, since droplets assuming barrel morphology in this region comprise a great amount of the results found in the literature.

2 - Contact Angle of a Microdroplet on a Fibre

X.-F. Wu and Y. A. Dzenis [142] used a free energy variation analysis to model the geometrical shape, wetting length, and contact angle of a microdroplet on a fibre. By calculating the geometrical

[1] Refer to Eötvös's number.

shape of the droplet as a combination of Legendre's elliptical functions of the first and second kinds (see Caroll [271]), they were able to derive an efficient semi-analytic approach to extract the contact angle from experimental data [2].

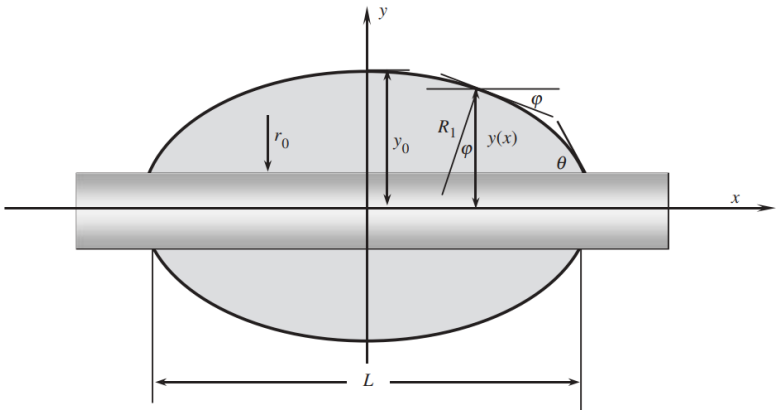


Figure 8.2: Schematic diagram of a microdroplet on a fibre.

For a microdroplet whose morphology is defined by L, y_0, and r_0, respectively, its length along the axial direction, maximum diameter (where 0 refers to the origin, placed at intersection between the droplet symmetry plane and axis) and fibre diameter (see Fig. 8.2), all parameters that can be obtained from imaging analysis, the contact angle θ can be calculated using the following dimensionless semi-analytic polynomial approximation of the drop axial length (coefficients are presented at the end of this section).

$$l(\lambda) = C_0 + C_1\lambda + C_2\lambda^2 + C_3\lambda^3 + C_4\lambda^4 + C_5\lambda^5 + C_6\lambda^6 + C_7\lambda^7 + C_8\lambda^8 + C_9\lambda^9 + C_{10}\lambda^{10} + C_{11}\lambda^{11} + C_{12}\lambda^{12} \quad (8.1)$$

which dependent on $l(\lambda) = L/(2r_0)$, $\rho_0 = y_0/r_0$, $\lambda = \frac{y_0\cos\theta - r_0}{y_0 - \cos\theta}$, where l is the dimensionless droplet length, ρ_0 is the dimensionless droplet aspect ratio and λ is a dimensionless variable that accounts for the contact angle variation.

Eq. 8.1 with the coefficients defined in Appendix A has only one root λ_0 for a given l_0, consequently, only one root in the considered domain, which is related to a value of $\theta \in [15°, 180°]$ (so-called middle range contact angles, interval in which, according to the author, it presents very high accuracy, with cutoff error lower than 0.5° [3]),

$$\theta = \cos^{-1}[(1 + \lambda_0\rho_0)/(\lambda_0 + \rho_0)] \quad (8.2)$$

[2]Here only the practical results are presented. A reader looking for further understanding of the model is encouraged to refer to Caroll [271] and to the simple derivation by X.-F. Wu and Y. A. Dzenis [142]

[3]The equation is derived via an expansion in Taylor's series, that is why it is not well defined for contact angles below 15°.

Coefficients to be used in Eq. 8.1 for approximation until the 13th term:

$C_0 = \sqrt{\rho_0^2 - 1}$,

$C_1 = -\ln(\rho_0 - \sqrt{\rho_0^2 - 1})$,

$C_2 = -\frac{1}{2\rho_0}\ln(\rho_0 - \sqrt{\rho^2 - 1})$,

$C_3 = \frac{1}{2\rho_0^2}\left[\frac{\rho_0}{2}\sqrt{\rho_0^2 - 1} - \frac{1}{2}\ln(\rho_0 - \sqrt{\rho_0^2 - 1})\right]$,

$C_4 = \frac{3}{8\rho_0^3}\left[\frac{\rho_0}{2}\sqrt{\rho_0^2 - 1} - \frac{1}{2}\ln(\rho_0 - \sqrt{\rho_0^2 - 1})\right]$,

$C_5 = \frac{3}{8\rho_0^4}\left[\frac{\rho_0^3}{4}\sqrt{\rho_0^2 - 1} + \frac{3\rho_0}{8}\sqrt{\rho_0^2 - 1} - \frac{3}{8}\ln(\rho_0 - \sqrt{\rho_0^2 - 1})\right]$,

$C_6 = \frac{5}{16\rho_0^5}\left[\frac{\rho_0^3}{4}\sqrt{\rho_0^2 - 1} + \frac{3\rho_0}{8}\sqrt{\rho_0^2 - 1} - \frac{3}{8}\ln(\rho_0 - \sqrt{\rho_0^2 - 1})\right]$,

$C_7 = \frac{5}{16\rho_0^6}\left[\frac{\rho_0^5}{6}\sqrt{\rho_0^2 - 1} + \frac{5\rho_0^3}{24}\sqrt{\rho_0^2 - 1} + \frac{5\rho_0}{16}\sqrt{\rho_0^2 - 1} - \frac{5}{16}\ln(\rho_0 - \sqrt{\rho_0^2 - 1})\right]$,

$C_8 = \frac{35}{128\rho_0^7}\left[\frac{\rho_0^5}{6}\sqrt{\rho_0^2 - 1} + \frac{5\rho_0^3}{24}\sqrt{\rho_0^2 - 1} + \frac{5\rho_0}{16}\sqrt{\rho_0^2 - 1} - \frac{5}{16}\ln(\rho_0 - \sqrt{\rho_0^2 - 1})\right]$,

$C_9 = \frac{63}{128\rho_0^8}\left[\frac{\rho_0^7}{8}\sqrt{\rho_0^2 - 1} + \frac{7\rho_0^5}{48}\sqrt{\rho_0^2 - 1} + \frac{35\rho_0^3}{192}\sqrt{\rho_0^2 - 1} + \frac{35\rho_0}{128}\sqrt{\rho_0^2 - 1} - \frac{35}{128}\ln(\rho_0 - \sqrt{\rho_0^2 - 1})\right]$,

$C_{10} = \frac{63}{256\rho_0^9}\left[\frac{\rho_0^7}{8}\sqrt{\rho_0^2 - 1} + \frac{7\rho_0^5}{48}\sqrt{\rho_0^2 - 1} + \frac{35\rho_0^3}{208*}\sqrt{\rho_0^2 - 1} + \frac{35\rho_0}{128}\sqrt{\rho_0^2 - 1} - \frac{35}{128}\ln(\rho_0 - \sqrt{\rho_0^2 - 1})\right]$,

$C_{11} = \frac{231}{512\rho_0^10}\left[\frac{\rho_0^9}{10}\sqrt{\rho_0^2 - 1} + \frac{9\rho_0^7}{80}\sqrt{\rho_0^2 - 1} + \frac{21\rho_0^5}{160}\sqrt{\rho_0^2 - 1} + \frac{63\rho_0^3}{504}\sqrt{\rho_0^2 - 1} + \frac{63\rho_0}{256}\sqrt{\rho_0^2 - 1} - \frac{35}{128}\ln(\rho_0 - \sqrt{\rho_0^2 - 1})\right]$,

$C_{12} = \frac{231}{512\rho_0^11}\left[\frac{\rho_0^9}{10}\sqrt{\rho_0^2 - 1} + \frac{9\rho_0^7}{80}\sqrt{\rho_0^2 - 1} + \frac{21\rho_0^5}{160}\sqrt{\rho_0^2 - 1} + \frac{63\rho_0^3}{504}\sqrt{\rho_0^2 - 1} + \frac{63\rho_0}{256}\sqrt{\rho_0^2 - 1} - \frac{35}{128}\ln(\rho_0 - \sqrt{\rho_0^2 - 1})\right]$.

9 Appendix D: System Compliance

Introduction Direct extension measurements (e.g., using gauge extensometers) in the case of elementary and technical fibres tensile testing is not practical since the devices used, when attached to small samples, are often bulky and can interfere with the measurements [252]. As a convenient replacement, the system crosshead or actuator displacement is often used to measure the specimen extension, which results in an error associated to the equipment (load frame, load cell and grips) deformation under load, which increases with the system compliance. As a result, tensile moduli calculated without accounting for system deformation will be lower than the real value. The present document briefly discusses how and when the contribution of the non-specimen deformation can be considered in terms of system compliance.

Compliance Theory Let us assume that both, the equipment and the fibre, are in the elastic regime over the entire experiment such that the whole setup and tested specimen can be modelled in terms of an association of springs in series with stiffnesses k_{sys}, related to the system components (outside fibre) and k_f, related to the fibre [272].

$$\frac{1}{k_f^{eff}} = \frac{1}{k_{sys}} + \frac{1}{k_f} \tag{9.1}$$

where k_f^{eff} is the effective stiffness measured.

Here it is convenient to use the inverse of the stiffness, the Compliance (C), which is additive for in series association.

$$C_{tot} = C_{sys} + C_f \tag{9.2}$$

From Hooke's law,

$$E = \frac{F/A}{\Delta L/L_0} = k\frac{L_0}{A} = \frac{L_0}{CA} \tag{9.3}$$

where F is the tensile force under an elongation distance ΔL, L_0 is the gauge length, and A is the cross-sectional area.

Using the relation obtained in Eq. 9.3 in Eq. 9.2, it is possible to obtain the following relation for the system compliance as a function of the effective and real tensile moduli.

$$\frac{L_0}{E_f^{eff}A} = C_{sys} + \frac{L_0}{E_f A} \tag{9.4}$$

Compliance-Associated Error A few important conclusions can be derived from Eq. 9.4:

- In a plot $L_0/E_f^{eff}A$ v L_0, C_{sys} and L_0/E_fA are respectively the y-intercept and the slope of the resulting linear function;
- The error introduced by C_{sys} increases in the following cases:

- High compliance system;
- High stiffness fibres;
- Small gauge length;
- High cross-sectional area.

For a known system compliance, the error associated with it can be defined as follows,

$$\epsilon(\%) = \frac{E_f - E_f^{eff}}{E_f} 100 = \frac{C_{tot} - C_f}{C_{tot}} 100 = \frac{C_{sys}}{C_{tot}} 100 \tag{9.5}$$

Assuming an approximately constant cross-sectional area, it is possible to derive the minimum gauge length (L_{min}) that keeps the system compliance-associated error below a given value by introducing Eq. 9.5 into Eq. 9.4

$$L_{min} = C_{sys} E_{eff} A \left(\frac{100}{\epsilon(\%)} - 1 \right) \tag{9.6}$$

Similarly, if the system compliance is known, the elongation at break can be corrected as follows,

$$\Delta L_{corr} = \Delta L_{eff} - C_{sys} F \tag{9.7}$$

Conclusion As the mathematical development presented in this document shows, it becomes unpractical to evaluate whether the compliance-associated error is important not knowing its value. In this case, guidelines such as low stiffness fibres, large gauge length and small cross-sectional area become vague.

Differently from the batch-to-batch, specimen and cross-sectional variabilities observed in natural fibres, the system compliance does not result in a scattering of the measured values around a mean, rather it introduces a bias, resulting in measured values that are either less (Tensile Modulus) or greater (Elongation at break) than the real value.

UNIVERSITÉ CATHOLIQUE DE LOUVAIN
École polytechnique de Louvain
Rue Archimède, 1 bte L6.11.01, 1348 Louvain-la-Neuve, Belgique | **www.uclouvain.be/epl**